Fall 12-5-2011

DEVELOPMENT OF SELF-STRESSING SYSTEM FOR BRIDGE APPLICATION WITH EMPHASIS ON PRECAST PANEL DECK SYSTEM

Marcelo Ferreira da Silva

University of Nebraska-Lincoln, marcelofsilva@gmail.com

www.manaraa.com

DEVELOPMENT OF SELF-STRESSING SYSTEM FOR BRIDGE APPLICATION WITH

EMPHASIS ON PRECAST PANEL DECK SYSTEM

by

Marcelo Ferreira da Silva

A DISSERTATION

Presented to the Faculty of

The Graduate College at the University of Nebraska

In Partial Fulfillment of Requirements

For the Degree of Doctor of Philosophy

Major: Interdepartmental Area of Engineering

(Civil Engineering)

Under the Supervision of Professors Elizabeth Jones & Atorod Azizinamini

Lincoln, Nebraska

December, 2011

DEVELOPMENT OF SELF-STRESSING SYSTEM FOR BRIDGE APPLICATION WITH EMPHASIS ON PRECAST PANEL DECK SYSTEM

Marcelo Ferreira da Silva, Ph.D.

University of Nebraska, 2011

Advisor: Elizabeth Jones & Atorod Azizinamini

Steel girder bridges often utilize continuity over the pier to reduce interior forces on the spans. In continuous structures with composite concrete decks, the location of maximum negative bending moment is over the interior supports. This moment produces tensile stresses in the concrete deck and compressive stress in the bottom flanges of the girders. The tensile stress in the deck leads to cracking which allow intrusion of moisture and road salt, causing corrosion of the reinforcement and supporting girders. Continued maintenance is required to forestall the deterioration; however, replacement of the deck is eventually required.

To overcome this problem, a "self-stressing" system was developed. The method induces a compressive force in the deck that is accomplished by raising the interior supports above their final elevation while the deck is cast or placement (precast panels). Once the concrete has cured the supports are lowered to their final elevation. Continuity of the steel member and the composite action with the deck produce a compressive stress in the concrete slab, which is balanced by tensile stresses in the bottom of the steel member. As a result, the cracking over interior support is diminished increasing durability and the need of girder splices may be eliminated making the overall bridge design more efficient and cheaper when compared to conventional design.

The experimental investigation was conducted to observe the behavior of the system. Time-dependent effects and behavior of the system under ultimate load were analyzed. Overall,

the specimen performed as expected, shown good stability, delayed cracking, and sufficient amount of ductility. Based on the experimental program, the system appears to be a simple and viable alternative to more common method of post-tensioning the deck to obtain an initial compressive force in the concrete deck. As a result, a design guide was developed to aid bridge engineers with the implementation of the Self-stressing Method Design in practice.

Dedication

This dissertation is dedicated to the memory of my father, Marcelo José da Silva and to my mother Cleise Ferreira Gomes, who have been my role-model and mentor throughout the years. I would love to sincerely thank them for their hard work, persistence and personal sacrifices for me to have the best education. They have always emphasized the importance of education and encouraged me to set high goals and have strong confidence to achieve them.

Acknowledgement

First of all, I would like to thank my advisor, Dr. Atorod Azizinmaini. I am deeply grateful for his guidance, advice, and valuable suggestions throughout the duration of the research conducted at the National Bridge Research Organization (NaBRO).

Thank you to Dr. Jones for stepping in to serve as a chair of my committee so that our main supervisory professor, Dr. Atorod Azizinamini, could continue to serve as co-chair of my committee after leaving the University of Nebraska-Lincoln for his current position as Department Chair of Civil and Environmental Engineering at Florida International University.

I offer my thanks to Dr. Andrzej Nowak, Dr. Mehrdad Negahban, and Dr. Fred Choobineh who have served on my committee and evaluated my work.

I would like to thank Dr. Aaron Yakel for his assistance and expertise. As well as to Peter Hilsabeck, for all the long hours in the structures laboratory and hard work during the construction of many test specimens that we have worked on.

Last but not least, I offer my sincere thanks and love to my parents, Marcelo José da Silva (in memoriam) and Cleise Ferreira Gomes, who have raised and supported me, and siblings Michelle Ferreira Wright and Sandro Ferreira da Silva for their love and friendship. Special thanks to my girlfriend Emily for her unconditional love and support throughout the years.

I also appreciate the assistance, cooperation, and friendship provided by many colleagues, whose numbers have now grown too great to be individually mentioned.

Table of Contents

List of Figures

List of Tables

Chapter 1

Introduction

1.1 Problem Statement

Probably the most common composite steel-concrete structural member is a composite tee-beam, which is comprised of a concrete slab connected to a steel I-beam section by shear stud connectors. Composite beams find extremely widespread used in both building and highways bridges. The attraction of standard composite beams is that the steel component is subjected predominantly to tensile stresses, and the concrete to compressive stresses, thereby making the most efficient use of both materials.

Frequently, steel girder bridges often utilize continuity over the pier to reduce interior forces on the spans. In continuous structures with composite steel-concrete section, the location of maximum negative bending moment is over the interior supports. This moment produces tensile stresses in the concrete deck and compressive stress in the bottom flanges of the girders. Although, this reversal of the benign characteristics of the steel and concrete in negative bending reduces the efficiency of composite construction below those subjected to positive bending only, there are still both strength and stiffness advantages if continuous construction is used.

This stress inversion lead to two commonly knows issues. The first refers to the bucking of the steel beam under compressive forces and cracking of concrete under tensile forces. The flexural capacity due to buckling is often solve by increasing the cross-section properties of the beam. Thus, expensive and labor intensive steel-splices are often considered to change the beam lighter section to a much heavy section.

On the other hand, since concrete tensile strength is practically negligible, cracking are often expected in the negative bending region. When precast concrete decks are considered, cracks are expected to be developed first at the joint locations since these are considered weak areas due to the discontinuities in steel reinforcement. Consequently, the extensive of cracks leads to durability issues such as chloride intrusion and corrosion of reinforcement which required periodical maintenance to diminish the corrosion rate thus resulting in high life cycle cost of highway bridges. In some case where maintenance is neglected due to budget cuts, bridge deterioration become so extreme that replace the entire bridge is the only alternative.

Figure 1-1. Example of mapping cracks in the concrete deck and steel girder splice.

In order to improve durability and consequently reduce life cycle cost of bridges, construction and design procedures have been developed to deal with the problems. The two of the most common procedures are:

1. **Cast-in-place concrete deck approach:** Providing additional reinforcement in the slab in the negative moment regions so that composite action is developed between the steel reinforcement of the deck and the steel girder. This approach does not eliminate the cracks completely but only control the crack width to a certain level.

2. **Precast concrete deck approach:** Prestressing the panels using embedded steel tendons, so that the concrete is always in compression. This may completely mitigate the appearance of cracks but needs well-trained personnel and extra time for execution, hence higher initial cost is expected when this solution is considered. Also, the tendons are susceptible to corrosion which may lead to loss of prestressing force and further to cracking and corrosion of reinforcing steel.

Although both solutions are commonly used to diminish the issue related to deck cracking, none of them resolve the issue of steel-splice requirement when steel girders are considered.

1.2 Objective and Scope

The main objective of this research is to develop guidelines of the Self-Stressing Method (SSM) system for use on multi-span continuous structures with composite cast-in-place or precast bridge decks.

One of the biggest advantages of the system is precompress the deck without the need of the costly and time consuming post-tensioning techniques, thus reducing the cost and time for bridge construction. In addition, because no prestressing strands are used, possible corrosion of strands and lost of prestressing force are completely removed from the picture.

In negative region where durability issues are always expected due to cracking of the deck due to tensile force in concrete, the application of a compressive force would reduce cracking thus increasing durability and service life of bridges. Another advantage of the system is the demand reduction at the interior support region due to compressive force in girder. Though, when steel girders are considered, the bridge design becomes more cost efficient since a

single girder cross-section can be used throughout the whole bridge length. In other words, the method eliminates the need of expensive, labor intensive steel-splice details.

Consequently, this project focuses on develop guidelines for use of the self-stressing deck system in practice. The self-stressing system or prestressing by cambering can be a cheaper alternative to post-tensioning for imparting a longitudinal compressive stress in the bridge deck and minimize the size if not completely eliminate the extent of cracking of the concrete bridge deck. Although steel girders are used throughout the discussion, the concept could be adapted for concrete girder as well.

The scope of the research project to evaluate the feasibility of the self-stressing system is as follows:

Step 1 – Identify various approaches to create prestress force in the deck.

Step 2 – Evaluate existing prestressing practices to determine the level of prestress required to create a desired results with respect to crack abatement.

Step 4 – Assess the benefit of prestressing the deck by monitoring the crack behavior over the middle support.

Step 3 – Perform time history analysis to determine the stressing loss due to the effects of creep and shrinkage.

Step 5 – Develop and calibrate finite element models in order to evaluate behavior of the system.

Step 6 – Based on the results of steps 1 thru 5, develop recommendations for determining the amount of initial pre-stressing and displacement required.

Step 7 – Identify avenues for future research. A final step will be to identify the potential for future research, specifically with an aim to develop field trials of the proposed system.

1.3 Report Organization

Chapter 2 presents the literature review providing background information for the research.

The test specimen selection and the resulting geometry are given in Chapter 3. The experimental setup, instrumentation, and testing procedures are also described.

In Chapter 4 presents the results of the different testing considered. The obtained results are compared with analytical solutions in order to later develop guidelines to use the method in practice.

The development of the finite element models are detailed in Chapter 5. General modeling considerations are explored and methods for addressing materials are discussed. The results obtained are compared with the experimental and analytical results.

Chapter 6 provides a simplified design example considering both conventional method and self-stressing method for easy comparison. Important procedure and construction stages are discussed. Analytical equations are provided to aid bridge engineers while designing the self-stressing deck system in practice.

Finally, Chapter 7 presents the main conclusions obtained and suggests avenues of potential future research.

Reference and Appendices are also provides. In Appendix A is introduced a draft of the AASHTO formatted design guide to use the self-stressing method. Appendix B includes additional experimental data not included in the main body of the dissertation. Appendix C provides additional pictures took during the experimental program. Appendix D shows some supplementary analysis and calculations carried out.

Chapter 2

Literature Review

This chapter provides a summary of previous research project related to topic researched herein. The idea of prestressing the bridge deck using the bridge's continuity is simple; however, the technique has never been extensively researched or used in practice. Very little research has been conducted on this type of a system. Thus did not allow for extensive literature review.

2.1 NDOR P539 research project

The NDOR Research Project Number SPR-PL-1 (038) P539, titled as "Three Innovative Concepts for Short Span Steel Bridges", reports three innovative bridge concepts in response to a series of design challenges. Two of the concepts were aimed at quick construction with the elimination of costly elements such as intermediate stiffeners and cross frames, while the third concept attempted to improve the performance of a composite girder deck in the negative moment region. Dr. Aaron Yakel, Dr. Mohammadreza Farimani, Ms. Nazanin Mossahebi, and Dr. Atorod Azizinamini, investigated the three designs using a combination of theory, finite element analysis and experimentation.

2.1.1   Test Description

Yakel et al. (2007) had conducted a preliminary investigation of cast-in-place deck system considering the self-stressing method system under the project previous mentioned. The system consisted of a continuous I-shape steel girder (W14x22) over two equal spans of 15 ft. A concrete slab was poured to act compositely with the steel girder. The center support was

shimmed upward 0.3 inch above the elevation of the outer supports before the pouring of the concrete. Since the test specimen considered was a reduced scale of bridge, additional weight was added to simulate the dead weight of a larger section. After the deck was poured and allowed to cure, the shim was released to create compression in the concrete. The creep in the deck was monitored for 100 days. Finally, an ultimate load test was performed by applying point loads in the middle of each span. Figure 2-1 shows the pouring of the deck and the self-stressing test specimen before shim removal.

| a) Deck pour | b) Test specimen |

Figure 2-1. Self-stressing test specimen considering CIP deck (Yakel et. al, 2007)

2.1.2   Experimental Results

Part of the results is here discussed. Figure 2-2 (a) shows a very good agreement between the estimated value of compressive force of 500 psi and the measured values of 480 psi. Regarding the long-term results, it was reported that the deck underwent additional compressive strains due to the creep of the concrete based on the shape of the curves in Figure 2-2 (b). Also it was observed that after long period, the strain did not increased much as was observed at early stages of the monitoring.

a) Compressive force measured   **b) Long-term monitoring**
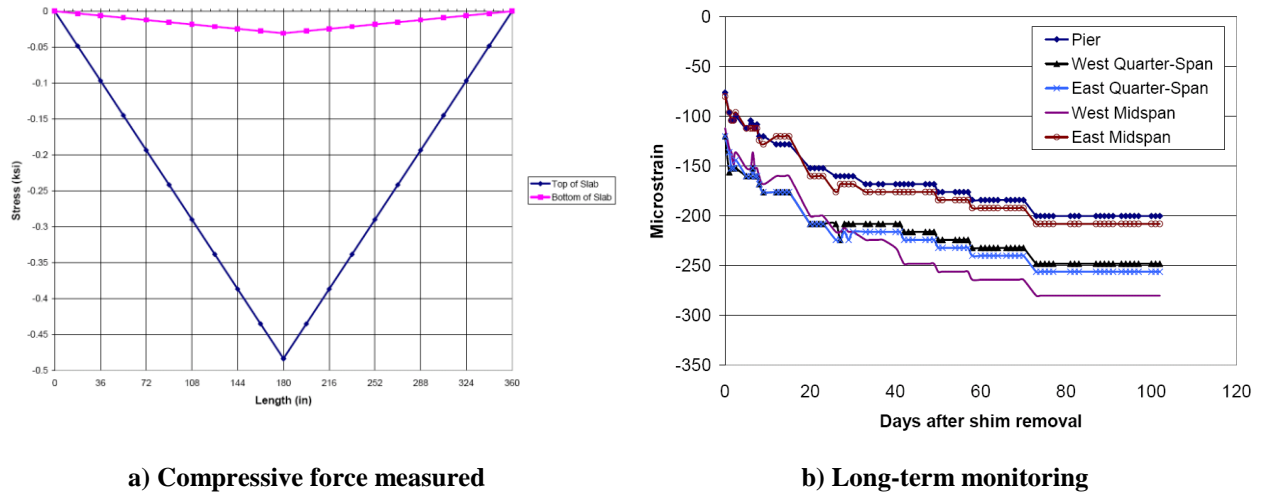
Figure 2-2. Prestressing force and long-term monitoring (Yakel et. al, 2007)

After the center support had been lowered and the concrete had been monitored for 100 days, the ultimate load test was conducted. The test was conducted by applying point load at the each mid-span. Figure 2-3 show the load-defection curve from the ultimate load test. It was reported that load-defection response of the system was nearly linear until a deflection of approximately 0.25 inches, which corresponded to an applied load of 55 kips. Yakel et al. (2007) reported that an unloading of the system at about 60 kips was done to correct the loading frame. After correction the loading was resumed. At 72 kips, yielding of the web occurred near the pier. This corresponded to a deflection of 1.1 inches at mid-span. It was also mentioned that the specimen exhibited a sufficient amount of ductility.
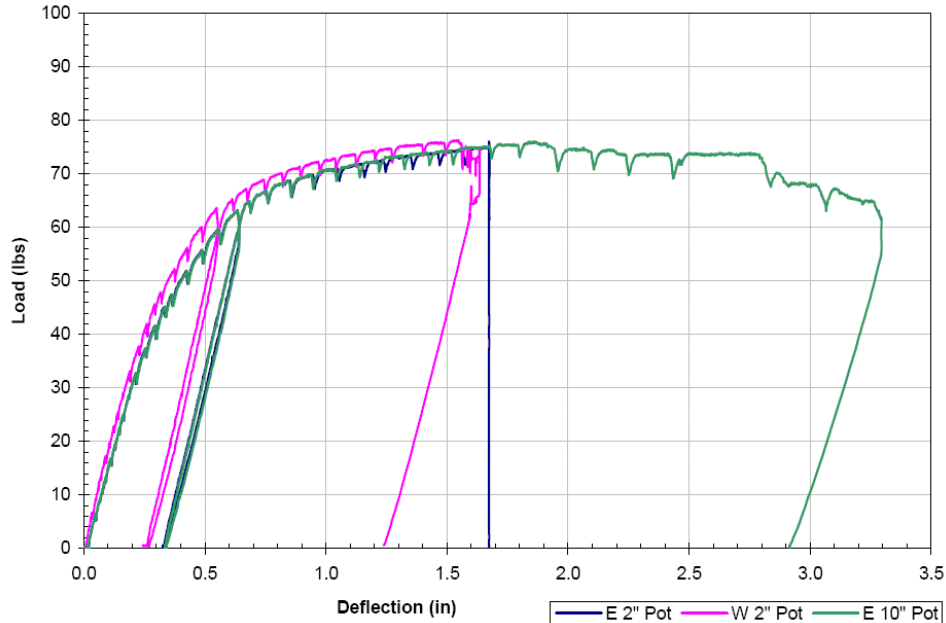
Figure 2-3. Load-defection curve of ultimate load test (Yakel et. al, 2007)

2.1.3   Findings

During the test very few observable events prior to the reaching of ultimate load was observed (Yakel, Farimani, Mossahebi, & Azizinamini, 2007). At a load of 65 kips the transverse crack pattern was first observed. The load ceased to increase after reaching 75 kips, at which point the vertical deflection at the middle of the east span was 1.65 inches. The deflection continued to increase with no increase in load until crushing was observed at the top of the deck. Beyond this point, the specimen was able to absorb additional deflection, but at a reduced level of loading. The maximum deflection at the end of the test was approximately 3.25 inches at midspan. The observed ultimate load was slightly lower than the predicted failure load of 81 kips (Yakel, Farimani, Mossahebi, & Azizinamini, 2007). They attributed to the fact that during the design calculations were made assuming yield strength of 50 ksi but the material testing showed that the actual yield strength of the beam was slightly lower at 47.6 ksi.

a) Crushing the concrete slab at the point load   b) Crack pattern over the center support

Figure 2-4. Concrete behavior under positive and negative moment (Yakel et. al 2007)

Figure 2-5 show the points of interest of the system after failure.
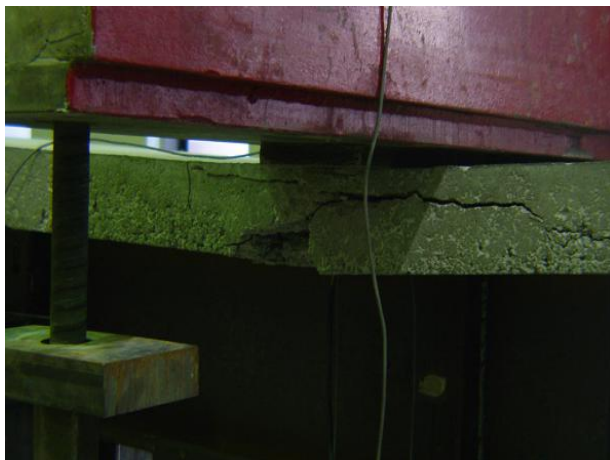
a) Deck crushing failure mode   b) Large defection (yielding/bucking) failure mode

Figure 2-5. Mode of failure observed (Yakel et. al 2007)

2.1.4   Conclusions

Their final comments were the failure of the specimen was initiated by the yielding of the steel web close to the pier further intensify to local buckling of the web and crushing of the concrete deck. This is typical for a continuous steel I-girder, only with this specimen it was observed that the cracking of the concrete deck was reduced (Yakel et al. 2007). The system performed satisfactorily and as expected, exhibiting good stability, sufficient ductility and a

delayed crack occurrence over the pier. Based on this experimental program, Yakel et al. (2007) reported that system seems to be a simple and viable method when compared to the more common method, post-tensioning of the deck slab. The initial precompression of the slab had prevented any observable cracks from forming in the negative flexure region over the interior support until well within the ultimate load test (Yakel et al. 2007).

They also pointed out some major topics which may affect the performance of the self-stressing system, such as, level of prestress and amount of displacement required, effect of long-term creep and shrinkage, effect of overload, effect of cyclic loading.

2.2 Chidorinosawagawa Bridge

Chidorinosawagawa was designed in 1998 as a four span continuous composite two-I-girder bridge with a prestressed concrete (PC) slab. It was the first application of this bridge type to highway bridges in Japan. Before then, from 1980 to 1998, almost all steel bridges with reinforcement concrete slabs were designed as a noncomposite girder and the lateral distance between steel girders was restricted within 10 ft (Nagai, et al., 2000).

They had mentioned that during the design of this kind of bridge, it should be pay close attention to the time-dependent stress variation. Thus after the completion of the concrete slab, the stress in the concrete and girder had been monitored, i.e. the effect of creep and shrinkage had been monitored. Further, they conducted an analytical approach to simulate time-dependent behavior and the results are compared with those obtained from measured data (Nagai, et al., 2000).

Figure 2-6. Concrete Casting with Movable Form at Chidorinosawagawa Bridge (Nagai, et al., 2000).

2.2.1   Bridge Outline

Chidorinosawagawa Bridge was constructed in Hokkaido Island, northern part of Japan. It is a four span continuous composite two-l-girder bridge and has a total bridge length of 194 meters (46.5+53.0+53.0+40.4 m). Figure 2-7 shows a cross section of the bridge and a total width of the bridge is 11.4 meters. The prestressed concrete slab with a thickness of 320 millimeters is supported by two I-girders only. These two girders have a depth of 2.9 meters, and are connected with small-sized cross beams arranged at a distance of 8.5 meters in the longitudinal direction.
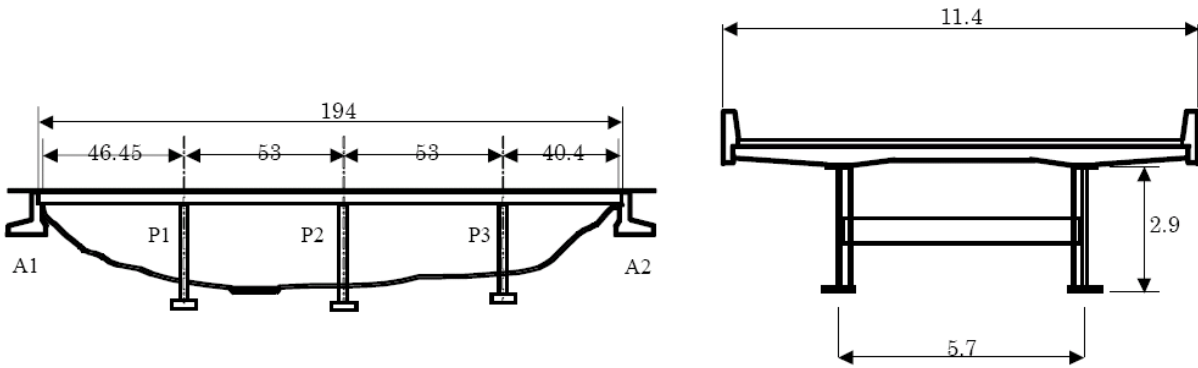
Units of length in meter (m)

Figure 2-7. Side View and Cross Section of Chidorinosawagawa Bridge (unit: m) (Nagai, et al., 2000).

Besides some innovative detailing regarding the lighter section stiffeners considered in this bridge. The design of composite girder bridges should consider the stress transfer from a concrete slab to steel girders due to creep and shrinkage effects. For this bridge, a creep coefficient of 2.0 was employed according to Japanese bridge code (JSHB) and since the expansive concrete was used, an ultimate shrinkage of 150 με was employed, which is smaller than 200 με specified in JSHB for conventional composite girder bridges (Nagai, et al., 2000).

2.2.2   Bridge Erection

A launching erection method was employed for the construction of the steel girder. Then, the concrete slab was cast. Figure 2-8 shows the casting sequence of the concrete slab in which the numbers are the order of concrete casting. This procedure is sometimes called "piano method". In this procedure, in order to avoid concrete cracking, jack-up and down was carried out at intermediate supports (Nagai, et al., 2000).
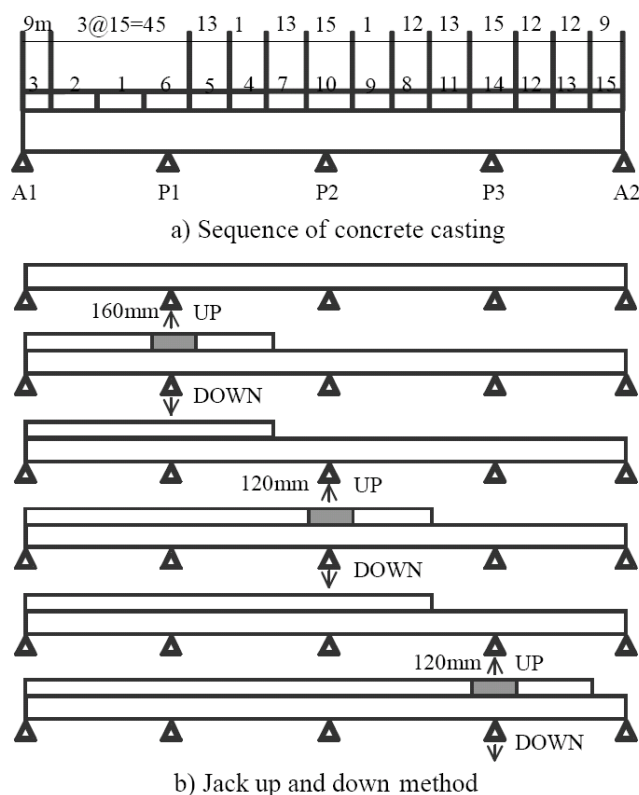
Figure 2-8. Sequence of segmental concrete casting and jack up and down procedure (Nagai, et al., 2000).

2.2.3   Field Measurement and Analytical Study

The field measurement was considered to confirm whether or not the expected prestress had been introduced and identification of the time-dependent stress variation. The monitoring using strain gauges and thermometers was started just after the completion of the concrete work at both concrete and steel girder surfaces.

To assess the prestress loss, Nagai et al., (2000) had carried out time-dependent analysis using finite element model simulating the construction stages. The concrete slab and steel girders were modeled with different beam elements and the creep behavior in the concrete element was modeled as viscoelasticity with the Kelvin chain model (DIANA, 1996).

The analytical prediction was verified with the field stress measurements (one and half year monitoring period) in the steel girder at support P1. Figure 2-9 shows a comparison of

measured and analytical results of the steel stress at P1. Although the monitoring stresses are scattered by nature owing to temperature effect and so on, both calculated and measured values show a good agreement after 300 days. From this result, it is confirmed the expected prestress was introduced by assuming approximately 50% of prestress loss (Nagai, et al., 2000).

Stress in concrete slab

Reduction of Concrete Prestress due to Creep and Shrinkage at Interior Support

Stress in steel girder

Comparison between Analytical Results and Monitoring Data
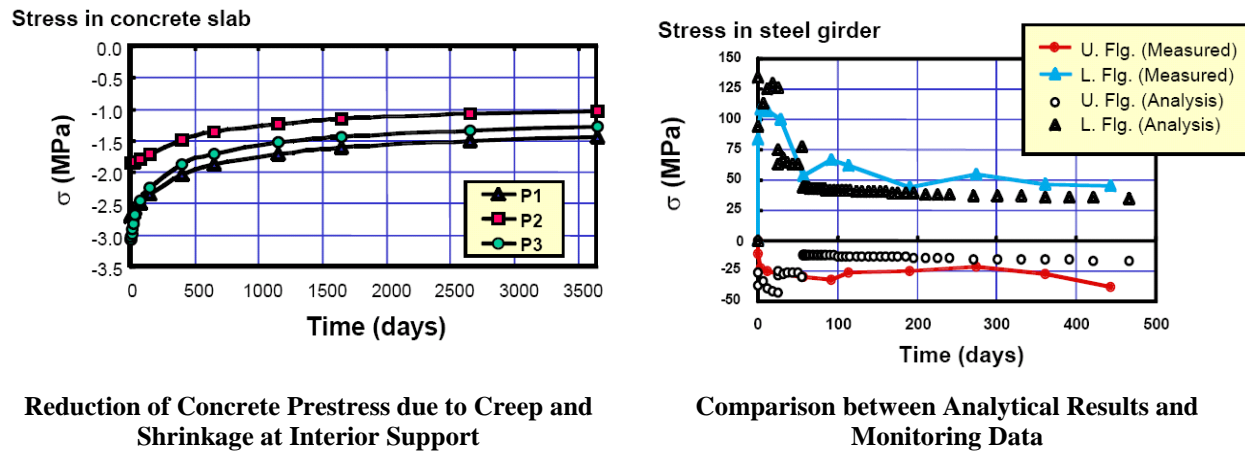
Figure 2-9. Field measurements and Analytical Results (Nagai, et al., 2000).

2.2.4   Conclusions

Nagai el al. (2000) had shown the outline of Chidurinosawagawa Bridge including an innovative web stiffening design method. They emphasized that time-dependent stress variation in the concrete has an important factor in the design of composite bridges. They carried out study confirmed that: (1) The designed value of prestress was achieved in the bridge. (2) After 1 one year monitoring, the reduction of compressive stress obtained from measured and calculated values shows a good agreement with each other. (3) From the reported results, a predicted reduction of prestress obtained from calculation is expected (Nagai, et al., 2000).

2.3 Oregon Demonstration Project

The Highways for LIFE (HfL) pilot program is an initiative of the Federal Highway Administration (FHWA) to accelerate innovation in the highway community. The program

promotes and documents improvements in safety, construction-related congestion, and quality that can be achieved by setting performance goals and adopting innovations.

A great example of the HfL program is the Oregon Department of Transportation's (ODOT) HdL demonstration project. This particular project involved alternate project delivery, innovative staged construction, and innovative removal and replacement of five bridges on Oregon 38 between the towns of Drain and Elkton (Ardani, Mallela, & Hoffman, 2010).

2.3.1 Project Overview

The Oregon HfL project consisted of removing and replacing five bridges on an 11-mi stretch of OR-38 between the towns of Drain and Elkton (see Figure 2-10). These bridges, built in the late 1920s and early 1930s, were near the end of their useful life and required immediate attention (Ardani, Mallela, & Hoffman, 2010). The reasons for chosen these bridge includes repair cost exceeding one-half of the replacement cost, narrowed bridge width and insufficient load rating.
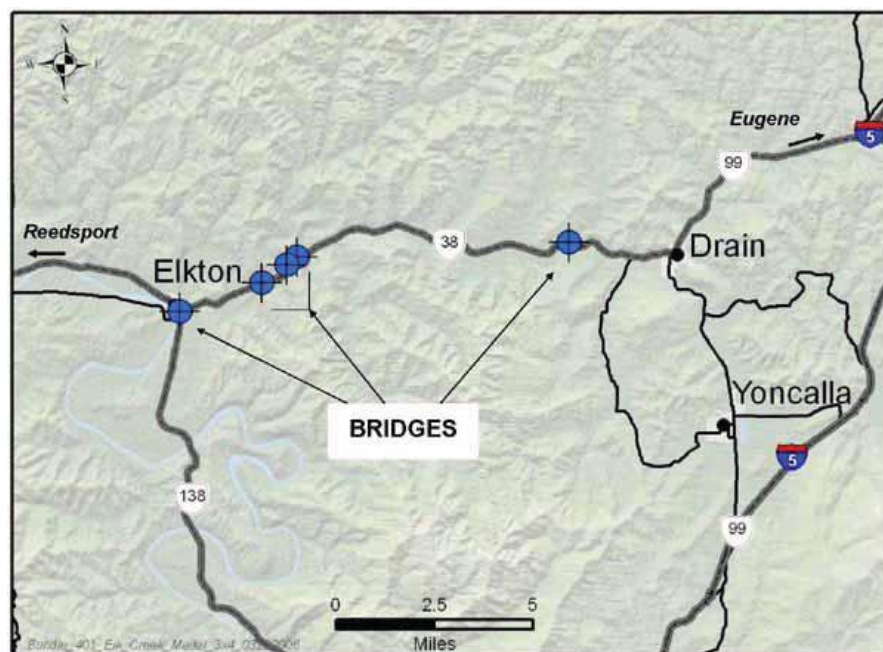
Figure 2-10. OR-38 bridge replacement project locations.

In order to achieve the goals, ODOT considered the following strategies (Ardani, Mallela, & Hoffman, 2010):

- Use of the D-B method of project delivery, which combines the design and construction phases of the project. Thus dramatically reducing the time required for the project.

- Offsite construction of the entire superstructure of two bridges (crossings 3 and 4) on temporary supports, which included girders, decks, curb, gutter, and side railings.

- Construction of substructures beneath crossings 3 and 4 and outside the bounds of OR-38 with little or no disruption of OR-38 traffic.

- Dramatically minimizing traffic disruption and maintaining normal traffic flow without altering the present roadway configuration through the use of an innovative, emerging technology: the hydraulic sliding system (HSS). HSS made it possible to remove the old crossings 3 and 4 and replace them during two weekend closures.

- Implementation of an innovative public information and outreach program that went beyond conventional public meetings.

- Implementation of a context-sensitive and sustainable solutions (CS3) approach that minimized environmental impacts and put communities and stakeholders at the heart of decision-making.

2.3.2   Removal and Replacement of OR-38 Crossings

Although all five bridges along the OR-38 had challenging site conditions, two (crossings 3 and 4) stood out because of the close proximity to tunnel entrances and the presence of Elk Creek. Thus construction of detour bridges at this location was impossible since these bridges were only a short distance (50 to 70 ft) from either end of the Elk Creek Tunnel.

Crossings 3 was a 340-ft long, six-span, reinforced concrete deck girder (RCDG) structure with steel truss and Crossings 4 was a 240-ft-long, five-span, RCDG bridge with steel truss were built in 1932 and 1931 respectively were situated at each end of the Elk Creek Tunnel (Ardani, Mallela, & Hoffman, 2010).
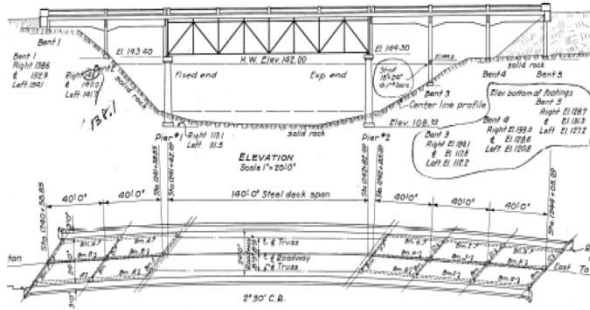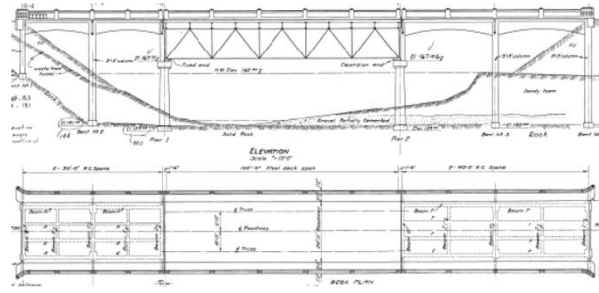
Crossing 3 drawings   Crossing 4 drawings

Figure 2-11. Crossing 3 & 4 old typical section.

The new bridge at the west portal of the tunnel (crossing 3) is a three-span structure constructed with steel deck girders with the overall length of 320 ft. The new bridge at the east portal of the tunnel is a two-span; 220-ft-long bridge constructed using precast concrete deck girders.
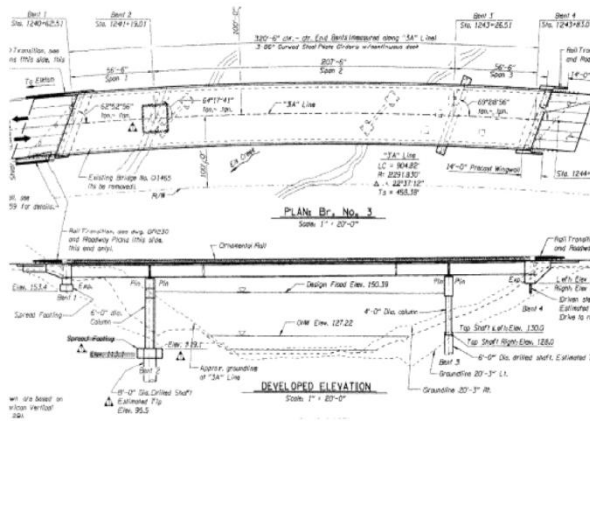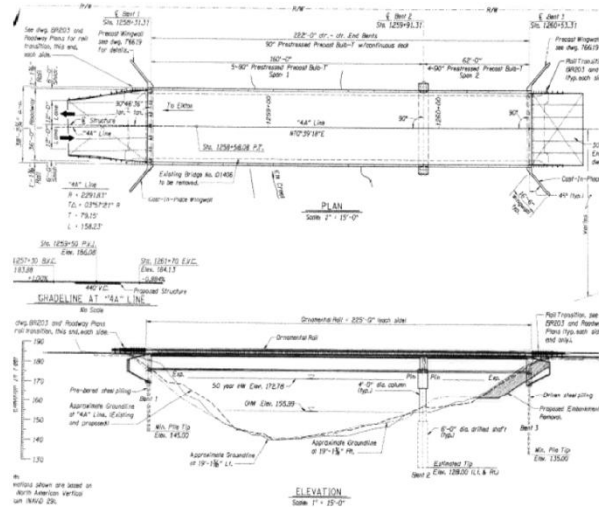
Crossing 3 drawings   Crossing 4 drawings

Figure 2-12. Crossing 3 & 4 proposed typical section.

Both crossings were successfully removed and replaced during a weekend closure using HSS rapid bridge replacement technology differently from the standard construction which would take years to be completed. In this system of bridge relocation, hydraulic jacks mounted on a sliding rail lift the new superstructures and hydraulic pumps slide them into their final position. HHS was also used to slide the old superstructure onto temporary supports before sliding in the new superstructure. In general, the rapid removal and replacement of bridges using HSS involves four stages (Ardani, Mallela, & Hoffman, 2010).

Table 2.1. Construction stages of rapid bridge removal using HSS.

Stage 1:	Construction of the temporary support for the old;
	Construction of the new substructure.
Stage 2:	Construction of the temporary support next to the old bridge for the new superstructure;
	Construction of the new superstructure.
Stage 3:	Demolition of the approach panels to the old bridge and translation of the old superstructure sideways onto its temporary support using HSS;
	Translation of the new superstructure onto its new substructure.
Stage 4:	Placement of the backfill materials and installation of the prefabricated components of the bridge, including wing walls, sleeper slabs, and approach pavement panels;
	Preparing the approach roadway for paving, installing the remaining guardrails, and striping the pavement and the bridge surface;
	Dismantling and removing the old superstructure and temporary support systems and hauling them away.

Figure 2-13 shows the rapid removal and replacement of bridges using HSS.
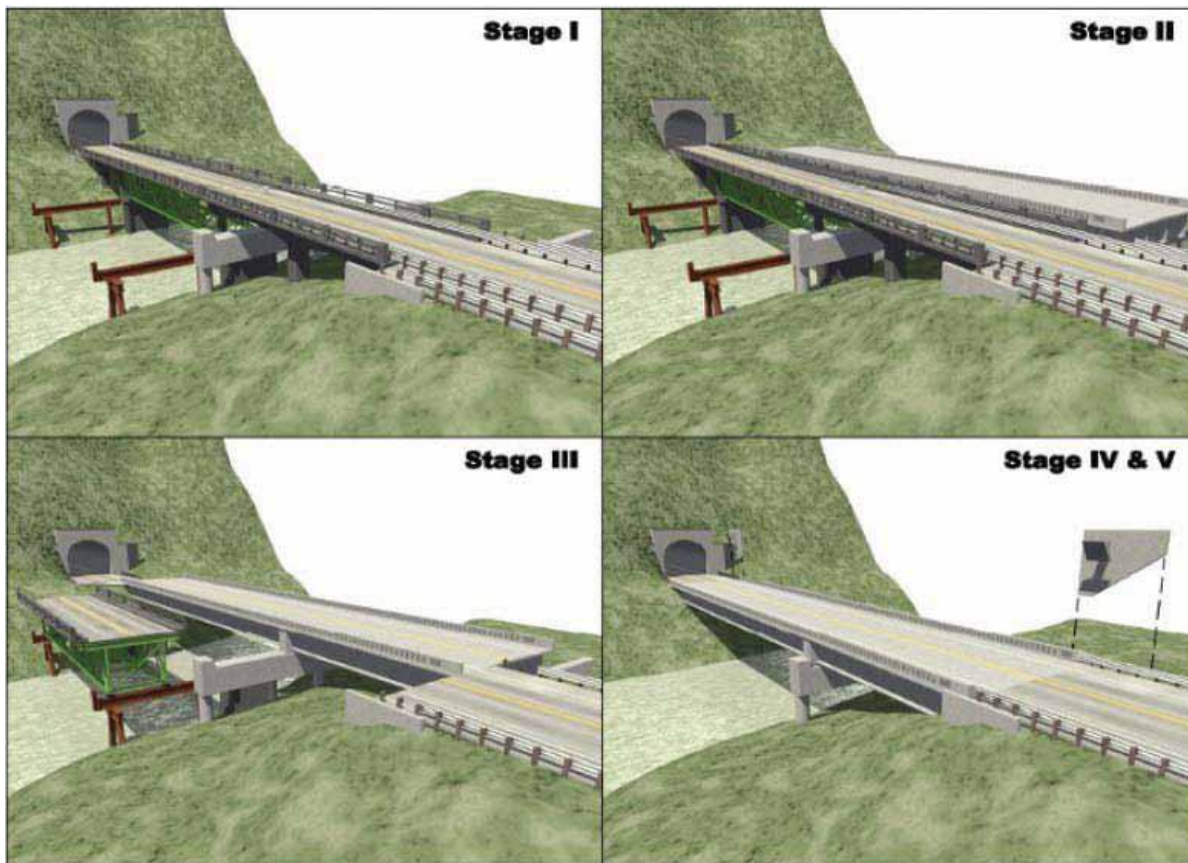
Figure 2-13. Conceptualized stages of rapid bridge removal using HSS (Ardani, Mallela, & Hoffman, 2010).

View of a complete hydraulic sliding system

Demolition and dismantling of end panels

| View of old and new superstructures | Replacement of superstructure and end panels. |

Figure 2-14. Sequence of removal and replacement of crossing 3 (Ardani, Mallela, & Hoffman, 2010).

2.3.3   Design Challenges and Solution

Crossing 3 was by far the most difficult site. Besides the extreme topography, the bridge featured long span, curved alignment, super elevation, high skew angle and steel-plate girder bridge with short end spans. Due to the short end spans configuration, uplift of the bridge end is produced which would be required by code some restraint system to avoid the lifting. However, the restraint system is complex and difficult to install in a short period of time.

The solution adopted was to construct bridge with "low" ends to elastically deform upon placement and "pre-stresss" a downward force onto the abutments. This solution was not sufficient to offset all code required load combination, but it did cover the service loading combination.

2.4 INVERSET™ Bridge System

Inverset™ is a proprietary product developed by Stanley Grossman, P.E., from Oklahoma, in the early 1980s. "Inverset is defined as a precast, precompressed, concrete/steel, composite superstructure made up of steel beams (typically two or more) and a concrete slab,

which act as a composite unit to resist its own dead load" (Fort Miller Company, Inc., 1998).
Figure 2-15 shows a typical cross section of an Inverset deck unit.
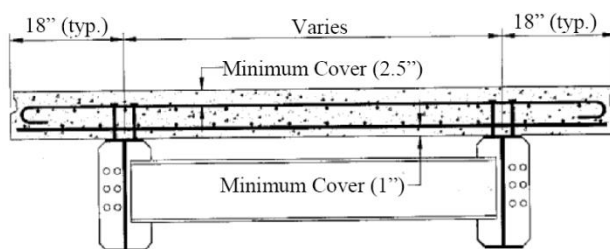
Figure 2-15. Typical cross section of an Inverset™ deck unit.

2.4.1   System description

The system is composed of modular components that are prefabricated upside down by casting the concrete deck slab in forms suspended from steel I-beams that will become its support members with the unit in its final inverted position.

The amount of prestress induced in the member is directly related to the amount of displacement thus deflection control device is used at mid-span during casting process, as shown Figure 2-16.
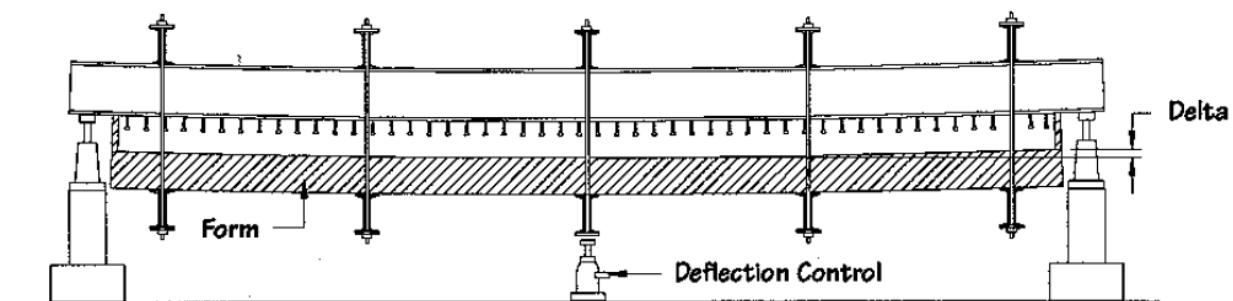
Figure 2-16. Schematic of the Inverset™ casting process.

The stress distribution in the section during casting can be seen in Figure 2-17 (a). The top flange of the beam is in compression and the bottom flange in tension, as is typically the case with any beam subjected to vertical loads. After the concrete cures and reaches its design strength, the entire unit is turned right side up (i.e., turned 180 degrees), with the concrete deck

now compositely cast over the steel beams. The section now undergoes stress reversals, as shown in Figure 2-17 (b). The concrete deck is in compression, the top flange of the steel beam (which was the bottom flange during casting) remains in tension, and the bottom flange of the beam (the top flange during casting) is decompressed to a near zero stress.
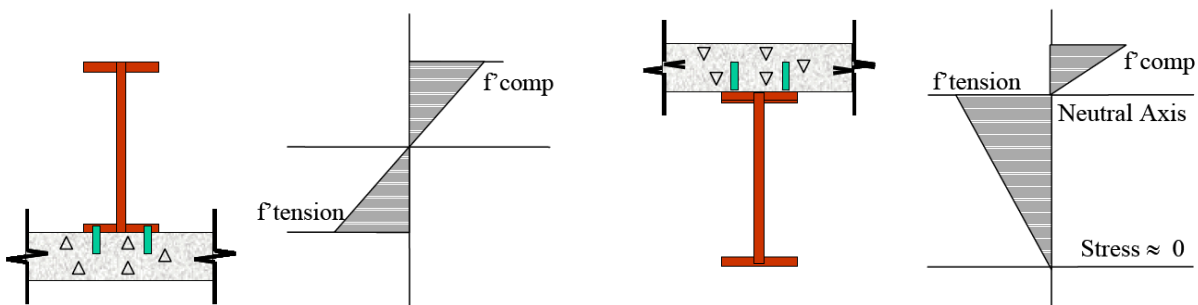
a) noncomposite section (during casting)   b) composite section (with only dead loads)

Figure 2-17. Stress distribution in Inverset™ deck unit (Fort Miller Company, Inc., 1998).

a) Casting upside down   b) Turning the unit

Figure 2-18. Inverset bridge deck system

2.4.2   Characteristics of the system

A typical unit consists of two beams made composite with a concrete deck. Each Inverset module is manufactured with relatively short overhangs to promote an efficient slab design and to facilitate load transfer. The units are connected by a series of field-installed steel diaphragms that distribute load to adjacent units (see Figure 2-19). Joints between units are filled with non-shrink grout and/or elastomeric concrete to prevent leakage.

The primary advantages to using the Inverset Bridge System are:

- Rapid construction: Construction can be completed within a few hours, under traffic conditions.

- Durability: The unit is cast under controlled conditions, and the densest concrete is at the surface.

- Design flexibility: The unit can be cast in a standard size or customized to fit any application.

- Easy handling: The units are designed to withstand handling and shipping operations. The units can be transported easily to the job site, picked up at any point, and even rolled into place.

- Cost effective: Time savings using this precast deck construction can result in overall cost effectiveness.

- Year-round installation: Construction operations can be scheduled all through the year, and the units may be installed even in cold winter months, day or night.

- Reduced superstructure depth: The use of an efficient system with shallow depths allows more clearance underneath the superstructure while maintaining the roadway profile.

- Minimal cracking: Prestressing minimizes cracking and chloride intrusion.

INVERSET™ BRIDGE SYSTEM DETAILS
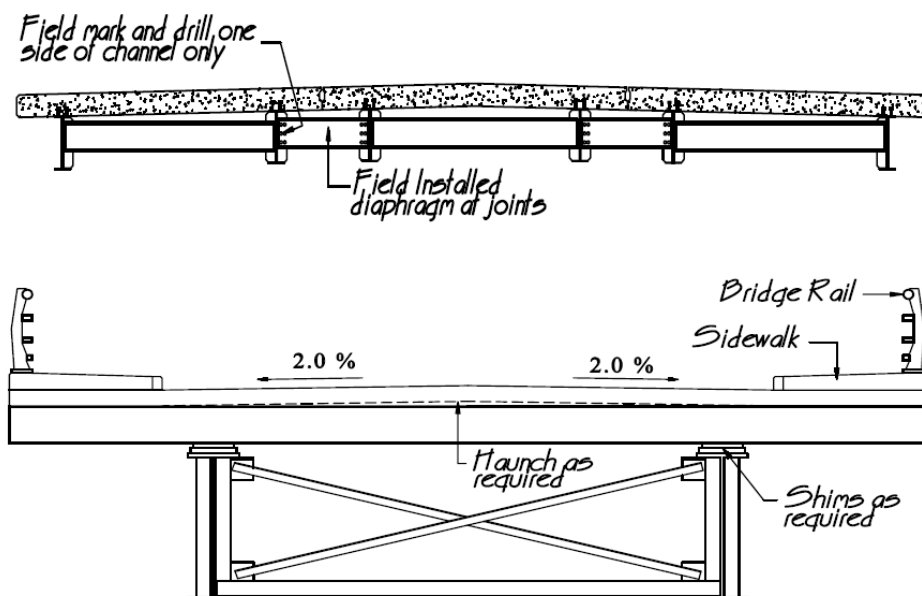
Figure 2-19. Inverset bridge system detail (NYDOT, 2010).

2.4.3   Bridge Application

The modular units provide flexibility and can be designed for a wide range of widths, lengths, and load requirements. Spans have been designed using these units to span in excess of 100 feet and 45º skew. The units can be designed and fabricated as full bridge span length units that are modular in width so that multiple units can be placed side by side to complete the full bridge width. Alternately, they can be designed and fabricated as full bridge width units that are modular in length so that multiple units can be placed end to end, in the longitudinal direction, on top of the span support members to complete the full bridge span. The units can be made composite (or non-composite) with the main members, typically longitudinal plate girders or trusses. Typical uses for transverse Inverset units are: long span deck trusses; long span through trusses; long girder spans; and curved decks supported by straight girders or trusses (NYDOT, 2010).

2.4.3.1   Transverse Inverset (Inverset II)

Inverset II is a bridge erection technique used for the construction of the San San River Bridge near Guabito, Panama (Grossman S. , 1994). The technique creates a pre-compressed composite steel and concrete deck that is free from aggregate segregation and is weather and traffic resistant. The bridge is 182 feet long and 28 feet wide. Deck segments are each 10 feet 1 inch wide and 28 feet long, and supported by two W14 x 22 steel beams. The thickness of the deck segments is 7 inches. Each of the 18 segments is cast upside down near the bridge. The main support for the single span bridge consists of two 7 foot 3 inch plate girders. These girders were assembled with their diaphragms at one abutment. They were then rolled across the river from one abutment to the other over two temporary supports 50 feet apart in the center of the span. With the girders supported on the temporary supports and the abutments, the deck segments were inverted and rolled into position along the top chords of the girders. With all deck segments in place, the girders were jacked up from the temporary supports until their ends were free from the abutments. The deck segments were then welded to the girders and the spaces between them were grouted to create a continuous roadway. The girders were then jacked down to seat the girders on the abutments and the temporary supports were removed. The dead weight of the structure thus pre-compressed the deck in two directions without the use of tendons (Grossman S. , 1994).

2.4.4   Conclusions

Virtually any bridge that can be built by conventional composite construction can be built with Inverset superstructure modules. Practical limitations on shipping restrict piece sizes to approximately 100 feet long and 75 tons. Shipping width should also be considered.

2.5 Full-depth precast deck (general discussion)

Many advantages to using a precast panel system for bridge decks exist. First, all of the deck panels can be manufactured at a concrete precasting facility prior to the start of construction at the bridge site. Thus, eliminates the time it would otherwise take to cast and cure a concrete deck and also minimizes the amount of cast-in-place material. Beside simplifies the construction process, the precast panels allow for a much faster bridge deck replacement or repair, which significantly reduces the duration of bridge closure and the corresponding disruptions of traffic. In most cases, the flow of traffic can be maintained on a portion of the bridge while precast panels are used to fix segments of the bridge deck in other locations. The precast system is an economical option due to the savings in required field labor and the reduced inconvenience of delays for bridge users. Finally, the precast system can be a practical solution for a variety of transportation infrastructure needs, including new bridge construction as well as bridge deck rehabilitation or replacement (Issa, Yousif, Issa, Kaspar, & and Khayyat, 1995).
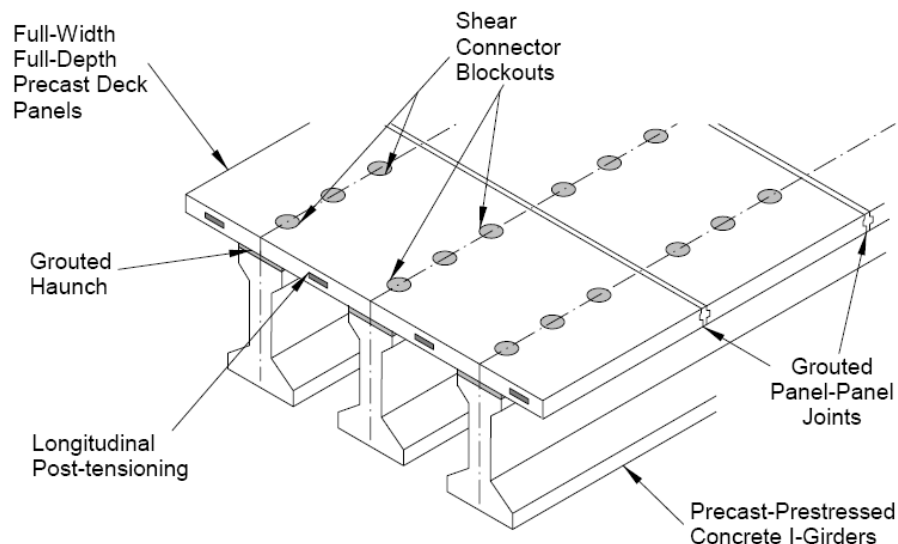
Figure 2-20. Precast Concrete Bridge Deck Panel System (Scholz, 2004).

2.5.1   Panel to Superstructure Connection

Since 1974, significant advances have been made in the construction of bridge decks built with full-depth precast concrete deck panels. Most of the bridges built during this period were made composite with the superstructure. This was achieved by extending steel shear studs or structural steel channels into the precast deck through prefabricated pockets. Shear pocket connections are the most commonly used connection between the full-depth panels and the girders. The spacing between pockets ranged from 18 in. to 24 in., and the number of studs per pocket ranged from 4 to 12 (Badie & Tadros, 2008).

a) Deck/superstructure connection details of the Delaware River bridge.   **b) Panel dimensions and cross section of the I-80 overpass project, Oakland, California.**
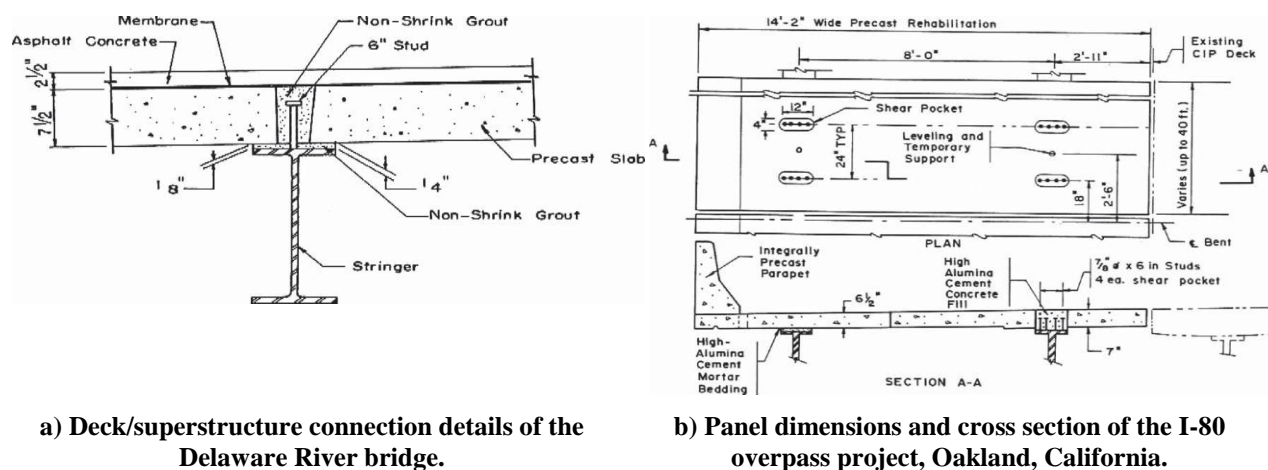
Figure 2-21. Example of panel to superstructure connection (Badie & Tadros, 2008).

As an alternative to steel shear studs, standard channel sections welded to the top flange of the stringer beam can be used. Some experimental study had showed that the channel welded sections performed well, thus was limited use because of the relatively high labor cost. On the same experimental bridge, a bolted connection was evaluated. In this connection, the panels were first placed using steel shims for leveling. The holes are drilled thought all the components (top flange of the steel girder, sleeves, and precast panels) and later high-strength bolts were fastened. Though, the bolts cannot be fully tensioned because of concerns the precast slab would break (Badie & Tadros, 2008).
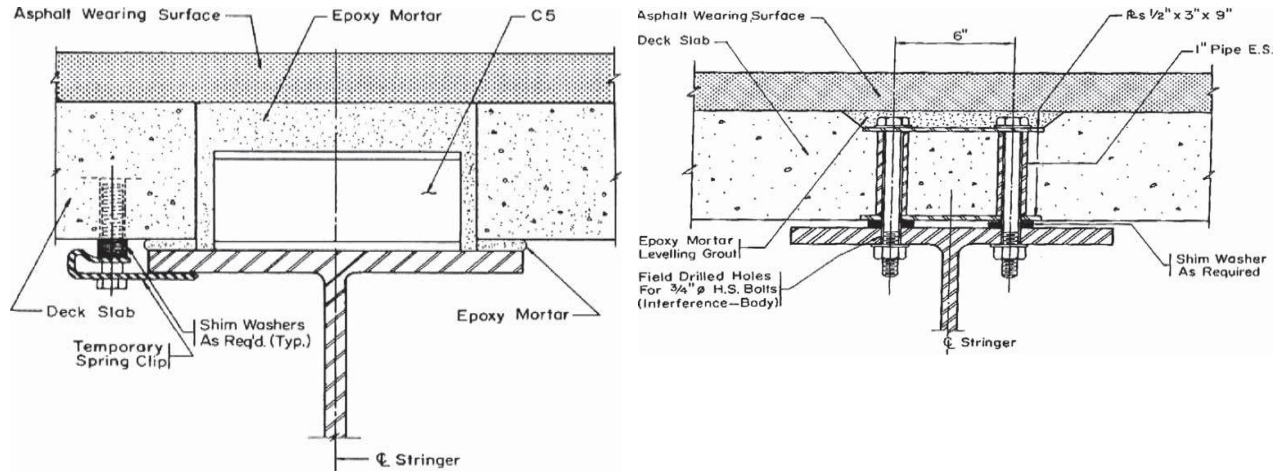
a) Welded channel section detail used in the New York Thruway experimental bridge.

b) Bolted detail used in the New York Thruway experimental bridge.

Figure 2-22. Example of alternative panel to superstructure connection (Badie & Tadros, 2008).

Differential camber among bridge girders and other fabrication variations can cause the bearing of the full-depth deck panels on the girders to be uneven (Hieber, Eberhard, Wacker, & Stanton, 2005). To alleviate this problem, leveling screws can be used to adjust the panel elevation. Two screws per panel were typically used at every girder-line. These screws should be designed to support the panel weight and expected construction loads. After the grout that filled the haunches and pockets gained strength, the screws were removed or were flame cut (Badie & Tadros, 2008).
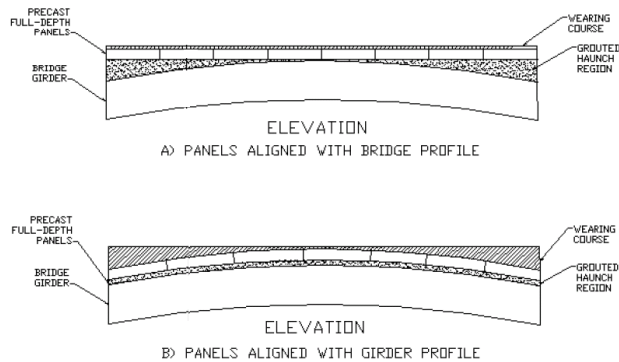
a) Methods of leveling full-depth panels to account for bridge profile
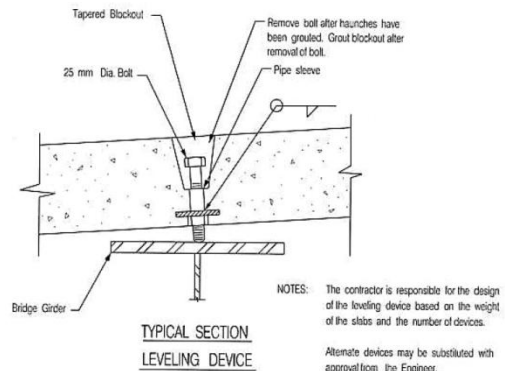
b) Leveling screw detail.

Figure 2-23. Method of leveling and leveling screw details (Hieber, Eberhard, Wacker, & Stanton, 2005)

2.5.2   Transverse Panel to Panel Connection

The transverse edges of the precast panels were usually provided with shear keys, which play an important role in the service performance of the finished deck. The shear key must be designed to protect adjacent panels from relative vertical movement and to transfer the traffic load from one panel to the next without failure of the panel to panel joint. Under traffic load, a panel to panel joint experiences two types of forces: (a) a vertical shear force that tries to break the bond between the panel and the grout filling the joint, and (b) a bending moment that puts the top half of the joint in compression and the bottom half in tension (Badie & Tadros, 2008). Two types of shear keys have typically been used with full-depth precast concrete panels:

- **Nongrouted match-cast shear key:** This type of shear key was used with longitudinal post-tensioning on the Bloomington Bridge in Indiana. Thin Neoprene sheets were installed between adjacent panels to avoid high stress concentrations. Although match casting can be achieved in a controlled fabrication environment, such as in a precast concrete plant, it was difficult to achieve a perfect match in the field as a result of construction tolerances and the necessary elevation adjustment of the panels. After 5 years of service, cracking and spalling was observed in the concrete at the panel joints, which eventually led to leakage problems at the joints (Badie & Tadros, 2008).
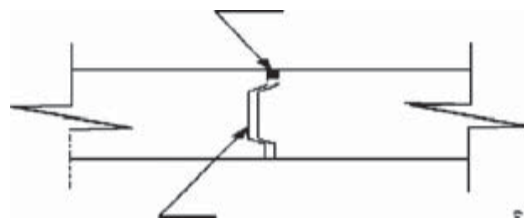
Figure 2-24. Nongrouted match-cast joint used in Bloomington Bridge in Indiana (Badie & Tadros, 2008).

- **Grouted female-to-female joints:** In this type of joint, grout was used to fill the joint between adjacent panels. Inclined surfaces were provided in the shear key detail to enhance the vertical shear strength of the joint. Vertical shear forces applied at the joint

were thus resisted by bearing and bond between the grout and the panel. The shear key was recessed at the top to create a relatively wide gap that allowed casting the grout in the joint (Badie & Tadros, 2008).

a. Trapezoidal-shape shear key detail. **b. Semi-circle shear key detail.**

c. V-Shape shear key detail **d. Rectangular shear key detail**
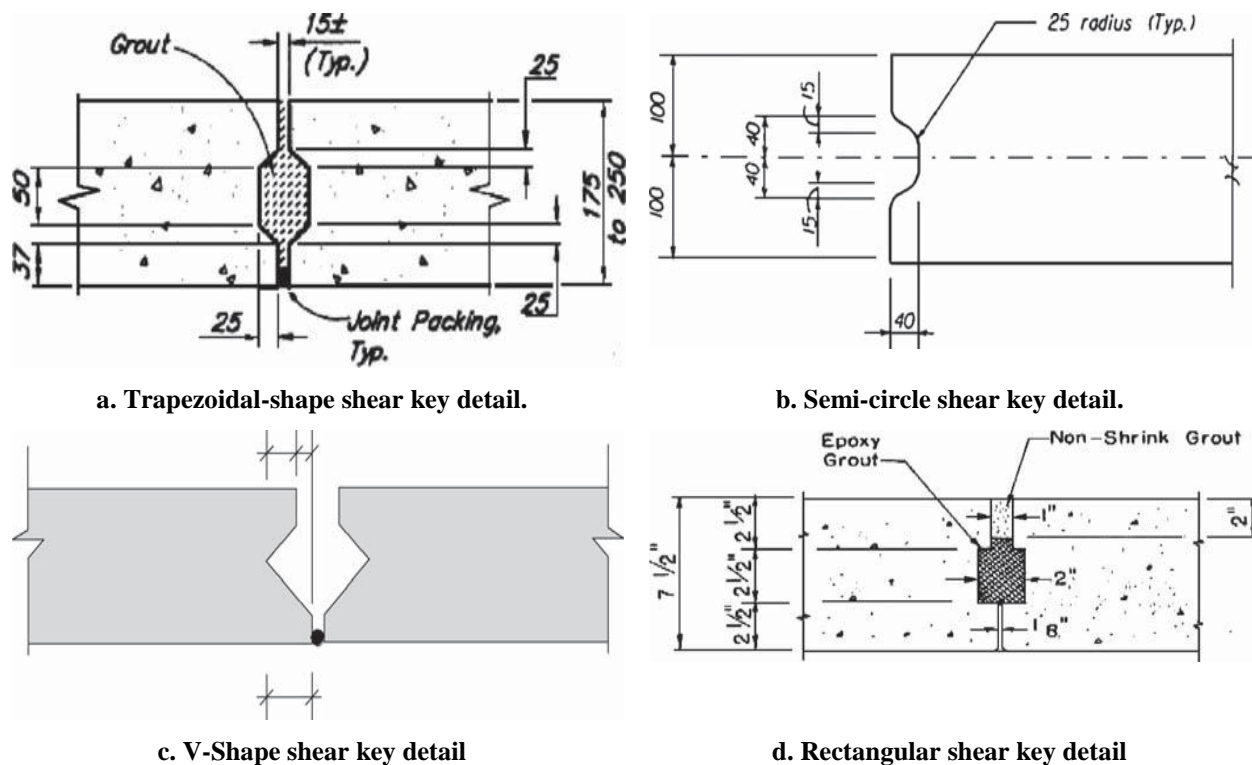
Figure 2-25. Various grouted female-to-female joints details. (Badie & Tadros, 2008).

When grouted joints are considered, a form must be provided at the bottom surface of the panels to prevent the grout from leaking during casting. Two methods of forming have been used (Badie & Tadros, 2008).

- **Polyethylene backer rods:** The polyethylene backer rods are placed in the tight space between panels at the bottom of the joint. The detail does not require any construction work to be done from below, however it has been reported that, as a result of fabrication and construction tolerances, joints in some cases ended up partially full which can cause high stress concentrations.
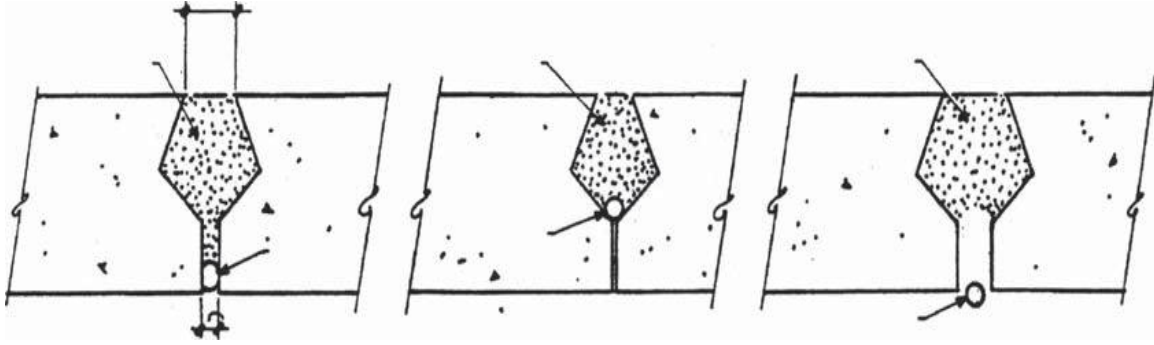
Figure 2-26. Detail of foam packing rods misaligned as a result of panel misalignment (Nottingham, 1996).

- **Wood forming:** Wood forming is installed from under the panel. In this detail, a gap of 1 to 3 in. is maintained between adjacent panels. The forms are hung from the top surface of the precast panels using threaded rods and nuts. This detail usually results in a full-height grouted joint with excellent performance (Issa, Yousif, Issa, Kaspar, & and Khayyat, 1995) & (Nottingham, 1996). This technique allows the joint to be completely filled with grout, but it requires access from below for form erection and removal. The bond between the grout and the shear key surface can be significantly enhanced by roughening the surface of the shear key (Badie & Tadros, 2008).
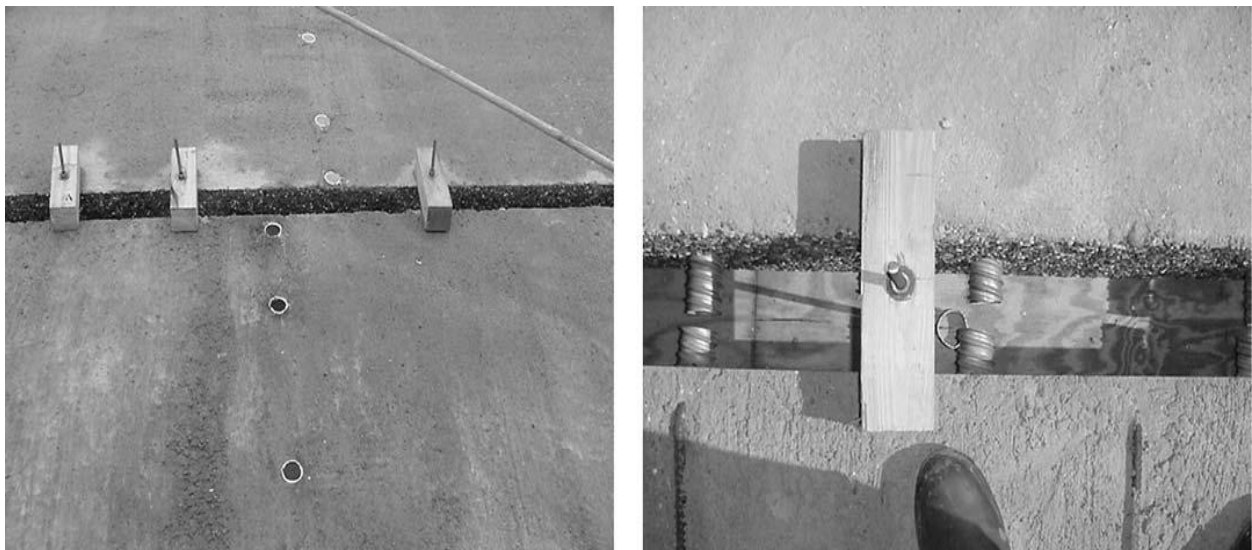
Figure 2-27. Wood forming of the panel-to-panel joint used in the tied-arch bridges, TX (Badie & Tadros, 2008).

2.5.3   Longitudinal Reinforcement

Longitudinal reinforcement in deck slabs is used to distribute the concentrated live load in the longitudinal direction. It is also used to resist the negative bending moment due to superimposed dead and live loads at the intermediate supports of continuous span bridges. For deck slabs made with full-depth precast panels, splicing this reinforcement at the transverse joint between panels is a challenge for design engineers for the following reasons:

- The panels are relatively narrow (usually 8 to 10 ft). Therefore, a wide concrete closure joint (2 to 3 ft) would be needed to splice the reinforcement. Thus increasing wood forming under the panels and an extended period of time for curing (Badie & Tadros, 2008).

- The longitudinal reinforcement is spliced at the transverse grouted joint between panels that is considered the weakest link in the system.

- Splicing the longitudinal reinforcement requires a high level of quality control during fabrication to guarantee that the spliced bars will match within a very small tolerance.

- Splicing the longitudinal reinforcement requires creating pockets and/or modifying the side form of the panels, which increases the fabrication cost.

As a result, a few highway agencies, such as the Alaska DOT and the New Hampshire DOT, have opted not to splice the longitudinal reinforcement on simply supported span bridges. However, most highway agencies prefer to provide some type of reinforcement across the transverse joints. Thus, various methods are available such as lap splice, U-shaped pin bar, spiral confinement, and longitudinal post-tensioning (Badie & Tadros, 2008).
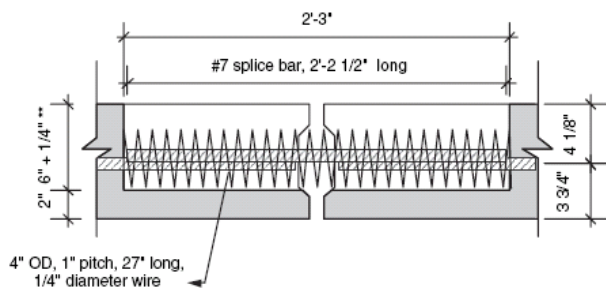
a) Panel-to-panel connection using spiral confinement.
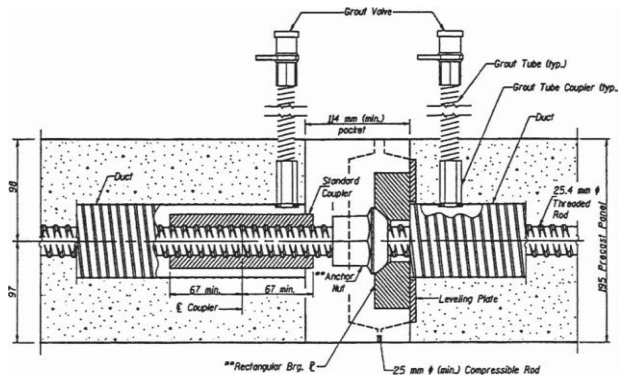
b) Posttensioning detail used on Bridge-4 constructed on Route 75, Sangamon County, Illinois.

Figure 2-28. Methods of longitudinal reinforcement splice (Badie & Tadros, 2008).

Longitudinal post-tensioning has been used on the majority of bridges built with full-depth precast panels during the past 30 years.   In recent applications, longitudinal post-tensioning has been incorporated to place the joint in compression which helps to prevent cracking due to applied loads or shrinkage of the concrete, and helps prevent subsequent leakage through the joint. The amount of post-tensioning stress on the concrete after seating losses used in bridge decks ranges from 150 to 450 psi (Issa, Yousif, Issa, Kaspar, & Khayyat, 1998) & (1995).
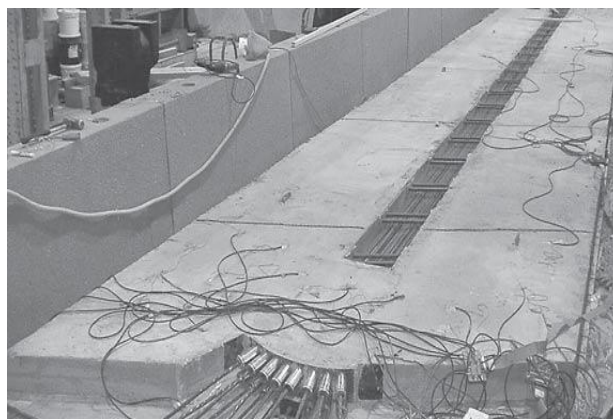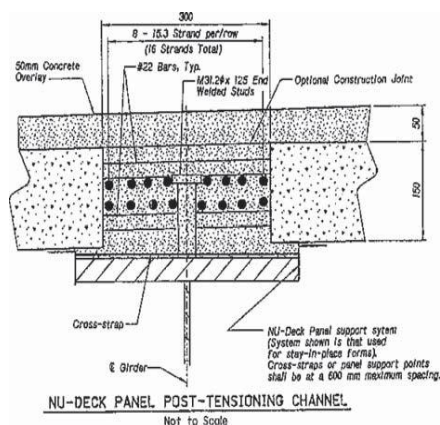
Figure 2-29. Longitudinal post-tensioning concentrated at girder lines used on the Skyline Drive bridge, Omaha, NE (Badie & Tadros, 2008).

2.5.4   Conclusions

The long-term performance of full-depth panels is still uncertain. The majority of the decks on which observations have been documented are relatively young. Supporters of full-depth deck panels also believe that the durability problems have been caused by inadequate details that were used in early applications (Issa, Yousif, Issa, Kaspar, & and Khayyat, 1995).

Typically, headed steel studs are used to compositely connect the girder with the deck. Limited amount of research regarding the panel to concrete girder connection has been reported.

Female-to-female joints (i.e., shear key details) filled with cast-in-place nonshrink grout provide superior performance compared with match-cast, male-to-female joints. The design criteria for a successful joint detail include no cracks under repeated service loads and no water leakage (Badie & Tadros, 2008).

Although longitudinal post-tensioning, which puts the joint in compression and secures it against leakage, increases the cost of the deck system, it was used with the majority of full-depth precast concrete deck panel systems. U-shaped pin bars and/or lap splice details require a wide joint and/or a thick precast panel to provide for the required lap splice length and concrete cover (Badie & Tadros, 2008).

2.6 Findings of literature review

The findings from the literature review are the following:

- Overall, it was observed that bridge construction using precast panel is the method of choice. Since it offers many advantages such as reduction of construction time, labor, cast-in-place elements, better concrete quality, etc.

- It was noted that the weak spot in bridge using precast panel is the panel-to-panel transverse connection. Although, the female-to-female joints (i.e., shear key details) filled with cast-in-place nonshrink grout is the detail of choice.

- Different solution has been given to solve the panel-to-panel connection problem such as reinforcement splice, U-shape bar, spiral, and post-tensioning. However, it seems unanimous that applying compressive force to alleviate the tensile stress is the best approach.

- Different techniques are available to induced compressive force in the deck. Self-stressing, piano method, inverset, post-tensioning.

- Nagai et al. (2000) had reported a real application of the piano method, which is similar to the self-stressing method reported by Yakel et al. (2007). They emphasized the need for time-dependent analysis to predict the creep and shrinkage effect in the induced compressive force.

- The post-tensioning is reported in the literature as an expensive method to apply compressive stress in the deck. Also, the prestressing strands as susceptible to corrosion which could aggravate to future loss of prestressing force.

- The self-stressing method seems to be a cheaper and a viable way to precompress the deck without the use of strands. Thus corrosion problems and prestressing lost are completely eliminated. Yakel et al. (2007) had shown the application of the method for cast-in-place deck with good agreements among the experimental and analytical prediction.

Therefore, the research will focus on the proof-of-concept of self-stressing method applied to bridges built with precast deck panels.

Chapter 3

Test Specimen and Procedures

This chapter described the test specimen and procedures considered for the experimental investigation. Method of constructions used to build the test specimen is also described. The final geometry of specimen, dimensions of the main components such as girder and deck are presented. Detailed drawings of the slab reinforcement, shear key and closure pour is reported. The different material used is characterized by ASTM standard tests. The instrumentation components considered to monitor the specimen is also presented. Finally, the loading procedures are discussed.

3.1 System Description

The test specimen was built with two I-shape steel girders over three equally spaced supports. Full-depth concrete precast panels were placed over the girders and made composite with the girder through shear studs.

The self-stress system was accomplished firstly by setting the girders over the supports and shimmed upward the internal support above the elevation of the outer supports. As the precast panels are placed over the girder, the panel-to-panel connections were accomplished by using high-strength epoxy spread over the match-cast shear key. Once all panels are set in place, the block-out shear pockets and the center panel-to-panel connection were filled with non-shrink grout. After allowing the grout to harden, the shim was released. This creates compressive force (self-stressing) in the specimen. The creep and shrinkage in the deck was monitored for two

months to evaluate and further estimate the long-term prestressing lost. Finally, an ultimate load testing was performed to determine the failure mode.

Figure 3-1 shows a 3D sketch of the test specimen.
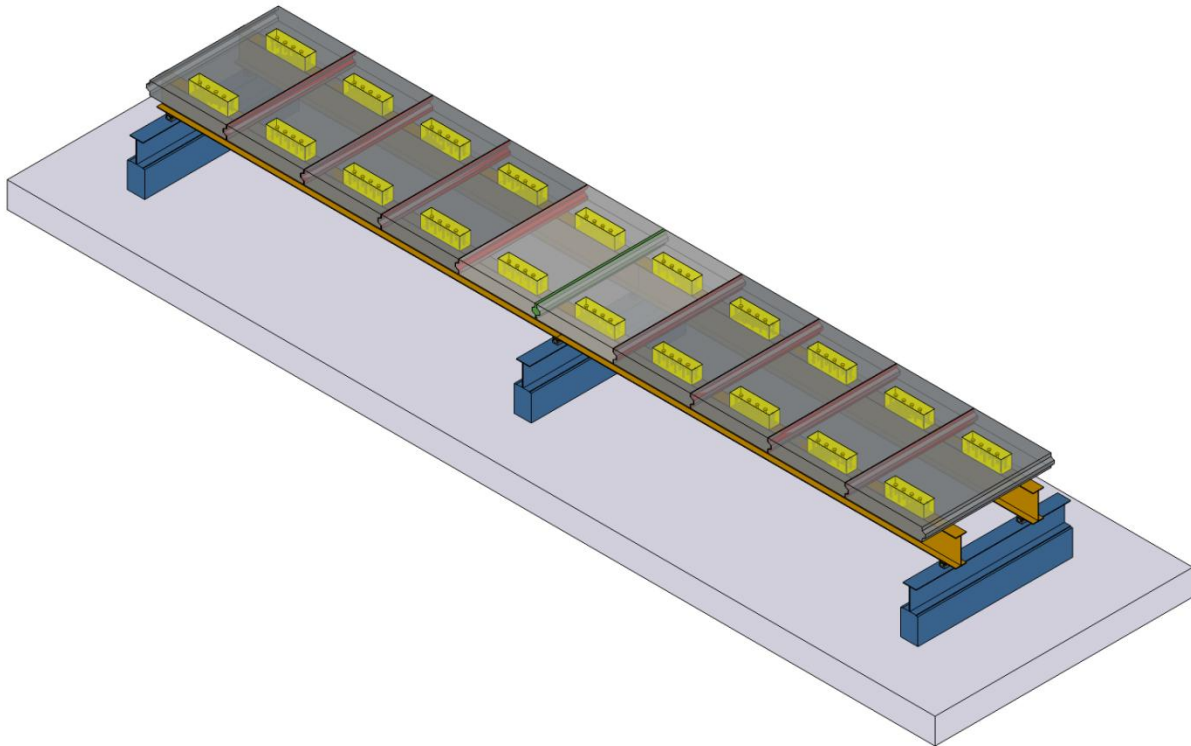
Figure 3-1. 3D view of self-stress system specimen

3.2 Test Specimen Components

A small-scale test specimen was considered to investigate the parameter that may affect the performance of the self-stressing system. Dimensions, geometry, and detailing are described as follows. Figure 3-2 and show the longitudinal, top view and cross-sectional view of the test specimen. The main components are identify and the primarily dimensions are shown.

Longitudinal view

Top view

Cross-section view
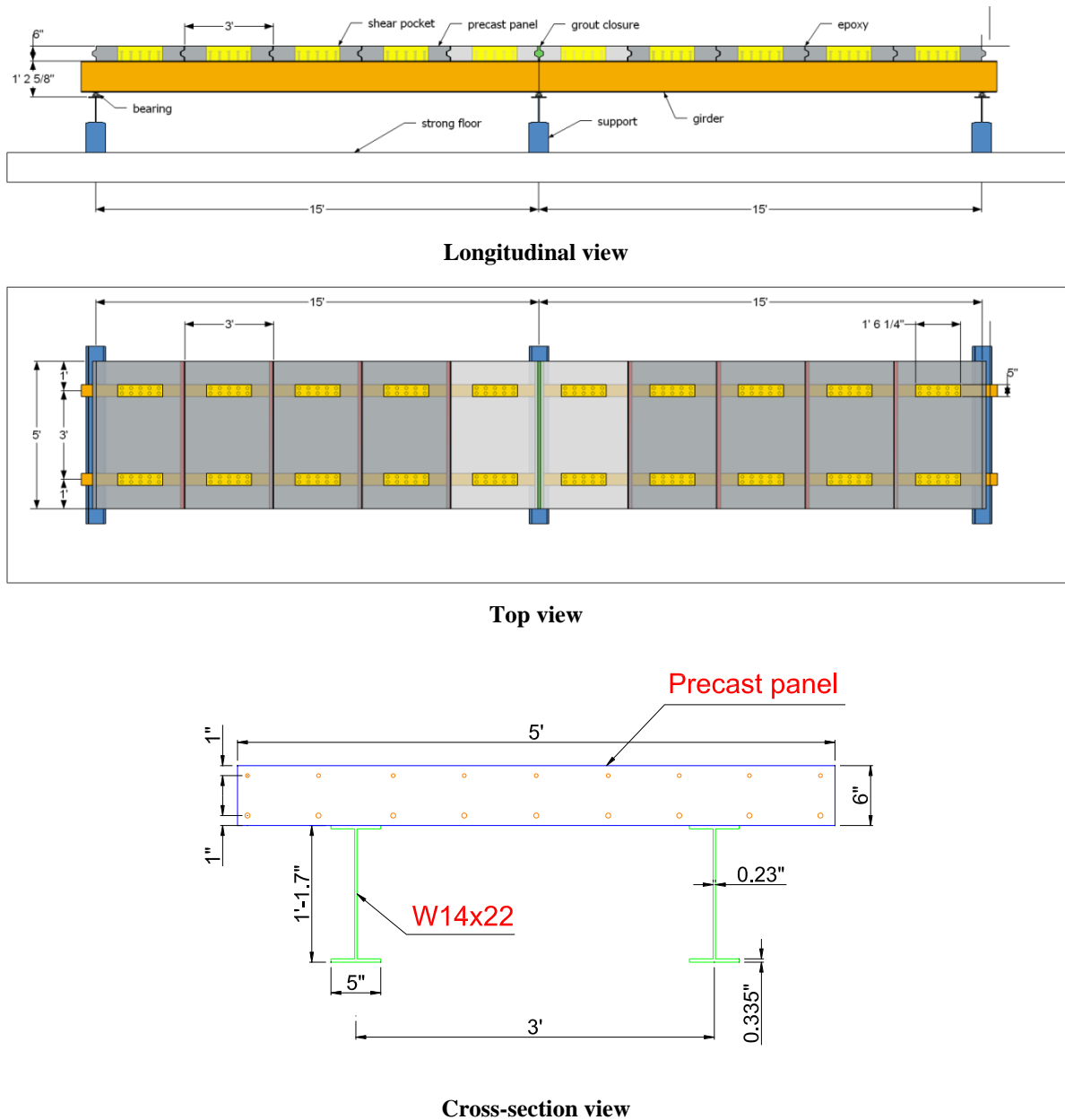
Figure 3-2. Test specimen primarily dimensions and views.

The main components needed to construct the test specimen are discussed as follows.

3.2.1   Steel components

The girders and all steel components were provided by Steel Works, Inc in which Mr.

Ron Ediger was the primarily contact. Table 3.1 describes the list of material ordered.

Table 3.1. List of material ordered from Steel Works, Inc.

Quantity	Description	Comments
2	I-beam profile W14x22, 31 ft long	
5	Channel beam profile C12x25	Grade 36
10	Stiffener plates 13"x3.5", 3/8" thickness	With 3 holes
10	Stiffener plates 13"x2.5", 3/8" thickness	
200	Shear studs, 5/8" diameter, 4" height	Grade 60
36	Heavy hex structural bolts, washers, knots	ASTM A325
16	Channels beam profile C10x15.3, 10" long	Grade 36
16	Plates 2"x7", 1/4" thickness (front)	
8	Plates 9"x7", 1/4" thickness (back)	

Figure 3-3 show the detailed drawing provided for fabrication.
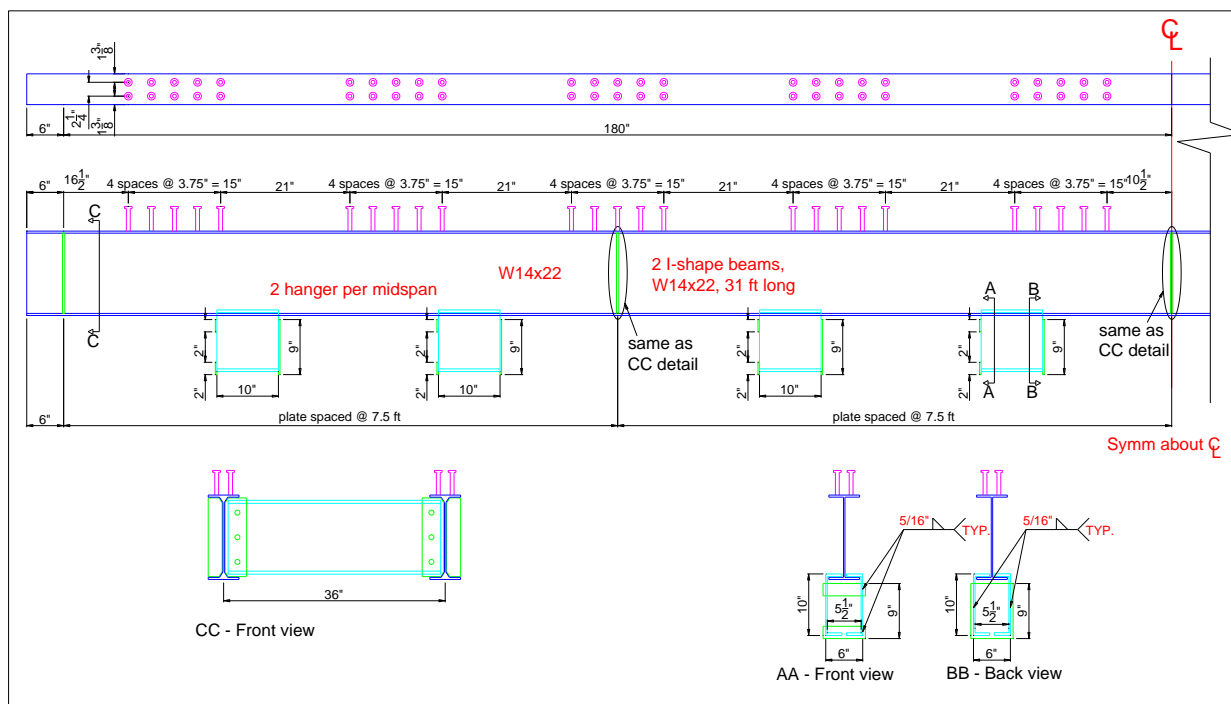
a) Girder and bracing details
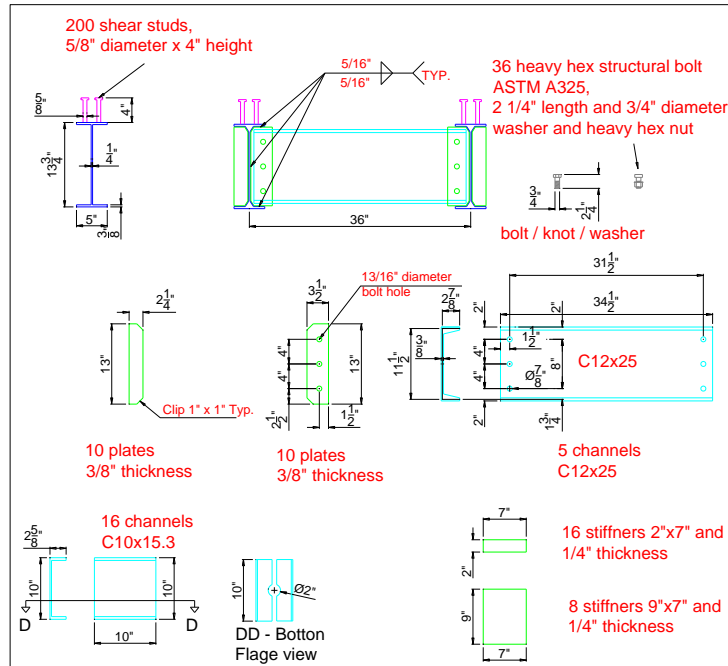
b) Additional details

Figure 3-3. Steel work detailed drawings

Figure 3-4 shows the final product being delivered and later assembled in the structural laboratory.

| Bottom flange view | Top flange view |

Final assembling of girders and bracing system.

Ballast hanger

Shear studs

Figure 3-4. Girders, bracing system and addition steel components.

3.2.2 Concrete components

The precast concrete panels were fabricated by Concrete Industries Inc. Prior submitting the final drawing for fabrication, couple meets were held with Mr. Mark Lafferty (company's COO). During the meetings, it was discussed the best approach and detailing for the fabrication. Mr. Lafferty had provided practical comments and recommendations which were later considered during the design and detailing of the precast panels. One of the concerns was whether a reduced thickness (since the specimen was a reduced scale of a real bridge) would be possible to be fabricated. Another concern was the shear key detailing and dimensions. Also, practical question on how to placing the panels over the girder and the material it should be used for the panel-to-panel connections and for the shear studs blockout and closure region.

Finally, the simplest and considered best approach was selected. Table 3.2 summarizes some of the final details and dimensions.

Table 3.2. List of material ordered from Concrete Industries

Quantity	Description	Comments
8	Precast panels 5'x3', 6" thick	See drawing
2	Precast panels 5'x2'11.5", 6" thick	See drawing
250 lbs	Steel reinforcement #3	ASTM A615
450 lbs	Steel reinforcement #4	ASTM A615
25 bag	Sikagrout 212 (nonshrinkage grout) 25lbs	
3 gal	Sikadur 31 (two-part epoxy)	
3 yd^3	High strength concrete	f'$_c$ = 7 ksi

Figure 3-5 show the detailed drawing provided for fabrication.
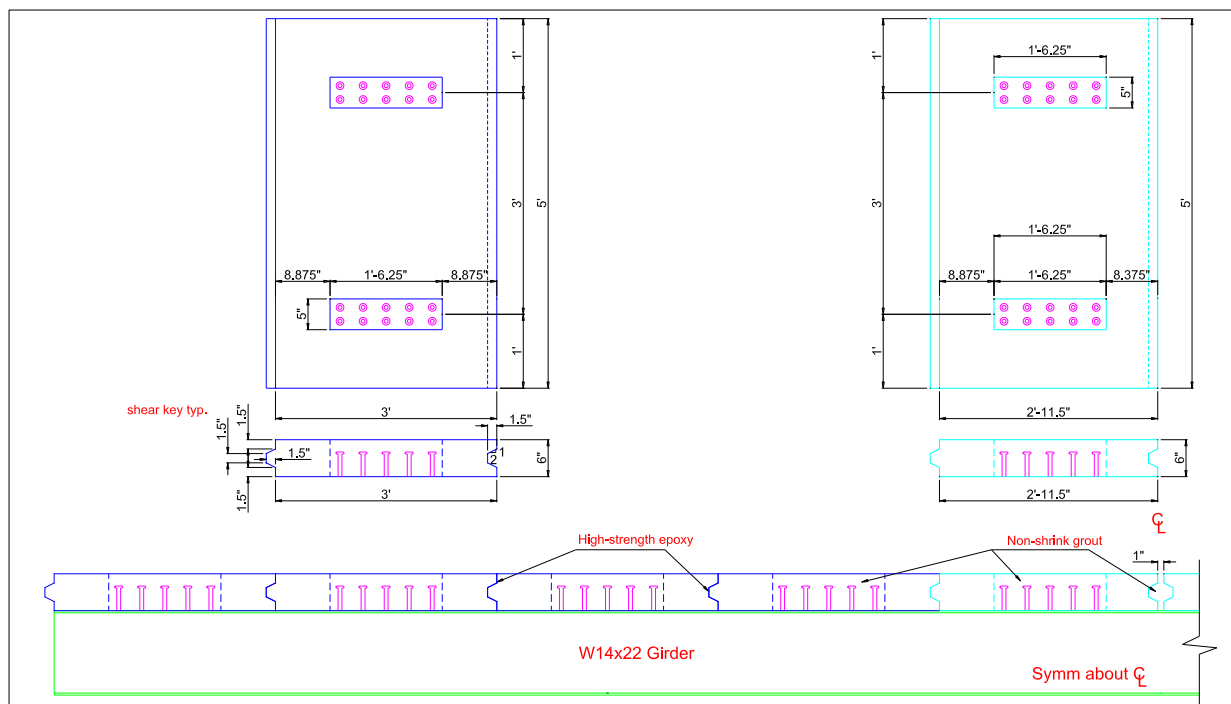
a) Precast panels overall dimensions
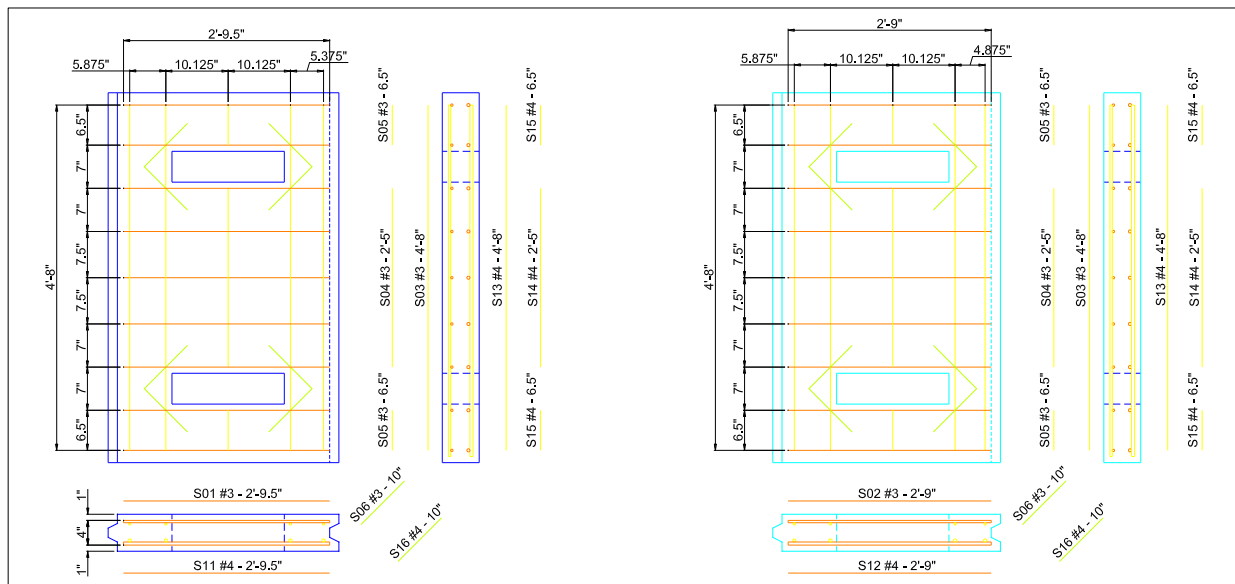
b) Steel reinforcement detailing

Figure 3-5. Precast concrete panels detailed drawings

In order to obtain the match casting connections between each precast panel, the casting sequence shown in Figure 3-6 was considered. At first panels A, C and E were poured. Three days later the forms were removed. The previously casted and hardened panels were used as formwork for the remaining panels B and D. One day later, panels B and D were released and all five panels were moved to the yard to cure. The same procedure was used to cast the other five precast panels. The information regarding the casting sequence is important since during the placement of precast panels over the girder, the same sequence was kept in order to maintain a "perfect" connection between each panel.
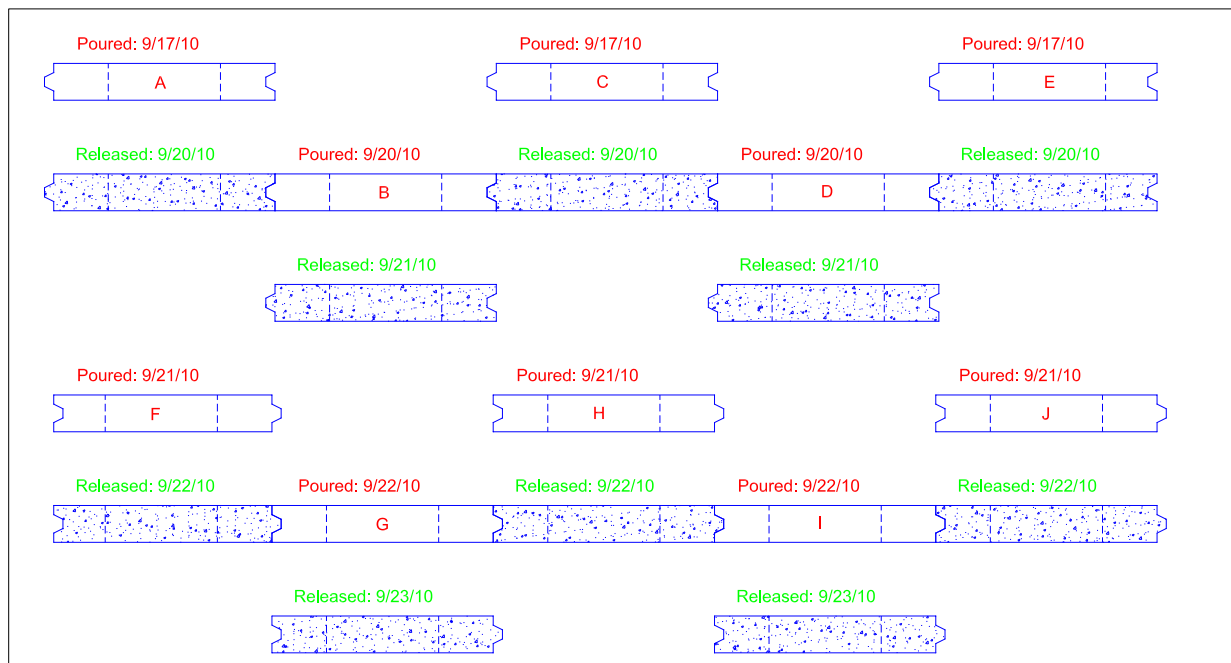
Figure 3-6. Pouring sequence of precast concrete panels

Figure 3-7 shows the epoxy and grout used. The grout and epoxy were mixed based on instructions provided in the Sika product catalog(SIKA, 2010).

SikaGrout 212 (nonshrinkage grout)   **SikaDur 31 (high-strength epoxy)**

Figure 3-7. Grout and epoxy used.

Figure 3-8 show the final product being delivered and some close-up of the full-depth precast concrete deck panels.

Precast panel delivering

Match cast detail

Precast panels organized in sequence

Panel I damaged

Panel E damaged

Figure 3-8. Precast concrete deck panels.

3.3   Construction of Test Specimen

The test specimen was built in the structural laboratory at the University of Nebraska-Lincoln. The reduced scale bridge had 3 supports equally spaced by 15 feet. The test specimen represents a ¼ scaled model of a prototype structure. Since the simulation largely depends on self-weight of the structure, ballast load was used to indirectly increase weight of the specimen. More explanations regarding the ballast load is provided in Section 3.6.1. Stacks of five train wheels were used as ballast. The each stack was weighted and moved to the basement. After

aligning the stack with the hole, high-strength rod was lowered and the stack was hanged in place. This process was repeated 15 times.

| Preparation of 5 train wheels stacks | Stacks hanging in the basement |

Figure 3-9. Stacks of train wheels used as ballast load.

Gypsum cement (hydro-stone) was used under each supporting beam to level it and prevent from moving. Stiffeners were welded to the supporting beams at the alignment of bearing to strengthening the supporting beams. Two rocking bearing were placed over each support (total of six) and tack-welded to prevent from moving. The end bearings had a sheet of 1/8 inch of Polytetrafluoroethylene (PTFE) to allow the bridge to move longitudinally during test, i.e., these bearing were roller type and the two internal bearings were fixed bearings.

| Supporting beam leveled with hydro-stone | End bearings with sliding surface |

Figure 3-10. Supporting beam and bearings details.

With the supporting elements ready in place, the girders assembling were initiated. The two girders were made with grade 50 structural steel. The rolled I-shaped beams with profile W14x22 had a total length of 31 ft. Stiffeners were welded to the girder at five different locations. At the same locations, C-shaped beams profile C12x25 were bolted to each girder stiffeners in order to bracing the girder laterally. Later, whole system was placed over the bearings with the help of laboratory's crane.

Assemble of girders and bracing system   **Girder placed over bearing/supporting beams**

Figure 3-11. Girder assemble and final placement of supporting elements

The installation of instrumentation needed to monitor the bridge responses was initiated at this stage. Linear strain gauges and potentiometer were the two type used at this time. In the meantime, 10 precast concrete panels were delivered to the laboratory. The precast concrete panels measures 3 ft long, 5 ft wide, 6 in tall. Each panel had a label with the casting date. This information is very important since all panels were made with match-cast shear key connection. Hence during the unloading process, the sequence of casting was kept as they had been made.

| **Delivery of 10 precast panels** | **Precast panel being placed on sequence** |

Figure 3-12. Delivery and unloading of precast panels.

The first step to introduce the self-stressing method to the specimen starts with the lifting of intermediate support to a predetermined height. Two pancake jacks were placed under the central beam to shim the girder 1 (one) inch. Metal sheet were used to temporarily hold the shim. Prior to shim the girders, calculations were made to determine whether or not the girder ends would be lifted. Based on the approximated analysis, it was estimated that that only end ballast close to the end supports would need to be dropped in order to avoid lifting (total of 4 ballasts, 2 on each end). In a real construction, the lifting would be avoided by anchoring the ends to the abutments. Since, the estimation made considered an average ballast weight and only a simplified beam (no consideration of the 3-dimensional response), after shim the girder 1 inch, it was noted that only one end was lifted. At this point, decision was made to drop 4 more ballast in order to completely remove the lifting. Appendix D provides the calculations.

| Pancake jacks used to shim the system | Central support shimmed 1.0 in. |

Figure 3-13. During and after shim up the girders

During the placement of precast panels, Mr. Jim Kaiser (Construction Services Manager, of Concrete Industries, Inc.) personally came to oversee the process. The placement of precast panels started from the ends towards the middle support. Each panel was simulated put in place so that one could anticipate any issues during its final placement. High-strength epoxy mixed and applied to match-cast shear key from panel already set in place. Further, the next panel was placed and pushed against each other to eliminate any voided between the panels. This process was repeated until all panels were placed. It was allowed 1 day for the epoxy to harden.

| Placing precast panels | Epoxy matching cast shear key |

Figure 3-14. Placement of precast concrete panels.

After the epoxy had harden, the grout was poured into the shear studs blockouts and the closure region between two central panels. A power-drill and buckets were used to mix the grout material with a predefined water amount recommended by Sika's catalog (SIKA, 2010). The grout was had a fluid like consistence so no vibration was applied. A total of 4 small grout cylinder samples were casted and later tested to determine the compressive strength. Also, it was used plastic sheet and wet burlap to cover the exposed surface in order to avoid rapid lost of moisture. It was allowed 14 days for grout to harden and 2 samples were tested to determine the strength.

Grouting shear studs blockout   **Grouting closure region**

Figure 3-15. Grouting shear studs blockout and closure region at interior support.

Further in the test specimen construction, surface strain gauges were installed on the deck surface to measure the concrete deformation. In addition, demountable mechanical strain gauges (DEMEC) were installed to measure the strain through the deck thickness. The initial reading was taken and the shim was removed to induce the compressive force in the system. The maximum amount of compressive stress applied was 2.3 ksi at the interior support region. This value matches with initial estimations. At this point, the long-term monitoring, which last for 63 days, was initiated in order to observe the strains changes in both concrete and steel components.

Removing shim   **Monitoring concrete creep**

Figure 3-16. Removing shim and monitoring specimen for concrete creep.

Throughout the extended monitoring, it was observed the strains development in the specimen. It was observed after 63 days that the strains were not change much so decision was made to stop the monitoring and start with the ultimate load test. The ultimate load conducted to determine whether or not the self-stressing method would alter the maximum capacity of the system. Also, the test would provide in-depth information and better understating of the critical section of the bridge such the mid-span (maximum positive moment) and interior support (maximum negative moment).
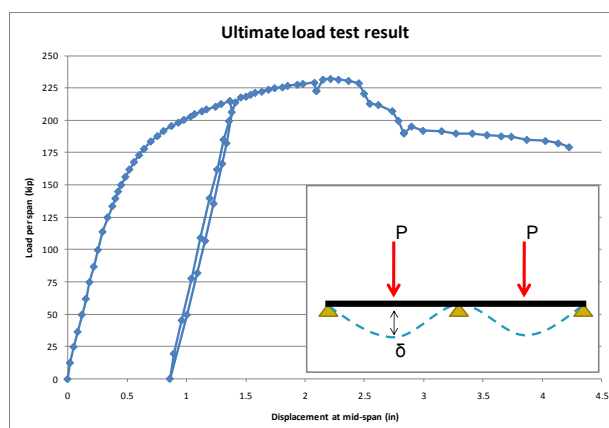
Ultimate test setup   **Load-displacement curve**

Figure 3-17. Ultimate test setup and load-displacement curve.

Finally observations regarding the failure models of self-stressing system were documented. Based on the test conducted, self-stressing method guidelines were developed to aid the dissemination of the method in the bridge industry.

Yield of bottom flange and concrete crushing at load point section

Web/flange buckling and large crack width over center support section

Figure 3-18. Failure mode observations.

3.4 Instrumentation

This section discusses briefly the equipment and instrumentations used to monitor the test specimen.

3.4.1.1 Data Acquisition System

Automated data acquisition MEGADAC system was used for monitoring the specimen. Strains in the SS system were monitored through the use of shorter (steel) and longer (concrete) surface strain gauges. These gages were wired to the MEGADAC 3407DC data acquisition system, developed by Optim Electronics (see Figure 3-19). The potentiometers which are used to measure deflections in the SS system were also wired to the data acquisition system. An external computer was connected to the MEGADAC to gather and analysis the data while running the test.
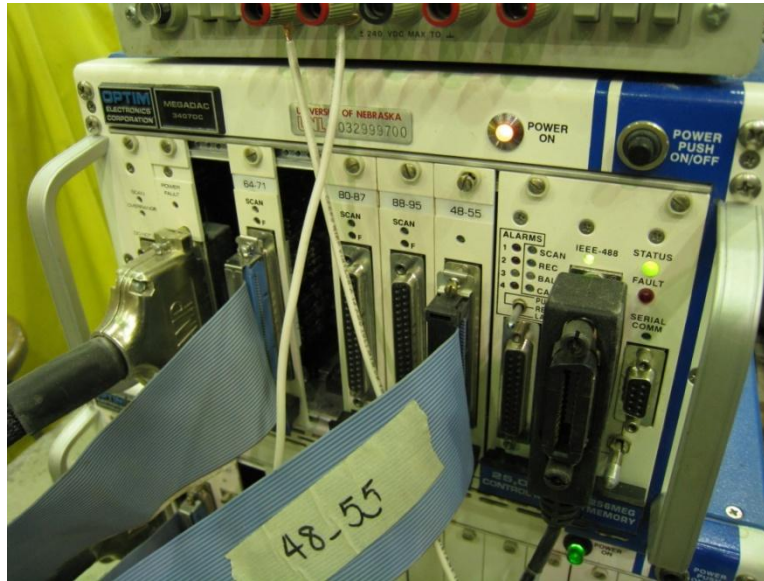
Figure 3-19. MEGADAC Data Acquisition System.

Three different gauge types were used to monitor the response of test specimen. These gauges are as follows: steel strain gauges, concrete surface gauges, and linear potentiometers. Wires ran from each of the gauges to the monitoring station positioned at a safe distance away from the test specimen. At the monitoring station the wires were connected to module containing 8 inputs channels. These modules are subsequently connected to the MEGADAC system for data acquisition.
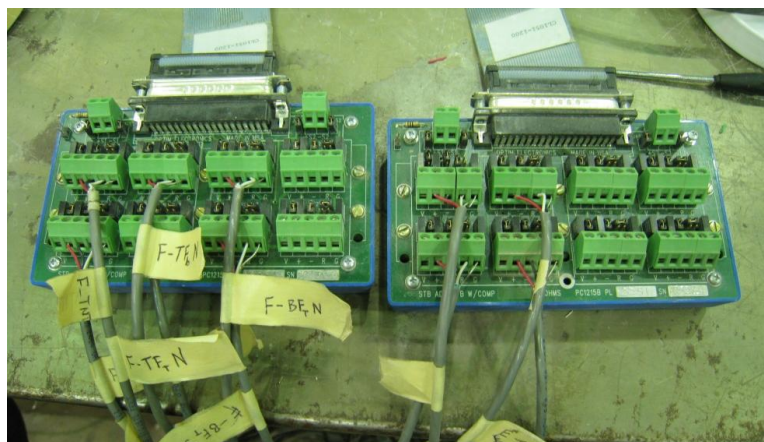
Figure 3-20. Data collection modules.

3.4.1.2   Strain Gauges

General purpose linear strain gauges were used on the steel girder surface. Due to doubly symmetry of the test specimen, a large number of gages were used in some location than the others. A total of 25 strain gauges identical to Figure 3-21 (a) were used in the entire specimen.

Concrete surface gauges were used on the top surface of the composite precast deck to evaluate the strains. Figure 3-21 (b) shows the concrete surface gages used during testing. Ten surface gages were installed only after the concrete precast panels were placed over the girder and the shear studs blockouts were grouted.
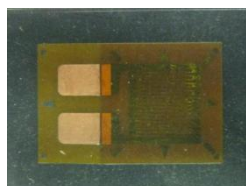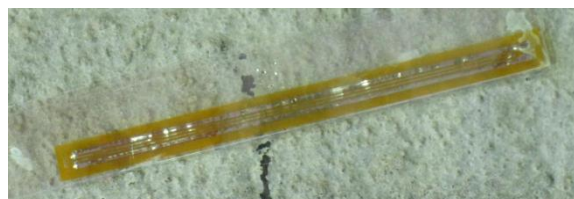
| a) Steel gauges | b) Concrete gauges |

Figure 3-21. Steel and concrete strain gauges.

3.4.1.3   Potentiometer

The deflection was measured though potentiometer (pot) located throughout the entire test specimen. The potentiometers were attached to a wooden base, which was attached to the floor in order to eliminate any movement.

| a) Potentiometer on the base floor | b) String line from the bottom of girder |

Figure 3-22. Potentiometer

3.4.2   Monitored Sections and Labels

The location in which the instruments previously described (strain gauges and potentiometers) were installed is discussed in this section. The test specimen was divided into 7 sections which was assigned a capital letter from A to G. In order to minimize the amount of instruments thus reducing the redundancy of the results and therefore optimized distribution of instruments, the bridge symmetry was considered. Since the bridge presented double symmetry, i.e. transversal symmetry due to 2 identical girders side by side and longitudinal symmetry based on the equal span length, some locations were heavily instrumented more than the others. Figure 3-23 shows scheme adopted.
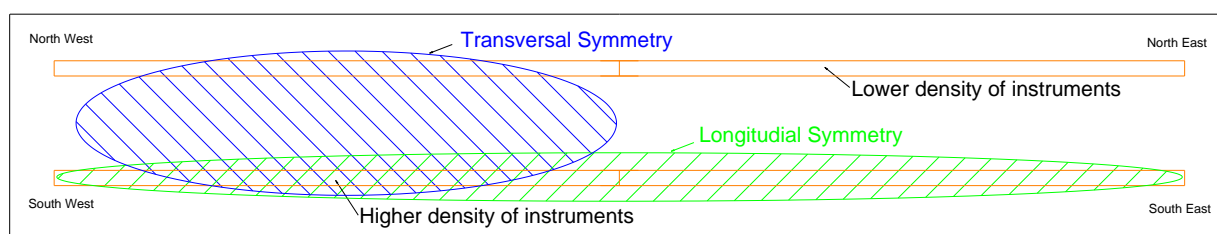
Figure 3-23. Distribution of instrumentation.

Beside the symmetry, some location such as maximum positive moment (mid-span) and maximum negative moment (interior support) were heavily instrumented since those locations were considered critical and possibly would dictate the bridge design.

Figure 3-24 shows the section location. The section of interesting are: 1/4 west span (A), west mid-span (B), 3/4 west span (C), in
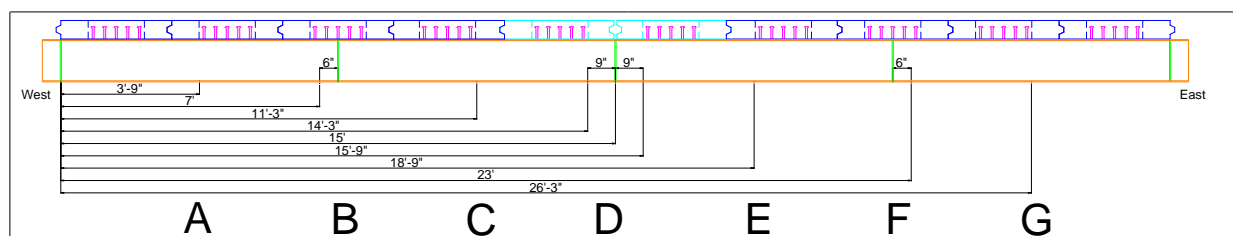
Figure 3-24. Section letter assigned and distances.

Figure 3-25 shows the assigned label for the strain gauges installed at the girders. The labeling assigned was based on the section location (A-G), which girder (north or south girder), and location at the girder (top flange, web, or bottom flange). A total o 25 strain gauges were installed.
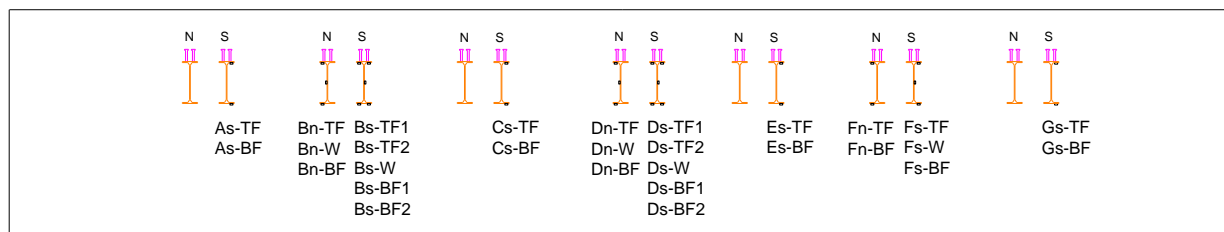
Figure 3-25. Strain gauges installed on the girders.

Figure 3-26 shows the location and the labels assigned for the concrete stain gauges. The gauges were installed on the surface of the precast panels. The labeling refers to the section location (A-G), which girder (north or south), the letter "C" (concrete) and a number (1-10). A total of 10 concrete gauges were installed. In addition, 9 demountable mechanical strain gauges, known as DEMEC points, were installed.

Concrete strain gauges
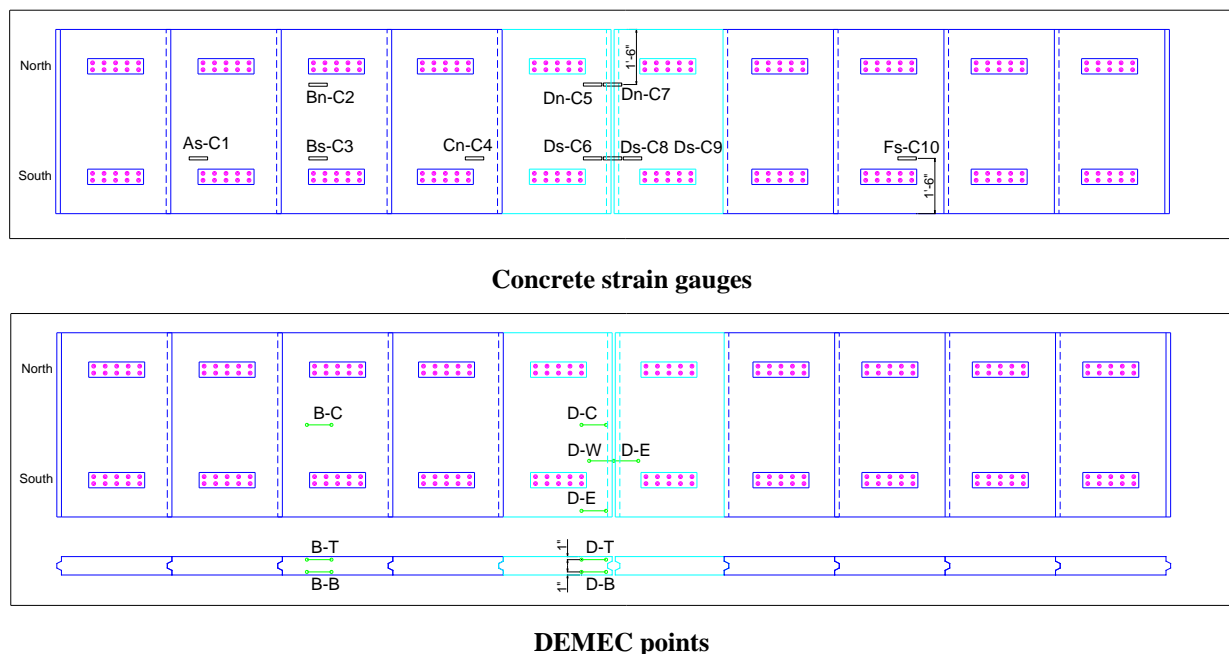
DEMEC points

Figure 3-26. Concrete strain gauges and DEMEC points installed on the deck.

Finally, Figure 3-27 shows the location of the potentiometer installed. Once again similar labeling format is considered. The label refers to section location (A-G), which girder (north or south) and the letter "P" (potentiometer) followed by a number (1-10). A total of 8 potentiometers were used to monitor the displacement of the test specimen.
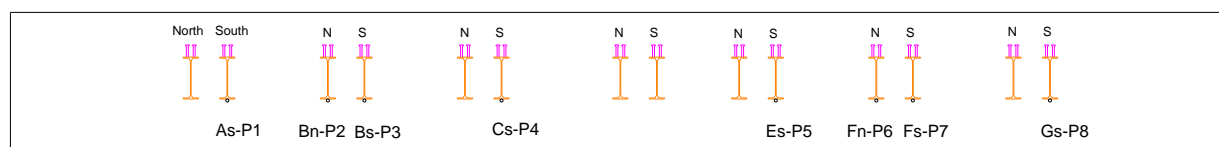
Figure 3-27. Potentiometers installed at girders bottom flange.

3.5 Material Properties

The materials used in the test specimen were characterized following the testing procedure described in the American Society for Testing and Materials (ASTM, 2010). Additional parameters were assumed based on commonly known values reported in the literature.

3.5.1 Concrete

The concrete compressive strength testing results were provided by the Concrete Industries, Inc. Table 3.3 shows the results.

Table 3.3. Concrete compressive strength testing results

Date poured	1 day (release)	7 day	28 day
9/17/2010	5.453*	6.361	7.537
9/20/2010	3.923	7.113	8.676
9/21/2010	4.496	8.210	9.728
9/22/2010	4.927	8.912	10.240

Units in 1000 pounds per square inch (ksi).

* Released 3 days after poured.

The additional concrete parameters were assumed based on AASHTO LRFD specification (AASHTO, 2007).

Table 3.4. Additional concrete parameters

Properties	Assumed value
Concrete density γ_c	0.150 kcf
Linear elastic limit $0.45 f_c'$	3.6 ksi
Modulus of elasticity $E_c = 33000 \gamma_c^{1.5} \sqrt{f_c'}$	5422 ksi
Tensile strength $f_r = 0.23 \sqrt{f_c'}$	0.65 ksi

After the ultimate load testing, four cores were extracted from two end precast panels. This location was chosen because the concrete panels were visually undamaged, although, at this region the maximum shear force is applied in the bridge cross-section. Nevertheless, the samples were taken to have an idea of the compressive strength of concrete after the ultimate test was concluded. Prior to core removal, guiding lines were drawn in the precast surface to indicate the expected location of the reinforcement. The lines follow the reinforcement detailing previously presented. Besides the effort to avoid the reinforcement, two samples were extracted with part of the reinforcement on it.

Lines drawn to guide during core removal

4" diameter core driller

| Skew sample | Sample with rebars |

Figure 3-28. Precast panels concrete core removal.

It can be noted that one sample clearly preset some skew also in two samples at opposite span also reinforcing rebars were found. Though, it may explain the low compressive strength result measured during the compression test. Table 3.5 shows the compression test results.

Table 3.5. Compressive strength testing results

Location	East	West
North	6.647	4.447
South	7.259*	3.146*^
28 day testing	**9.728**	**7.537**

Units in 1000 pounds per square inch (ksi).

* Reinforcement found in the sample.
^ Sample was skewed

3.5.2   Grout

The grout used to fill the shear pockets and closure region was manufactured by Sika Corporation US. SikaGrout 212 is a nonshrink, cementitious grout sold in 25 lbs bags. The Sika catalog reports 3 typical water amounts (SIKA, 2010). The amount of water added was selected based on desired strength and flow condition. Thus, the bag was mixed with 7 US pints

(approximately 200 in^3) of water so that an approximately compressive strength at 28 days of 6.10 ksi and flowable-fluid consistence would be obtained (SIKA, 2010).

In order to determine the compressive strength of the grout used, 4 cylinder grout samples (4" diameter, 8" height) were made. Two sample were tested prior the shim removed (application deck precompression) and the remaining two were tested after the ultimate test. Figure 3-28 shows the grout being mixed and grout cylinder sample after the compression test.

Mixing grout using power drill   **Grout cylinder after compression test**

Figure 3-29. Grout being mixed and after tested

Table 3.6 shows the compression test results.

Table 3.6. Grout compressive strength testing results

Date poured	14 day	77 day
10/20/2010	6.481	5.362
10/20/2010	5.456	7.078
Average	**5.969**	**6.220**

Units in 1000 pounds per square inch (ksi).

3.5.3   Structural Steel

The specified steel strength for this self-stressing specimen was 50 ksi. Material testing was performed once testing was completed to determine the exact strength of steel used. Sections were cut from both ends of the each girder and later machined to meet ASTM standard

dimensions (ASTM, 2010). The reason for taken the samples from the girders ends was because at this location the bending moment is minimal, thus the samples would have the least possible residual stress. This is important because if the samples were taken from other locations which were subjected to previous yield, the tensile test results would be irrelevant and the stress-strain curve wrong. Nevertheless, a total of four samples were taken, two from each girder.

Figure 3-30 show a sequence of picture: starting from cutting the steel piece from the bottom flange of the girder and ending with the final product which is four samples machined to meet ASTM standard dimensions (ASTM, 2010).

Torch cutting the bottom flange

Bottom flange after the cut

Steel sample taken from bottom flange

Steel tensile samples

Figure 3-30. Steel sample removal and machine shop

A micrometer was used to measure the steel sample at 3 different locations in order to obtain an average cross sectional area.

Table 3.7. Tensile sample dimensions

Sample	Dimensions (thickness x width)			Average area
	Location 1	Location 2	Location 3	
Girder N - East	0.3350 in x 0.5045 in	0.3340 in x 0.5040 in	0.3340 in x 0.5030 in	0.168449 in^2
Girder N - West	0.3335 in x 0.4900 in	0.3300 in x 0.4925 in	0.3325 in x 0.4930 in	0.163288 in^2
Girder S - East	0.3350 in x 0.4960 in	0.3350 in x 0.4960 in	0.3350 in x 0.4910 in	0.165602 in^2
Girder S - West	0.3385 in x 0.4810 in	0.3370 in x 0.4850 in	0.3370 in x 0.4790 in	0.162562 in^2

Figure 3-31 shows the average engineering stress versus strain results. The plot was obtained based on the average values of three tensile samples. The fourth test result was disregarded because the sample had shown relatively low yield stress and also an early strain hardening.

Steel Tensile Testing Results
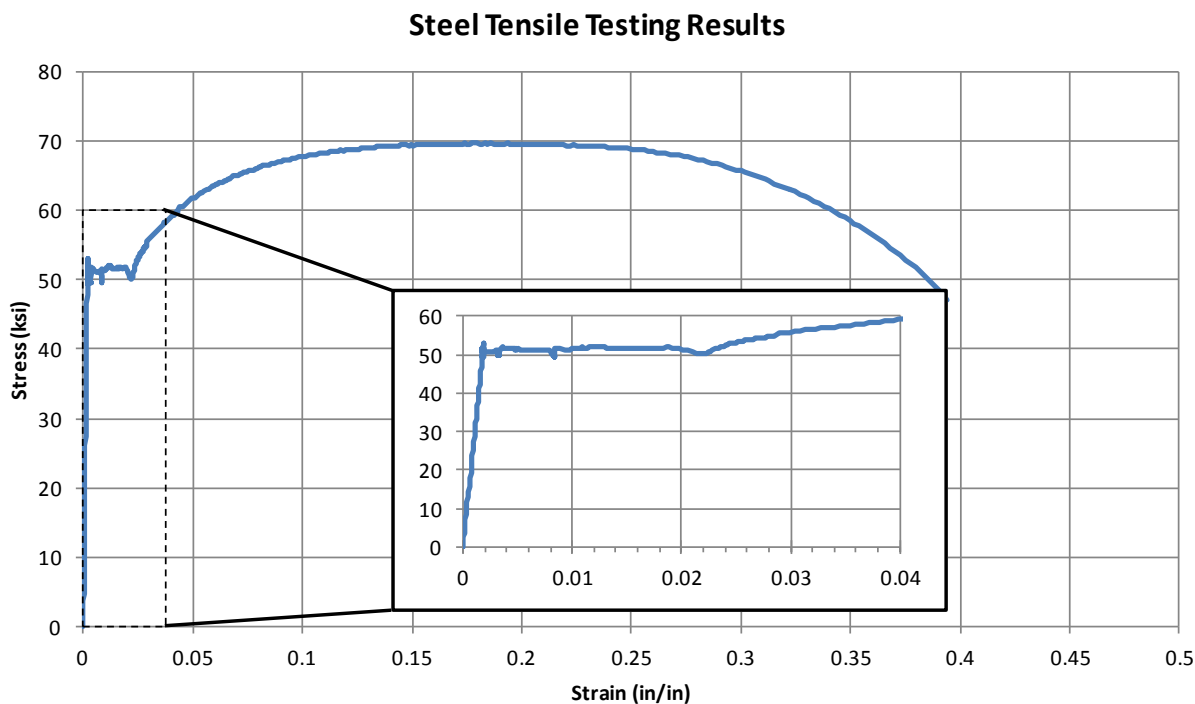
Figure 3-31. Average results of steel tensile testing.

Table 3.8 provides a summary of the structural steel material properties.

Table 3.8. Average structural steel material properties

Properties	Average values
Yield stress	50 ksi
Ultimate stress	70 ksi
Initial modulus of elasticity	29000 ksi
Tangential modulus of elasticity	350 ksi
Steel density (assumed)	0.490 kcf*

3.6 Test Procedure

The test procedure considered to investigate the self-stressing method system can be divided into six stages. The first stage refers to the placement of the girder over level supports followed by the next stage which includes the raising of interior support. The third step consists of cast (or placement) of concrete deck. Up to this point, only the girder (noncomposite section) is carrying the loads. After allowing time for concrete to harden, so that the composite action

between girder and deck is acquired, the fourth stage is carried out where the shim is removed to induce the self-stressing force. Since concrete change its properties over the time due to creep and shrinkage, the next stage was carried out over a period of time. Finally, the system is put to the task and an ultimate loading test is carried out.

The first column of Table 3.9 is shown the description of each stage. Next column shows the structure condition which can be either noncomposite or composite. Third column presents the loading type either distributed, concentrated or induced curvature. Columns five and six show, respectively the moment and deflection shapes due to the each load.

Table 3.9. Summary of test procedure

Stage	Structure	Loading	Moment	Deflection
1 Place Girder on Level Supports				
2 Raise Interior Support				
3 Ballast load				
4 Cast Concrete				
5 Lower Interior Support				
6a Relaxation (time dependent effect)				
6b Restoring Force (time dependent effect)				
7 Ultimate Loading				

The following sections briefly discuss some of the loading stage considered.

3.6.1   Ballast Load

The test specimen represents a ¼ scale model of a prototype structure. Since the simulation largely depends on self-weight gravity loading in order to maintain similitude, the density of the materials would need to be increased. This can be demonstrated considering a simply supported beam with rectangular cross-section of width b and height h. The length of the beam is L and the unit weight is γ. The stress at the bottom of the beam at mid-span can be found to be ¾ γ L^2 / h. If the geometric parameters (L and h) are scaled by a factor α, the resulting stress is (α ¾ γ L^2 / h), i.e. the stress has been scaled as well. In order to obtain the same stress levels, as is desired, the unit weight would need to be factored by 1/α. A similar result can be obtained for the actual structure.

Since it is be impossible to alter the unit weight of the materials to the required level, ballast load was attached to the structure to obtain the desired correct stresses. The level of stresses was determined from analysis of the full-sized prototype structure. A series of point ballasts were applied as a substitute for the more correct uniform distributed ballast.

The ballast load used in this study was made by stacking five train wheels on top of each other. After each stack was made, they were weighted and later moved to the basement to be hanged by high-strength rods.

Figure 3-32. Overview of ballast load stack and digital scale

Figure 3-33 shows the final configuration of ballast loads to be applied to self-stressing system. The average load per stack was 3835 lbs. This is equivalent to a uniform distributed load of approximately 1.28 kip/ft.

Top view

Side view
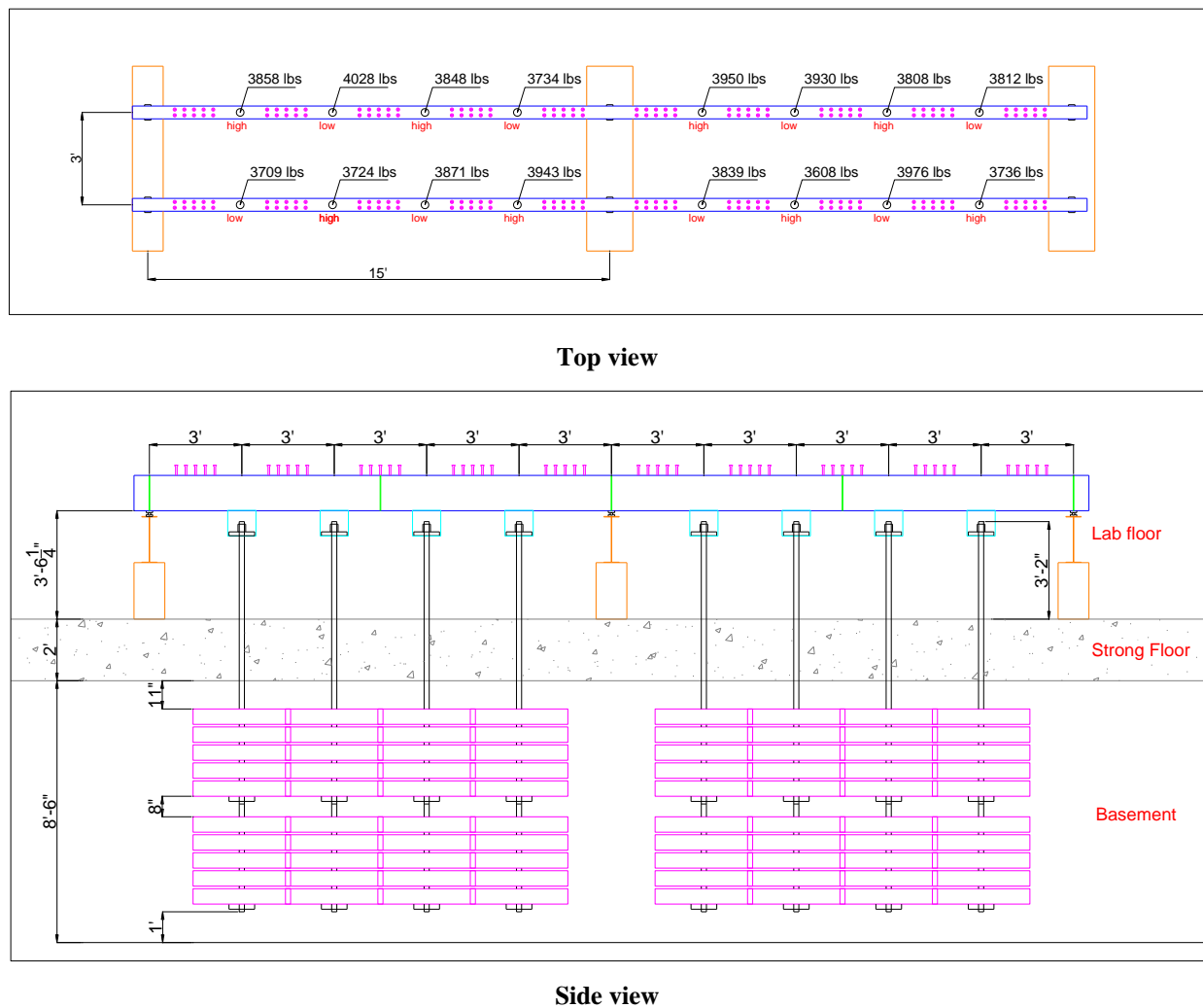
Figure 3-33. Schematic view of ballast loading.

Figure 3-34 show the ballast load organized in the basement of the structural laboratory.

Figure 3-34. Stacks of ballast loads in the basement.

3.6.2   Creep and Shrinkage Monitoring

Creep and shrinkage can either increase or decrease the amount of prestress initially induced into the bridge system. Therefore, the creep and shrinkage was monitored in order to determine their influence into the whole system behavior.

The data acquisition system recorded all the strains and defections during this period. Additional strain measurements obtained from the DEMEC points were also collected. The analysis of long-term monitoring is presented in Chapter 4 and further comparison with the AASHTO LRFD creep and shrinkage prediction models was carried out. The models are described as follows.

3.6.2.1   Shrinkage Model

Shrinkage is influenced by factors such as volume-to-surface ratio, ambient relative humidity, concrete age, type of curing, and age of concrete under service. It is conveniently expressed as a dimensionless strain under uniform conditions of relative humidity and temperature. The AASHTO LRFD specifications provided formulas for estimating shrinkage (AASHTO, 2007).

For accelerated curing, shrinkage strain ε_{sh} is calculated from:

$$\varepsilon_{sh} = 560 \times 10^{-6} k_{td} k_s k_{hs} \text{ (for accelerated curing)}$$

3.1

For moist curing, shrinkage strain ε_{sh} is calculated from

$$\varepsilon_{sh} = 510 \times 10^{-6} k_{td} k_s k_{hs} \text{ (for moist curing)}$$

3.2

The time development factor for shrinkage k_{td} is determined by

$$k_{td} = \frac{t}{55+t} \quad \text{for 1 day to 3 days of accelerated curing;}$$

$$k_{td} = \frac{t}{35+t} \quad \text{for after 7 days of moist curing}$$

3.3

where

t = drying time after end of curing, days

The size factor k_s is determined by

$$k_s = \left[\frac{\dfrac{t}{26e^{0.36V/S}+t}}{\dfrac{t}{45+t}} \right] \left[\frac{1064 - 94V/S}{923} \right]$$

3.4

where

V/S = volume-to-surface ratio of the exposed surfaces of the component

Finally, the humidity factor for shrinkage k_{hs} is calculated by

$$k_{hs} = \frac{140 - RH}{70} \qquad \text{for RH} < 80\%$$

$$k_{hs} = \frac{3 \ 100 - RH}{70} \qquad \text{for RH} \geq 80\%$$

3.5

3.6.2.2 Creep Model

The creep coefficient $\psi(t,t_i)$ is the ratio of creep strain occurring in the period t to the elastic strain at t_i caused by a constant stress applied to concrete of age t_i and sustained in the period t, where t is the age of concrete between time of loading for creep calculations, end of curing for shrinkage calculations, and time being considered for analysis of creep or shrinkage effects and t_i is the age of concrete when load is initially applied. Creep strain will reach its ultimate value at the end of the service life of the structure. The creep coefficient is influenced by the same factors that influence shrinkage as well as the age of concrete at the time of loading. The coefficient is defined in such a way that the applied stress has to be a constant sustained stress within the levels that usually prevail for in-service conditions. It is not intended to be used for excessively high compressive stress. Structural analysis modeling allows use of the creep coefficient for cases where the stress in concrete varies with time, such as in the case of prestress losses and with deck or girder differential creep and shrinkage. Following equations are the AASHTO LRFD specifications creep-prediction formulas (AASHTO, 2007).

$$\psi(t,t_i) = 3.5 k_f k_c k_{hc} k_{la} k_{td}$$

3.6

where

k_f = concrete strength factor

k_c = size factor for creep

k_{hc} = humidity factor for creep

k_{la} = loading age factor

k_{td} =   time development factor

Each term can be determined by

$$k_f = \frac{1}{0.67 + \dfrac{f_c'}{9}} \tag{3.7}$$

$$k_c = \left[\frac{\dfrac{t}{26e^{0.36\,V/S} + t}}{\dfrac{t}{45 + t}} \right] \left[\frac{1.80 - 1.77e^{-0.54\,V/S}}{2.587} \right] \tag{3.8}$$

$$k_{hc} = 1.58 - \frac{RH}{120} \tag{3.9}$$

$$k_{la} = t_i^{-0.118} \tag{3.10}$$

$$k_{td} = \frac{t - t_i^{\;0.6}}{10 + \;t - t_i^{\;0.6}} \tag{3.11}$$

3.6.3   Ultimate Load

The ultimate loading was conducted to determine the failure mode that may govern the design of self-stressing method system. The loading was be applied to the specimen by two spreader-beam located at each mid-span. The beams were connected to four hydraulic rams (2 per beam) through high-strength rods as shown in Figure 3-35. Elastomeric pad were place under the spread beams to transfer the load to the deck.

Side view

Top view
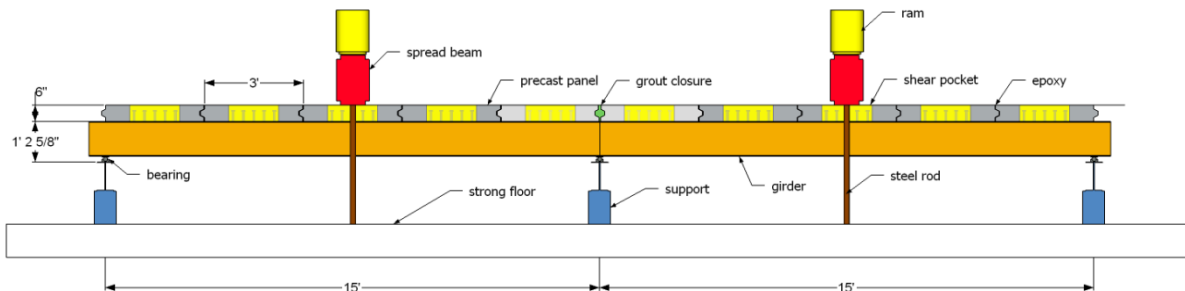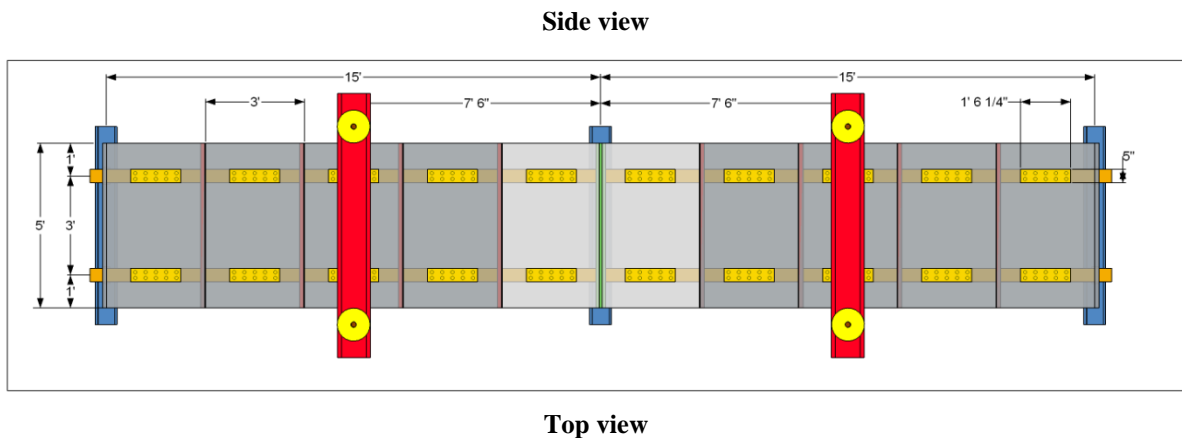
Figure 3-35. Sketch of the ultimate load test setup.

During the test, the data acquisition system was used to record all strains in both concrete and steel, defections, and rams hydraulic pressure (loading). The analysis of the recorded data and observed mode of failure are discussed in the following Chapter 4.

Figure 3-36 show the ultimate load test setup in the structural laboratory.

Figure 3-36. Ultimate load test setup.

Chapter 4

Test Results and Discussion

The test results regarding the different loading stages are here presented and discussed. The chapter starts with the general assumptions considered to analysis the bridge response. In the next section, the bridge analyses under three different constructions loading are considered. The long-term behavior is analyzed in the following section. The creep and shrinkage prediction models are considered. Finally, the bridge behavior under service and ultimate loading are discussed. Additionally, the failure modes are evaluated.

4.1 General considerations

For simplification purpose, the following assumptions were considered in order to analysis the bridge response during the different load stages. The assumptions are as follows:

- Plane section remains plane, i.e. the strain distribution on any section at any time is linear. Euler-Bernoulli beam assumption.

- Slip at the steel-concrete interface and between the concrete and any embedded reinforcement, is negligible. Full composite section is acquired.

- The short-term stress-strain relationship for concrete is linear-elastic in compression and in tension prior to cracking.

- The concrete in tension carries no stress after cracking, and the tensile strength $f_t = 0.23\sqrt{f_c^{'}}$, where $f_c^{'}$ is the 28 day characteristic cylinder strength of the concrete in ksi units. Tension in the concrete is neglected after cracking,

- The stress-strain relationship for steel in both compression and tension is linear elastic, with elastic modulus of E_s.

- The age-adjusted effective modulus method (AEMM) is suitable for the inclusion of creep and shrinkage effects.

- Tension is positive, compression is negative and positive bending causes negative curvature, with tensile strains in bottom fibers of the section.

The bridge analysis is divided in four stages. The first considered the construction load, and includes the girder weight, lifting of interior support and the precast deck weight. The next analysis considers the short-term analysis and includes the shim removal in order to induce the prestressing force into the bridge system. Third analysis considers the long-term monitoring. The creep and shrinkage prediction models are used to estimate the concrete strains after the time-dependent effects. Finally, the ultimate load is conducted to understand how the bridge using the self-stressing method behaves under low load (service limit) and ultimately under high load (strength limit). In addition, the failures modes are described.

4.2 Before self-stressing (construction)

This section summarized the results during the first three construction stages. This includes the placement of the girder over the level supports, raising the interior support to a predetermined elevation and placement of concrete deck over the girders. In addition, the ballast load was also considered.

4.2.1 Bending moment analysis

The bending moment diagram due the girder self-weight, ballast load and concrete deck can be determined by Equation 4.1. Similarly, the bending moment diagram due the raising of

interior support can be determined by Equation 4.2 as follows. Since the bridge is symmetrical, the moments in Span 2 are symmetrical to those in Span 1.

$$M_{girder,ballast,deck}(x) = \frac{3wL}{8}x - \frac{w}{2}x^2 \qquad for \ x \leq L \qquad \textbf{4.1}$$

where

w = Girder self-weight (0.035 kip/ft)
Ballast load weight (1.279 kip/ft)
Concrete deck weight (0.188 kip/ft)

L = Span length (15 ft)

and

$$M_{lift}(x) = \frac{3E_s I_g}{L}\delta\left(\frac{x}{L}\right) \qquad for \ x \leq L \qquad \textbf{4.2}$$

where

E_s = Steel modulus of elasticity (29000 ksi)

I_g = Moment of inertia of girder (192.03 in^4)

δ = Lifting displacement (-1.0 in)*

NOTE: negative sign was a convention for upward displacement.

The moment diagram resulted from all the load within this stage of construction is plotted in Figure 4-1. At this stage only the girder (noncomposite section) carries the loads. The diagram includes the moments due to girder self-weight, ballast load, concrete deck and lifting.

Bending moment diagram
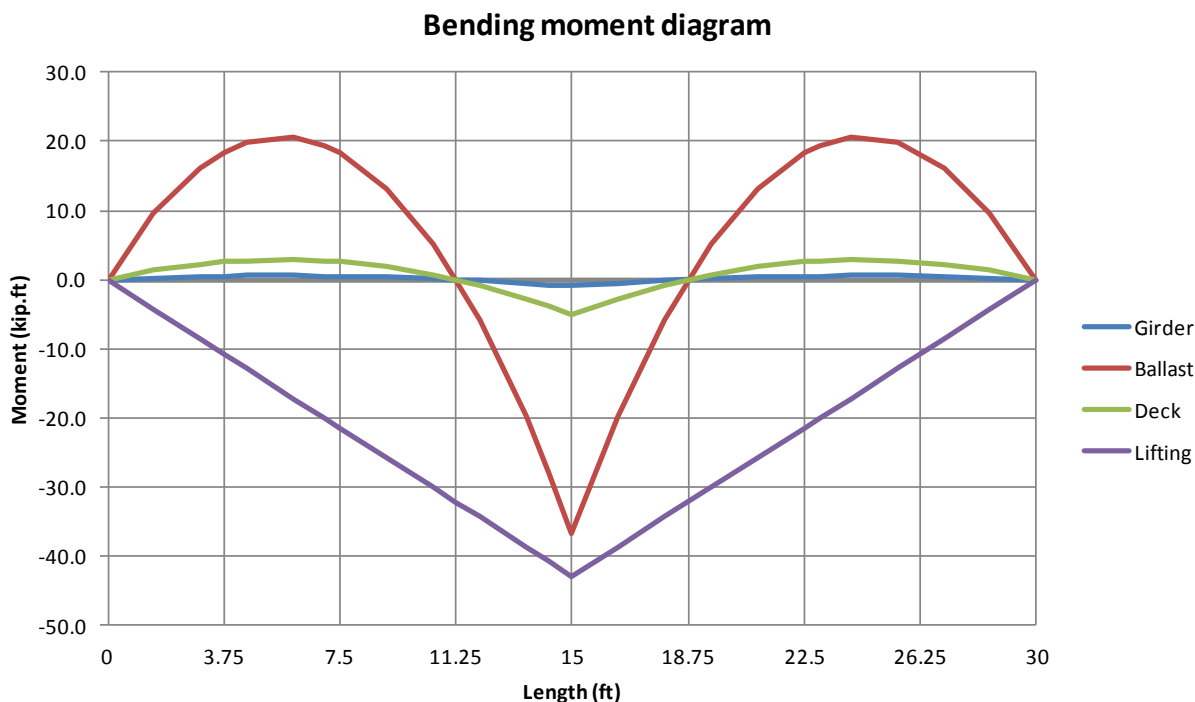
Figure 4-1. Bending moment diagram during construction load

Since the stress levels are within the linear elastic limits, the principle of superposition can be applied. As a result, both displacements and stresses are calculated using linear elastic theory and compared with the measured values provided by the potentiometers and strain gauges installed only the final stage of construction.

4.2.2　Deflection analysis

Figure 4-2 shows the displacement development during the construction of the test specimen. Initially, the plot starts showing a small drop in the displacement readings (1), this was due to initial drop of part of the ballast load to avoid the girder ends to be lifted. Following, the displacement star to increase due to lifting of interior support. The potentiometers at section "E" and "F" located close to the interior support show measurement close to the maximum shimmed value of 1.0 inch (2). The displacement held constant prior the placement of the deck where the remaining ballast loads are dropped. Since the precast deck panels were placed first at one span

moving towards the middle, it can be observed that potentiometers "A", "B" and "C" show a displacement decreasing due to precast weight and ballast load drop (3). At the conclusion of the first span, the deck placement is started at second span. As expected, the displacement readings once again meet each other after the construction conclusion (4).
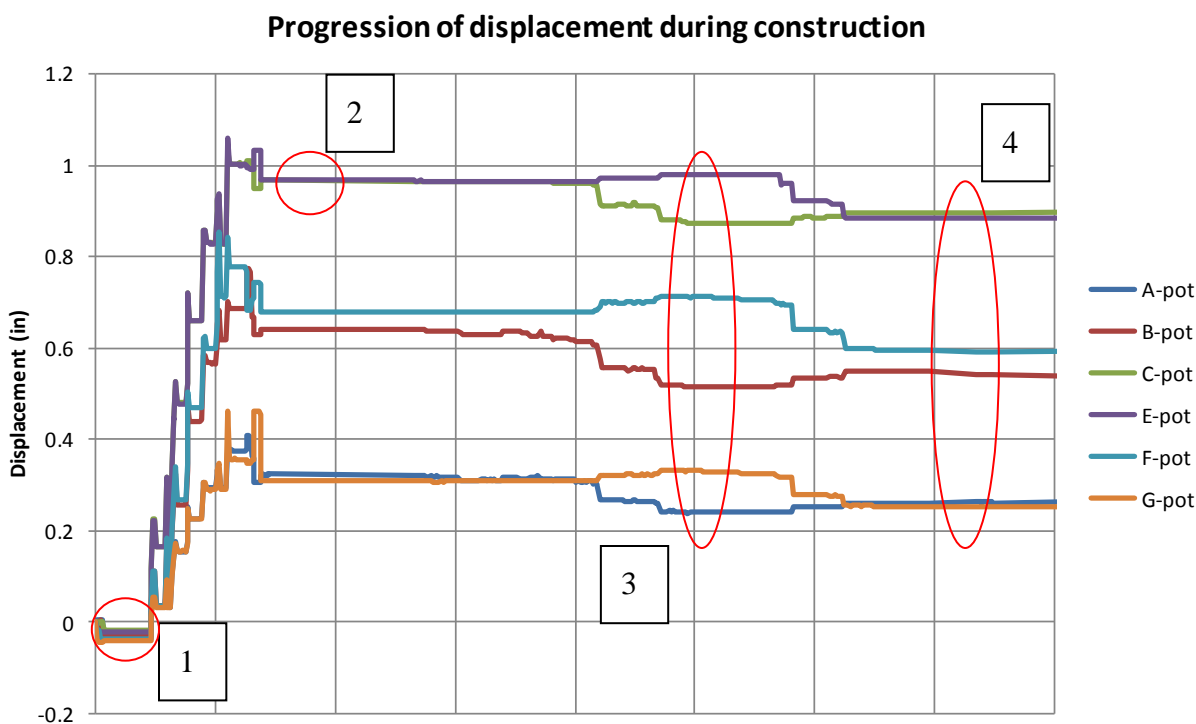
Figure 4-2. Progression of displacement during construction

In order to verify the applicability of the linear elastic theory to analyze the results, the measurements were compared with the calculated values using the linear elastic beam theory. Table 4.1 shows both theoretical and experimental results. It can be seen a very good agreement between the calculated and measured values.

Table 4.1. Displacement comparison after construction load.

Section	Theoretical	Measured
A (3.75 ft)	0.26	0.27
B (7.5 ft)	0.56	0.54
C (11.25 ft)	0.86	0.90
E (18.75 ft)	0.86	0.88
F (22.5 ft)	0.56	0.60
G (26.25 ft)	0.26	0.25

Units of displacement in inch (in).

4.2.3   Stress and strain analysis

The following analysis considers the stress comparison. Since at this point, the stresses levels fall within the elastic limits, Hooke's law can be used to calculate the stresses. The stresses were calculated based on the material properties determined during the tensile sample tests and the strains measured by the gauges installed in the specimen.

Figure 4-3 shows the stresses values at the bottom flange of the girder calculated based on beam theory and the measured values at the location of installed strain gauges. Since in some locations more the one strain gauge were installed (see Figure 3-25), an average between this them is plotted in the chart. It is observed a very good agreement between the calculated and measured values.

Stress at girder bottom flange
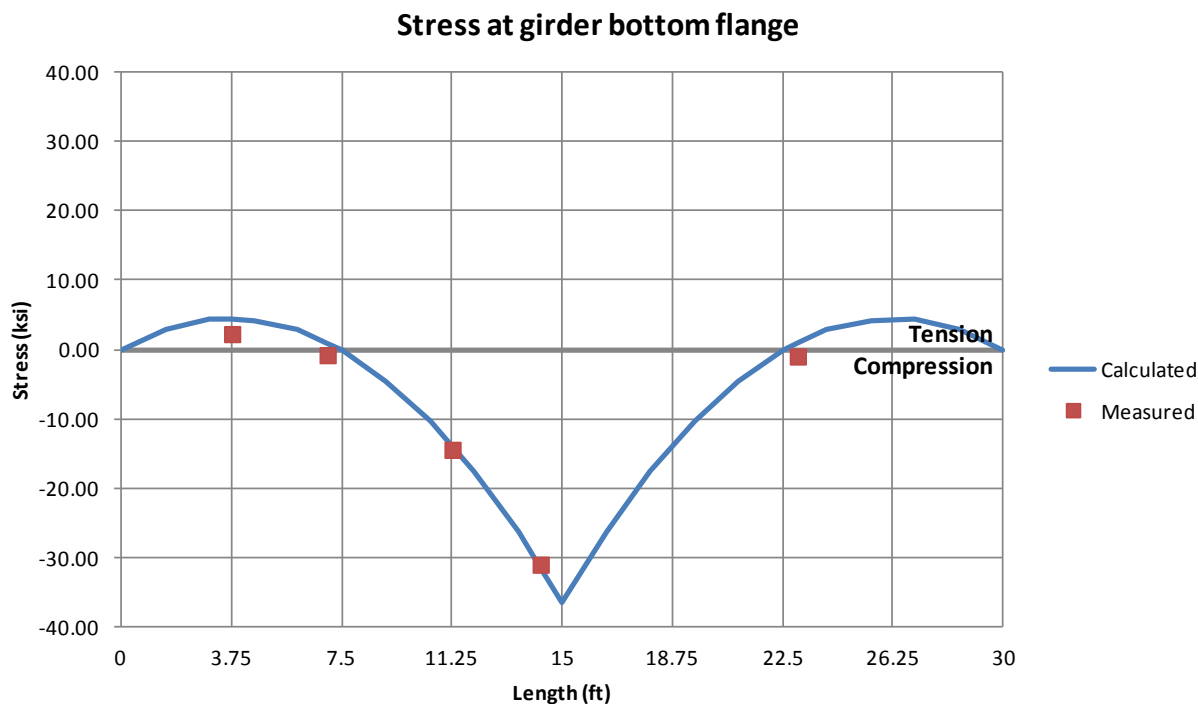
Figure 4-3. Stress at girder bottom flange due to construction load.

The next comparison considers the stresses measured at the top flange of the girder. Once again the theoretical is compared with the experimental. Figure 4-4 shows a small difference between the experimental and theoretical values. During the beam analysis, it was assumed that only the girder (noncomposite section) would carry the load; however, in reality this is not true. Although the deck is only placed over the girder at this stage, the friction between concrete/steel creates some partial (small) composite action. Thus a reduction of the stress at girder top flange is expected.
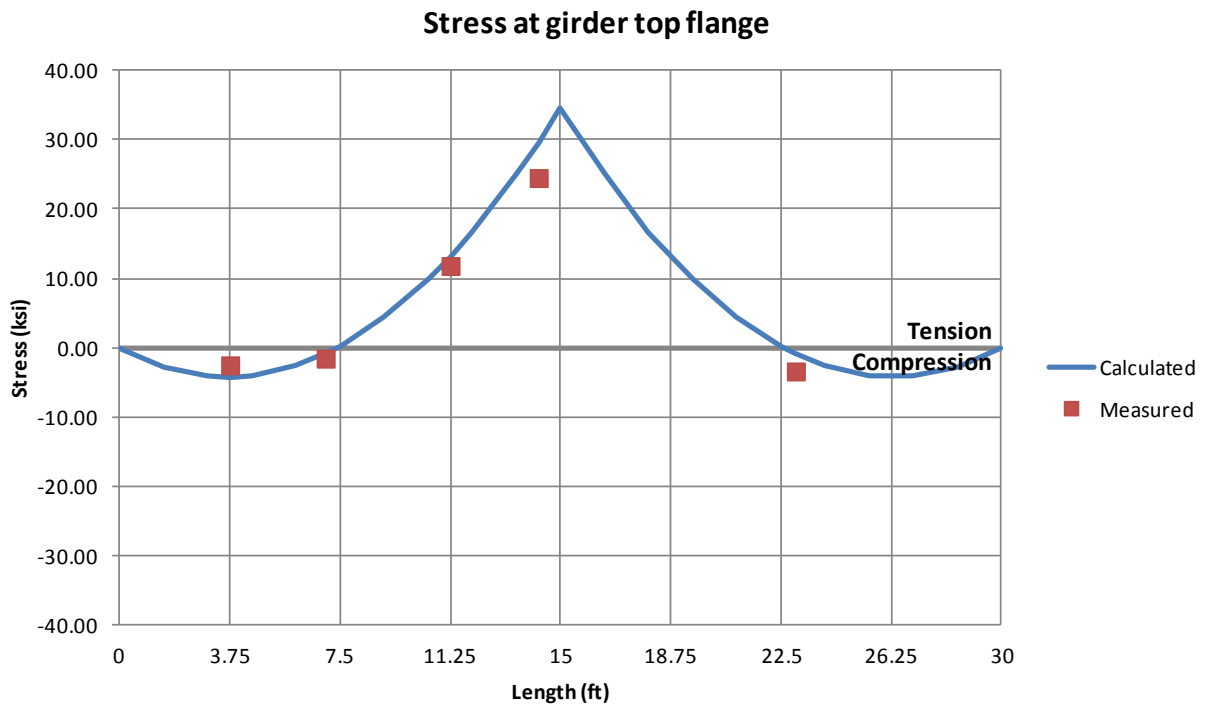
Figure 4-4. Stress at girder top flange due to construction load.

The next section discusses the results obtained after the grout was hardened and the concrete deck and steel girder acts as a composite section.

4.3 At self-stressing (short-term)

This section summarized the results during the application of prestressing force in the bridge. This was achieved by releasing the 1 inch shim previous introduced at interior support. At this stage, the concrete deck and steel girder acts as a composite section. Therefore, the force induced by releasing the shim is applied to the composite section.

4.3.1 Bending moment analysis

Similarly to the previous section, Equation 4.3 can be used to calculate the bending moment diagram due to lowering of interior support. The moment equation is very similar to Equation 4.2 used to calculate the lifting moment with the exception of the material and cross-

section properties which now assumes the composite (transformed) section values. Since the specimen is symmetrical, the moments in Span 2 are symmetrical to those in Span 1.

$$M_{release}(x) = \frac{3 E_s I_{transformed}}{L^2} \delta\left(\frac{x}{L}\right) \qquad for\ x \le L \qquad \textbf{4.3}$$

where

$I_{transformed}$ = Moment of inertia of transformed cross-section (811.01 in^4)

δ = Releasing displacement (+1.0 in)

The moment diagram resulted from shim removal is plotted in Figure 4-5. It can be seen that the moment applied due to shim releasing is 4 times greater the moment due to lifting. This difference is due to the increasing of the moment of inertia from 192 in^4 (noncomposite) to 801 in^4 (composite). Also, the sign had changed since shim removal occurs in the opposite direction of lifting.

Bending moment diagram
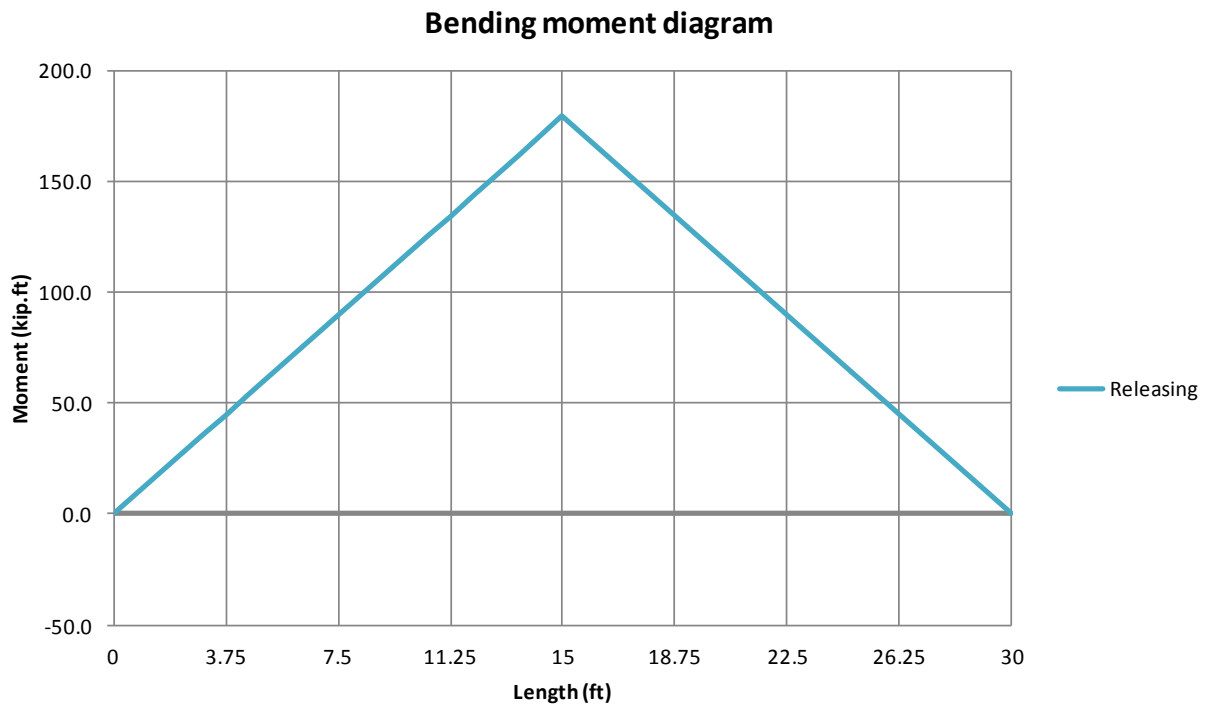
Figure 4-5. Bending moment diagram due to lowering

Followed are the comparison for both displacement and stress.

4.3.2 Deflection analysis

Figure 4-6 shows the displacement development during the shim removal process. The plot starts showing the same end-values presented in Figure 4-2 (1), since this stage is a continuation of the construction sequence. It can be noted a plateau at the chart (2) resulted by the changing of the hydraulic rams. This changing was necessary because the first jacks used had a small stroke which would extend the total time required for remove the shim. After the completion of this construction stage, it can be noted the sign inversion (3). This is expected since the supports are now leveled.
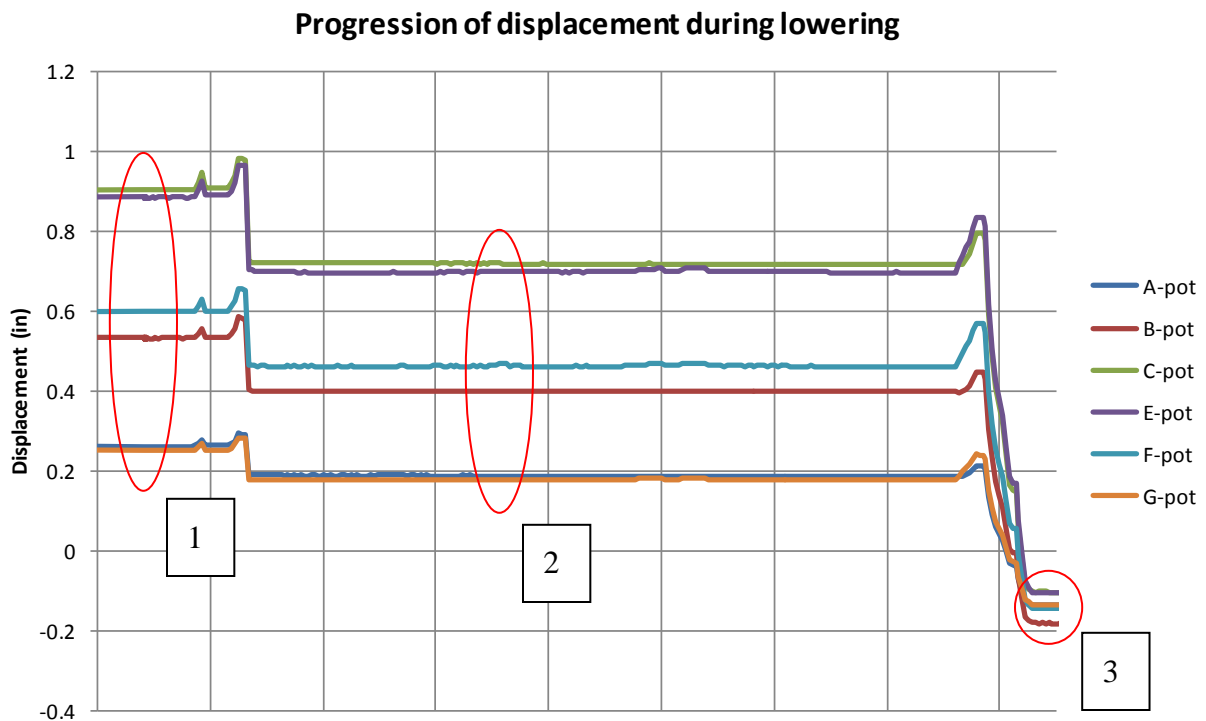
Figure 4-6. Progression of displacement during shim removal.

The measured values were compared once again against the theoretical values calculated from the linear elastic beam theory. Table 4.2 shows both theatrical and experimental results. It can be seen a very good agreement between the calculated and measured values.

Table 4.2. Displacement comparison after shim removal.

Section	Theoretical	Measured
A (3.75 ft)	-0.11	-0.14
B (7.5 ft)	-0.13	-0.18
C (11.25 ft)	-0.06	-0.10
E (18.75 ft)	-0.06	-0.11
F (22.5 ft)	-0.13	-0.15
G (26.25 ft)	-0.11	-0.14

Units of displacement in inch (in).

In the following stress analyses, the principle of superposition are applied, since the stress levels are within the linear elastic region.

4.3.3   Stress and strain analysis

The following stress analysis considers the same assumptions as previously mentioned. Figure 4-7 shows the stresses values at the bottom flange of the girder calculated based on both beam theory and the measured values from strain gauges.

In conventional bridge design, the negative region (vicinity of interior support) is susceptible to lateral torsional buckling since the bottom flange is subject to compression forces. Therefore, the girder cross-section is increased in this region to overcome this issue. This solution results in cost increasing since a larger amount of steel is considered and also the use of expensive and labor intensive steel splices are required.

However, when the self-stressing method is considered the compressive stress in the vicinity of interior support is reduced. Thus one single cross-section can be used throughout length of the bridge. Figure 4-7 shows the results obtained from the test specimen. It can be noted that the expected compressive stress at the bottom flange was completely eliminated. Also a very good agreement is observed between the calculated and measured values.
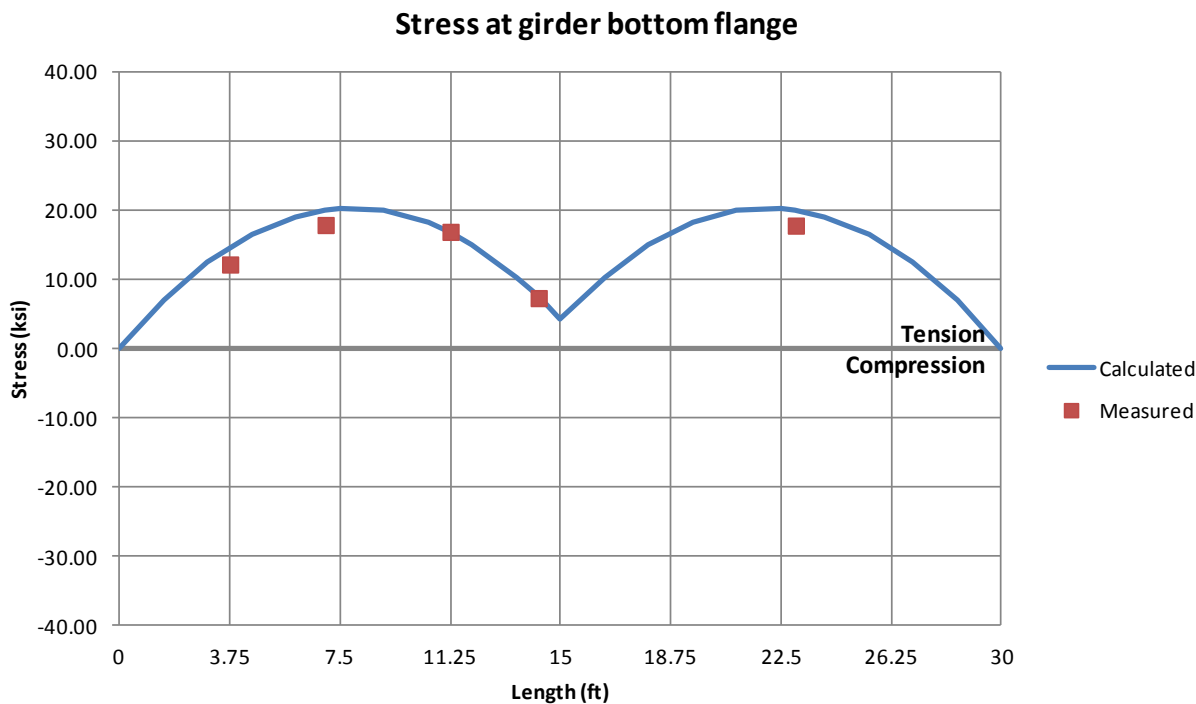
Figure 4-7. Stress at girder bottom flange after shim removal.

Differently from bottom flange measurement which it can seen greater difference in the measured stress before and after the prestressing force. The stresses measured at the top flange did not change as much. Figure 4-8 shows stresses at the girder top flange after shim has been removed. The reason for the small increasing of top flange stresses is due to the location of the neutral axis of the composite section which falls very close to the girder top flange (about 1.4 inches above it). Once again a very good agreement between the measured and calculated values is observed.
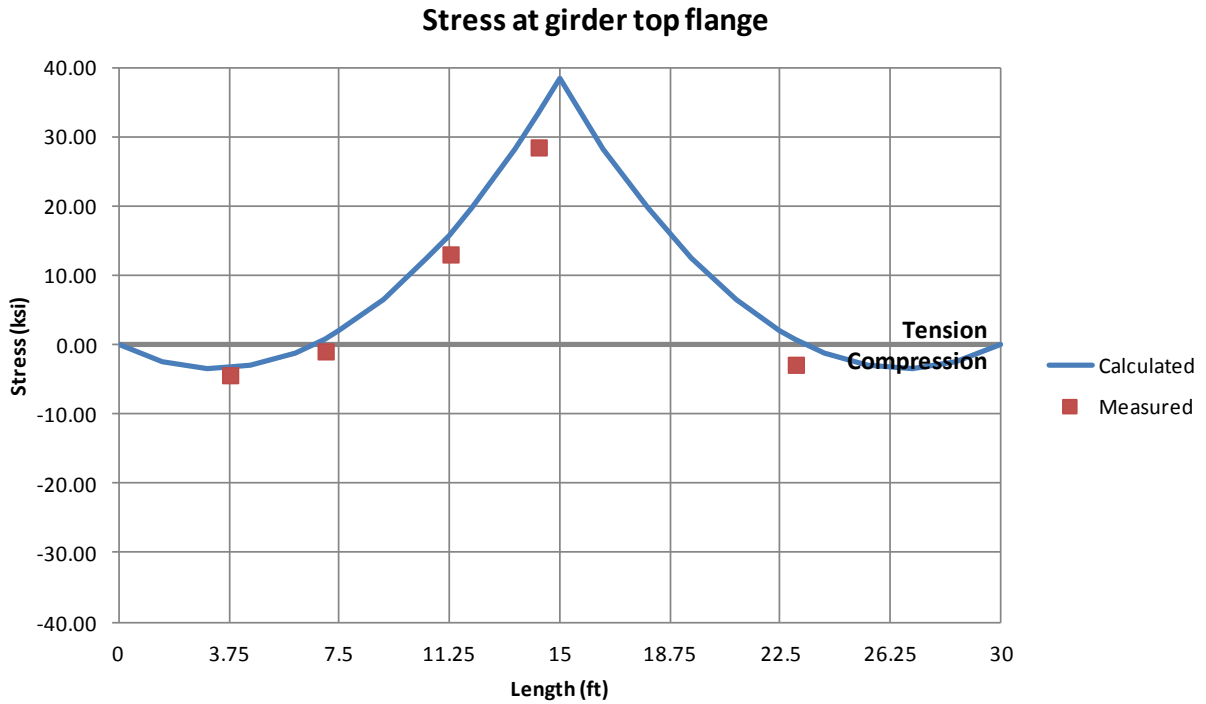
Figure 4-8. Stress at girder top flange after shim removal.

One of the biggest advantages of the self-stressing method over the conventional prestressing method is the application of prestressing force without the need of the expensive and corrosion prone post-tensioning techniques. The amount of prestressing achieved is directly proportional to the amount of displacement initially introduced during the construction. Equation 4.4 can be used to calculate the maximum compressive stress applied to the top fiber of the concrete deck. The formula was developed based on the 2-span bridge, although the methodology can be applied of n-span bridges.

$$\sigma_{ts}(x) = \frac{c_{ts}}{n\, I_{transformed}} M_{release}(x) \qquad for\ x \le L \tag{4.4}$$

where

c_{ts} = Distance from the N.A. to the top surface of concrete deck (4.56 in)

n = Modular ratio ($E_s / E_c = 5.35$)

σ_{ts} = Compressive stress at top surface of concrete deck

Figure 4-9 shows the compressive stress measured at the top surface of the concrete deck and calculated values based on Equation 4.4. The maximum compressive stress located at the interior support was 2.30 ksi or approximately 30% the concrete compressive strength. A very good agreement between the measured and calculated values is observed.
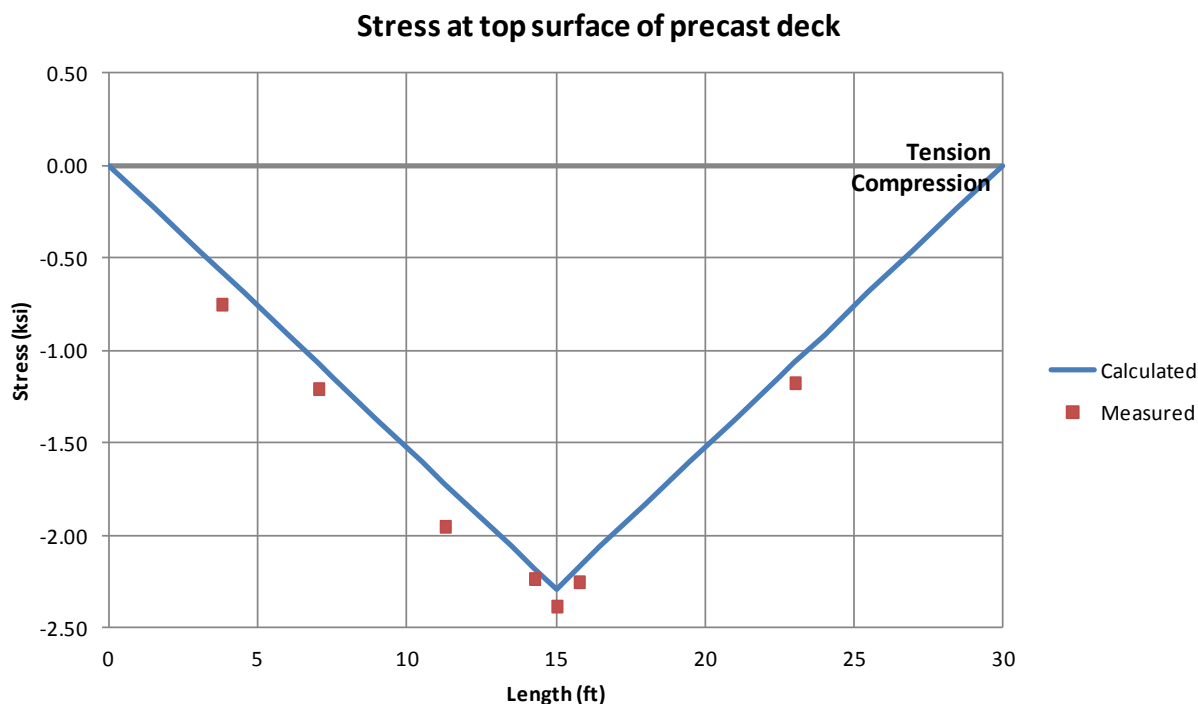
Figure 4-9. Stress at top surface of precast deck panels after shim removal.

Besides the measurement provides by the concrete strain gauges installed at the top surface of concrete deck, additional demountable mechanical strain gauge, commonly known as DEMEC points, where used to provide additional strain readings in both top surface and through the deck thickness. Table 4.3 shows very good agreement between the theoretical values and the readings taken by the concrete surface gauges and DEMEC points.

Table 4.3. Stress comparison through the deck thickness comparison

Section	Theoretical	Concrete Gauge	DEMEC
B top (7.0 ft)	-1.07	-1.20	-1.21
B bottom (7.0 ft)	0.16	-	0.09
D top (14.25 ft)	-2.18	-2.24	-2.43
D bottom (14.25 ft)	0.33	-	0.30

Units of stress in 1000 pounds per square inch (ksi)

Sign conversion: positive sign for tension and negative sign for compression.

The following results and discussions refer to the long-term monitoring of the self-stressing test specimen.

4.4 After self-stressing (long-term)

The long-term observations are summarized in this section. This extended monitoring was required to determine the influence of creep and shrinkage in the self-stressing system.

4.4.1 Deflection analysis

The long-term monitoring of the test specimen had a total time-span of 63 days. Manual readings of the concrete strain were made at the at the DEMEC points locations. In addition, the first 21 days was fully monitored by the data acquisition system. After that, the MEGADAC and some potentiometer were disconnected to be used in other laboratory testing and only the manual readings were conducted. Later, for preparation for the ultimate load test, the data acquisition and new potentiometer were reconnected and a final reading was performed.

Figure 4-10 shows the displacement from all 6 potentiometers installed at different locations through the length of test specimen (1). At day 21, the MEGADAC and some potentiometers were disconnected and only reconnected after 42 days. Hence, a drop in the reading for potentiometers "C", "E", and "G" is observed (1). Further analyzing the results,

potentiometer "F" had shown some inaccurate reading during the initial stages of monitoring (2). 63 days after initially apply the prestressing force, the system was reconnected and a final reading of displacement was conducted (3).
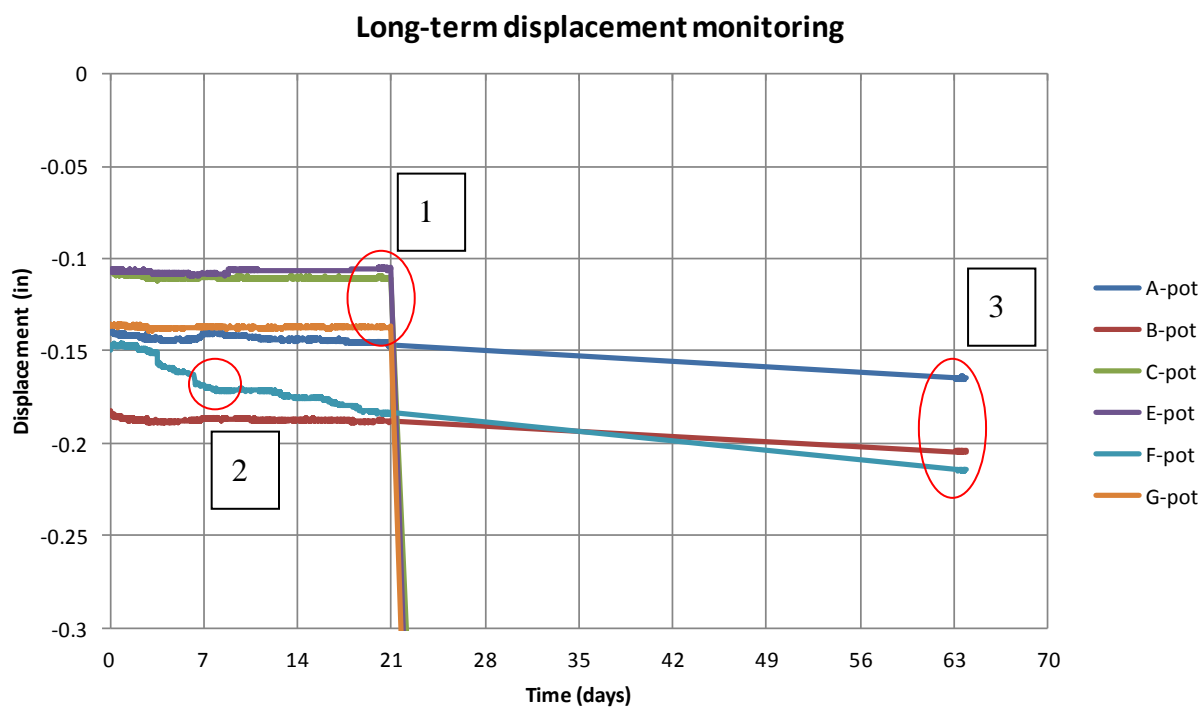
Figure 4-10. Displacement development during long-term monitoring

Table 4.4 summarized the results plotted in Figure 4-10.

Table 4.4. Short and long-term displacement comparison

Section	Initial	21 days	Final
A (3.75 ft)	-0.139	-0.147	-0.165
B (7.5 ft)	-0.184	-0.188	-0.204
C (11.25 ft)	-0.106	-0.110	-
E (18.75 ft)	-0.106	-0.105	-
F (22.5 ft)	-0.147	-0.184*	-0.214*
G (26.25 ft)	-0.136	-0.137	-

Units of displacement in inch (in).

* Possible mal-function of potentiometer.

Overall, it was observed a slightly increasing in the displacement due to the time-dependent effect. The increasing was only attributed to the concrete creep that softens the concrete elastic modulus and consequently decreases the bridge stiffness which increases the displacement. The shrinkage effect was neglected because the precast panels after fabricated were set outside to cure thus losing the rapidly the moister which results in acceleration of the shrinkage process. Figure 4-11 shows a picture taken at the Concrete Industries, Inc. yard showing the precast panel outside prior to delivery.

Figure 4-11. Precast concrete deck panel at Concrete Industries Inc yard.

In the following section will be discussed stress and strain analyses.

4.4.2   Stress and strain analysis

The following analysis considers the stress and strain analysis. The stresses were calculated based on the material properties and strains measurement in the specimen by the strain gauges installed. The long-term strains due to creep and shrinkage were predicted using the model described in AASHTO LRFD Specification.

4.4.2.1   Creep and shrinkage analysis

The total concrete strain can be divided into three distinct terms (Figure 4-12). The first term refers to the concrete shrinkage and is variable since it mainly depends on how the concrete dry during the curing period. The elastic and creep term only happens if the concrete is subject to external load. The elastic term is constant throughout the time and proportional to the applied load. On the other hand, the creep term is variable since the concrete "relax" its modulus of elasticity with time due to sustained load.
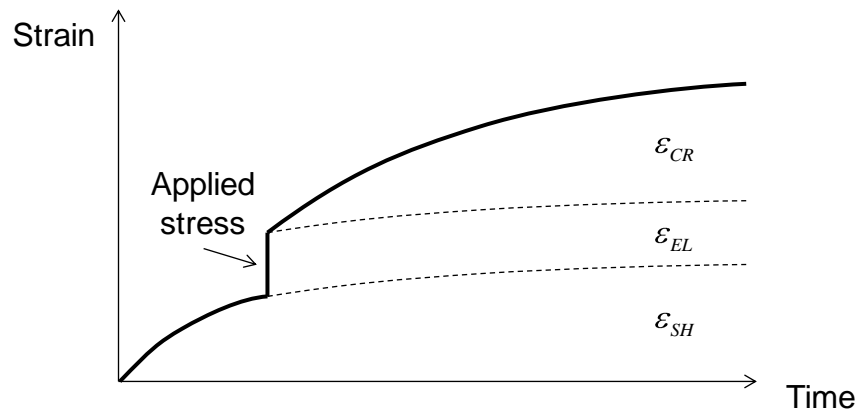
Figure 4-12. Graphical representation of different strain components over time.

As noted in Figure 4-12, the total strain is linear combination of all three terms which includes the elastic, shrinkage and creep strains as defined by Equation 4.5.

$$\varepsilon_T = \varepsilon_{EL} + \varepsilon_{CR} + \varepsilon_{SH} \qquad\qquad \textbf{4.5}$$

Equation 4.6 defines the elastic strain ε_{EL} as a function of the initial prestressing force divided by the initial modulus of elasticity of concrete.

$$\varepsilon_{EL} = \frac{\sigma_{ts}}{E_{ci}} \qquad\qquad \textbf{4.6}$$

The creep strain ε_{CR} defined by Equation 4.7 is a function of the creep coefficient and the initial deformation due to prestressing force.

$$\varepsilon_{CR} = \varepsilon_E \, \psi(t, t_i) \qquad\qquad \textbf{4.7}$$

in which,

$\psi(t, t_i)$ = Creep coefficient as a function of time

The creep coefficient $\psi(t, t_i)$ as described in Article 5.4.2.3.2 of AASHTO is defined in Equation 4.8. Concrete creep can be influenced by many factors such as aggregate characteristics and proportions, average humidity at the bridge site, W/C ratio, type of cure, volume to surface area ratio of member, duration of drying period, magnitude and duration of the stress, maturity of the concrete at the time of loading, and temperature of concrete. However, the creep shortening of concrete under permanent loads primarily depending on concrete maturity at the time of loading and generally assumes values in the range of 0.5 to 4.0 times the initial elastic shortening (AASHTO, 2007).

$$\psi(t, t_i) = 1.9 \, k_s \, k_{hc} \, k_f \, k_{td} \, t_i^{-0.118} \qquad\qquad \textbf{4.8}$$

Further, the creep coefficient can be used to predict the modulus of elasticity of concrete as function of time-dependent effects. Equation 4.9 defines the effective modulus of elasticity as described in Article 5.14.2.3.6 (AASHTO, 2007).

$$E_{eff} = \frac{E_{ci}}{1 + \psi(t, t_i)} \qquad\qquad \textbf{4.9}$$

Moreover, the changing in the concrete stress due to time-dependent effect can be estimated by knowing the effective modulus at the time of interest.
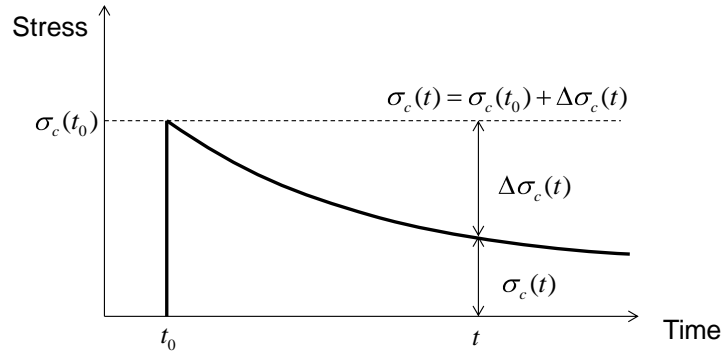
Figure 4-13. Gradual reduction of stress over time.

The shrinkage strain ε_{SH} assumed only to occur at the two inches closure region can be determined by Equation 4.10 as defined in Article 5.4.2.3.3 of AASHTO. Although, the model was calibrated and developed to predict the shrinkage strain of concrete, the model had shown great agreement in prediction the final strain in the grouted closure region.

$$\varepsilon_{SH} = 510 \times 10^{-6} k_s k_{hs} k_{td} \qquad \textbf{4.10}$$

Shrinkage is affected by aggregate characteristics and proportions, average humidity at the bridge site, W/C ratio, type of cure, volume to surface area ratio of member, and duration of drying period. It can assumes values from nearly nil to 0.0008 for thin sections made with high shrinkage aggregates and sections that are not properly cured (AASHTO, 2007).

The following values were determined based on the test specimen dimensions, amount of prestressing, location where the concrete was made and concrete material properties. These values were used as input values to estimate the creep coefficient and strain, concrete effective modulus, and shrinkage strain.

Table 4.5. Input values for creep and shrinkage calculation

		Concrete (precast panels)	Grout (closure region)
V/S	=	2.38 in	1.5 in
H	=	70 %	70 %
f'_{ci}	=	8 ksi	6 ksi
t	=	0-3650 days	0-3650 days
t_i	=	43 days	14 days

Table 5.6 shows the creep coefficient and the concrete effective modulus prediction for different days.

Table 4.6. Creep coefficient and effective modulus prediction.

	Concrete		Grout		
Time	$\psi(t,t_i)$	E_{eff}	$\psi(t,t_i)$	E_{eff}	ε_{SH}
Days	-	ksi	-	ksi	με
0	0.000	5422	0.000	4696	0
1	0.085	4997	0.152	4078	-14
3	0.153	4702	0.270	3697	-41
7	0.235	4392	0.405	3341	-86
14 (1w)	0.325	4092	0.546	3038	-147
28 (4w)	0.440	3767	0.706	2752	-228
60 (2m)	0.589	3412	0.894	2479	-323
63	0.600	3390	0.906	2464	-329
180 (3m)	0.816	2986	1.148	2186	-428
365 (1y)	0.941	2794	1.284	2056	-466
730 (2y)	1.037	2661	1.389	1965	-487
1825 (5y)	1.126	2550	1.490	1886	-501
3650 (10y)	1.171	2498	1.542	1847	-505

The results based on the prediction model are further compared in order to validate the

models. Figure 4-14 shows the strain results obtained from the experiment and the predicted

values using creep model. It is observed a very good agreement between the calculated and measured values.
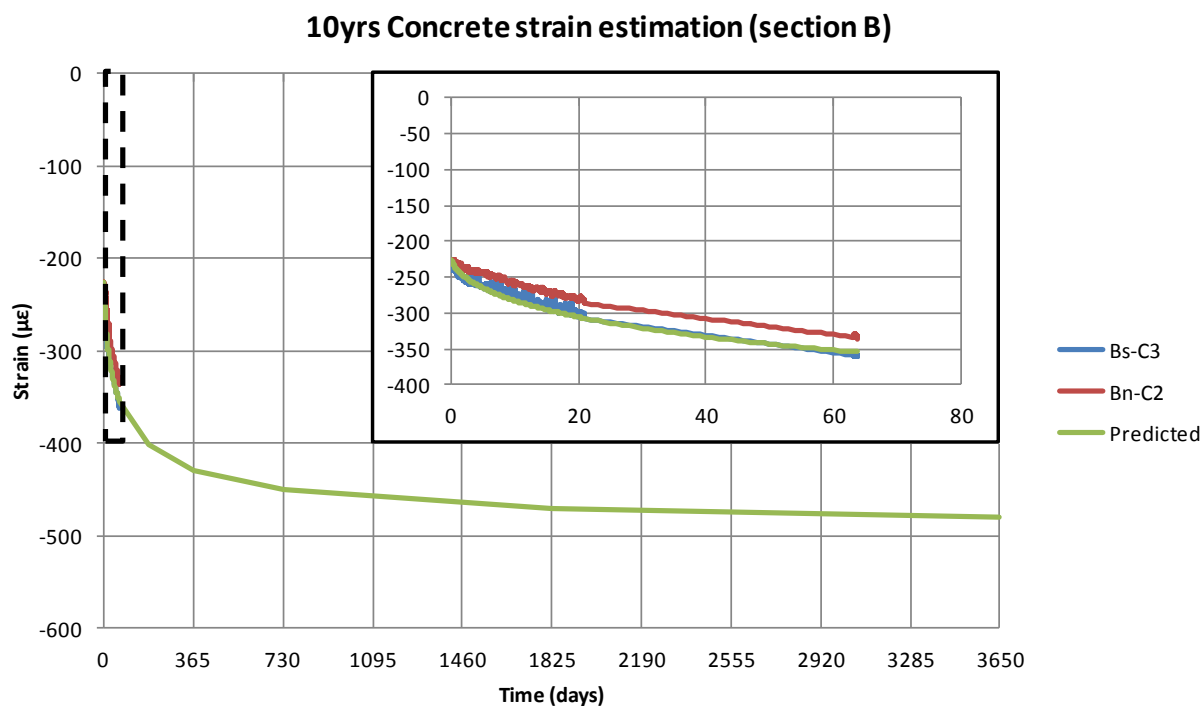
Figure 4-14. Concrete strain at section B - 10 years prediction.

Similarly, the creep model was used to predict the concrete strain at the interior support region (section D). At this section, the prestress force applied to the deck surface was twice as much as in the mid-span section. It is observed in Figure 4-15 a small divergence between the measured strain and the predicted values. Besides the difference, the model is considered suitable since in this case conservatively predicts the time-dependent effect in concrete.

10 yrs Concrete strain estimation (Section D)
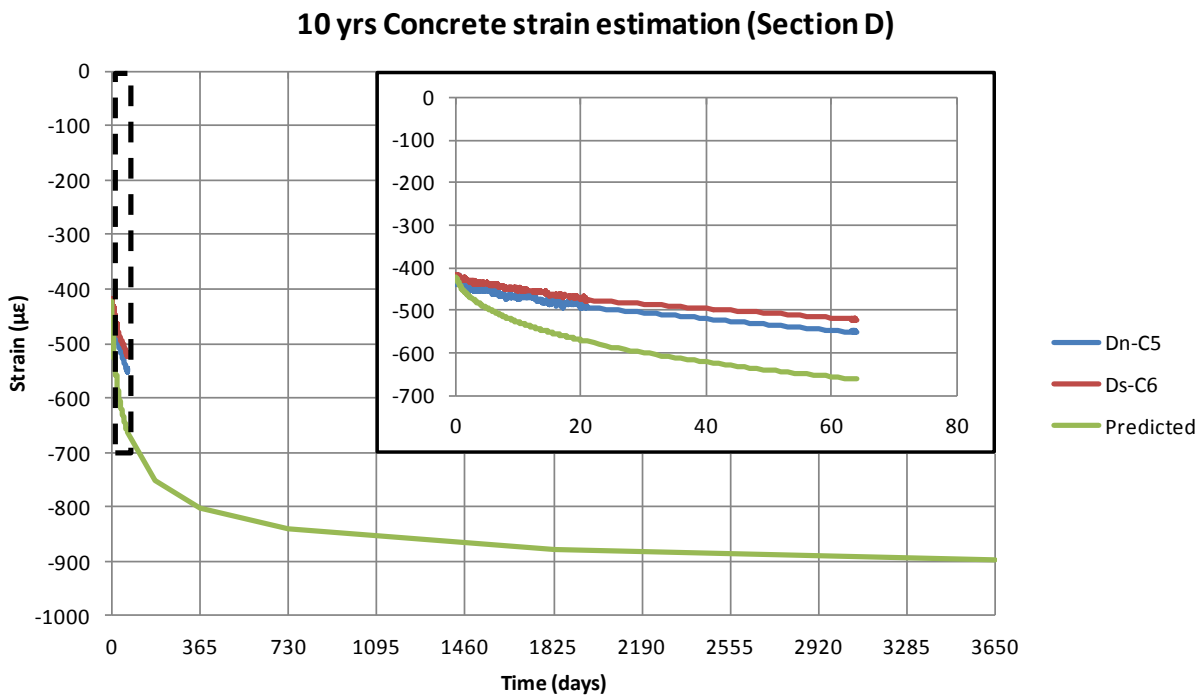
Figure 4-15. Comparison between measured concrete strain and predicted values.

Although, the prediction model was developed based on concrete specimen, the model was capable to predict the grout strain. Figure 4-16 shows the strain measurements at the grout region and the predicted values.

10 yrs Grout strain estimation (Section D)
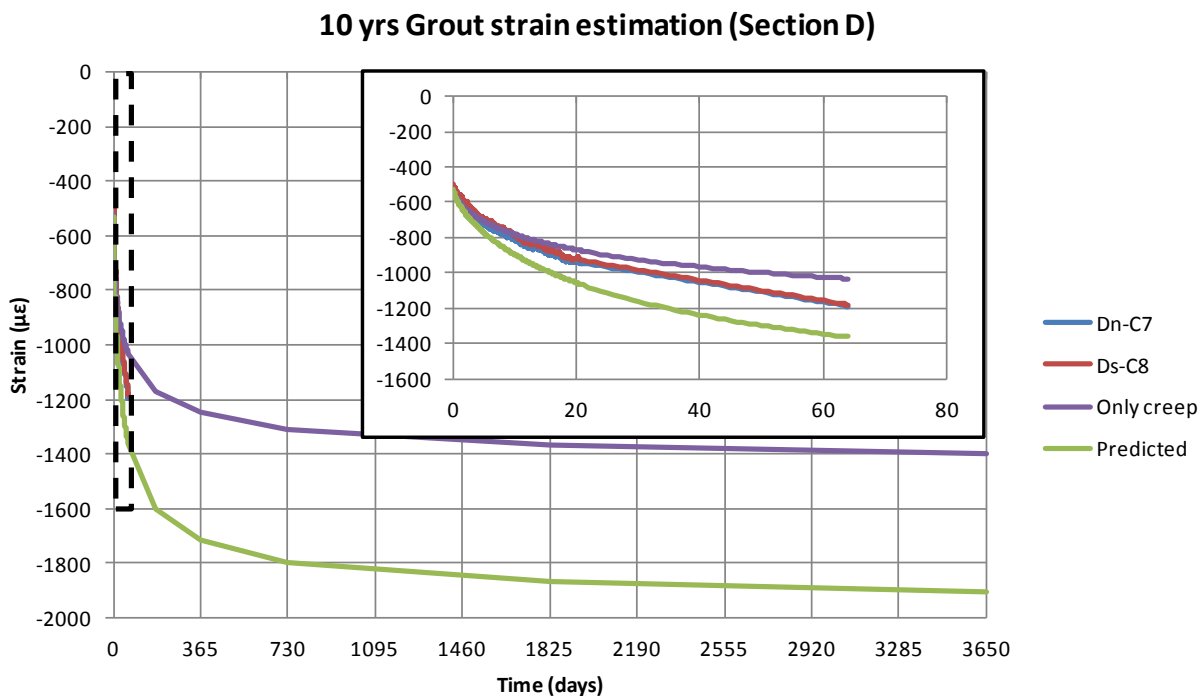
Figure 4-16. Comparison between measured grout strain and predicted values.

Based on the comparison between the predicted model and the measured values, it can be concluded that AASHTO model conservatively predicts the strain variation due to the time-dependent effect. Also, the initial assumption that the strain variation was caused only by the creep effect was verified.

4.4.2.2   *Steel section analysis*

Figure 4-17 shows the strain variation measured on the steel girder at mid-span (section B). It can be observed a decreasing in the strain measurements due to time-dependent effect (concrete creep). In average, the mid-span section had a $\Delta\varepsilon = -105\mu\varepsilon$ which is equivalent to a stress reduction of approximately 3 ksi at girder cross-section.

Steel strain variation at Section B
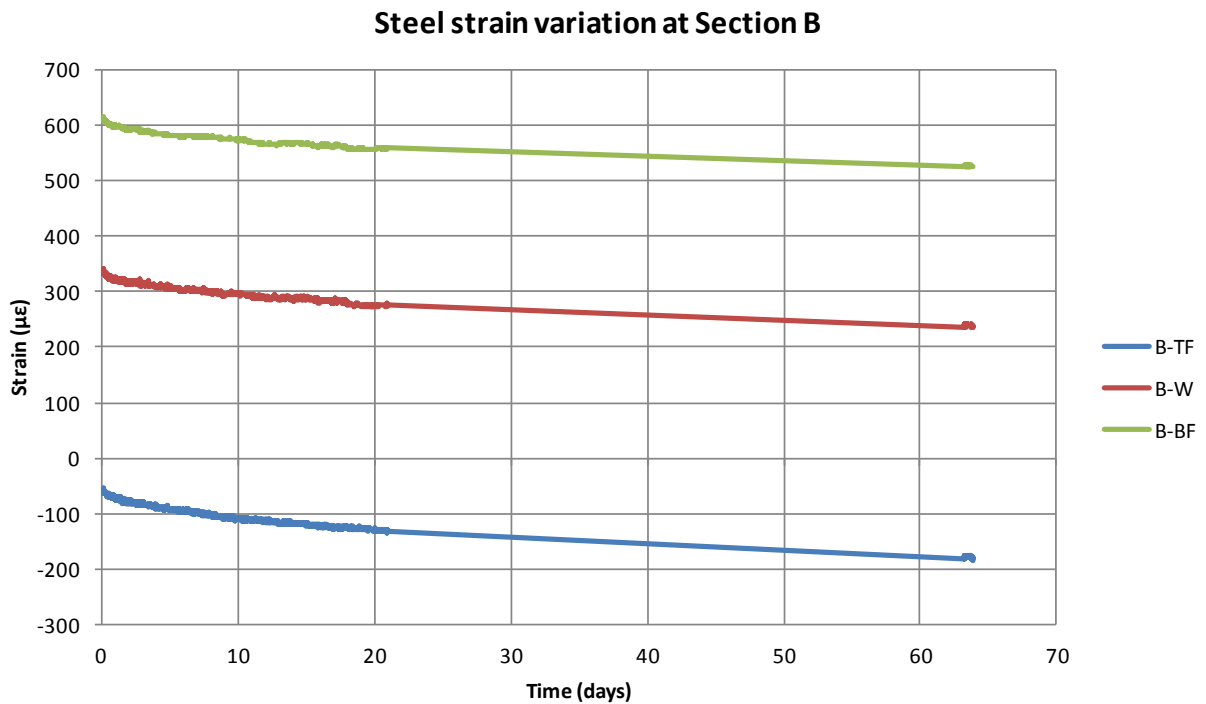
Figure 4-17. Stress at girder bottom flange due to time-dependent effect.

Figure 4-18 shows the strain variation measured on the steel girder at interior support region (section D). It can be observed a decreasing in the strain measurements due to time-dependent effect (concrete creep). In average, the interior support section had a $\Delta\varepsilon = -210\mu\varepsilon$ which is equivalent to a stress reduction of approximately 6 ksi at girder cross-section.

As expected, since the concrete creep is dependent of the amount of stress applied, the stress variation is more pronounced at section close to the interior support than in section near the ends.

Steel strain variation at Section D
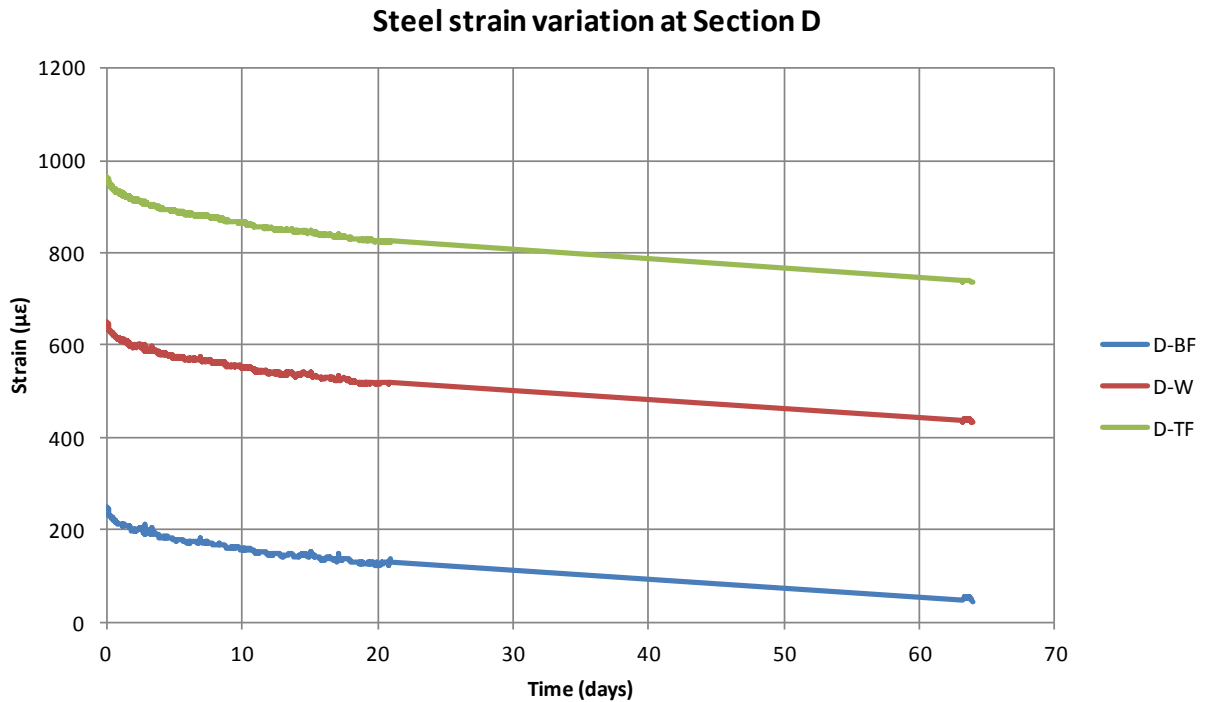
Figure 4-18. Stress at girder top flange due to time-dependent effect

Additional strain measurements at other sections of the test specimen are provided in the Appendix B.

4.4.2.3   *Time-dependent analysis*

The short- and long-term analyses were carried out using the AEMM (Gilbert R. I., 1988) & (Gilbert & Ranzi, 2001). Figure 4-19 show very good agreement between the predicted and measured results. Due to the time-dependent effect, additional compressive stress was induced in the steel girder.

Figure 4-20 shows the comparison between the short- and long-term at the girder top flange. The AEMM for this particular analysis did not predict well the stress at the girder.

Stress at girder bottom flange
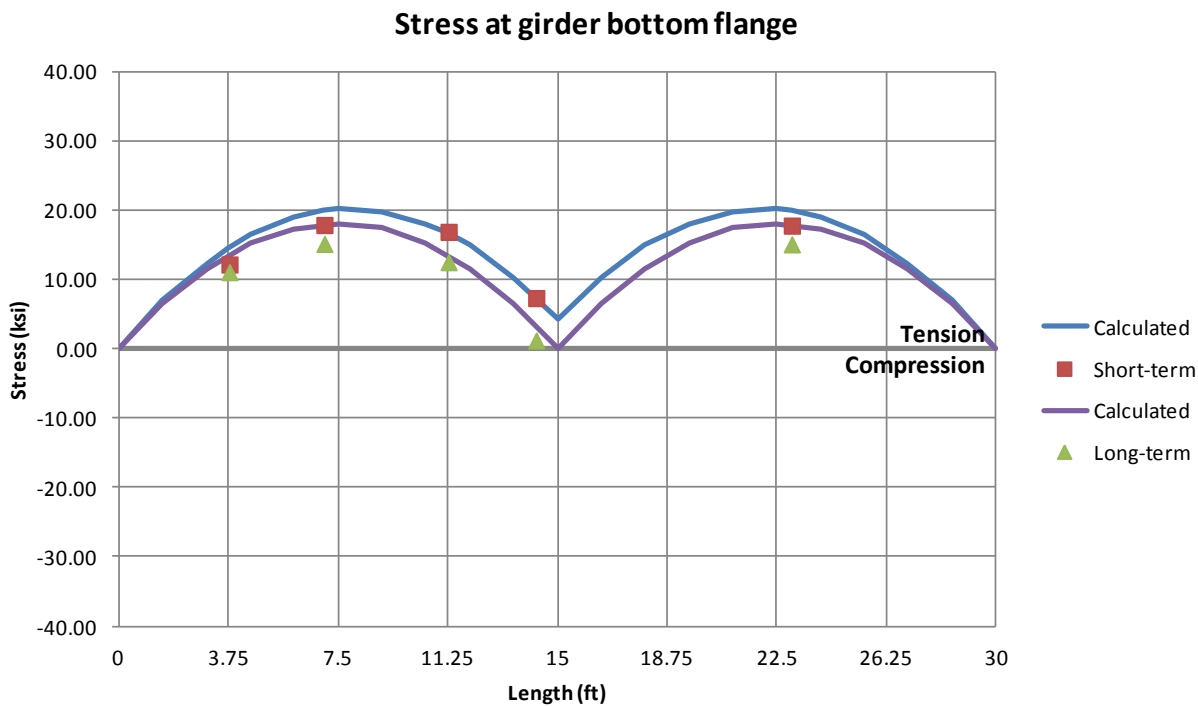
Figure 4-19. Stress variation girder bottom flange due time-dependent effect.

Stress at girder top flange
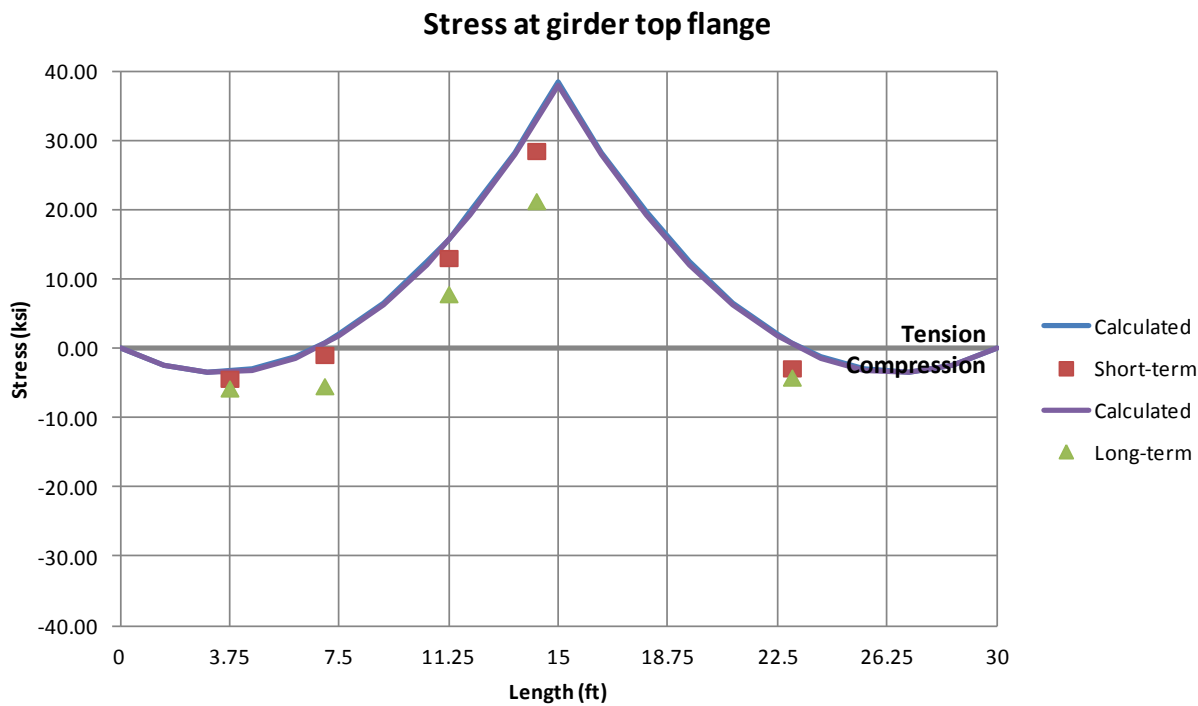
Figure 4-20. Stress variation girder bottom flange due time-dependent effect.

Based on the time-dependent analysis, it was estimated a 30% of precompression loss after the time-dependent effect, i.e., the maximum compressive stress was reduced from 2.3 ksi to approximately 1.6 ksi.
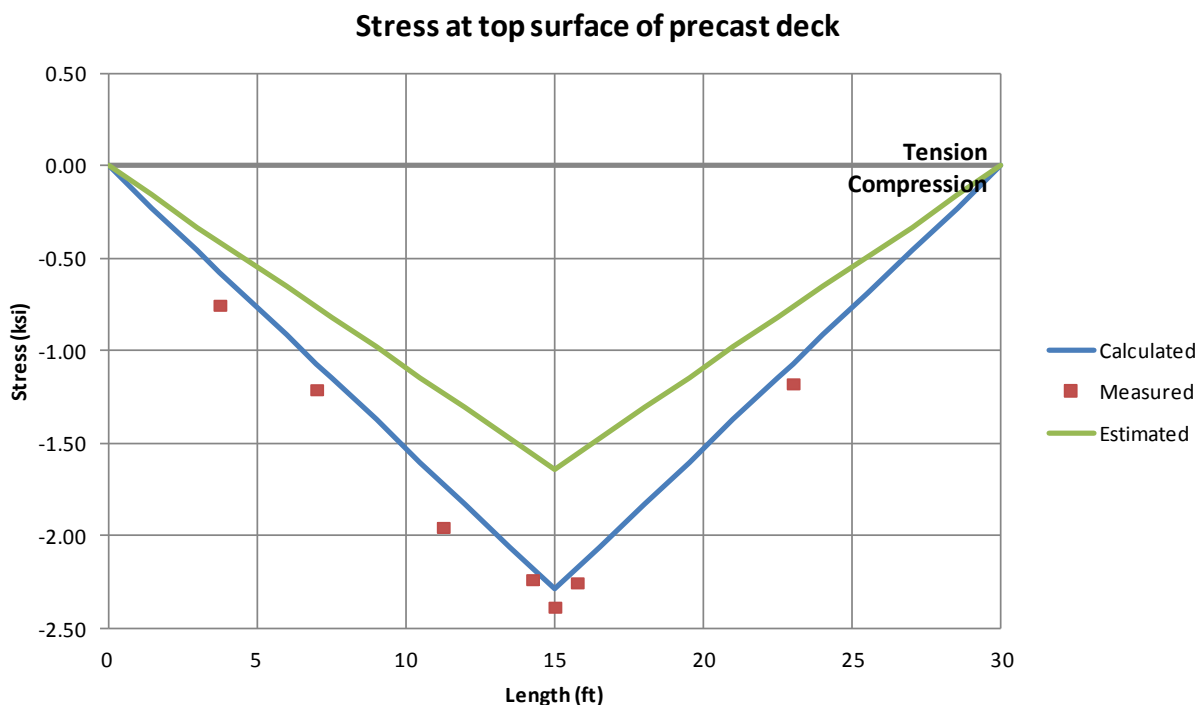
Figure 4-21. Estimation of final compressive stress.

In Appendix D is provided the short- and long-term analysis considering the AEMM. The ultimate test results are discussed in next section.

4.5 Ultimate load testing

The ultimate load testing was conducted to determine the mode of failure of the self-stressing bridge. The test was conducted by applying two point loads, one on each span, at mid-span.

Figure 4-22 provides an overview of the entire ultimate loading test. The test took a little over 3 hours to be completed. Initially, a preload test was conducted in order to check whether or not all the instrumentations (gauges and potentiometers) were working properly (1). After

checking the equipment the ultimate load test was started. The main load stage took about 1.5 hours be completed (2). During this load stage, it was observed yield of steel at girder bottom flange at mid-span. The ultimate load testing was temporally stopped because some irregularity at one of the end supports (3). The test specimen was fully unloaded and the support was fixed (4). After a 30 minute break, the test was resumed and the load was once again applied to the specimen. The maximum load experienced by the bridge was 230 kips. At this point, the girder bottom flange at interior support start to yield and also web and flange buckle was observed. The maximum capacity of the bridge cross-section was finally reached after concrete crushing. A sudden drop in load was observed (5). After the bridge failure, a good amount of ductility in the system was observed.
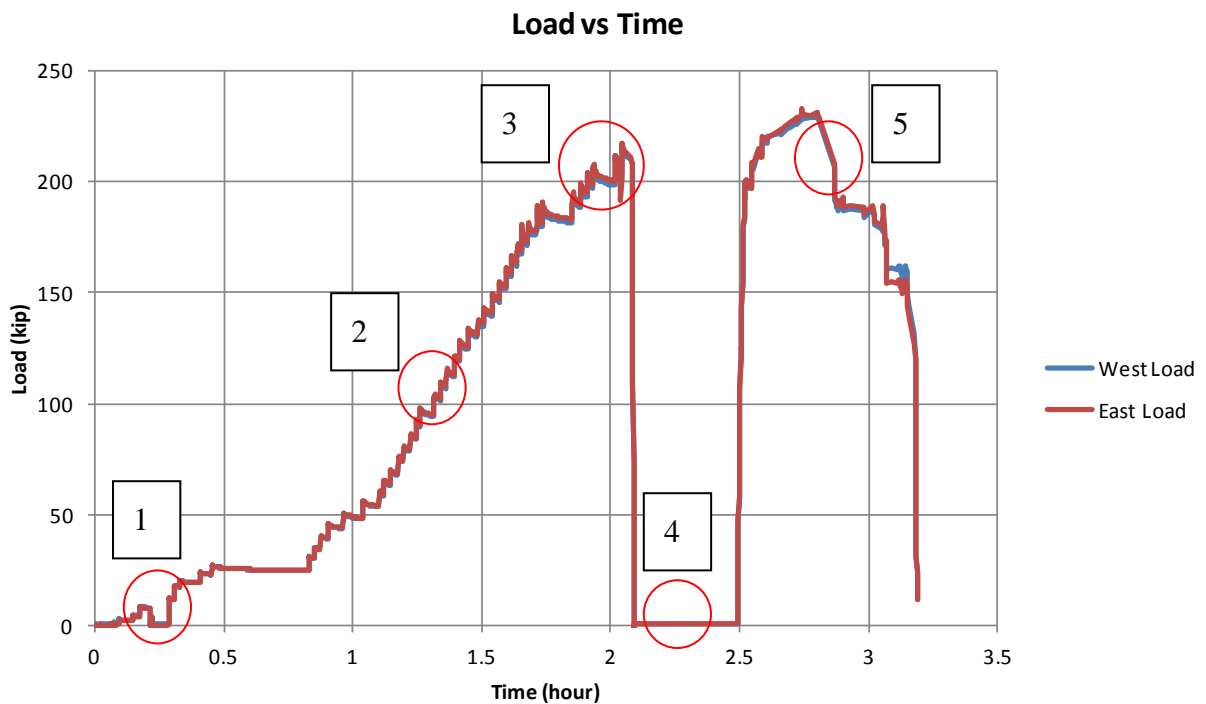
Figure 4-22. Load development during the ultimate load test

4.5.1   Steel strain analysis

The study of the steel strain is discussed in this section. This analysis will provides in-depth understanding on how the bridge using the self-stressing method behaves under service load. The strain analyses will be performed in two critical sections. The first section is the bridge mid-span where the maximum positive moment is located. The other critical section is located over the interior support where the maximum negative moment is located. Additional strain measurements are provided in the Appendix B.

For the case of positive moment, the girder bottom flange often reaches stress close to the yield stress. Therefore, bridge engineers must design the bridge so that this critical section does not reach yield stress under service load.

For the negative moment region, the girder is susceptible to bucking since the bottom flange is subjected to compressive stresses. Consequently during the conventional bridge design, bridge engineers are often required to increase the steel cross-section in order to overcome this issue. Since the bucking capacity is often less than yielding capacity and the absolute value of negative moment in continuous bridge is always greater than the positive moment, the interior support region is considered to be the most critical section during the conventional bridge design.

However, when a bridge is designed using the self-stressing method. The stresses at bottom flange around interior support are reduced which is a great advantage in term of bridge design and safety. Also, by considering the method, one single beam cross section may be used which reduces the steel cost and the additional cost and labor required by the steel splices.

4.5.1.1   Mid-span section

The first sections of the bridge analyzed are section B and F. Each are located at mid-span, one on west span and the other on east span, respectively. A total of eight and five steel strain gauges were installed in section B and F, respectively.

Figure 4-23 shows the strain readings in the both sections B & F measured by the gauges installed on the girder bottom flange. It can be observed a great symmetrical behavior of the bridge as all the strains are clustered together during initial loading stage. When the load value reaches approximately 110 kip, the girders bottom flange start to yield by meeting the yield line (1). The yield point is defined as the steel yield stress divided by steel modulus of elasticity, i.e. $\varepsilon_{yield} = \sigma_y / E_s = 50 ksi / 29000 ksi = 1724 \times 10^{-6}$. It can be observed that west span yields first than east span. As the load keeps increasing, the strain grows quickly reaching values greater than 3000 με which is the maximum range of the strain gauges. Values beyond that are considered unreliable (2). Although, the bottom flange had yield, the bridge still carry the load reaching a maximum loading of 215 kips which is 2 times more the load at yield point (3). The unloading was performed to fix the support and later resumed. Even though, after the steel had yield in most of the girders mid-span, the bridge was capable of carrying more load reaching a maximum of 230 kips. At this point concrete crushes and the test was finalized.
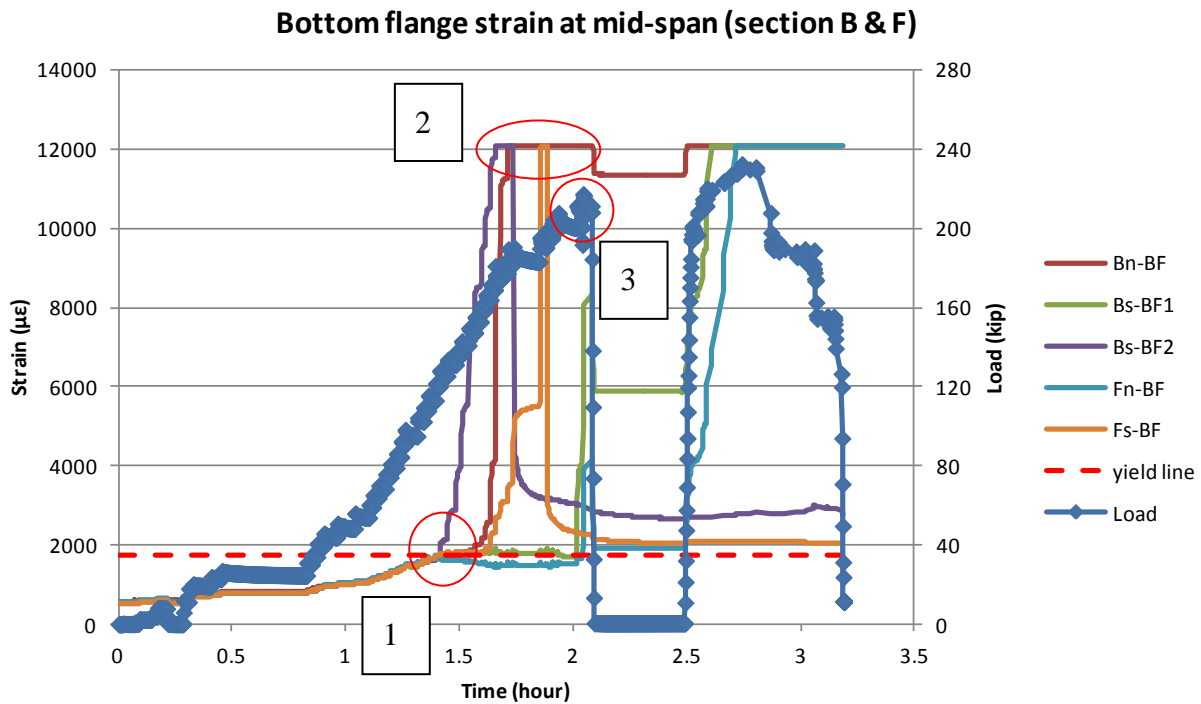
Figure 4-23. Bottom flange steel strain at mid-span during ultimate load

Due to the doubly symmetry of the test specimen, Figure 4-24 only shows the strain measurements in section B of south girder. It can be seen that after the bottom flange yields, the gauge located in the mid-height of the girder only reach the yield line after the load levels close to 160 kips (1). Further, with the increasing of loading, the top flange strain reached values close to yield point before the concrete crushes dropping the load (2). Base on this observation, it is correct to say that steel cross-section fully plasticizes. Thus, the assumption of full plastification of steel beam during the estimation of ultimate capacity of composite steel-concrete sections hold true. Hence, the self-stressing method did not change the bridge response.
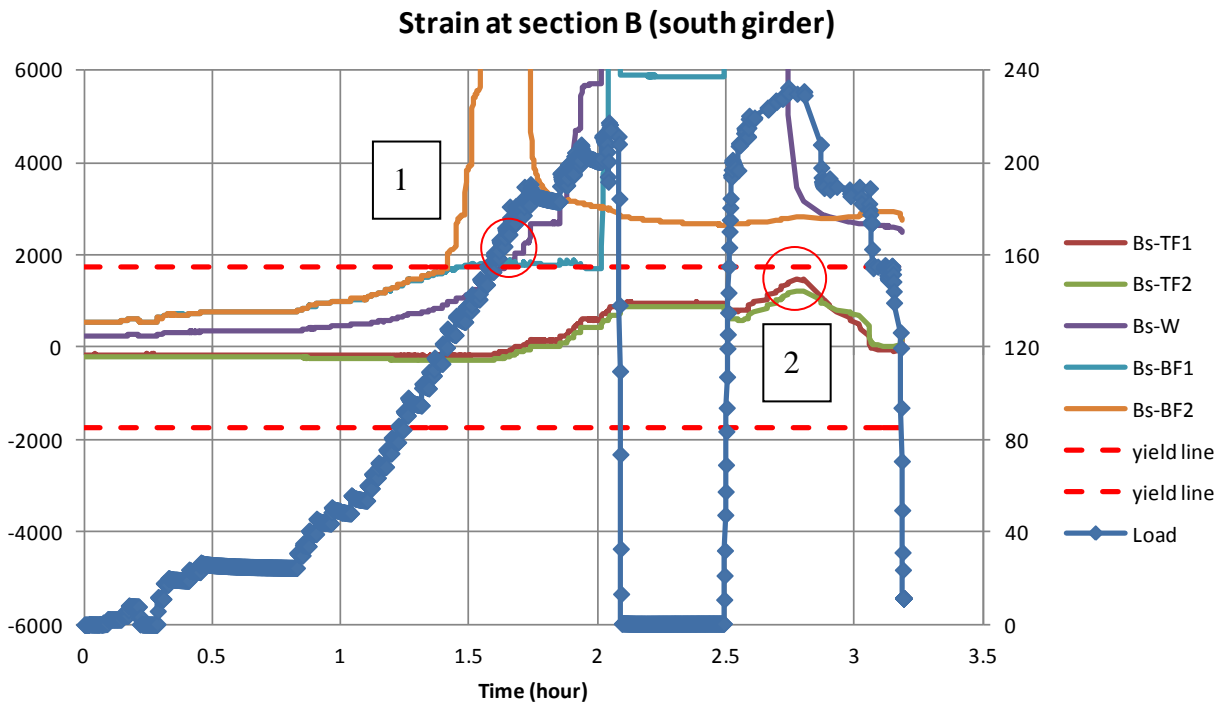
Figure 4-24. Steel strains at mid-span of south girder during ultimate load

4.5.1.2   *Interior support section*

The region around the interior support is here analyzed. The section D in test specimen refers to the instrumentation installed in the vicinity of interior support. A total of eight steel strain gauges were installed in this region.

Figure 4-25 shows the strain measurements at the girder bottom flange. As expected, the self-stressing method had reduced the demand in the negative region. For the same loading level of 110 kip (bottom flange at mid-span had yield), the strain in bottom flange did not reach the yield line (1). As the load increases to values of 215 kip, the strains are close to yield line but not plastic deformation is observed since the strain comes back to its initial values after unloading (2). Further, after resetting the support, the load is increased reaching the ultimate load of 230 kip and finally making the bottom flange of the interior region to yield (3).
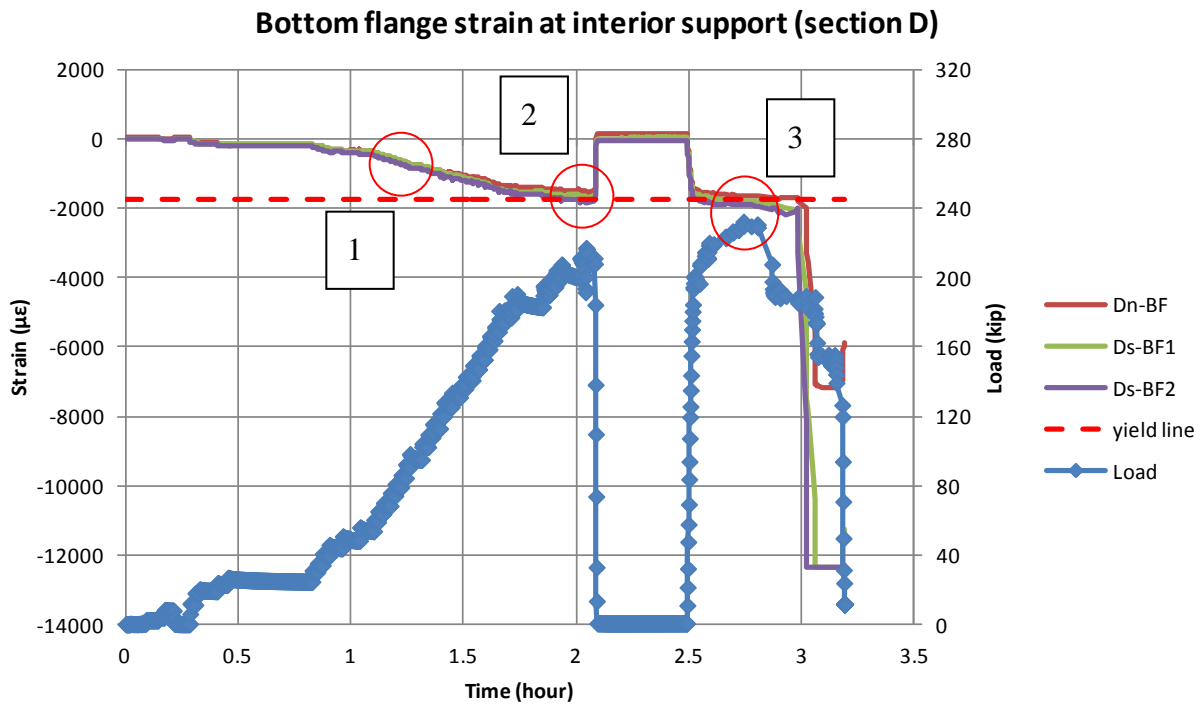
Figure 4-25. Bottom flange steel strain at interior support during ultimate load

Similarly to section B discussion, Figure 4-26 only shows the strain measurements in section D of south girder. During the load stage 75 kip, it was observed that a crack developed over the closure region had fully propagated through deck thickness. As a result, the section properties at that location (initially composite) had its value decreased to the steel section properties (noncomposite). From this point on, the strain in both top and bottom increases proportional to each other (1). Also, the web strain goes to zero as the neutral axis of the section is now located in the mid-depth of the girder. Further, at load level at its maximum, the steel section fully plasticizes as noted by the strains measurement. Both top and bottom reaches the yield line in tension and compression, respectively (2). After concrete crush at mid-span, the strain in the web starts to increase to values beyond yield which characterizes web buckling (3).

Strain at section D (south girder)
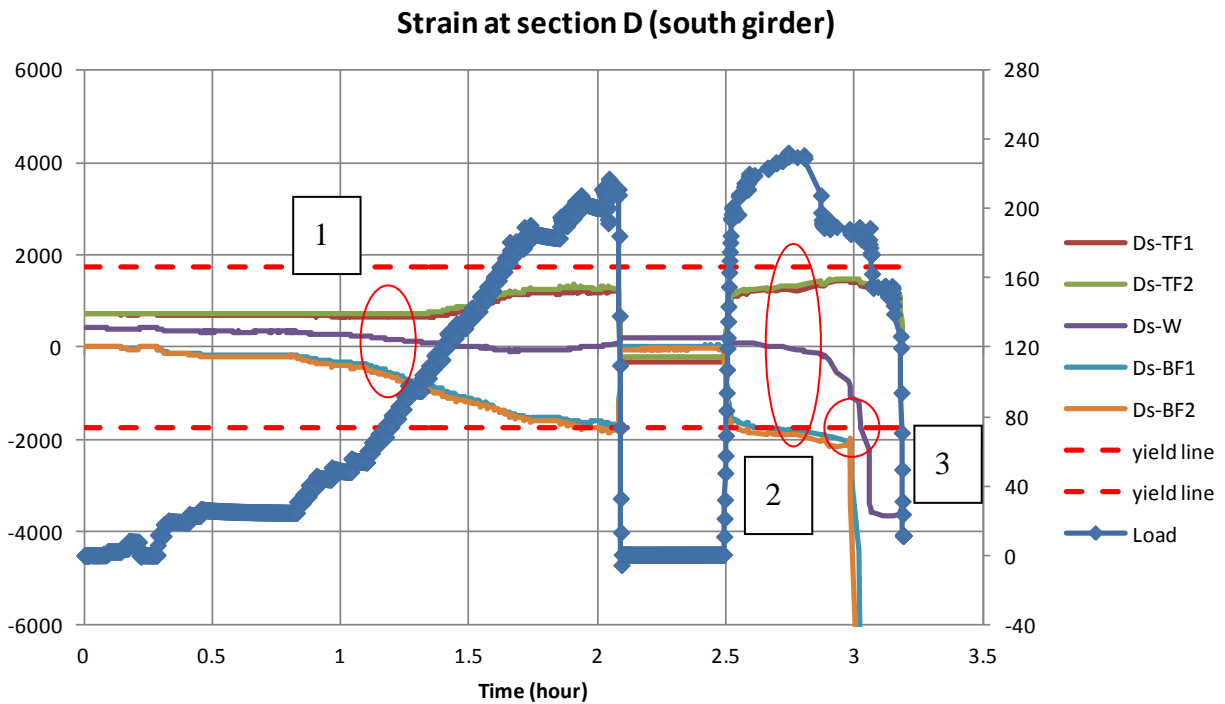
Figure 4-26. Steel strains at mid-span of south girder during ultimate load

4.5.2   Concrete strain analysis

The study of the concrete strain is discussed in this section. The analyzes of the test results play a important rule in better understanding how the bridge built using the self-stressing method technique behaves under service load. Similarly to the steel strain analyses, the concrete strain analysis will be performed in two critical sections. The first section is the bridge mid-span where the maximum positive moment is located. The other critical section is located over the interior support where the maximum negative moment is located.

For the case of positive moment, the concrete is subjected to maximum compressive force which may lead to concrete crushing under service load. Therefore, bridge engineers must design the bridge so that this critical section does not reach nominal concrete compressive strength under service load.

For the negative moment region, the concrete section is susceptible to tensile force that may lead to crack and further corrosion of reinforcement due to chloride intrusion. Consequently during the conventional bridge design, engineers are often required to increase the amount of reinforcement in order to meet both service and strength limit states and also the control crack width.

However, by considering the self-stressing method during the bridge designing, the corrosion and crack issues are mitigated, if not completely eliminated. The method provides a compressive force in the deck without any prestressing cable in which is susceptible to corrosion and further lost of prestress. Also, the compressive force enhances the concrete permeability by closing the crack which mitigates the corrosion of reinforcement.

4.5.2.1   Mid-span section

The first sections of the bridge analyzed are section B and F. Each are located at mid-span, one on west span and the other on east span, respectively. A total of two and one concrete strain gauges were installed in section B and F, respectively.

Figure 4-27 shows the strain readings in the both sections B & F measured by the gauges installed on the deck top surface. It can be observed a small different between the strains measured at east and west spans. This small discrepancy was already expected since in Table 3.5 different compressive strength was reported, thus different elastic modulus (1). Further in the test results, it is noted that before reaching the maximum load of 230 kip, the concrete strain in section B suddenly drop the due to concrete spalling. However the strain readings were very close to its maximum strain of 3000 micro strains which is a value commonly assumed as the ultimate compressive strain of concrete (2) (ACI Committee 318, 2008). At the maximum

loading stage of 230 kip, the strain on section F (east span) never reached the ultimate limit because the bridge failure happen in the west span due to concrete crushing (3).
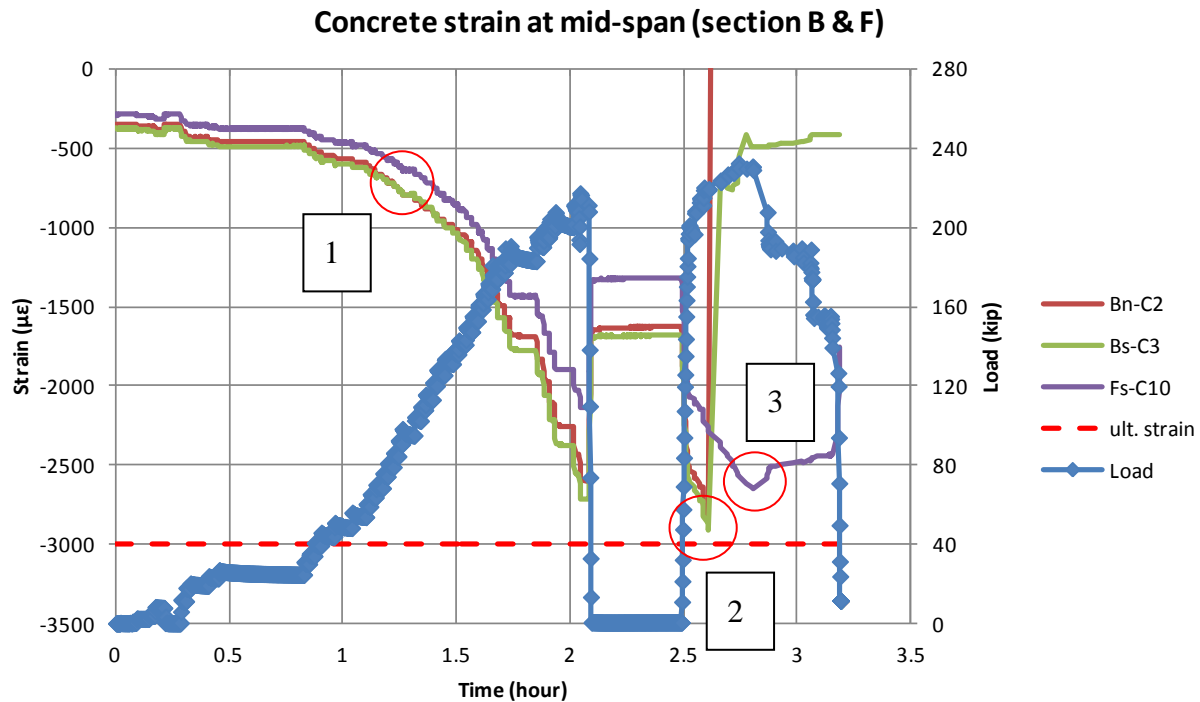
Figure 4-27. Concrete strain at mid-span during ultimate load

4.5.2.2   *Interior support section*

The region around the interior support is here analyzed. The section D in test specimen refers to the instrumentation installed in the vicinity of interior support. Figure 4-28 shows the strain measurements at top surface of concrete deck. Initially, it is observed a small discrepancy in the concrete strain gauge which is attributed to different concrete (material properties) used in each precast panel (1). In conventional bridge design, addition reinforcement would be considered to control (not eliminate) the cracks over the interior support region. However, the self-stressing method reduced the demand by inducing compressive stress in the deck. The crack at the closure region was only observed after reaching 43% of ultimate load. At this location no

reinforcement was considered. After the crack happen, the readings in both gauges C7 and C8 stop to change (2).
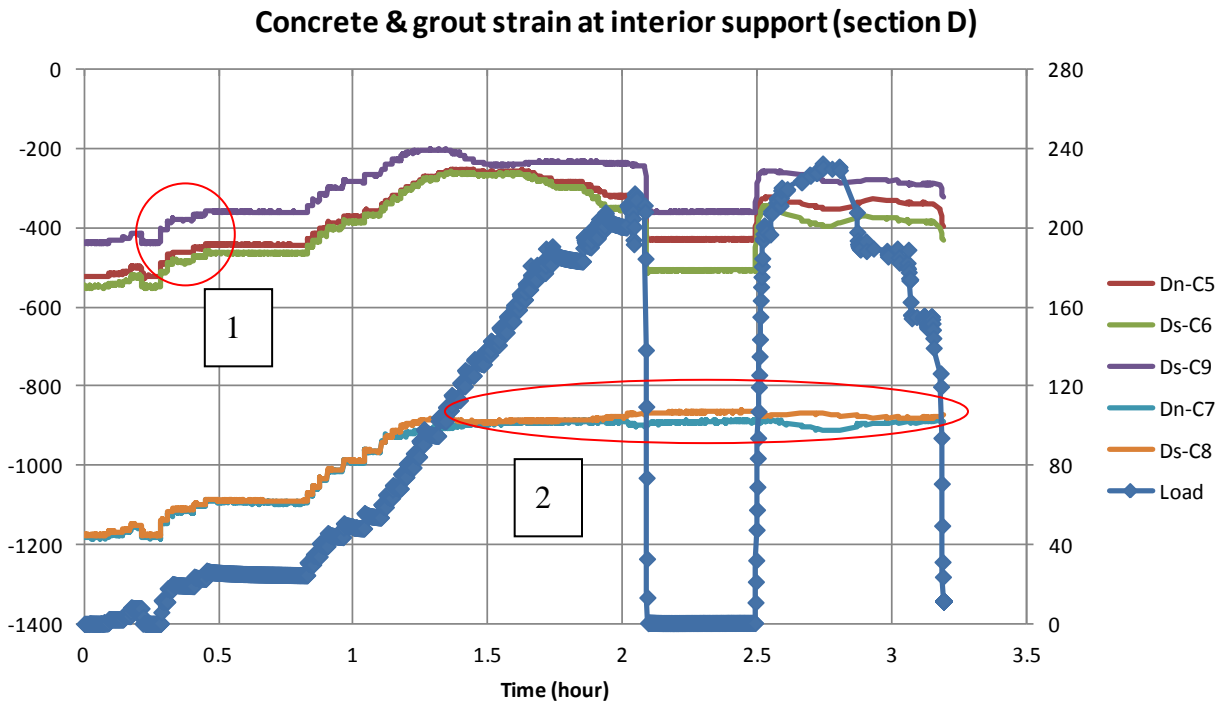
Figure 4-28. Concrete and grout strain at interior support region during ultimate load

In order to show the benefit of the precompress the deck, Figure 4-30 shows an estimation of cracking moment. (a) shows the stress analysis for a conventional construction with no deck precompression. (b) shows the stress analysis for a self-stressing construction. It can be noted that the required moment (force "P") to crack the deck at interior support was 3 times greater. In this calculation was assumed 40% of precompression loss to account for the time-dependent effects. Thus, a final compressive stress of 1.38 ksi $\left(2.3ksi \times 60\%\right)$ was assumed.

(a) Conventional method	**(b) Self-stressing method**
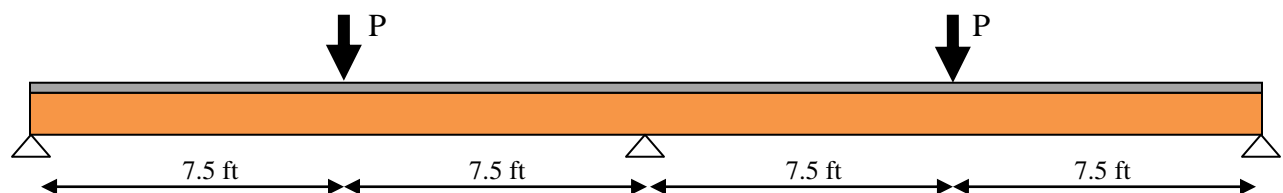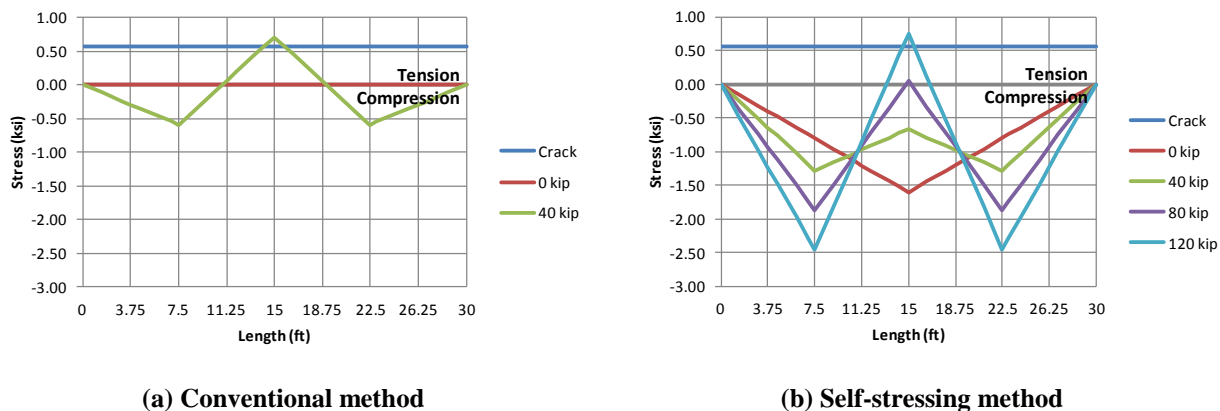
Figure 4-29. Stress analysis between conventional and self-stressing construction.

The ultimate capacity of the test specimen is discussed in the following section.

4.5.3　Ultimate Strength

The ultimate strength of the bridge built using the self-stressing method is here considered. Figure 4-30 shows the load-displacement curve of the self-stressing test specimen. It is observed that after 110 kip (0.3 inch) the test start to show nonlinear behavior due to the yield of girder bottom flange (1). The specimen showed some residual deformation (0.75 inch) after unloading stage to fix the support. Although, the girder had some plastic deformation, the slope during the reloading stage appears similar to the beginning of test (2). The specimen had a maximum loading capacity of 230 kip which corresponding twice of the linear elastic limit of 110 kip (3). The bridge shows great ductility by deforming 2.3 inches at 230 kip which is about 7 times more than the elastic deflection at 110 kip. Also, after concrete crushes, the specimen still carry load at a reduced level and very large deformation under goes the bridge (4). The maximum predicted ultimate capacity based on strain compatibly method was 217 kip.

Load-displacement curve
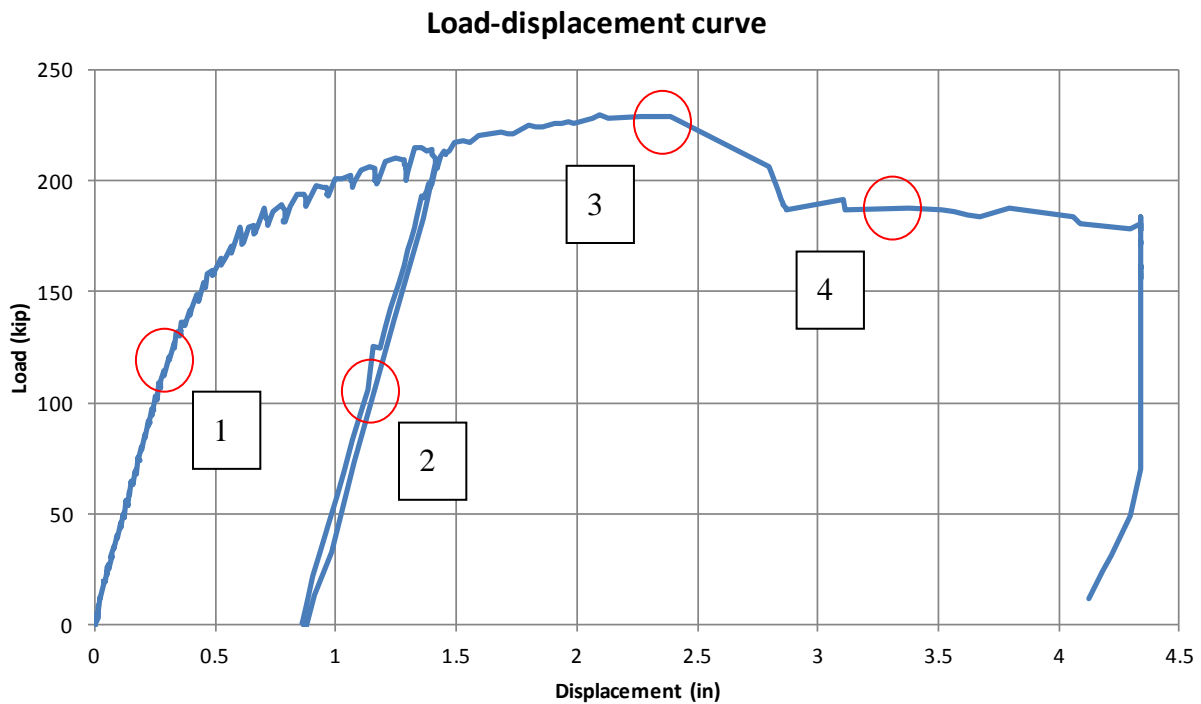
Figure 4-30. Load-displacement for ultimate load testing

4.5.3.1   Failure Modes

The modes of failures are here presented. Although, the bridge was constructed using an innovated method never used in practice, the modes of failures are identical to if the bridge were built using conventional method. Following are presented a list of observed failures:

1. Cracking in the vicinity of interior support;

2. Yielding of girder bottom flange (large deformation);

3. Combination of web and bottom flange buckling;

4. Concrete crushing;

All listed modes of failures are commonly observed in two-span continuous composite steel-concrete bridges.

Figure 4-31 shows the only tensile crack located at the closure region. Since steel reinforcement was not considered in this region, the crack width is much greater than if reinforcement were used to distribute the cracks.

Figure 4-31. Crack at the closure region due to tensile force over interior support

Figure 4-32 shows the final deformed shape of the bridge after the ultimate load testing. It is clearly visible the bridge had undergone large deformation due yielding of girder bottom flange.

Figure 4-32. Large deformation due to yielding of bottom flange at mid-span

Figure 4-33 shows a combination of web and flange local buckling observed over the interior bearing support.

Figure 4-33. Web and flange local bucking over interior support.

Figure 4-34 shows the crushed concrete after the bridge reaches its maximum load capacity.

Figure 4-34. Concrete crushing under the loading location at mid-span (west side).

Chapter 5

Finite Element Analyses

This chapter describes the development of the finite element (FE) model. The numerical simulation offers engineers a sophisticated approach to analyze bridges considering the three dimensional behavior. The numerical model was created based on the dimensions and material properties used in the test specimen and the numerical results were compared with the testing results in order to validate the finite element model.

5.1 General considerations

The general purpose finite element program, ABAQUS, is a highly sophisticated software designed primarily to model the behavior of solids and structures under externally applied loading. ABAQUS main features include:

- Capabilities for both static and dynamic problems;

- The ability to model very large shape changes in solids, in both two and three dimensions;

- A very extensive element library, including a full set of continuum elements, beam elements, shell and plate elements, among others;

- A sophisticated capability to model contact between solids;

- An advanced material library, including the usual elastic and elastic-plastic solids; models for foams, concrete, soils, piezoelectric materials, and many others;

- Capabilities to model a number of phenomena of interest, including vibrations, coupled fluid/structure interactions, acoustics, buckling problems, and so on.

Although, finite element based software offers many capabilities to the users. A reliable numerical model should be able to predict both global behavior (such as load deflection) and local responses (such as local strains and stresses) consistent with results obtained experimentally. In general, numerical models produce results that are very much dependent on the assumptions made during analysis. For instance, assumptions related to the type of stress-strain curve, boundary conditions, element type, and other factors could potentially alter significantly the numerical results.

The following sections will be presented general information regarding the constitutive models, element type and boundary condition considered while creating the FE model.

5.1.1   Material Model

The material library in ABAQUS includes many different constitutive models to model a variety of materials. This section will be covered briefly the material model and the input data used.

5.1.1.1   Concrete model

The model used to predict the concrete response is known as CONCRETE DAMAGE PLASTICITY (ABAQUS, 2010). The model is a continuum, plasticity-based, damage model for concrete. It assumes that the main two failure mechanisms are tensile cracking and compressive crushing of the concrete material. The evolution of the yield (or failure) surface is controlled by two hardening variables, the tensile $\tilde{\varepsilon}_t^{pl}$ and compressive $\tilde{\varepsilon}_c^{pl}$ equivalent plastic strains, linked to failure mechanisms under tension and compression loading, respectively.

The main attributes of the concrete damaged plasticity model in Abaqus/Standard and Abaqus/Explicit are:

- Provides a general capability for modeling concrete and other quasi-brittle materials in all types of structures (beams, trusses, shells, and solids);

- Uses concepts of isotropic damaged elasticity in combination with isotropic tensile and compressive plasticity to represent the inelastic behavior of concrete;

- Can be used for plain concrete, even though it is intended primarily for the analysis of reinforced concrete structures;

- Can be used with rebar to model concrete reinforcement;

- Is designed for applications in which concrete is subjected to monotonic, cyclic, and/or dynamic loading under low confining pressures;

- Consists of the combination of nonassociated multi-hardening plasticity and scalar (isotropic) damaged elasticity to describe the irreversible damage that occurs during the fracturing process;

- Allows user control of stiffness recovery effects during cyclic load reversals;

- Can be defined to be sensitive to the rate of straining;

- Can be used in conjunction with a viscoplastic regularization of the constitutive equations in Abaqus/Standard to improve the convergence rate in the softening regime;

- Require that the elastic behavior of the material be isotropic and linear.

Figure 5-1 shows the uniaxial behavior of plain concrete based on the damaged plasticity constitutive model.

(a) compression **(b) tension**
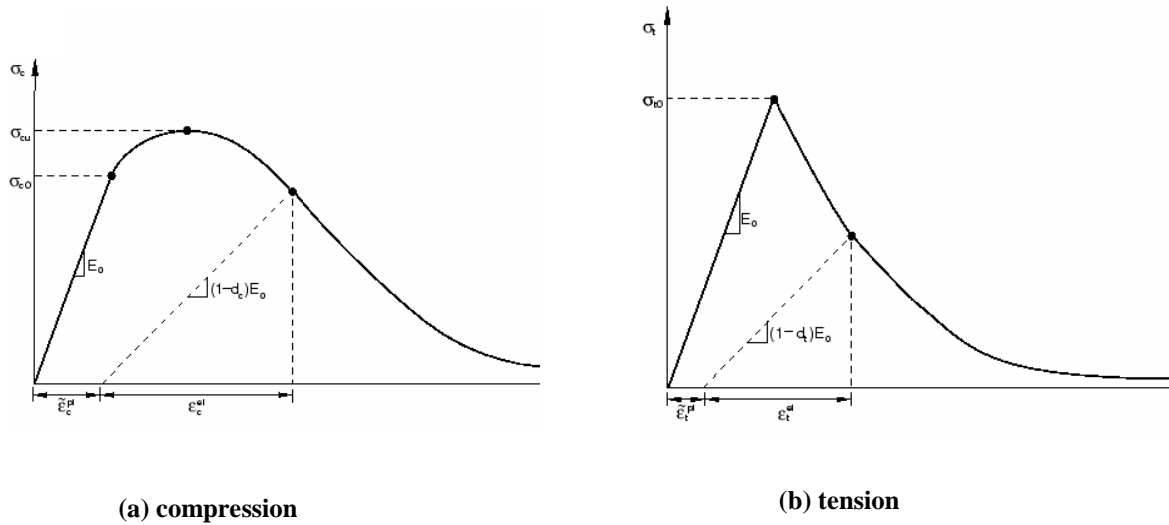
Figure 5-1. Uniaxial behavior of plain concrete for damaged plasticity model.

The following concrete material properties were assumed in the FE model.

Concrete density $\quad = \quad \gamma_c = 0.150 kcf$

Modulus of elasticity $\quad = \quad E_c = 33000 \gamma_s^{1.5} \sqrt{f_c'} = 5422 ksi$

Concrete strength $\quad = \quad f_c' = 8 ksi$

Tensile strength $\quad = \quad f_t = 0.23\sqrt{f_c'} = 0.65 ksi$

Since the only material testing considered was the compressive strength of concrete. Other concrete properties required by the concrete damage plasticity were estimated. Equation 5.1 and 5.2 define the concrete model used to estimate the stress-strain curve for concrete under uniaxial compression and tension, respectively (CEB-FIP, 1993).

$$\sigma_c \ \varepsilon_c \ = \frac{0.85 f_c' \left[6193.6 \ 0.85 f_c' + 1.015 \ ^{-0.953} - 206000\varepsilon_c \right] \varepsilon_c}{1 + \left[8074.1 \ 0.85 f_c' + 1.450 \ ^{-1.085} - 850 \right] \varepsilon_c} \tag{5.1}$$

and

$$\sigma_t \ \varepsilon_t \ = f_t e^{-19500\left(\varepsilon_t - \frac{f_t}{E_c} \right)} \tag{5.2}$$

NOTE: US customary units.

Table 5.1 present the input data assumed in the FE model.

Table 5.1. Concrete input in FE model (ABAQUS)

Compression		Tension	
$\sigma_{compression}$	ε_c^{pl}	$\sigma_{tension}$	ε_t^{pl}
ksi	**-**	**ksi**	**-**
3.40	0	0.65	0
3.95	0.000065	0.44	0.000059
4.68	0.000200	0.30	0.000105
5.31	0.000315	0.20	0.000143
5.83	0.000411	0.14	0.000175
6.23	0.000485	0.09	0.000203
6.52	0.000539	0.06	0.000228
6.70	0.000571	0.04	0.000252
6.75	0.000582		
6.69	0.000570		
6.51	0.000536		
6.19	0.000478		
5.75	0.000397		
5.18	0.000292		
4.48	0.000162		

In addition, the default values recommended by ABAQUS documentation were used in order to fulfill the model input data (ABAQUS, 2010).

$$\text{Dilation angle} \quad = \quad \psi(\theta, f_i) = 36^o$$

$$\text{Ratio of biaxial/uniaxial} \quad = \quad \sigma_{b0}/\sigma_{c0} = 1.16$$

$$\text{Flow eccentricity} \quad = \quad \varepsilon(\theta, f_i) = 0.1$$

$$\text{Ratio of second invariant} \quad = \quad K_c = 0.667$$

$$\text{Viscoplastic regularization} \quad = \quad \varepsilon_v^{pl} = 0$$

5.1.1.2   Steel Model

The model used to predict the steel plastic response is known as PLASTICITY (ABAQUS, 2010). This model uses standard Mises or Hill yield surfaces with associated plastic

flow. The model is adequate for common applications such as crash analyses, metal forming, and general collapse studies; the models are simple and adequate for such cases.

The main attributes of the classical metal plasticity model are:

- use Mises or Hill yield surfaces with associated plastic flow, which allow for isotropic and anisotropic yield, respectively;

- use perfect plasticity or isotropic hardening behavior;

- can be used when rate-dependent effects are important;

- are intended for applications such as crash analyses, metal forming, and general collapse studies

- can be used in any procedure that uses elements with displacement degrees of freedom;

- can be used in a fully coupled temperature-displacement analysis or an adiabatic thermal-stress analysis that plastic dissipation results in the heating of a material;

- must be used in conjunction with either the linear elastic material model or the equation of state material model.

The four tensile testing results were used as input data for the model. Since ABAQUS require the input of true stress-strain data, Equation 5.3 was used. The equation holds true for values below the maximum engineering stress (prior to necking effect). As the simulation will never reach high values of stress, the equation can be used.

$$\varepsilon_{true} = \ln(1 + \varepsilon_{eng})$$
$$\sigma_{true} = \sigma_{eng}(1 + \varepsilon_{eng})$$

5.3

where

$\sigma_{true}, \varepsilon_{true}$ = True stress and true strain, respectively

$\sigma_{eng}, \varepsilon_{eng}$ = Engineering stress and engineering strain, respectively

Table 5.2 provides true stress and true strain values used.

Table 5.2. Steel input in FE model (ABAQUS)

Steel		
σ_{true}	ε_{true}	ε_{true}^{pl}
ksi	**-**	**-**
0	0	-
25	0.00086	-
50	0.00172	0
51	0.02175	0.019988
55	0.02551	0.023614
60	0.03609	0.034017
65	0.05030	0.048063
70	0.07048	0.068069
75	0.10128	0.098695
80	0.15069	0.14793

In addition to the stress and strain input data, the following material properties were also used in FE model.

Steel density $= \gamma_s = 0.490 kcf$

Modulus of elasticity $= E_s = 29000 ksi$

5.1.2 Element Type

The three different element types are briefly discussed in this section. Figure 5-2 shows the three element type considered.

(a) Truss Element   **(c) Shell Element**   **(d) Solid Element**
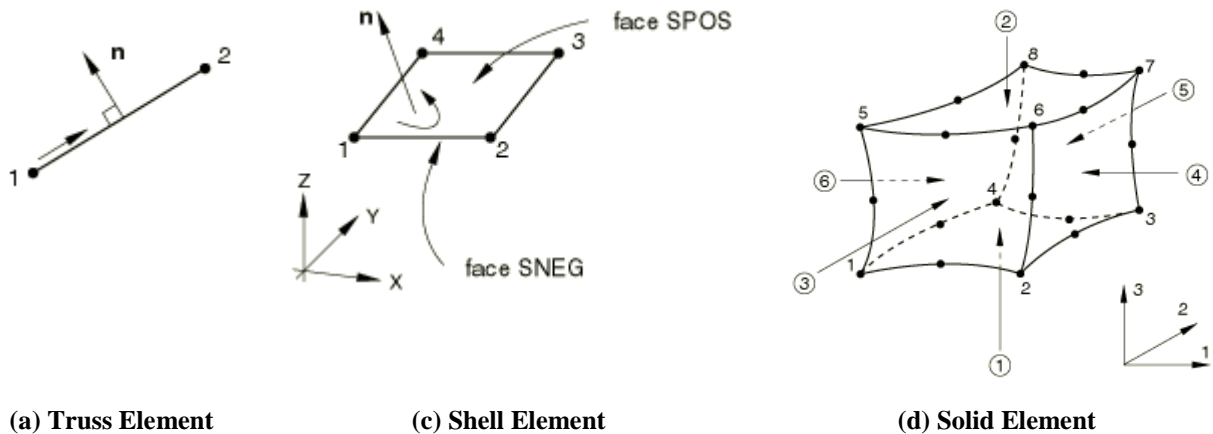
Figure 5-2. Different element type

5.1.2.1   Truss element

Truss element in ABAQUS is one-dimensional element used in two and three dimensional models which is often used to model slender, line-link structures that support loading only along the axis or the centerline of the element. Consequently, no moments or forces perpendicular to the centerline are supported. The truss element known as T3D2 was used to model all steel reinforcements (T = truss element, 3D = 3-dimensional models, and 2 = two node with linear interpolation) (ABAQUS, 2010).

5.1.2.2   Shell element

Shell elements are used to model structures in which one dimension, the thickness, is significantly smaller than the other two dimensions. Conventional shell elements use this condition to discrete a body by defining the geometry at a reference surface. In this case the thickness is defined through the section property definition. Conventional shell elements have displacement and rotational degrees of freedom. The shell element known as S4 were used to model the I-girders, C-channel bracing and the stiffness. (S = shell element and 4 = four node with linear interpolation) (ABAQUS, 2010).

5.1.2.3   Solid Element

The solid (or continuum) elements in ABAQUS can be used for linear analysis and for complex nonlinear analyses involving contact, plasticity, and large deformations. They are available for stress, heat transfer, acoustic, coupled thermal-stress, coupled pore fluid-stress, piezoelectric, and coupled thermal-electrical analyses. Also, ABAQUS element library includes first-order (linear) interpolation elements and second-order (quadratic) interpolation elements in one, two, or three dimensions. The solid (brick) element known as C3D8 was used to model the concrete deck. (C = continuum (brick) element, 3D = 3-dimensional models, and 8 = eight node with linear interpolation) (ABAQUS, 2010).

5.1.3   Constraints and Boundary Conditions

5.1.3.1   Tie constraints

A surface-based tie constraint can be used to make the translational and rotational motion as well as all other active degrees of freedom equal for a pair of surfaces. By default, the nodes are tied only where the surfaces are close to one another. One surface in the constraint is designated to be the slave surface; the other surface is the master surface (ABAQUS, 2010). The tie constraint was used to connect the deck and the girder together so that no slip between them would happen (full composite action).

5.1.3.2   Embedded elements

The embedded element technique is used to specify that an element or group of elements is embedded in "host" elements. The embedded element technique can be used to model rebar reinforcement (ABAQUS, 2010). Hence, the embedded element constraint was used to insert the truss element (steel reinforcement) into the solid element (concrete deck).

5.1.3.3 *Boundary conditions*

Boundary conditions can be used to specify the values of all basic solution variables (displacements, rotations, warping amplitude, fluid pressures, pore pressures, temperatures, electrical potentials, normalized concentrations, acoustic pressures, or connector material flow) at nodes (ABAQUS, 2010). The displacement restrictions were used to create either roller or fixed bearing in the bridge model.

5.1.3.4 *External Loading*

External loading can be applied to the model as concentrated and distributed loads. Concentrated forces or moments can be only applied to any nodal degree of freedom. Three types of distributed loads can be defined: body loads, surface loads, and edge loads. Distributed body loads are always element-based. Distributed surface loads and distributed edge loads can be element-based or surface-based. Body loads, such as gravity, centrifugal, Coriolis, and rotary acceleration loads, are applied as element-based loads. The three different external loading were used. The gravity acceleration needed to calculate the components self-weight, the ballast load applied to the girder and the precast panel weight to simulate the stage construction of placing each panels.

5.2 Finite element model

The finite element model was created based on the dimensions and material used in the test specimen. Figure 5-3 shows the different part created using FE software ABAQUS.

a) I-Girder part   **b) Deck part**   **c) Channel bracing part**
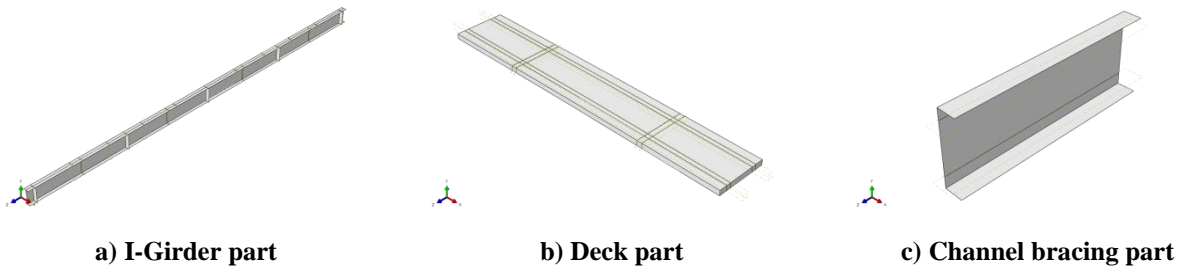
Figure 5-3. Different parts created.

The next step while creating the FE model is to assemble the part together. At this point, no constraints (e.g. tie constraint) between the parts are assigned. Figure 5-4 shows the three main parts were been assembled.

a) Top view   **b) Bottom view**
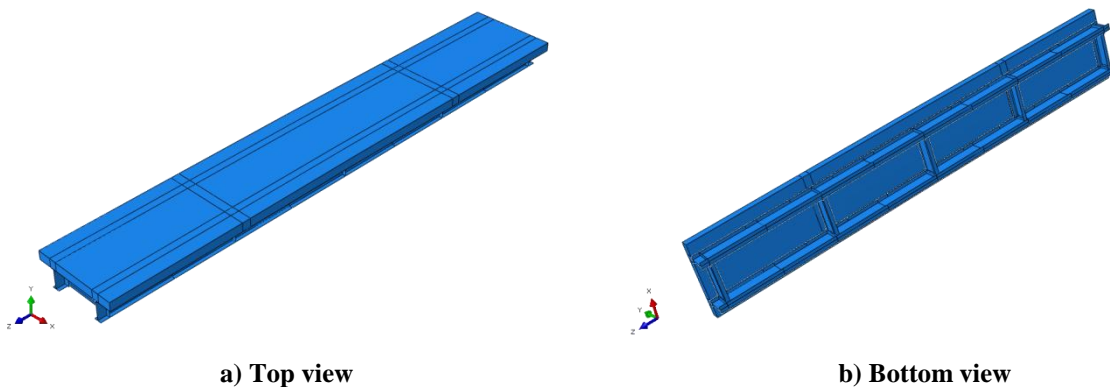
Figure 5-4. Assembled parts.

Figure 5-5 shows the FE meshing applied to the whole model. The average element size considered was 3 inches. Although, finite element model accuracy often depends on the meshing size and/or order of element considered, the results obtained had shown very good agreement with the experimental and analytical results. Thus, no meshing refinement was conducted. The total number of elements was 7449 elements (1052 each girder, 77 each bracing, and 4960 for deck).

a) Girders and bracing meshing   **b) Deck meshing**
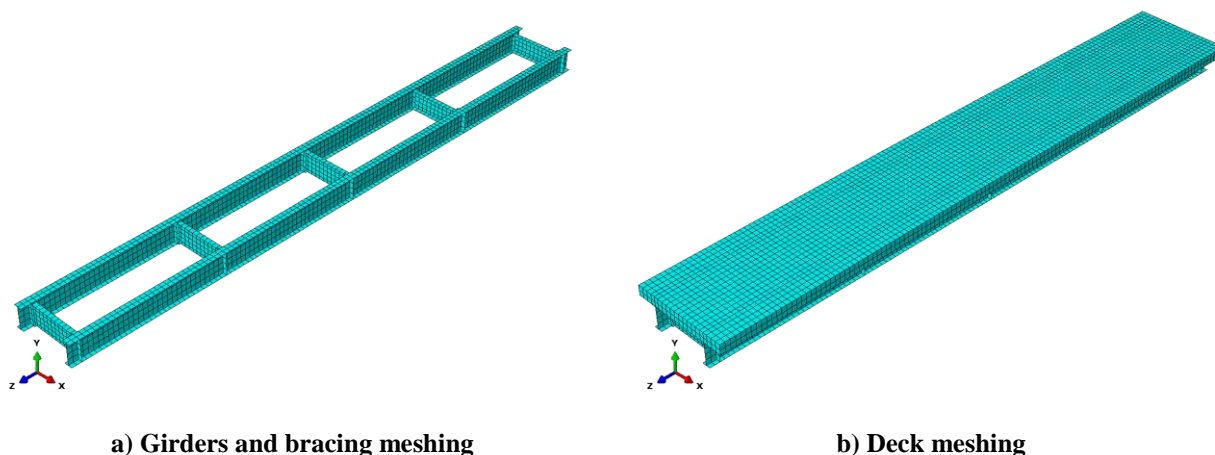
Figure 5-5. Finite element meshing.

Figure 5-6 show the two tie constraints assigned to the FE model. The first constraints was used to tie the bracing (channel beam) to the girder stiffeners (a). This was considered to simulate the bolted connecting considered in the test specimen. The other constraints tie the bottom of the deck with the top flange of the girder (b). This simulates the shear studs connection between the deck and girder in the test specimen.

a) Tie constraints (bolts)   **b) Tie constraints (shear studs)**
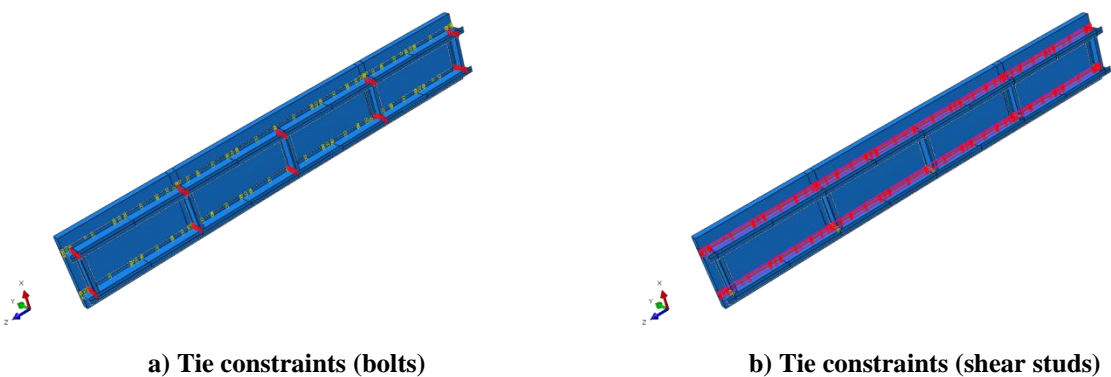
Figure 5-6. Tie constraints assignments.

Figure 5-7 shows the loading conditions applied to the model. The point loading was used to simulate the ballast load (1). Distributed load were used to simulate the concrete deck (2). This approach was considered to better simulate the sequence of placement of deck over the girders. Since the test specimen was built using roller at the girder ends and fixed bearing over

the interior support. Similar, boundary conditions were assigned to the model to simulate both bearing types (3).
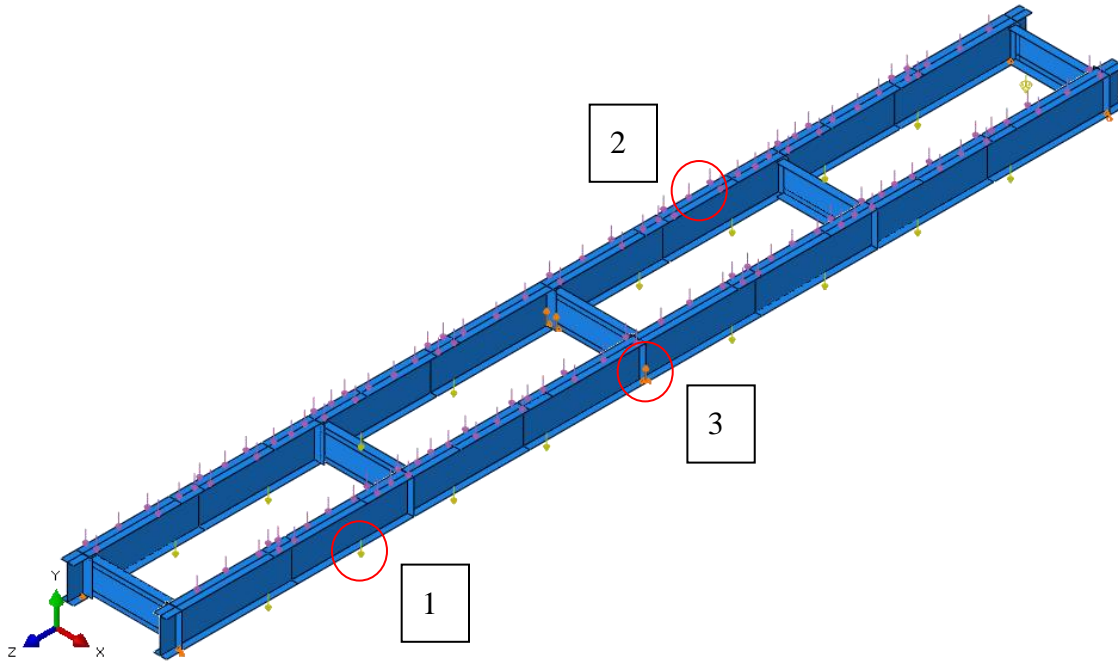
Figure 5-7. Boundary conditions, point and distributed loading assigned.

Finally, the FE model created is ready to be submitted for analysis. The results obtained are discussed in the following section.

5.3 FE Model Results

For easy comparison between all three results i.e. experimental, analytical and numerical, this section follows the same layout presented in Chapter 4. The results presented only considers two loading stage. First is discussed the results based on the construction loading analysis which includes the self-weight loading, lifting of interior support and placement of concrete deck panels. The second analysis refers to the shim removal. At this analysis, the composite action between deck and girders is considered. The time-dependent effects and ultimate load analysis

are not considered. For easy comparison, the results provided in the following tables are related ¼ of the FE model. In other words, only the results from the south girder west span are provided.

5.3.1   Before self-stressing (construction)

The construction loading stage includes the girder self-weight, lifting of interior support and placement of precast panels. At this point, the only the girder (noncomposite section) carry the loads. Two approaches are considered to discuss the results from the numerical simulation, one considers the global behavior where the displacements are compared and the other considers a local response where the stresses are analyzed.

Table 5.3 compares the displacement based on all three outcomes, i.e. experimental, numerical and analytical results. It can be seen that FE model created was capable of predicting the overall (global) behavior of the test specimen.

Table 5.3. Displacement comparison during construction.

Section	Experimental	Analytical	Numerical
A (3.75 ft)	0.26	0.27	0.266
B (7.0 ft)	0.56	0.54	0.523
C (11.25 ft)	0.86	0.90	0.849

Units of displacement in inch (in)

Table 5.4 compares the stresses based on all three methods, i.e. experimental, numerical and analytical results. It can be seen that numerical model was capable of predicting with good agreement the local responses of the test specimen.

Table 5.4. Stress comparison during construction.

Section	Experimental	Analytical	Numerical
Top flange stress			
A (3.75 ft)	-2.56	-4.38	-2.97
B (7.0 ft)	-1.59	-1.09	-0.19
C (11.25 ft)	11.78	13.12	12.60
D (14.25 ft)	24.47	29.92	27.47
Bottom flange stress			
A (3.75 ft)	2.24	4.60	2.93
B (7.0 ft)	-0.80	1.15	-0.19
C (11.25 ft)	-14.46	-13.80	-13.48
D (14.25 ft)	-31.04	-31.46	-29.22

Units of stress in 1000 pounds per square inch (ksi)

Figure 5-8 shows different stresses (S22) plots for different stage of construction.

a) After placing girder over support

b) After dropping 4 ballast to avoid lifting

c) After displacing interior support

d) After placing 5 panels (west span)
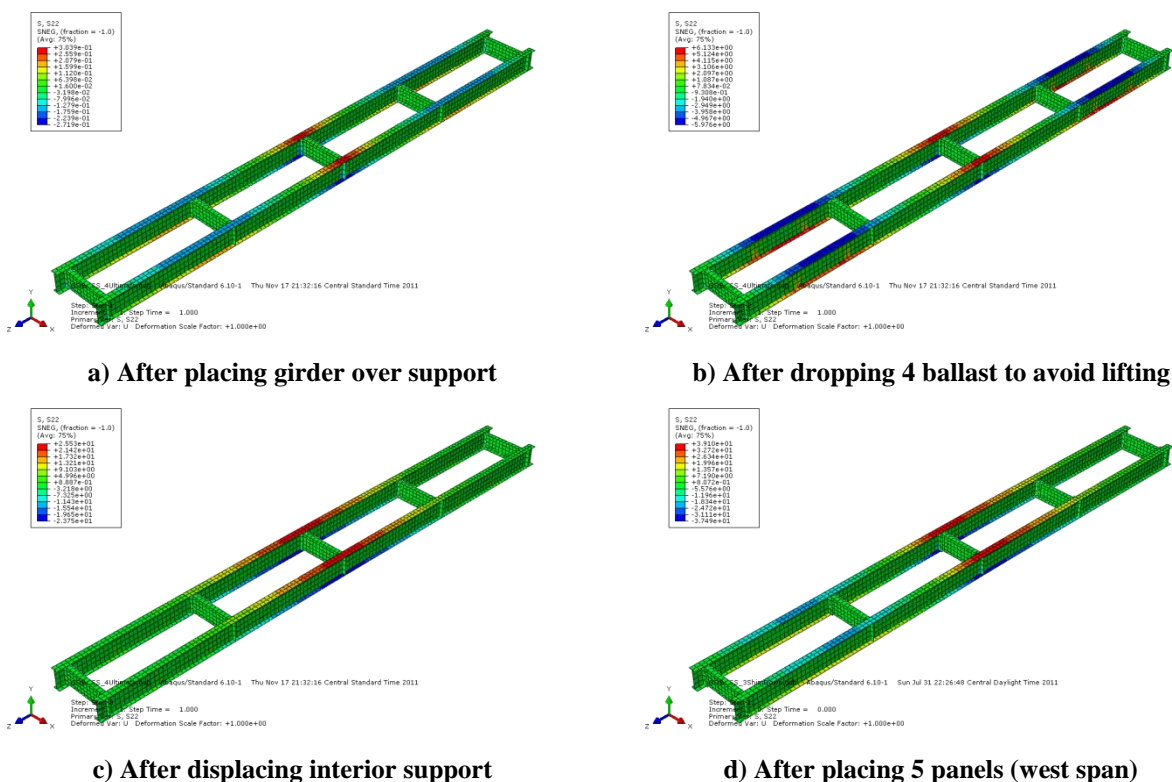
Figure 5-8. Stress on girder during different stages of construction.

Figure 5-9 shows the final stress after all construction loads (girder self-weight, ballast and precast panel weight) are applied over the bare steel section (girders only).
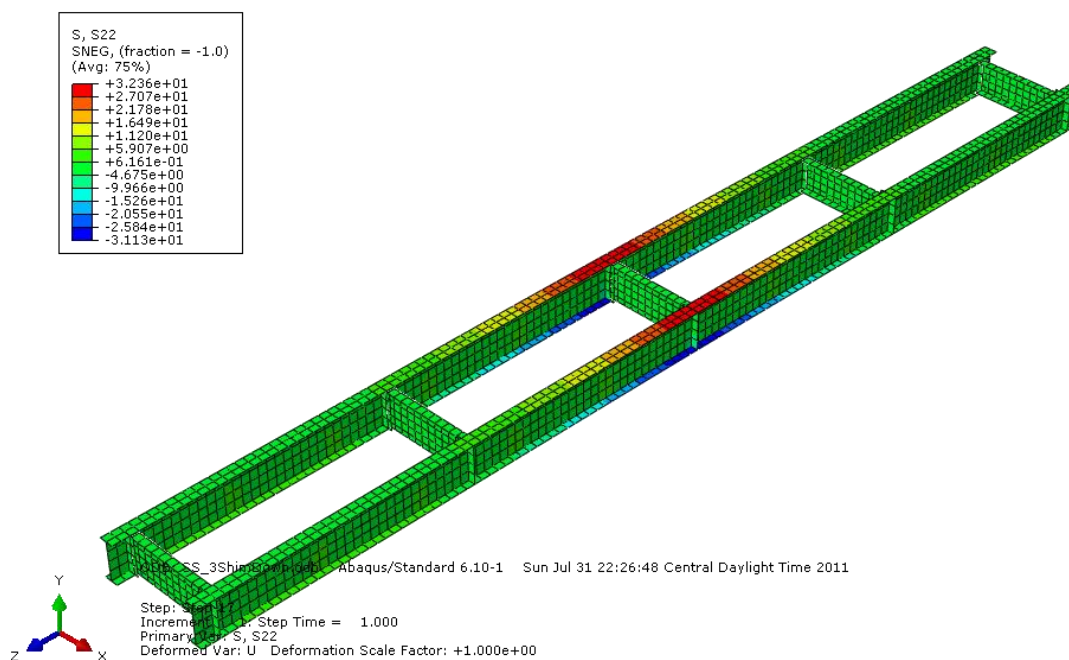
Figure 5-9. Final stress on the girder after construction load.

Next section is discussed the results associated with the self-stressing force induced after removing the shim.

5.3.2   At self-stressing (short-term)

The short-term response of the FE model is discussed in this section. After completion of the initial construction stages, grout was poured into the shear studs blockouts and the closure region over the interior support. After allowing two weeks for grout to harden, the shim was removed in order to prestress the deck. Once again in order to validate the FE model, the numerical results are compared with the experimental data and the analytical solution based on linear elastic theory. Two approaches are considered to discuss the results from the numerical simulation, one considers the global behavior where the displacements are compared and the other considers a local response where the stresses are analyzed.

Table 5.5 compares the displacement based on all three outcomes, i.e. experimental, numerical and analytical results. It can be seen that FE model developed shows close results to ones collected during the experimental program. Thus, the numerical simulation was capable of precisely predicting the global behavior of the test specimen.

Table 5.5. Displacement comparison during self-stressing (shim removal).

Section	Experimental	Analytical	Numerical
A (3.75 ft)	-0.14	-0.11	-0.097
B (7.0 ft)	-0.18	-0.13	-0.119
C (11.25 ft)	-0.10	-0.06	-0.058

Units of displacement in inch (in).

Table 5.6 compares the girder stresses based all three analyses, i.e. experimental, numerical and analytical. It can be seen that numerical model was capable of predicting with good agreement stresses at monitored locations of the test specimen.

Table 5.6. Stress comparison at girder after shim removal.

Section	Experimental	Analytical	Numerical
Top flange stress			
A (3.75 ft)	-4.27	-3.46	-2.97
B (7.0 ft)	-0.83	0.62	0.21
C (11.25 ft)	13.15	15.87	15.96
D (14.25 ft)	28.60	33.41	32.28
Bottom flange stress			
A (3.75 ft)	12.28	14.76	12.45
B (7.0 ft)	17.98	20.12	17.72
C (11.25 ft)	16.99	16.69	16.07
D (14.25 ft)	7.43	7.15	7.66

Units of stress in 1000 pounds per square inch (ksi)

Figure 5-10 shows stress (S22) plot along the girders.
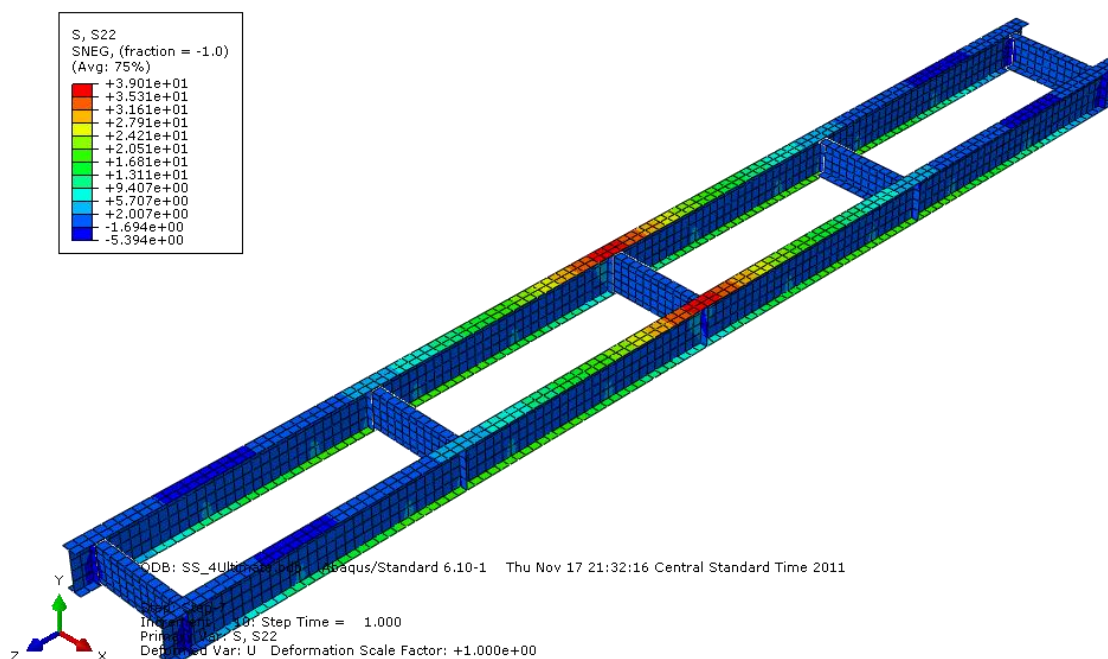
Figure 5-10. Stress on the girders after shim removal.

Overall, the FE analysis shows very good agreement with both experimental observation and analytical predictions. Table 5.7 compares the concrete stresses based all three analyses, i.e. experimental, numerical and analytical.

Table 5.7. Stress comparison at concrete deck after shim removal.

Section	Experimental	Analytical	Numerical
Deck top surface			
A (3.75 ft)	-0.75	-0.57	-0.55
B (7.0 ft)	-1.21	-1.07	-1.02
C (11.25 ft)	-1.95	-1.72	-1.64
D (14.25 ft)	-2.24	-2.18	-2.16

Units of stress in 1000 pounds per square inch (ksi)

Figure 5-11 shows stress (S33) longitudinal stress plot along the concrete deck.
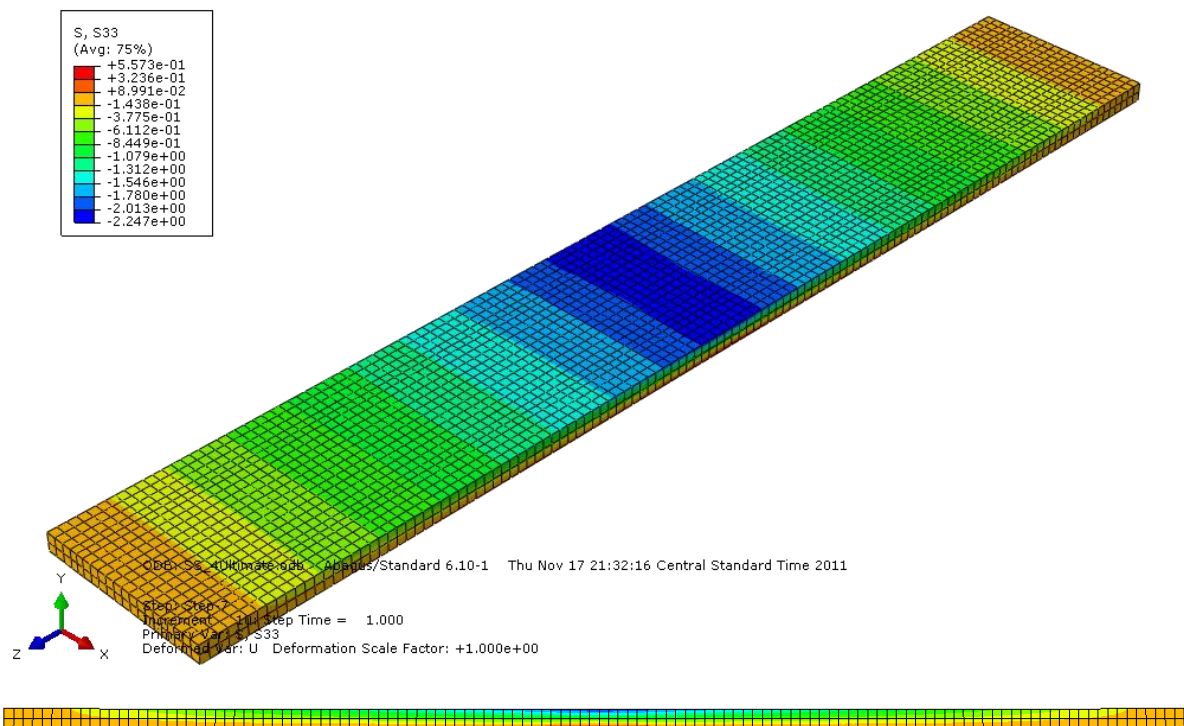
Figure 5-11. Stress on the concrete deck after shim removal.

5.3.3   After self-stressing (long-term)

The long-term response of the FE model is discussed in this section. The creep effect was simulated in the FE model by changing the concrete modulus of elasticity to the value equal to the concrete effective modulus. This approach was perfomed after the short-term analysis were completed. In Abaqus, the command *INITIAL CONDICTIONS was used to set the initial modulus of concrete and later within the analysis to change the modulus. The results of this analysis are summarized in Table 5.8 which compares the girder stresses based all three analyses, i.e. experimental, numerical and analytical. It can be seen that numerical model was capable of predicting with good agreement the stresses at monitored locations of the test specimen.

Table 5.8. Stress comparison at girder after time-dependent effect.

Section	Experimental	Analytical	Numerical
Top flange stress			
A (3.75 ft)	-5.67	-3.25	-2.53
B (7.0 ft)	-5.34	0.20	1.24
C (11.25 ft)	7.93	15.69	15.32
D (14.25 ft)	21.36	32.89	31.86
Bottom flange stress			
A (3.75 ft)	11.17	13.39	12.44
B (7.0 ft)	15.25	17.74	17.32
C (11.25 ft)	12.61	13.43	14.98
D (14.25 ft)	1.31	3.33	7.05

Units of stress in 1000 pounds per square inch (ksi)

Figure 5-12 shows stress (S22) plot along the girders.
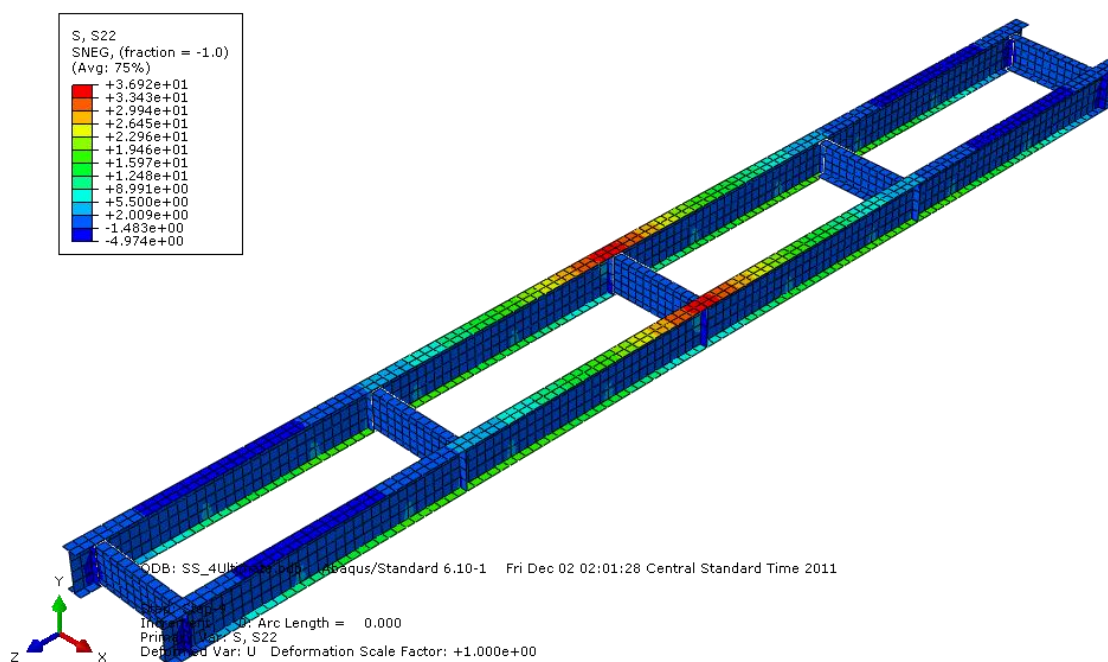
Figure 5-12. Stress on the girders after time-dependent effect.

Overall, the FE analysis shows very good agreement with both experimental observation and analytical predictions. Table 5.9 compares the concrete stresses based analytical and numerical results.

Table 5.9. Stress comparison at concrete deck after time-dependent effect.

Section	Experimental	Analytical	Numerical
Deck top surface			
A (3.75 ft)	-	-0.41	-0.40
B (7.0 ft)	-	-0.74	-0.73
C (11.25 ft)	-	-1.23	-1.16
D (14.25 ft)	-	-1.56	-1.55

Units of stress in 1000 pounds per square inch (ksi)

Figure 5-13 shows stress (S33) longitudinal stress plot along the concrete deck.
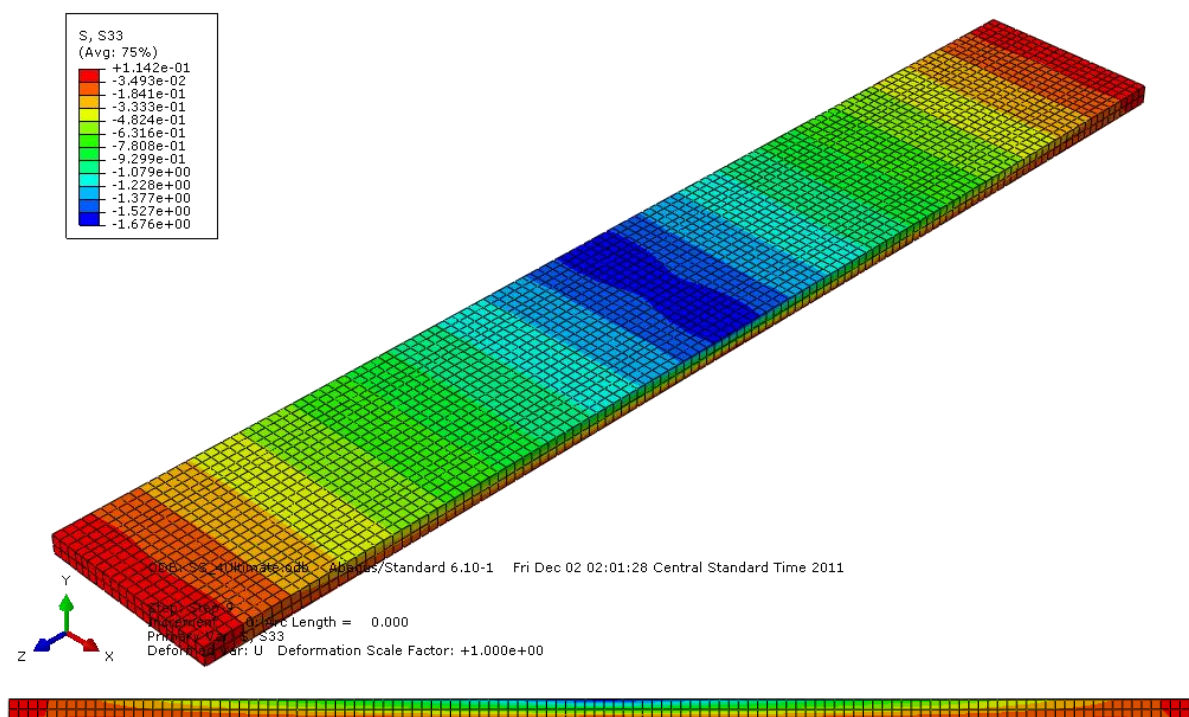
Figure 5-13. Stress on the concrete deck after time-dependent effect.

5.4 Interpretation and Appraisal

Based on the results presented in this chapter, the following can be concluded:

- The finite element model was capable of precisely predict the global behavior (displacements) and local response (stresses) of the self-stressing test specimen.

- The FE model was calibrated using the experimental data obtained from the tested specimen in the structural laboratory.

- The numerical results also had shown good agreement with the solution obtained from linear-elastic beam theory.

- Overall, the finite element method offers engineers an advanced tool to analyze bridges considering the 3-dimenional behavior of the structure. Thus, FE analysis can predict the bridge response better than using simplified methods such as beam theory.

Based on all results and discussing reported up to this point. The following chapter provides a simplified design example to aid engineers while considers the self-stressing method during a bridge design. The example assumes a bridge with real dimensions and both conventional and self-stressing (innovative) design method are considered for comparison.

Chapter 6

Self-stressing Design Example

This chapter consists of a simplified steel girder bridge design example, with instructional commentary based on the AASHTO LRFD Bridge Design Specifications. The design example and commentary are intended to serve as a guide to aid bridge design engineers while implementing the Self-stressing Design Method in practice.

This worked example follows similar outline presented in a FHWA report titled "LRFD Design Example for Steel Girder Superstructure Bridge," prepared by Michael Baker Jr., Inc. (Hartle, Wilson, Amrhein, Zang, Bouscher, & Volle, 2003).

6.1 General information

Section 6.1 is the first of several steps that illustrate the design procedures used for a steel girder bridge. It serves as an introduction to this design example and it provides general information about the bridge design.

The purpose of this worked example is to provide a basic design example for a steel girder bridge as an informational tool for the practicing bridge engineer. The example is also aimed at assisting the bridge engineer with designing using the self-stressing method while considering the AASHTO Load and Resistance Factor Design (LRFD) specifications (AASHTO, 2007).

The following is a list of parameters upon which this design example is based:

1. Two span, square, continuous structure configuration

2. Bridge width 46 feet curb to curb (two 12-foot lanes and two 10-foot shoulders)

3. Reinforced concrete deck with overhangs

4. Grade 50 steel throughout

5. QConBridge software to be used to generate superstructure loads (WSDOT, 2005)

6. Composite deck throughout, no shear connector design is provide

7. Only flexural stresses are calculated.

6.1.1 Determine the design criteria

The first step for any bridge design is to establish the design criteria. For this design example, the following is a summary of the primary design criteria:

6.1.1.1 Design Criteria

Table 6.1. Design criteria primarily dimensions.

Description	Value assigned
Governing specifications	AASHTO LRFD Bridge Design Spec.
Design methodology	Load and Resistance Factor Design
Live load requirements	HL-93
Bridge width (curb to curb)	W_{deck} = 46 ft
Roadway width	$W_{roadway}$ = 44 ft
Bridge length	L_{total} = 120 ft
Steel yield strength	F_y = 50 ksi
Reinforcement strength	f_y = 60 ksi
Steel ultimate strength	F_u = 65 ksi
Steel unit weight	W_s = 0.490 kcf
Concrete compressive strength	f'_c = 5 ksi
Concrete tensile strength	f_{ct} = 0.8 ksi
Concrete unit weight	W_c =0.150 kcf
Future wearing surface	W_{fws} = 0.0 kcf
Future wearing surface thickness	t_{fws} = 0.0 in

NOTE: No concrete barrier and future wearing surface are considered.

6.1.1.2 Design Factor

The first set of design factors applies to all force effects and is represented by the Greek letter η. These factors are related to the ductility, redundancy, and operational importance of the structure.

In this design example, it is assumed that all η (η_D, η_R, η_I) factors are equal to 1.0.

For loads for which the maximum value of γi is appropriate:

$$\eta = \eta_D \eta_R \eta_I \qquad \text{and} \qquad \eta \geq 0.95$$

For loads for which the minimum value of γi is appropriate:

$$\eta = \frac{1}{\eta_D \eta_R \eta_I} \qquad \text{and} \qquad \eta \leq 1.0$$

Therefore for this design example, use:

$$\eta = 1.0$$

The following is a summary of other design factors from the AASHTO LRFD Bridge Design Specifications.

- Load factor:

Table 6.2. Load Combinations and Load Factors.

Limit state	DC max	DC Min	DW max	DW Min	LL	IM
Strength I	1.25	0.90	1.50	0.65	1.75	1.75
Strength III	1.25	0.90	1.50	0.65	-	
Strength IV	1.25	0.90	1.50	0.65	1.35	1.35
Service I	1.00	1.00	1.00	1.00	1.00	1.00
Service II	1.00	1.00	1.00	1.00	1.30	1.30
Fatigue	-	-	-	-	0.75	0.75

NOTE: Only Strength I limit state and Service II limit states are considered in this design example.

- Resistance factor:

Table 6.3. Resistance Factors.

Material	Type of Resistance	Resistance Factor, φ
Structural Steel	For flexure	$\varphi_f = 1.00$
	For shear	$\varphi_v = 1.00$
	For axial compression	$\varphi_c = 0.90$
	For bearing	$\varphi_b = 1.00$
Reinforced Concrete	For flexure and tension	$\varphi_v = 0.90$
	For axial compression	$\varphi_a = 0.75$
	For compression with flexure	$\varphi = 0.75$ to 0.90

NOTE: Only structural steel for flexure is considered in this design example

- Multiple presence factors:

Table 6.4. Multiple Presence Factors.

Number of Lanes Loaded	Multiple presence factor, m
1	1.20
2	1.00
3	0.80
>3	0.65

NOTE: 2 lanes loaded is considered in this design example

- Dynamic load allowance:

Table 6.5. Dynamic Load Allowance

Limit state	Dynamic Load Allowance, IM
Fatigue and Fracture Limit state	15%
All other limit states	33%

NOTE: Fatigue and fracture are not considered in this design example

6.1.1.3 Perform Span Arrangement

For this design example, the span arrangement is presented in Figure 6-1. This span arrangement was selected to illustrate various design criteria and the established geometry constraints identified for this example.

Table 6.6. Longitudinal arrangement

Description	Value assigned
Bridge length	$L_{total} = 120$ ft
span length	$L = 60$ ft
number of spans	$N_{span} = 2$ spans

Longitudinal span arrangement is illustrated below:
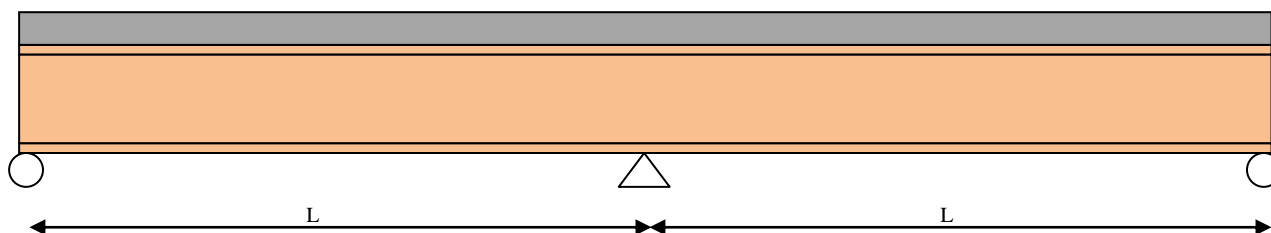
Figure 6-1. Stress on the girders after shim removal.

6.1.1.4   Cross-section Arrangement

For this design example, the superstructure cross section is presented in Figure 6-2. This superstructure cross section was selected to illustrate selected design criteria and the established geometry constraints.

Table 6.7. Transversal arrangement

Description	Value assigned
bridge width (curb to curb)	$W_{deck} = 46$ ft
Roadway width	$W_{roadway} = 44$ ft
number lanes	$n_{lanes} = 2$ lanes
Lane width	$w_{lanes} = 12$ ft
Shoulder width	$w_{shoulder} = 10$ ft
number girders	$N_{girders} = 5$ girders
girder spacing	$S = 10$ ft
overhang width	$S_{overhang} = 3$ ft

Superstructure cross section arrangement is illustrated below:
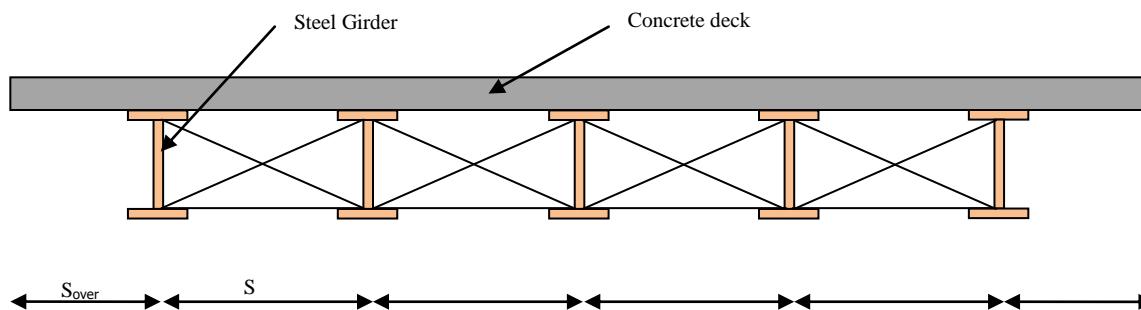
Figure 6-2. Superstructure Cross Section.

6.2 Concrete Deck Design Example

The first design step for a concrete bridge deck is to choose the correct design criteria. The following concrete deck design criteria are obtained from the typical superstructure cross section shown in Figure 6-2.

The next step is to decide which deck design method will be used. In this example, the cross section meets all the requirements given in Article 9.7.2.4; therefore, the empirical method design is used. Since deck design is not the main purpose of this example, the overhang design is not considered. Although, note that empirical method could not be used to design the overhang as stated in Article 9.7.2.2 (AASHTO, 2007).

6.2.1 Deck design criteria:

Table 6.8 provides a summary of all parameters needed for the empirical method deck design.

Table 6.8. Deck design parameter

Description	Value assigned
girder spacing	$S = 10$ ft
overhang width	$S_{overhang} = 3$ ft
number girders	$N_{girders} = 5$ girders
Deck thickness	$t_{deck} = 8$ in
Deck top cover	$Cover_t = 2.5$ in
Deck bottom cover	$Cover_b = 1.0$ in
concrete density	$W_c = 0.150$ kcf
Reinforcement strength	$f_y = 60$ ksi
concrete compressive strength	$f'_c = 5$ ksi

6.2.2   Empirical method deck design:

The requirement for using this method is as follows (Article 9.7.2.4) (AASHTO, 2007):

- Cross-frames or diaphragms are used throughout the cross-section at lines of support

- Intermediate diaphragms for torsionally stiff cross-section should be spaced not more than 25 ft, or supplemental reinforcement over webs is needed

- The supporting components (girders) are made of steel and/or concrete

- The deck is fully cast-in-place and water cured

- The deck has uniform depth, except for haunches at girders flanges and other local thickening

- The deck is made composite with the supporting structural components

- The girder spacing

$6\text{ft} \leq S \leq 18\text{ft}$ $\qquad\qquad$ $S = 10\text{ft}$ $\quad$ *OK*

- The core depth of the slab

$$t_{deck} - Cover_t - Cover_b \geq 4\text{in} \qquad\qquad 8\text{in} - 2.5\text{in} - 1.0\text{in} = 4.5\text{in} \geq 4\text{in} \quad OK$$

- The effective length as specified in Article 9.7.2.3

$$S - b_f \leq 13.5\text{ft} \qquad\qquad 10\text{ft} - 14\text{in} = 8.33\text{ft} \leq 13.5\text{ft} \quad OK$$

- The minimum depth of the slab

$$t_{deck} \geq 7\text{in} \qquad\qquad 8\text{in} \quad OK$$

- There is an overhang beyond the centerline of the outside girder and a structurally continuous concrete barrier is made composite with the overhang

$$S_{overhang} \geq 3 \times t_s \qquad\qquad 3\text{ft} \geq 3 \times 8\text{in} = 2\text{ft} \quad OK$$

- The specified 28-day strength of the deck concrete

$$f_c' \geq 4\text{ksi} \qquad\qquad f_c' = 5\text{ksi} \quad OK$$

- Reinforcement (9.7.2.5)

- Top layer (longitudinal and transversal)

$$A_{st\_req} = 0.18\text{in}^2/\text{ft} \qquad use \#4 @ 12\text{in in both ways} \qquad A_{st} = 0.20\text{in}^2/\text{ft} \quad OK$$

- Bottom layer (longitudinal and transversal)

$$A_{sb\_req} = 0.27\text{in}^2/\text{ft} \qquad use \#5 @ 12\text{in in both ways} \qquad A_{sb} = 0.31\text{lin}^2/\text{ft} \quad OK$$

6.3 Steel Girder Design Example

The main purpose of this section is to show how the self-stressing method relates to the conventional method. In this example, only the moments and stresses of interior girder are considered.

6.3.1 Girder Design Criteria

Table 6.9 provides a summary of all parameters needed for the steel girder design.
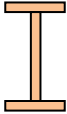
Table 6.9. Girder design parameter

Description	Value assigned
Number of spans	$N_{spans} = 2$
Span length	$L_{spans} = 60$ ft
Skew angle	Skew = 0deg
number girders	$N_{girders} = 5$ girders
girder spacing	$S = 10$ ft
overhang width	$S_{overhang} = 3$ ft
Cross-frame	$L_b = 15$ ft
Web yield strength	$F_{yw} = 50$ ksi
Flange yield strength	$F_{yf} = 50$ ksi
concrete compressive strength	$f'_c = 5$ ksi
Deck thickness	$t_{deck} = 8$ in
steel density	$W_s = 0.490$ kcf
concrete density	$W_c = 0.150$ kcf
Additional miscellaneous dead load/girder	$W_{misc} = 0.015$ klf
Deck width	$W_{deck} = 46$ ft
Roadway width	$W_{roadway} = 44$ ft

6.3.1.1 *Select Trial Girder Section*

Before the dead load effects can be computed, a girder section must be selected. The section properties and dead load effects will be computed. Checks will be performed to determine if the girder section successfully resists the applied loads. If the girder section does not pass all specification checks, then a new trial girder section must be selected and the design process must be repeated.

Table 6.10. Girder dimensions

W33x141	Description	Value assigned
	Girder total height	h = 33.30 in
	Top flange width	b_{tf} = 11.50 in
	Top flange thickness	t_{tf} = 0.96 in
	Web height	D = 31.38 in
	Web thickness	t_w = 0.61 in
	Bottom flange width	b_{bf} = 11.50 in
	Bottom flange thickness	t_{tf} = 0.96 in

The section properties before and after concrete hardened can be calculated after all the bridge components are determined.

6.3.2   Compute Section Properties

Since the superstructure is composite, several sets of section properties must be computed. The initial dead loads (or the noncomposite dead loads) are applied to the girder-only section. The superimposed dead loads are applied to the composite section based on a modular ratio of 3n or n, whichever gives the higher stresses.

The live loads are applied to the composite section based on a modular ratio of n.

For this design example, the concrete slab will be assumed to be fully effective for both positive and negative flexure for service. The steel reinforcement contribution is neglected.

For this design example, only the interior girder design is presented. In general, both the exterior and interior girders must be considered, and the controlling design is used for all girders, both interior and exterior.

The modular ratio is computed as follows:

$$W_c = 150 kcf$$
$$f_c^{'} = 5 ksi$$
$$E_c = 33000(W_c)^{1.5}\sqrt{f_c^{'}} \qquad E_c = 4287 ksi$$

$$E_s = 29000 ksi$$

$$n = \frac{E_s}{E_c} \qquad n = 6.76$$

The effective flange width is assumed to be the same as the girder spacing.

$$W_{effflange} = S = 10 ft$$

6.3.2.1 Positive region Section Properties

The noncomposite and composite section properties for the positive moment region are computed as shown in the following table. The distance to the centroid is measured from the bottom of the girder.

Table 6.11. Positive moment region section properties

	Area, A (in^2)	Centroid, d (in)	Inertia, I (in^4)	y_{botgdr} (in)	y_{topgdr} (in)	$y_{topslab}$ (in)	S_{botgdr} (in^3)	S_{topgdr} (in^3)	$S_{topslab}$ (in^3)
Girder only	41.1	16.7	7332.8	16.7	-16.7	-	440.4	-440.4	-
Composite (n)	183.0	32.7	21670.6	32.7	-0.6	-8.6	663.4	-34154.2	-2509.8
Composite (3n)	88.4	27.7	16958.6	27.7	-5.6	-13.6	612.1	-3030.4	-1247.3

6.3.2.2 Negative region Section Properties

Similarly, the noncomposite and composite section properties for the negative moment region are computed as shown in the following table. The distance to the centroid is measured from the bottom of the girder.

For simplification purpose, the deck is assumed to fully contribute for the section properties calculations and the steel reinforcements are neglected. In reality this assumption is false since it is expected that concrete would crack over high negative moment developed over the piers.

Table 6.12. Negative moment region section properties

	Area, A (in^2)	Centroid, d (in)	Inertia, I (in^4)	y_{botgdr} (in)	y_{topgdr} (in)	$y_{topslab}$ (in)	S_{botgdr} (in^3)	S_{topgdr} (in^3)	$S_{topslab}$ (in^3)
Girder only	41.1	16.7	7332.8	16.7	-16.7	-	440.4	-440.4	-
Composite (n)	183.0	32.7	21670.6	32.7	-0.6	-8.6	663.4	-34154.2	-2509.8
Composite (3n)	88.4	27.7	16958.6	27.7	-5.6	-13.6	612.1	-3030.4	-1247.3

6.3.3   Compute Dead Load Effects

All the calculations here considered follow into the linear elastic range of all materials considered; therefore, the principle of superposition can be applied when necessary.

6.3.3.1   Conventional Design (Flexure)

The girder must be designed to resist the dead load effects, as well as the other load effects. In addition, some dead loads are factored with the DC load factor and other dead loads are factored with the DW load factor.

For the steel girder, the dead load per unit length for an interior girder is computed as follows:

$$W_c = 0.490 kcf \qquad A_{gdr} = 41.1 in^2$$
$$DL_{gdr} = W_c.A_{gdr} \qquad DL_{gdr} = 0.140 klf$$

For the concrete deck, the dead load per unit length for an interior girder is computed as follows:

$$W_c = 150 kcf \qquad S = 10 ft \qquad t_{deck} = 8 in$$
$$DL_{deck} = W_c.S.t_{deck} \qquad DL_{deck} = 1.0 klf$$

For the miscellaneous dead load (including cross-frames, stiffeners, and other miscellaneous structural steel), the dead load per unit length is assumed to be as follows:

$$DL_{misc} = 0.015 klf$$

For the miscellaneous dead load (including cross-frames, stiffeners, and other miscellaneous structural steel), the dead load per unit length is assumed to be as follows:

$$DL_{misc} = 0.015klf$$

No load due to future wearing surface is considered

$$DL_{fws} = 0.0klf$$

The following table present the unfactored dead load moments computed by QConBridge software (WSDOT, 2005). Since the bridge is symmetrical, the moments in Span 2 are symmetrical to those in Span 1.

Table 6.13. Dead Load Moments

Location	0	0.1L	0.2L	0.3L	0.4L	0.5L	0.6L	0.7L	0.8L	0.9L	1.0L
Girder	0.0	16.4	27.7	34.0	35.3	31.5	22.7	8.8	-10.1	-34.0	-63.0
Deck	0.0	117.0	198.0	243.0	252.0	225.0	162.0	63.0	-72.0	-243.0	-450.0
Miscellaneous	0.0	1.8	3.0	3.6	3.8	3.4	2.4	0.9	-1.1	-3.6	-6.8
Future wearing	0.0	0.0	0.0	0.0	0.0	0.0	0.0	0.0	0.0	0.0	0.0

NOTE: Units of bending moment in 1000 pounds foot (kip.ft)

Bending moment diagram is shown as follows:
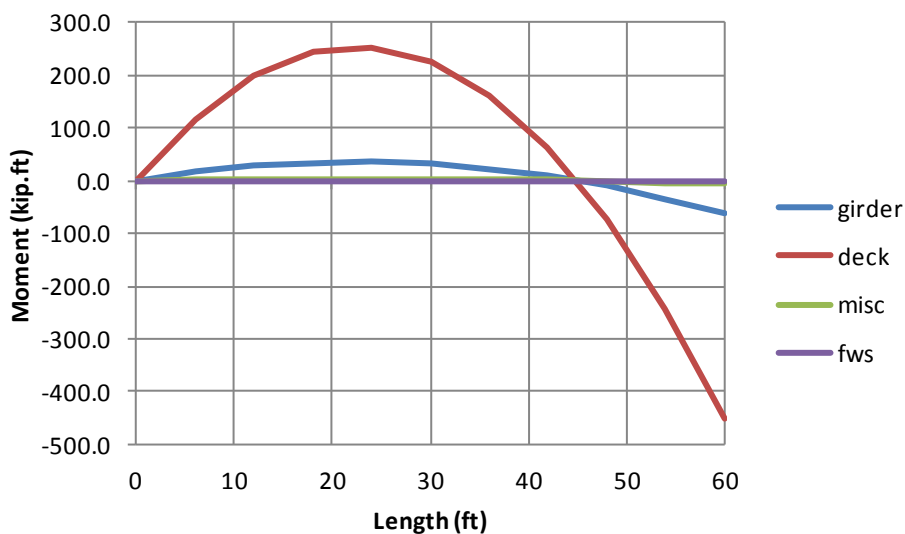
Figure 6-3. Dead Load Bending Moment Diagram in Span 1

6.3.3.2   *Self-stressing Method Design (Flexure)*

In addition to the dead load calculations previously carried out on Section 6.3.3.1, the following steps are required when the self-stressing method is considered.

6.3.3.2.1 Amount of compressive stress

The self-stressing method guide (Appendix A) recommends that the level of compressive prestress at the deck surface shall follow within the limits shown below.

$$0.75 \, ksi \leq \sigma_{top\_slab} \leq 0.6 \times f_c^{'}$$

6.1

For this example, the compressive stress selected is 30 percent of the concrete compressive strength.

$$\sigma_{top\_slab} = 0.3 \times f_c^{'} = 1.5 \text{ ksi}$$
.

6.3.3.2.1 Determine the amount of displacement

The self-stressing guide provides an analytical equation to determine the amount of displacement needed to induce the compressive stress chosen previously. Equation 6.2 was rewritten from the guide (Appendix A).

$$\delta = \frac{\sigma_{top\_slab} \, L^2}{3 \, E_{concrete} \, y_{top\_slab}}$$

6.2
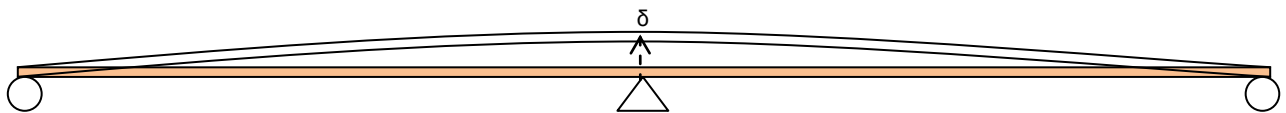
The following values were obtained from previous tables.

$$\sigma_{top\_slab} = 1.5 \text{ ksi}$$
$$E_{concrete} = 33000 \, (W_c)^{1.5} \sqrt{f_c^{'}} = 4286.8 \text{ ksi}$$
$$y_{top\_slab} = 8.6 \text{ in}$$
$$L = 60 \text{ ft}$$
$$\delta = \text{upward displacement}$$

$$\delta = \frac{1.5 \times \overline{60 \times 12}^{2}}{3 \times 4286.8 \times 8.6} = 7.0 \text{ in}$$

In order to induce compressive stress of 1.5 ksi at top surface of concrete deck, the 120 ft long bridge will required a 7 inches upward shim at interior support during construction.

6.3.3.2.2   Determine total lifting force

The guide developed provides provisions on how to calculate the force to raise the bare steel beam to a predetermined elevation. Equation 6.3 was here rewritten.

$$F_{lifting}^{shim} = 3 \times \frac{E_{steel} \times I_{steel} \times 2L}{L^{4}} \times \delta \qquad \textbf{6.3}$$

The total force to lift the bare steel girder 7 inches above its initial elevation is given by

$$F_{lifting}^{shim} = 3\frac{29000 \times 7332.8 \times (2 \times 60 \times 12)}{(60 \times 12)^{4}} \times 7.0 = 23.92 \text{ kip}$$

During the final stage of construction the upward shim is removed and the hydraulic jack will be subjected to the lifting force previous calculated (shim force) plus the weight of the bridge (girder weight, deck, miscellaneous, etc.). The addition force considered bridge's weight is given by (Equation was obtained from guide Appendix A).
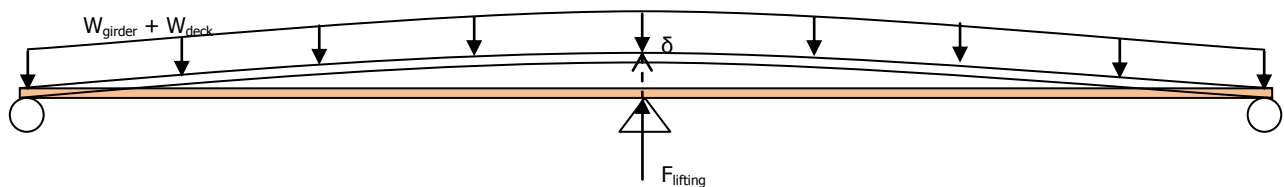
$$F_{lifting}^{girder+deck} = \frac{10}{8}(W_{girder} + W_{deck} + W_{misc}) \times L$$

$$F_{lifting}^{girder+deck} = \frac{10}{8}(0.14 + 1.0 + 0.015) \times 60 = 86.63 kip$$

*The hydraulic jack selected should capable of lifting the maximum **unfactored** load of 110.55 kip. Adequate safety factor should be considered while selecting a hydraulic jack system.*

6.3.3.2.3 Determine anchor force at girder ends

The anchor force was determined by following the recommendation provided in the guide. This force is maximum when the deck is poured (green concrete) at one span and the interior support is raised. The maximum anchor force is determined by Equation 6.4 here rewritten form the guide.

$$F_{anchor} = \frac{3LW_{steel}}{8} - 3\frac{E_{steel}I_{steel}}{L^3}\delta - \frac{LW_{deck}}{16} \qquad \textbf{6.4}$$
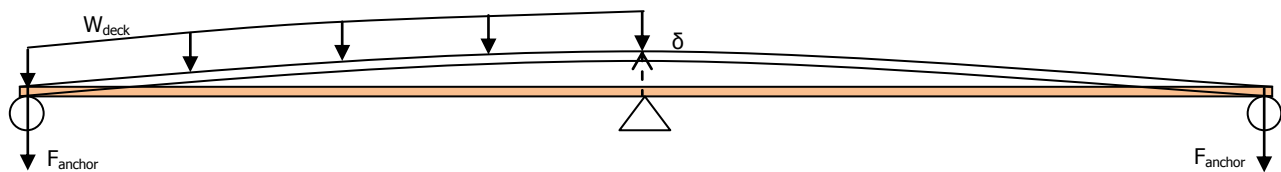
$$F_{anchor} = \frac{3 \times 60 \times 0.14}{8} - 3\frac{29000 \times 7332.8}{(60 \times 12)^3}7.0 - \frac{1.0 \times 60}{16} = 3.15 - 11.96 - 3.75 = 12.56 kip$$

The maximum unfactored anchor force is 12.56 kip. Adequate safety factor should be considered while designing the anchoring mechanism.

6.3.3.2.4 Determine Self-stressing moment

The forces caused by the self-stressing method are considered as DC1 type during the lifting since the force acts on the noncomposite section (girder only) and DC2 type during the releasing of shim when the forces act on the composite section. DC2 by definition is caused by weight of concrete barrier, closure pour, or any other load which will be acting over the bridge after concrete is hardened.

The moment due to lifting and releasing can be determined by following analytical equation

$$M \ x \ = 3\frac{E_{steel} \ I_{non/composite}}{L^2} \pm \delta\left(\frac{x}{L}\right) \quad for \ x \le L \qquad \textbf{6.5}$$

where

$$I_{noncomposite} = I_{steel}; \; -\delta \qquad during \; lifting$$

$$I_{composite} = I_{transformed\_section}; \; +\delta \qquad during \; releasing$$

Resulting:

Table 6.14. Lifting and Releasing Moments

Location	0	0.1L	0.2L	0.3L	0.4L	0.5L	0.6L	0.7L	0.8L	0.9L	1.0L
Lifting	0.0	-71.8	-143.6	-215.4	-287.1	-358.9	-430.7	-502.5	-574.3	-646.1	-717.9
Releasing	0.0	212.1	424.3	636.4	848.6	1060.7	1272.9	1485.0	1697.2	1909.3	2121.5

NOTE: Units of bending moment in 1000 pounds foot (kip.ft)

Bending moment diagram is shown as follows:
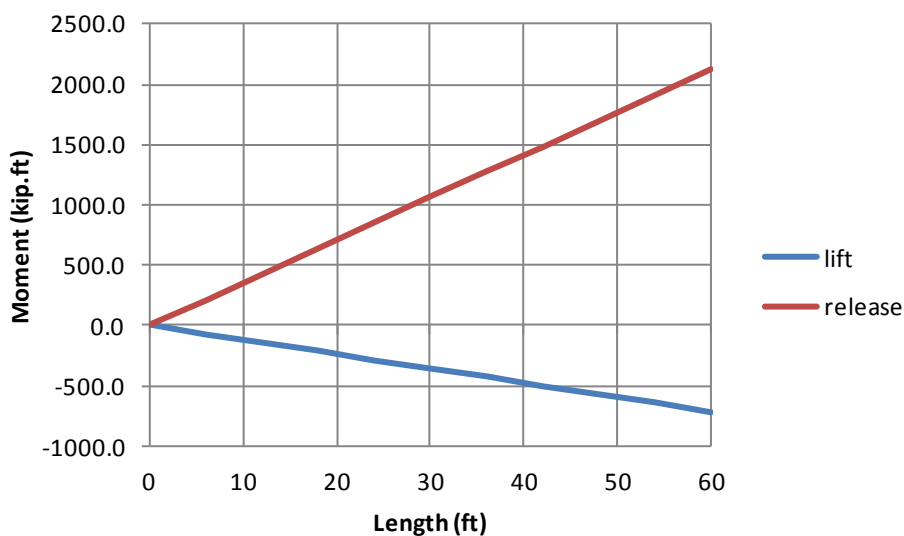
Figure 6-4. Lifting and Releasing Bending moment diagram in Span 1

6.3.4 Compute Live Load Effects

The girder must also be designed to resist the live load effects. The live load consists of an HL-93 loading. Similar to the dead load, the live load moments and shears for an HL-93 loading can be obtained from an analysis computer program.

The dynamic load allowance, IM, is as follows:

$$IM = 0.33$$

The live load distribution factors for moment for an interior girder are computed as follows:

The term which depends on longitudinal stiffness K_g is assumed to be one.

$$\left(\frac{K_g}{12.0\,L\,(t_{deck})^3}\right)^{0.3} = 1 \quad assumed$$

- For one design lane loaded, the distribution of live load per lane for moment in interior beams is as follows

$$g_{\text{int}\_moment\_1} = 0.06 + \left(\frac{S}{14}\right)^{0.4}\left(\frac{S}{L}\right)^{0.3}\left(\frac{K_g}{12.0\,L\,(t_{deck})^3}\right)^{0.1}$$

$$g_{\text{int}\_moment\_1} = 0.57$$

- For two or more design lanes loaded, the distribution of live load per lane for moment in interior beams is as follows

$$g_{\text{int}\_moment\_2} = 0.075 + \left(\frac{S}{9.5}\right)^{0.6}\left(\frac{S}{L}\right)^{0.2}\left(\frac{K_g}{12.0\,L\,(t_{deck})^3}\right)^{0.1}$$

$$g_{\text{int}\_moment\_2} = 0.80$$

- The selected distribution factor is the maximum between both values, Therefore,

$$g_{\text{int}\_moment} = \max\,(g_{\text{int}\_moment\_1},\, g_{\text{int}\_moment\_2}) = 0.80$$

The following table presents the unfactored maximum positive and negative live load moments and shears for HL-93 live loading for interior beams, as computed using an analysis computer program. These values include the live load distribution factor, and they also include dynamic load allowance. Since the bridge is symmetrical, the moments and shears in Span 2 are symmetrical to those in Span 1.

Table 6.15. Live Load plus Impact Moments

Location	0	0.1L	0.2L	0.3L	0.4L	0.5L	0.6L	0.7L	0.8L	0.9L	1.0L
Min moment	0.0	-51.5	-103.0	-154.4	-205.9	-257.4	-308.9	-360.4	-411.8	-531.5	-798.0
Max moment	0.0	393.2	659.7	806.4	871.2	852.0	768.4	594.4	349.4	136.7	0.0

NOTE: Units of bending moment in 1000 pounds foot (kip.ft)

Live load bending moment diagram is shown as follows:
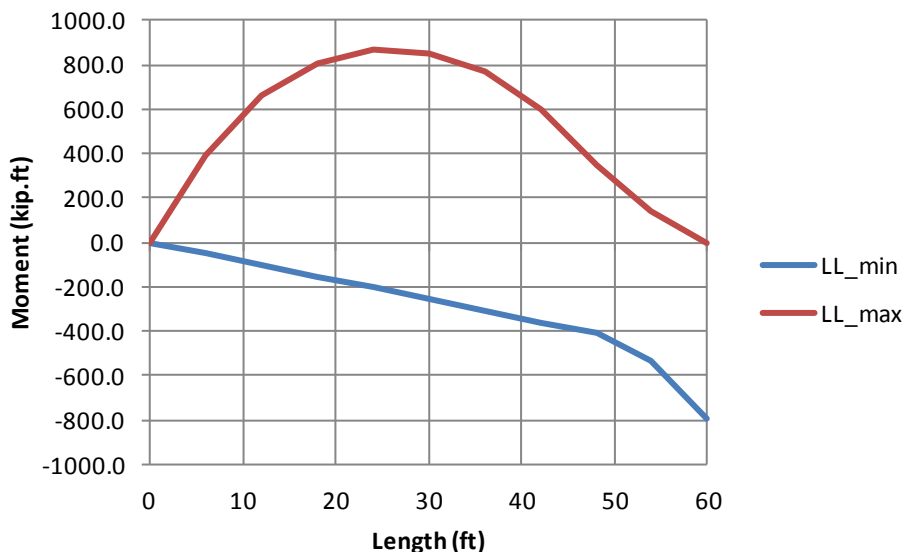
Figure 6-5. Live load bending moment diagram in Span 1

6.3.5   Combine Load Effects

After the load factors and load combinations have been established, the section properties have been computed, and all of the load effects have been computed, the force effects must be combined for each of the applicable limit states.

For this design example, η equals 1.00.

6.3.5.1   Conventional Design

6.3.5.1.1   Maximum positive moment

Based on the previous design steps, the maximum positive moment (located at 0.4L) for the Strength I Limit State is computed as follows:

$LF_{DC} = 1.25$

$M_{DC1} = 35.3 kip.ft + 252.0 kip.ft + 3.8 kip.ft$

$\qquad M_{DC1} = 291.1 kip.ft$

$LF_{DW} = 1.5$

$M_{DW} = 0.0 kip.ft$

$LF_{LL} = 1.75$

$M_{LL} = 871.2 kip.ft$

$M_{total} = LF_{DC}M_{DC1} + LF_{DW}M_{DW} + LF_{LL}M_{LL}$

$\qquad M_{total} = 1888.4 kip.ft$

6.3.5.1.2   Maximum stress

Similarly, the maximum stress in the top of the girder due to positive moment (located at

0.4L) for the Strength I Limit State is computed as follows:

Noncomposite dead load:

$M_{noncompDL} = 35.3 kip.ft + 252 kip.ft + 3.8 kip.ft$

$\qquad M_{noncompDL} = 291.1 kip.ft$

$S_{topgdrDL} = -440.4 in^3$

$f_{noncompDL} = \dfrac{M_{noncompDL}}{S_{topgdrDL}} \qquad\qquad f_{noncompDL} = -7.9 ksi$

Live load (HL-93) and dynamic load allowance:

$M_{LL} = 871.2 kip.ft$

$S_{topgdr} = -34154.2 in^3$

$f_{LL} = \dfrac{M_{LL}}{S_{topgdr}} \qquad\qquad f_{LL} = -0.31 ksi$

Multiplying the above stresses by their respective load factors and adding the products

results in the following combined stress for the Strength I Limit State:

$f_{Str} = LF_{DC}.f_{noncompDL} + LF_{LL}.f_{LL}$

$f_{Str} = -10.4 ksi$

6.3.5.1.3 Summary of combined forces

All combined moments and flexural stresses can be computed at the controlling locations. A summary of those combined load effects for an interior beam is presented in the following two tables, summarizing the results obtained using the procedures demonstrated in the above computations.

The maximum positive moment (located at 0.4L) for the Strength I and Service II Limit State is summarized as follows:

Table 6.16. Combined Effects at Location of Maximum Positive Moment (Conventional method)

Summary of unfactored values:				
Loading	**Moment (kip.ft)**	f_{botgdr} **(ksi)**	f_{topgdr} **(ksi)**	$f_{topslab}$ **(ksi)**
Noncomposite DL	291.1	7.9	-7.9	-
HL-93 LL	871.2	15.8	-0.3	-0.62
Summary of factored values:				
Limit state	**Moment (kip.ft)**	f_{botgdr} **(ksi)**	f_{topgdr} **(ksi)**	$f_{topslab}$ **(ksi)**
Strength I	1888.4	37.5	-10.4	-1.09
Service II	1423.6	28.4	-8.3	-0.81

The maximum negative moment (located at 1.0L) for the Strength I and Service II Limit State is summarized as follows:

Table 6.17. Combined Effects at Location of Maximum Negative Moment (Conventional method)

Summary of unfactored values:				
Loading	**Moment (kip.ft)**	f_{botgdr} **(ksi)**	f_{topgdr} **(ksi)**	$f_{topslab}$ **(ksi)**
Noncomposite DL	-519.8	-14.2	14.2	-
HL-93 LL	-798.0	-14.4	0.3	0.57
Summary of factored values:				
Limit state	**Moment (kip.ft)**	f_{botgdr} **(ksi)**	f_{topgdr} **(ksi)**	$f_{topslab}$ **(ksi)**
Strength I	-2046.2	-43.0	18.2	1.00
Service II	-1557.2	-32.9	14.5	0.74

It can be noted that in both limit states, the stress in the concrete is above the cracking limit assumed to be equal to 0.51 ksi. This value was calculated by $f_r = 0.23\sqrt{f_c^{'}} = 0.51 ksi$, which is an estimation of concrete direct tensile strength.

Since cracking would be expected at negative region, the initial assumption of uncracked section properties does not holds true, hence a cracked section properties should be considered for the stress calculations. Since the cracked section property is smaller than unckraced, the tensile stresses would increase even more, thus resulting in additional reinforcements to control the crack width at this region.

6.3.5.2   Self-stressing Method Design

6.3.5.2.1   Maximum positive moment

Based on the previous design steps, the maximum positive moment (located at 0.4L) for the Strength I Limit State is computed as follows:

For the self-stressing method design, M_{DC1} becomes a combination of dead load (girder weight, deck weight, miscellaneous, etc.) plus a new term related to the lifting of interior support.

$$LF_{DC} = 1.25$$
$$M_{DC1} = M_{DC1}^{conventional} + M_{DC1}^{lifting}$$
$$M_{DC1} = 291.1 kip.ft + (-287.1 kip.ft) \qquad M_{DC1} = 4.0 kip.ft$$

The moment of -287.1 kip.ft was obtained from Table 6.14 and refers to the moment caused by lifting the interior support while the section still noncomposite (girder only).

Similarly, M_{DC2} becomes also a combination of any dead load applied to the composite section plus a new term related to the shim release at interior support.

$$M_{DC2} = M_{DC2}^{conventional} + M_{DC2}^{releasing}$$
$$M_{DC2} = 0.0kip.ft + (848.6kip.ft) \times 0.70$$
$$M_{DC2} = 594.0kip.ft$$

The moment of 848.6 kip.ft was obtained from Table 6.14 and refers the moment caused by shim removal at interior support while the section is composite.
Since no advanced analysis is considered in this example, the long-term loss due to time-dependent effects was directly applied by considered 30% reduction of the compressive stress (Appendix A).

$$LF_{DW} = 1.5$$
$$M_{DW} = 0.0kip.ft$$
$$LF_{LL} = 1.75$$
$$M_{LL} = 871.2kip.ft$$
$$M_{total} = LF_{DC}(M_{DC1} + M_{DC2}) + LF_{DW}M_{DW} + LF_{LL}M_{LL}$$
$$M_{total} = 2272.0kip.ft$$

6.3.5.2.2 Maximum stress

The maximum stress in the top of the girder due to positive moment (located at 0.4L) for

the Strength I Limit State is computed as follows:

Noncomposite dead load:

$$M_{noncompDL} = 35.3kip.ft + 252kip.ft + 3.8kip.ft + (-287.1kip.ft)$$
$$M_{noncompDL} = 4.0kip.ft$$
$$S_{topgdrDL} = -440.4in^3$$

$$f_{noncompDL} = \frac{M_{noncompDL}}{S_{topgdrDL}} \qquad\qquad f_{noncompDL} = -0.1ksi$$

The maximum stress at top flange while considering the conventional method was $f_{noncompDL}$ = -7.9 ksi compared to the self-stressing method given by $f_{noncompDL}$ = -0.1 ksi.

Composite dead load:

$$M_{compDL} = 848.6kip.ft \times 0.70$$
$$M_{compDL} = 594.0kip.ft$$
$$S_{topgdr} = -34154.2in^3$$

$$f_{compDL} = \frac{M_{noncompDL}}{S_{topgdrDL}} \qquad\qquad f_{compDL} = -0.2ksi$$

Live load (HL-93) and dynamic load allowance:

$$M_{LL} = 871.2 kip.ft$$
$$S_{topgdr} = -34154.2 in^3$$
$$f_{LL} = \frac{M_{LL}}{S_{topgdr}} \qquad\qquad f_{LL} = -0.31ksi$$

Multiplying the above stresses by their respective load factors and adding the products

results in the following combined stress for the Strength I Limit State:

$$f_{Str} = LF_{DC}.(f_{noncompDL} + f_{compDL}) + LF_{LL}.f_{LL}$$
$$f_{Str} = -0.9ksi$$

The maximum stress at top flange while considering the conventional method was f_{Str} = -10.4 ksi compared to the self-stressing method given by f_{Str} = -0.9 ksi.

6.3.5.2.3 Summary of combined forces

All combined moments and flexural stresses can be computed at the controlling locations.

A summary of those combined load effects for an interior beam is presented in the following two

tables, summarizing the results obtained using the procedures demonstrated in the above

computations.

The maximum positive moment (located at 0.4L) for the Strength I and Service II Limit

State is summarized as follows:

Table 6.18. Combined Effects at Location of Maximum Positive Moment (Self-stressing method)

Summary of unfactored values:				
Loading	Moment (kip.ft)	f_{botgdr} (ksi)	f_{topgdr} (ksi)	$f_{topslab}$ (ksi)
Noncomposite DL	3.9	0.1	-0.1	-
Composite DL	594.0	10.7	-0.2	-0.4
HL-93 LL	871.2	15.8	-0.3	-0.62
Summary of factored values:				
Limit state	Moment (kip.ft)	f_{botgdr} (ksi)	f_{topgdr} (ksi)	$f_{topslab}$ (ksi)
Strength I	2272.0	41.1	-0.9	-1.62
Service II	1730.5	31.3	-0.7	-1.24

The maximum negative moment (located at 1.0L) for the Strength I and Service II Limit

State is summarized as follows:

Table 6.19. Combined Effects at Location of Maximum Negative Moment (Self-stressing method)

Summary of unfactored values:				
Loading	Moment (kip.ft)	f_{botgdr} (ksi)	f_{topgdr} (ksi)	$f_{topslab}$ (ksi)
Noncomposite DL	-1237.6	-33.7	33.7	-
Composite DL	1485.0	26.9	-0.5	-1.1
HL-93 LL	-798.0	-14.4	0.3	0.57
Summary of factored values:				
Limit state	Moment (kip.ft)	f_{botgdr} (ksi)	f_{topgdr} (ksi)	$f_{topslab}$ (ksi)
Strength I	-1087.3	-33.8	42.0	-0.33
Service II	-790.0	-25.6	33.6	-0.32

It can be noted that no tensile stress is induced in the deck at negative region. Since the

deck is fully under compressive force, no cracks are expected to appear at the deck surface.

Consequently, bridge durability is increased which also associated to increase of service life.
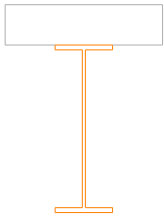
For this case since no cracks are expected, the initial assumption of concrete contributing

for negative section properties calculation holds true.

6.3.5.3   Final comparison of methods

For comparison purpose, both conventional and self-stressing methods results are summarized in the following tables.

At the positive moment section, the stress at bottom flange is closer to yield stress and the concrete stress is greater if the self-stressing method is considered. From a design prospective, the bridge cross-section is more efficient when the self-stressing design method is considered.

Table 6.20. Comparison of both design method considering Maximum Positive Moment
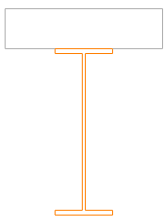
Method	Conventional			Self-stressing		
Loading	**Summary of unfactored values:**					
	f_{botgdr}	f_{topgdr}	$f_{topslab}$	f_{botgdr}	f_{topgdr}	$f_{topslab}$
Noncomposite DL	7.9	-7.9	-	0.1	-0.1	-
Composite DL	-	-	-	10.7	-0.2	-0.4
HL-93 LL	15.8	-0.3	-0.62	15.8	-0.3	-0.62
Limit state	**Summary of factored values:**					

Strength I: -1.09, -10.4, 37.5
Service II: -0.81, -8.3, 28.4
Strength I: -1.62, -0.9, 41.1
Service II: -1.24, -0.7, 31.3

NOTE: Units of stress in 1000 pounds per square inch (ksi)

At negative moment region, the concrete deck is in compression so the initial assumption of uncracked section properties holds true (no cracking at interior support region). Similarly to positive moment region, the self-stressing method had increased the effectiveness of the bridge cross-section, since the tensile stress at top flange stress is closer to yield and the compressive stress at bottom flange was reduced (reducing the risk of buckling). Consequently, same girder

cross-section (W33x141) can be used throughout the whole length of the bridge, i.e. no need for steel-splice.

Table 6.21. Comparison of both design method considering Maximum Negative Moment

Method	Conventional			Self-stressing		
Loading	Summary of unfactored values:					
	f_{botgdr}	f_{topgdr}	$f_{topslab}$	f_{botgdr}	f_{topgdr}	$f_{topslab}$
Noncomposite DL	-14.2	14.2	-	-33.7	33.7	-
Composite DL	-	-	-	26.9	-0.5	-1.1
HL-93 LL	-14.4	0.3	0.57	-14.4	0.3	0.57
Limit state	Summary of factored values:					

NOTE: Units of stress in 1000 pounds per square inch (ksi)

This design example clearly had shown the advantages and additional steps required during the bridge design when the self-stressing method is considered.

6.3.6   Design other components

As previously stated, no major changes from conventional method is expected during the design of other components such as stiffeners, bracing, bearings, abutments, piles, wing-walls, etc. Therefore, the design of remaining components is not covered in this example.

Chapter 7

Summary and Conclusions

This chapter provides a brief summary of the research performed, the conclusions and recommendations for future research.

7.1 Summary

The proof-of-concept was successfully conducted and validated. The self-stressing method was used to construct a prototype bridge using the precast concrete panel system.

The idea behind the self-stressing method was to prevent deck cracking in the negative moment region over the interior support by inducing an initial compressive force in the concrete deck. This was achieved by inserting a shim over the interior support before the precast panels are placed and later removed after the grout hardens. The design was deemed a success because the cracking was satisfactorily delayed. Additionally, the bottom flange stress at the interior support region was completely eliminate thus a single girder cross-section can be used throughout the bridge length.
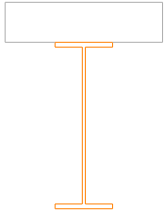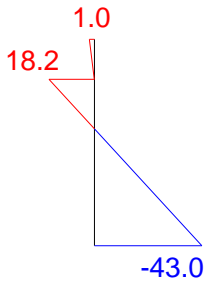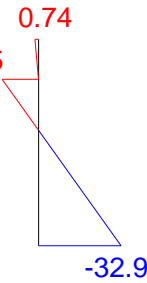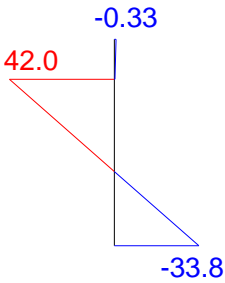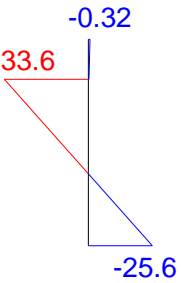
The self-stressing method applied to precast concrete deck is proposed as an alternative to the conventional post-tensioned concrete deck system used for preventing transverse deck cracking. Also, if the cast-in-place deck is considered, the self-stressing method can reduce and/or eliminate the shrinkage cracks often an issue even before the bridge is open to traffic.

Both analytical and numerical solutions have shown good agreement with the experimental results. Thus, both methods can be used to design a bridge using the self-stressing method. Furthermore, time-dependent analysis should be carry out in order to determine the

amount of precompression loss and additional stress induced in the girder due to the time-dependent effect.

A design example is provided to aid bridge engineers while considering the self-stressing method. In addition, guidelines were developed to facilitate the dissemination of the method. The following table clearly shows the advantage of the self-stressing method over the conventional method, such as, the reduction of compressive stress at the girder bottom flange (mitigating buckling) and the development of compressive stress in the deck (reducing cracking).

Comparison of both design method considering Maximum Negative Moment

AASHTO Limit state	Conventional method		Self-stressing Method	
	Strength I	Service II	Strength I	Service II
	1.0 18.2 -43.0	0.74 14.5 -32.9	-0.33 42.0 -33.8	-0.32 33.6 -25.6

NOTE: Units of stress in 1000 pounds per square inch (ksi)

7.2 Conclusions

The following sections detail the conclusions drawn from the research presented in this dissertation.

7.2.1 Experimental

Based on the experimental program, the following can be concluded:

- Overall, the specimen performed as expected, exhibiting good stability, delayed cracking, and a sufficient amount of ductility.

- During the ultimate load test, it was observed the failure modes. The first noticeable failure was yielding of bottom flange at mid-span. Followed by cracking of the closure region over the interior support. At the same location, it was observed local buckling of both web and bottom flange of the girder. Finally, concrete crushing was observed under the load application at mid-span.

- AASHTO creep and shrinkage prediction model is considered to be suitable for predicting the long-term strain variation of the concrete.

- The panel-to-panel connection reported in the literature as a weak spot, performed satisfactory showing full continuity between the panels, although no reinforcement was considered. The use of epoxy at the match-cast shear key seems an easy and practical solution to be implemented in the field.

- The self-stressing method did not alter the ultimate strength of the test specimen. The ultimate capacity measured shown good agreement with the predicted value.
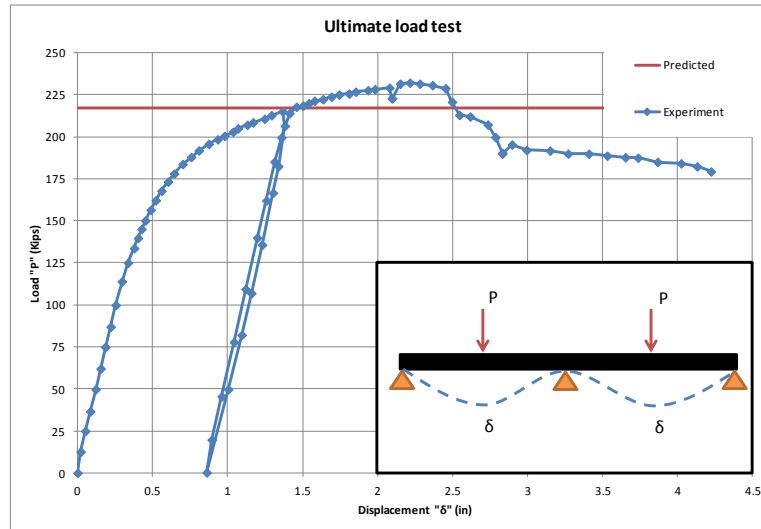
7.2.2 Analytical

Based on the analytical solution, the following can be concluded:

- The simplified beam theory can be used to analyze the bridge using the self-stressing method. Equations are provided throughout the dissertation and in the appendix.

- The AEMM was used to predict the time-dependent effect. The total loss of initial precompression stress was about 30%.

- For the case of a two span bridge, the following equation can be used to estimate the amount of displacement required.

$$\delta = \frac{\sigma_{ts} L_1 L_2}{3 E_{conc} c_{ts}}$$

Where:

δ = Amount of displacement required

σ_{ts} = Initial Prestress Stress

L_1 = Length of Span 1

L_2 = Length of Span 2

E_{conc} = Modulus of Elasticity of Concrete

c_{ts} = Distance from neutral axis to top fiber of slab

7.2.3 Numerical

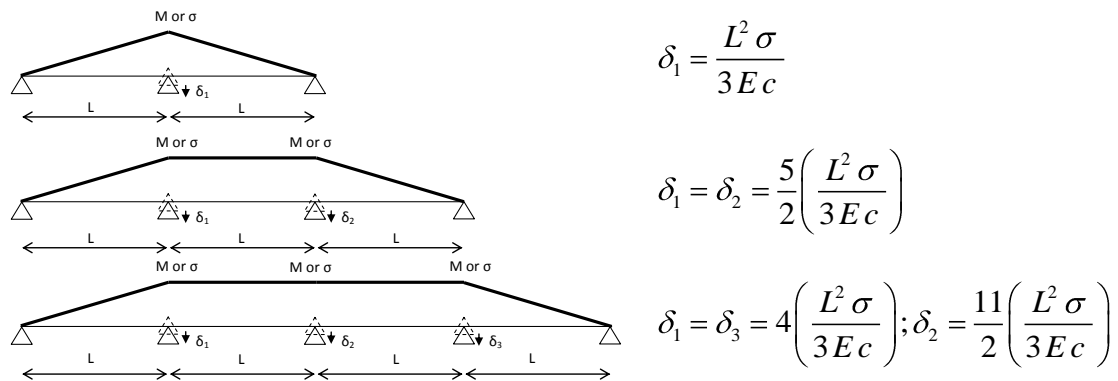The following can be concluded based on the numerical investigation:

- The finite element model was capable of precisely predicting the global behavior (displacements) and local response (stresses) of the self-stressing test specimen.

- The FE model was calibrated using the experimental data obtained from the tested specimen in the structural laboratory.

- The numerical results also have shown good agreement with the solution obtained from linear-elastic beam theory.

- The finite element method offers engineers an advanced tool to analyze bridges considering the 3-dimenional behavior of the structure.

- Overall, FE analysis was capable of predicting the bridge response better than using simplified methods such as beam theory.

7.3 Future Research

Below are some suggestions for future research.

- Evaluate alternative solution for the closure region. Since at this location, it is expected the development of large crack as observed during the ultimate testing. This crack may further leads to durability issues that should be avoided.

- Conduct cost analysis regarding the self-stressing method in order to show that the method is economically viable and apply the method for a real bridge project. In this case, extensive monitored should be considered to observe the system behavior.

- Evaluate the applicability of the self-stressing method for multiple span bridges. Although, the concept can be applied for bridge with more than two spans, the amount of displacement required may be too large for practical application. The following equations were developed assuming the same span length and material and section properties. It is noted that the amount of displacement required to induce the same level of stress (or moment) is increased when the number of span increases.

$$\delta_1 = \frac{L^2 \sigma}{3 E c}$$

$$\delta_1 = \delta_2 = \frac{5}{2}\left(\frac{L^2 \sigma}{3 E c}\right)$$

$$\delta_1 = \delta_3 = 4\left(\frac{L^2 \sigma}{3 E c}\right); \delta_2 = \frac{11}{2}\left(\frac{L^2 \sigma}{3 E c}\right)$$
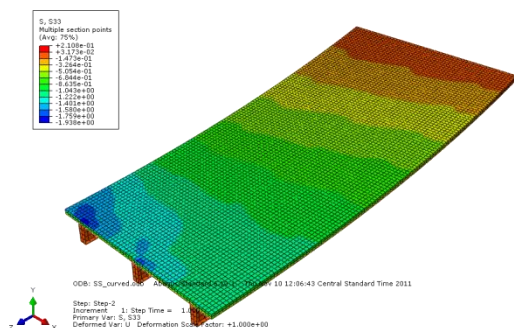
- Determine the influence of skew and curvature in the bridge design considering the self-stressing method. The FE model results below show clearly the difference between a curved and straight bridge.
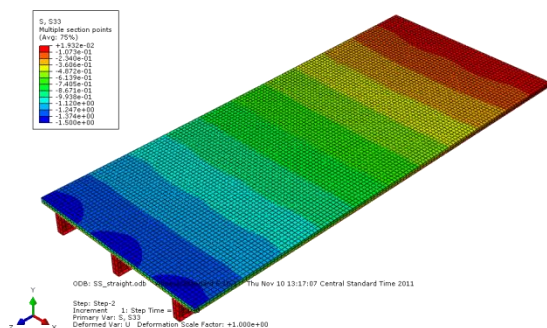
Straight 120ft long bridge (60ft span)

Curved 120ft long bridge (300ft radii, 60ft span)

Due to symmetry, only 1/2 of the bridge was modeled.

References

AASHTO. (2007). *AASHTO LRFD Bridge Design Specifications.* Washington, DC: American Association of State Highway and Transportation Officials.

ABAQUS. (2010). *Abaqus Analysis User's Manual, Version 6.10-1.* Pawtucket, RI: Simula.

ACI Committee 209. (2008). *Prediction of Creep, Shrinkage and Temperature Effect.* Farmington Hills, MI: American Concrete Institute.

ACI Committee 318. (2008). *Building Code Requirements for Structural Concrete.* Farmington Hills, MI: American Concrete Institute International.

Ardani, A., Mallela, J., & Hoffman, G. (2010). *Oregon Demonstration Project: Alternate Project Delivery and Accelerated Bridge Construction on OR 38, Drain to Elkton.* Washington, D.C.: Federal Highway Administration (FHWA).

ASTM. (2010). *Annual Book of ASTM Standards.* West Conshohocken, PA: American Society for Testing and Materials.

Badie, S. S., & Tadros, M. K. (2008). *Full-Depth Precast Concrete Bridge Deck Panel Systems.* Washington, D.C: National Cooperative highway research program (NCHRP Report 584).

Bowers, S. E. (2007). *Recommendations for longitudinal post-tensioning in full-depth precast concrete bridge deck panels. (M.S. Thesis).* Blacksburg, VA: Virginia Polytechnic Institute and State University.

CEB-FIP. (1993). *CEB-FIP Model Code 1990.* Lausanne, Switzerland: Comité Euro-International du Béton.

DIANA. (1996). *TNO DIANA Nonlinear Analysis User's Manual, Release 6.1.*

Fort Miller Company, Inc. (1998). *Inverset Bridge System - Design Installation and Technical Manual.* Schuylerville, NY: Product literature, 2nd Edition.

Gilbert, R. I. (1988). *Time Effects in Concrete Structures.* Amsterdam: Elsevier.

Gilbert, R. I., & Ranzi, G. (2001). *Time-Dependent Behaviour of Concrete Structures.* London and New York: Spon Press - Taylor & Francis Group.

Grossman, S. (1994). *Inverset II – Composite Steel, Segmental Bridge Deck Construction*. Retrieved October 2011, from Composite Steel Segmental Bridge Deck - 1994 NOVA Award Nomination 12.

Grossman, S. J. (1990). Prestressed Composite Steel Bridge Units - A Solution for Increasing Existing Bridge Capacity. *Proceedings of the Third International Conference on Short and Medium Span Bridges*, (pp. 393-400). Toronto, Canada.

Grossman, S. (1987). Stacked Steel Beams Add Economy to Prestressed Steel Bridge Units. *4th Annual International Bridge Conference (IBC)*, (pp. 105-111). Pittsburgh, PA.

Hartle, R. A., Wilson, K. E., Amrhein, W. A., Zang, S. D., Bouscher, J. W., & Volle, L. E. (2003). *LRFD Design Example for Steel Girder Superstructure Bridge with Commentary.* Washington, D.C.: Federal Highway Administration (FHWA NHI - 04-041).

Hieber, D. G., Eberhard, M. O., Wacker, J. M., & Stanton, J. F. (2005). *State-of-the-Art Report on Precast Concrete Systems for Rapid Construction of Bridges.* Seatle, WA: Washington State Transportation Center (TRAC) (Report WA-RD 594.1).

Issa, M., Yousif, A., Issa, M., Kaspar, I., & and Khayyat, S. (1995). Field performance of full depth precast concrete panels in bridge deck reconstruction. *PCI Journal , 40* (3), 82-108.

Issa, M., Yousif, A., Issa, M., Kaspar, I., & Khayyat, S. (1998). Analysis of full depth concrete bridge deck panels. *PCI Journal , 43* (1), 74-85.

Nagai, M., Okui, Y., Ohta, T., Nakamura, H., Inomoto, M., Nishio, K., et al. (2000). Time dependent stress variation of a composite two-I-girder bridge- Chidorinosawagawa Bridges. In *Bridge Management 4.* London: Thomas Telford.

Nottingham. (1996).

NYDOT. (2010). *Thruway Structures Design Manual - 4th Edition.* Albani, NY: NYDOT.

Okui, Y. (2007). Design issues for steel-concrete composite girders. *Proc. China-Japan Joint Seminar on Steel and Composite Bridges*, (pp. 85-93).

PCI. (2005). *Bridge Design Manual.* Chicago, IL: Precast/Prestressed Concrete Institute.

Rao, C., Tajirian, A., & Stubstad, R. (2003). *Lessons Learned from the Tappan Zee Bridge, New York.* Sacramento, CA: California DOT.

Scholz, D. (2004). *Performance Criteria Recommendations for Mortars Used in Full Depth Precast Concrete Bridge Deck Panels. (M.S. Thesis).* Blacksburg, VA: Virginia Polytechnic Institute and State University.

SIKA. (2010). *SIKA Corporation USA.* Retrieved October 2011, from http://usa.sika.com/en/solutions_products.html

Szerszen, M., & Nowak, A. (2007). *Practical Solution to Diminish Restrained Shrinkage Effects in Bridge Decks.* Arlington, VA: National Science Foundation (NSF).

WSDOT. (2005). *Bridge Engineering Software - QConBridge, Version 1.3.* Olympia, WA: Washington State Department of Transportation.

Yakel, A., Farimani, M., Mossahebi, N., & Azizinamini, A. (2007). *Three Innovative Concepts for Short Span Steel Bridges.* Lincoln, NE: NDOR Research Project Number SPR-PL-1 (038) P539.

Appendix A   Guidelines for Use of the Self-Stressing Method

The self-stressing method is a way to introduce compressive stresses in the concrete deck of a multispan continuous beam. These compressive stresses are generally located near the interior supports and therefore work to counter the tensile stresses that arise in this vicinity due to live loading. The result is a reduction in cracking and an accompanying increase in service life.
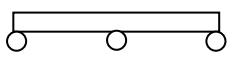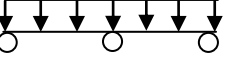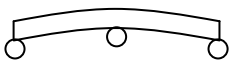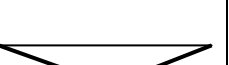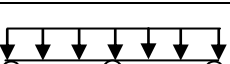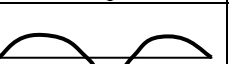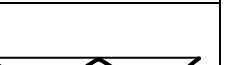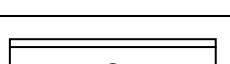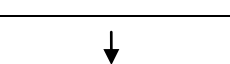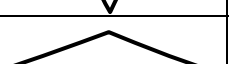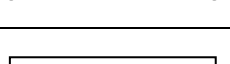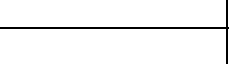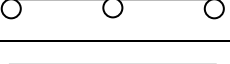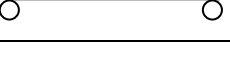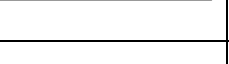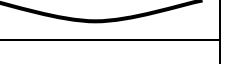
The prestressing is accomplished by raising the interior supports above their final elevation while the deck is cast. Once the concrete has cured the supports are lowered to their final elevation. Continuity of the steel member and the composite action with the deck produce a compressive stress in the concrete slab, which is balanced by tensile stresses in the bottom of the steel member. A more complete description of the process is provided in the following section.

This guide describes the construction procedure, design considerations, and implementation details for using the self-stressing method. The appendices provide a flow chart to aid in the implementation as well as simplified formulas applicable to two span bridges, which represents the most likely use of the method.

A.1 Construction Procedure Overview

This section provides a brief description to establish a frame of reference and vocabulary for the reader. These steps will be used as points of reference in the implementation chapter. Note that design sequence does not follow the construction sequence. Table A.1 illustrates the major steps required for the constructing a bridge using the self stressing method.

Table A.1. Self-stressing method major steps.

	Stage	Structure	Loading	Moment	Deflection
1	Place Girder on Level Supports				
2	Raise Interior Support				
3	Cast Concrete				
4	Lower Interior Support				
5a	Relaxation				
5b	Restoring Force				

The first stage is simply placing the girder onto the level supports and the resulting moments and deflections are those obtained from a continuous beam analysis.

During the second stage, the interior support is raised. During this event, the bare steel girder responds as a simply supported beam subjected to a point load at the location of the interior support. Note that the supports could be in the raised position prior to placing the girder. However, due to superposition, the analysis would be the same as described.

Next the concrete deck is cast, or precast panels are placed and grouted. The response of the structure is that of a continuous bare steel beam, just as it would be for conventional construction.

During the third step, the interior support is lowered to its final position. Just as in step two, the response is that of a beam supported at the exterior supports only. However, the structure is now composite. This action places the concrete deck over the supports into compression.

Over time, creep and shrinkage will occur in the concrete deck. This may be accounted for in two stages. First, the creep and shrinkage are seen as an applied curvature on the structure. If the beam were simply supported by the exterior supports, this applied curvature would result in additional deflection without inducing additional load. However, due to the continuity, a restoring force is generated that prevents the displacement and results in additional stresses.

A.2 Design Considerations

This section provides a discussion of the design issues specific to the use of the self-stressing method.

Design of bridges using the self-stressing method shall follow the provisions for I-Section and Box-Section flexural members contained in Section 6.10 and 6.11 respectively, except as modified herein.

A.2.1 General

The use of the self-stressing method is limited to straight I and Box section steel girders. The self-stressing method is only applicable to continuous multi-span structures with a composite deck. Simplified design aids are provided in Section A.5 for structures with two spans.

A.2.2 Analysis

Two options are provided for the analysis of the structure, which are described in the following section. Note that the analysis methods described herein are in reference to analyzing the construction steps associated with the self-stressing method only and not the overall analysis procedures as covered in AASHTO Chapter 4.

A.2.2.I Simplified

The simplified analysis method relies on first order techniques that disregard time effects in the concrete. These effects are accounted for using conservative correction factors presented in the Implementation Details portion of this guide. The correction factors account for the effects of creep and shrinkage in the evaluation of stresses and deflections. As an alternative, advanced methods of analysis may be used that directly evaluate these effects.

A.2.2.II Advanced

Advanced methods explicitly consider the effects of creep and shrinkage to evaluate the stresses and deflections.

Several such methods are the AEMM, EMM, SSM, and RCM.

When the creep and shrinkage strains are known, or otherwise assumed, AASHTO Section C4.6.6 describes a method for calculating the resulting stresses and deformations.

A.2.3 Forces

The forces and stresses in all components that arise due to the self-stressing construction procedure shall be considered in evaluating the load effects during design. For the purpose of design the locked in prestressing force shall be considered dead load force applied to the composite long term section (DC2).

AASHTO Section 3.4.1 states that where prestressed component are used in conjunction with steel girders the force effect should be considered locked in construction loads (EL). However, in this situation the prestressing forces are being developed by gravity effects rather than applied by prestressing devices. As such, the variability in the resulting stresses will be of the same magnitude as the variability of the dead load effects, which leads to the decision of considering the prestress stress as DC2 loading.

Note that the self-stressing procedure will generate tensile stresses in the bottom of the steel girders that will serve to offset some of the compressive dead and live load stresses. As such, the stresses due to the self-stressing procedure should be kept separate from other dead load stress sources and the minimum dead load factor should be used (0.9).

A.2.4 Deflections

The final deflected shape is necessary for determining the camber requirements of the girders. The final deflection is summation of deflections from the various construction stages.

A.3 Design Procedure and Implementation Details

This section provides a step by step procedure for designing a bridge incorporating the self stressing method.

A.3.1 Determine Required Amount of Prestress

The self-stressing method is a way to introduce compressive stresses in the concrete deck of a multispan continuous beam. The compressive stresses are generally located near the interior supports and therefore work to counter the tensile stresses that arise in this vicinity due to live loading. The result is a reduction in cracking and an accompanying increase in service life. The magnitude of the prestress that must be applied to achieve the desired effects has been determined based on past experience with decks that have been prestressed using traditional mechanical methods.

A.3.1.I Minimum Final

The recommended minimum level of prestress at the top fiber of the concrete deck over an interior support, after all losses, is 750 psi.

The simplified (Bernoulli assumption) analysis methods predict a linear variation of stresses through the thickness of the deck, which produces a maximum stress value at the face of

the concrete. In practice, creep effects quickly blunt this maximum stress value resulting in a more uniform stress profile through the depth of the concrete. The prescribed minimum prestress value at the face of the slab is intended to provide a final uniform value over the top half of the slab of 250 psi, which is the value recommended in Section 9.7.5.3 of the AASHTO Specifications for longitudinal prestressing of concrete slabs.

Figure 1 shows the initial stress distribution in the concrete deck and that which develops after some period of time has elapsed.
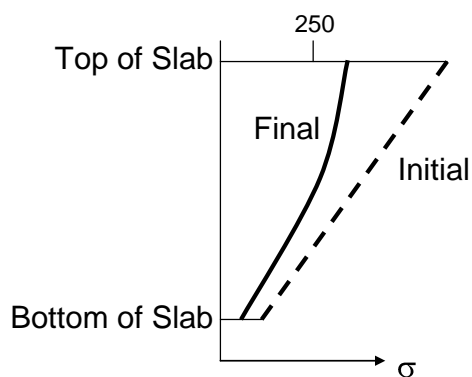
Figure 1. Stress Distribution in Concrete Deck

A.3.1.II Maximum Initial

The maximum initial prestress to be applied shall be no greater than 60 percent of the concrete compressive strength.

There is no upper limit recommendation in the literature because the material maximum strength is a natural upper bound. However, in order to maintain a safe margin the upper limit shall not be greater than 60 percent of the concrete compressive strength (0.6*f'c) which is the compressive stress limit recommended in Section 5.9.4.1.1 of the AASHTO Specifications for pretensioned and post-tensioned concrete components, including segmentally constructed bridges.

A.3.1.III Adjust for Losses

In lieu of an exact analysis, the prestress loss may be conservatively estimated as 20 percent when the initial prestress value is less than 40 percent of the concrete compressive strength and 30 percent when the initial prestress value greater than 40 percent of the concrete compressive strength.

The initial prestress at the top fiber that is to be applied is given by Equation 1.

$$\sigma_{pi} = \frac{\sigma_{pf}}{(1 - r_s)} \qquad \textbf{EQ 1}$$

Where:

σ_{pf}	=	Final Prestress Stress
σ_{pi}	=	Initial Prestress Stress
r_s	=	Loss due to Creep and Shrinkage

A.3.2 Calculate Amount of Deflection to Obtain Desired Prestress

Determine the height that the interior support must be raised that upon release will provide the desired amount of prestress.

The problem at hand is essentially that of support settlement. How far must the interior support settle such that the stress in the top of the deck is the value chosen in the previous design step (Section A.3.1).

For the following steps, the structure to be considered is the composite structure being supported at the exterior supports only, which is shown in Figure 2.

Figure 2. Equivalent structure used for calculating stresses during lowering of support.

a)   Determine the stress at the top fiber of the deck due to point loading applied at the interior support location.

b)   Use the result from the (a) to solve for the magnitude of the forces required to produce the desired prestress determined in the initial design step (Section A.3.1).

c)   Calculate the stiffness with respect to point load applied at the interior support location.

d)   Use the stiffness from (c) to solve for displacement required to produce the necessary force. For the structure shown in Figure 2, this displacement is given by Equation 2.

$$\delta = \frac{\sigma_{ts} L_1 L_2}{3 E_{conc} c_{ts}}$$ **EQ 2**

Where:

δ = Amount of displacement required

σ_{ts} = Initial Prestress Stress

L1 = Length of Span 1

L2 = Length of Span 2

EConc = Modulus of Elasticity of Concrete

Cts = Distance from neutral axis to top fiber of slab

A.3.3 Determine Forces Due to Lifting Bare Steel Beam

The results obtained from this step are used to complete the constructability check of the structure. For the following steps, the structure to be considered is the bare steel beam being supported at the exterior supports only, which is shown in Figure 3.
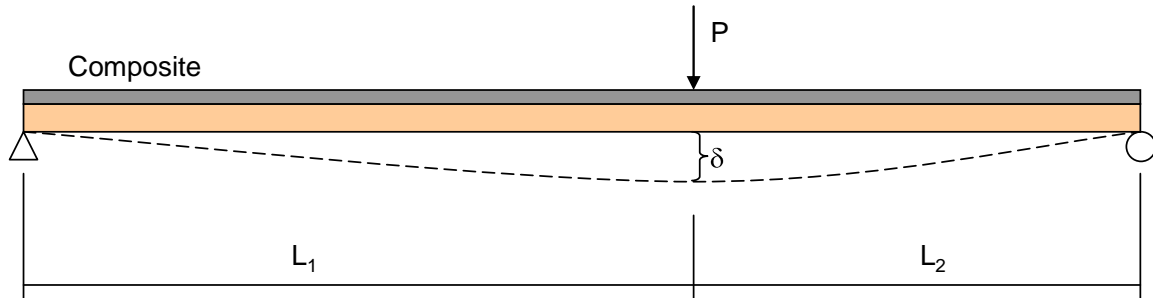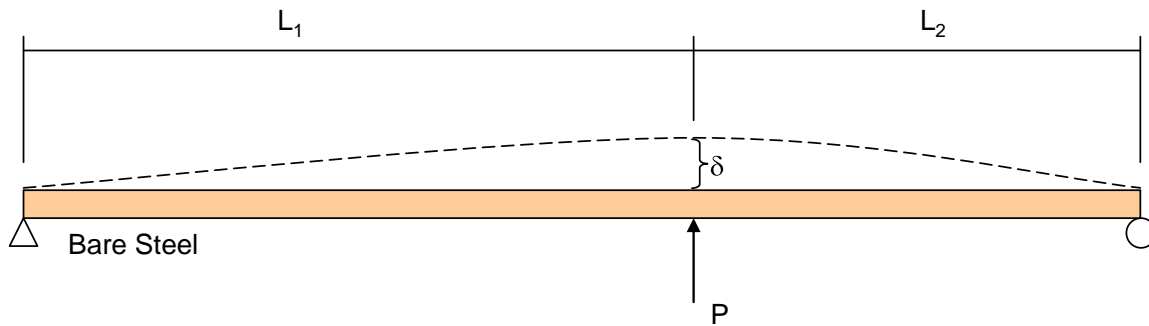
Figure 3. Equivalent structure used for calculating stresses during the raising of the support.

a)   Calculate the stiffness with respect to point loads applied at the interior support locations.

b)   Use the stiffness from (a) to calculate the force required to lift the interior supports to the height determined in the previous design step (Section A.3.2). For the structure shown in Figure 3, this force is given by Equation 3.

$$P = \frac{3E_{steel}I_{steel}(L_1 + L_2)}{L_1^2 \, L_2^2} \delta \qquad \textbf{EQ 3}$$

Where:

P = Reaction at Support due to Deflection of Support

δ = Deflection of Support

L_1 = Length of Span 1

L_2 = Length of Span 2

E_{steel} = Modulus of Elasticity of Steel

I_{steel} = Moment of Inertia of Bare Steel Girder

c)   Using the force given by (b), the reactions, moments, and stresses can be calculated as needed for design.

Author Note: The steel girders, and any support structures, temporary or permanent must be designed for the concentrated forces of lifting the girders.

A.3.3.I End Anchorages

The calculated vertical displacement may require a lifting force that is greater than the self-weight of the steel girder such that the girder would lift off of the end supports. In this

situation, the exterior ends of the girder may be anchored to prevent uplift. Once the concrete deck is in place, the weight of the deck will replace this anchorage force.

Also note that loading within the spans can affect uplift at the end supports. Consider the structure shown in Figure 4. Loading in the first span will create uplift at the end support of the opposite span. Therefore, the progression of deck casting or precast panel placement may affect the need for end anchorages. This possibility must be properly accounted for either through design or the specification of explicit procedures to avoid the condition described above.
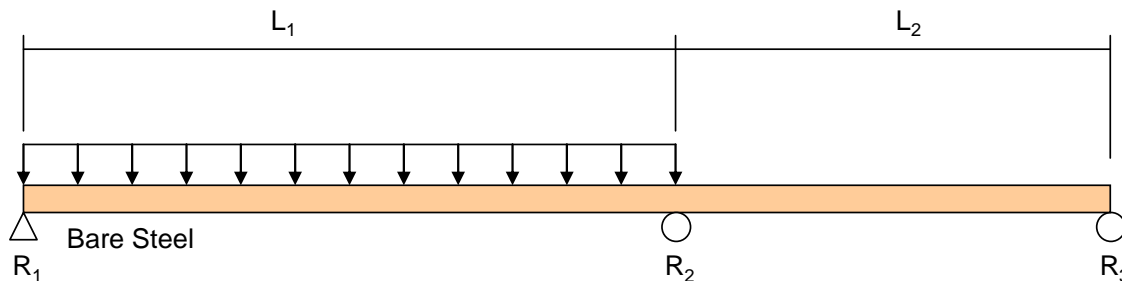
Figure 4. Loading in Span 1 Producing Uplift at Support 3.

Equation 4 gives the reaction at the end of Span 2 (unloaded span) due the following combination of loading:

- self weight of the steel girder (w_{steel})
- an upward displacement of the interior support (δ)
- uniform load within Span 1 due to deck placement (w_{deck})

This equation will aid in evaluating the need and magnitude of end anchorages. The critical condition occurs when span 1, the loaded span, is longer than Span 2. Therefore, when the spans are of different lengths, the deck within the short span should be cast first.

$$\frac{w_{steel}(3L_2^2 + L_1 L_2 - L_1^2)}{8L_2} - \frac{3E_{steel}I_{steel}}{L_1 L_2^2}\delta - \frac{w_{deck}L_1^3}{8L_2(L_1 + L_2)} \qquad \textbf{EQ 4}$$

Where:

w_{steel} = Uniform load due to Self weight of the steel

w_{deck} = Uniform load due to Deck Placment

$$\delta \quad = \quad \text{Deflection of Support (Positive Upward)}$$

L_1 = Length of Span 1

L_2 = Length of Span 2

E_{steel} = Modulus of Elasticity of Steel

I_{steel} = Moment of Inertia of Bare Steel Girder

For the case of two equal spans ($L_1=L_2=L$), Equation 5 can be simplified to:

$$\frac{3Lw_{steel}}{8} - \frac{3E_{steel}I_{steel}}{L^3}\delta - \frac{Lw_{deck}}{16} \qquad \textbf{EQ 5}$$

Where:

L = Length of Spans 1 and 2 (Equal)

Author Note: End Anchorages, when necessary must be designed to withstand the concentrated force that is to be applied.

A.3.4 Determine Forces and Stresses Due to Lowering Composite Bridge

The forces and stresses imparted on the structure due to lowering the composite bridge are obtained from a similar analysis to that performed when the amount of deflection was originally calculated (Section A.3.2).

For the following steps, the structure to be considered is the composite structure being supported at the exterior supports only, which is shown in Figure 5.
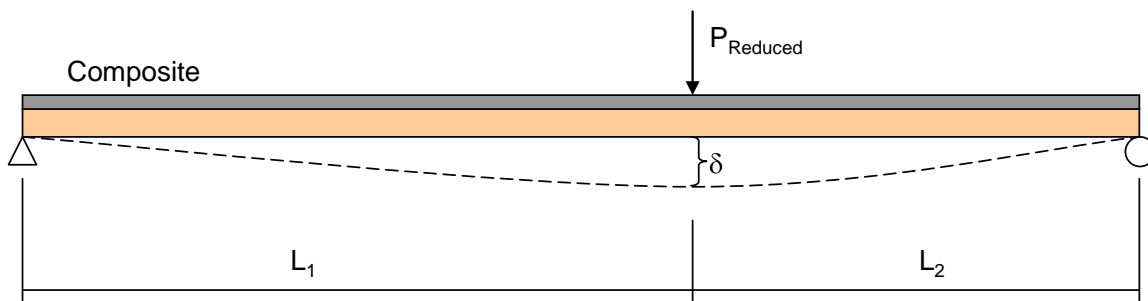
Figure 5. Equivalent structure used for calculating stresses during lowering of support.

a) Calculate the stiffness with respect to a point load applied at the interior support location.
b) Use the stiffness from the (a) to calculate the equivalent point force due to the lowering of the support.
c) Reduce the force calculated in (b) to account for the prestress loss due to creep and shrinkage, as determined in Section A.3.1.III.
d) Using the reduced force applied to the composite structure supported at the exterior supports, calculate the internal forces and stresses necessary for design.

The resulting forces and stresses from this step should be considered dead load forces

applied to the composite structure for the purpose of design.

A.3.5 Determine Deflected Shape

The final deflected shape is necessary for determining the camber requirements of the

girders. The final deflection is the summation of deflections from the various construction

stages.

A.3.5.I Bare Steel Deflection

Sources of deflection of the bare steel girder are:

- Self Weight of Steel
- Initial Lift of Interior Supports
- Casting of Wet concrete

Calculation of deflection due to the self weight of the steel and casting of the wet

concrete are calculated in a conventional manner using the continuous bare steel structure, as

shown in Figure 6. Equations for calculating the deformation along the length of the beam can

be found the Section A.5.
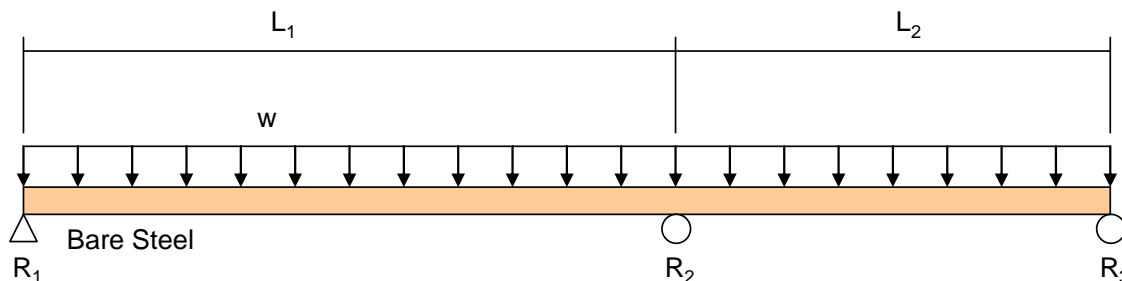
Figure 6. Structure for Calculation of Bare Steel Deflections

Calculation of the deflection due to the initial lift of the interior support is determined considering the bare steel girder supported at the exterior supports only, as shown in Figure 7. The structure is subjected to point forces applied at the interior supports as determined in Section A.3.3. Equations for calculating the deformation along the length of the beam can be found the Appendix B.
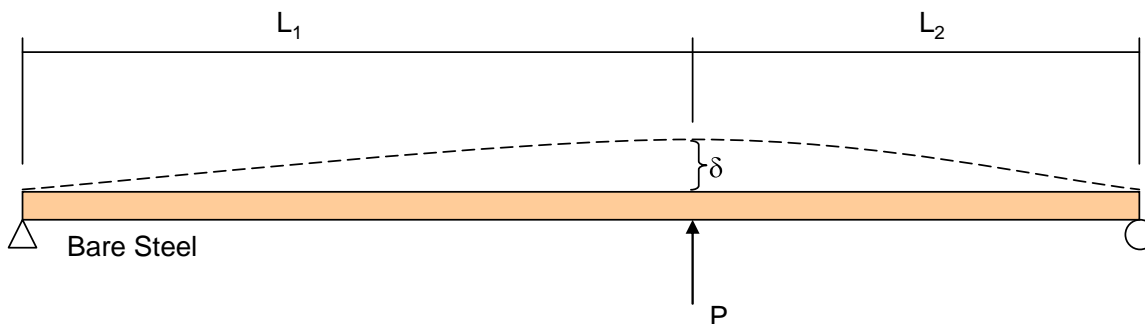
Figure 7. Structure for Calculation of Bare Steel Deflections due to Initial Lifting of Support

A.3.5.II Composite Deflection

Calculation of the deflection due to the lowering of the interior support is determined considering the composite bridge girder supported at the exterior supports only, shown in Figure 8. The structure is subjected to point forces applied at the interior supports as determined in Section A.3.4 **without** the reduction in load meant to account for creep and shrinkage. Creep and shrinkage will have the opposite effect resulting in an increase of the total deflection. This

effect is discussed in the following section. Equations for calculating the deformation along the length of the beam can be found in Section A.5.
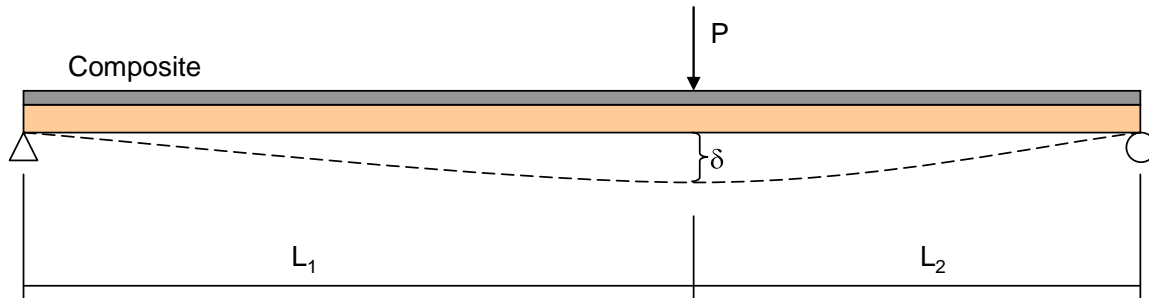
Figure 8. Structure for Calculation of Bare Steel Deflections due to Initial Lifting of Support

A.3.5.III Relaxation Deflection

Additional deflections arise due to curvature induced along the beam due to the effects of creep and shrinkage. The resulting loading can be seen in Figure 9.
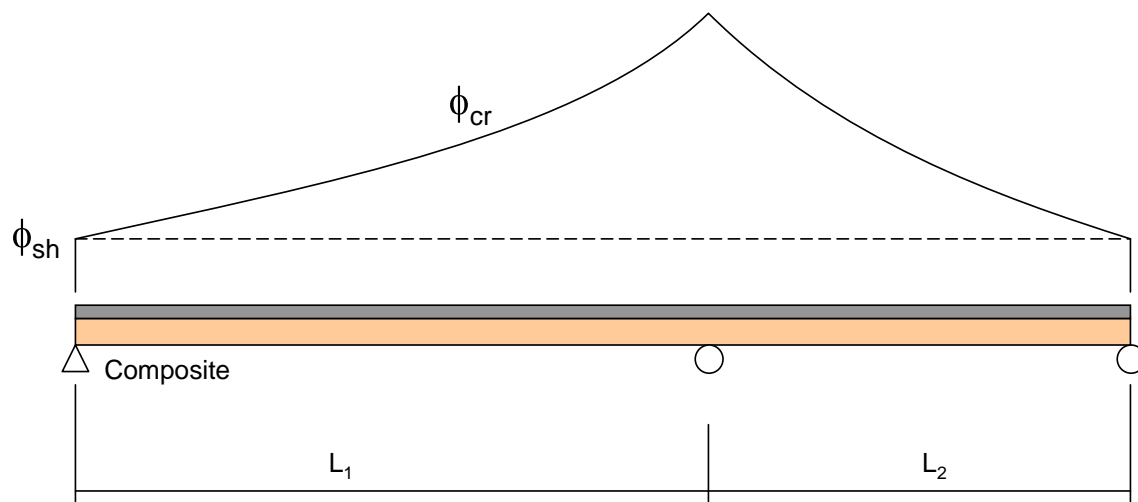
Figure 9. Curvature applied to continuous structure due to creep and shrinkage

The steps for calculating the deflected shape can be performed using the following steps considering the structure supported at the exterior locations only, as shown in Figure 10.
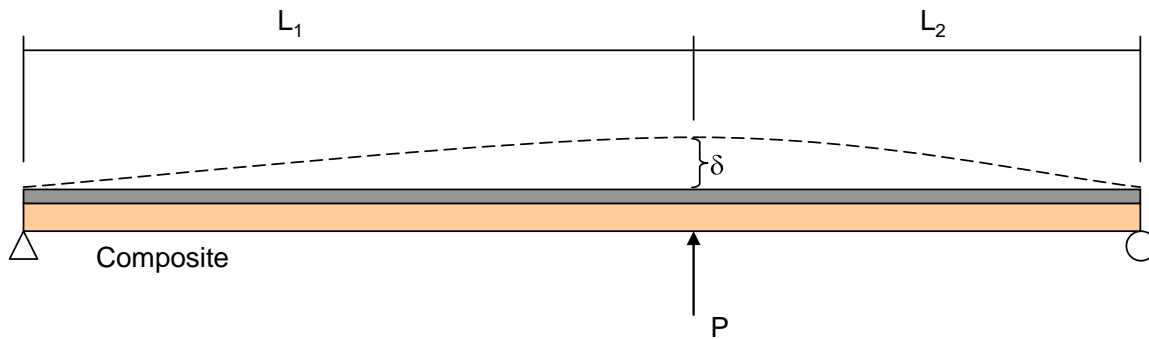
Figure 10. **Structure for determination of Restoring Force**

a)   Calculate the stiffness with respect to a point load applied at the interior support location.

b)   Determine the curvature along the length of the beam. The curvature at a section can be obtained from Equation 6. AASHTO Section 5.4.2.3.1 provides methods for determining the values of ε_{sh} and ε_{cr}.

$$\varphi = \frac{1}{I_c} \int (\varepsilon_{sh} + \varepsilon_{cr}) z \, dz \qquad \textbf{EQ 6}$$

Where:

Φ = Curvature of section

I_c = Composite Moment of Inertia

ε_{sh} = Strain due to shrinkage

ε_{cr} = Strain due to creep

z = Distance from Neutral Axis

c)   Calculate the displaced shape of the structure due to the applied curvature, shown in Figure 11. The displacement can be calculated using the integration given in Equation 7.
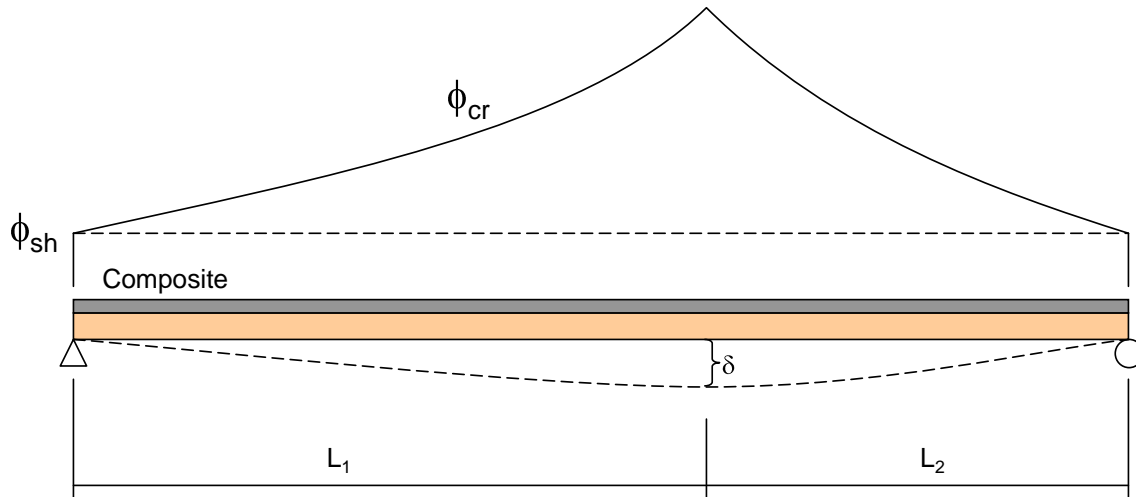
Figure 11. **Structure for determination of Deflection due to Curvature**

$$\delta(x) = \int_0^x \int_0^x \varphi(x)\,dx\,dx \qquad \textbf{EQ 7}$$

Where:

$\Phi(x)$ = Curvature along the length of the Beam

d) Using the stiffness from (a), determine the force required to offset the displacement at the support location calculated in (c). This force is given by Equation 8.

$$P = \frac{3E_c I_c}{L_1^2 L_2^2} \int_0^x \int_0^x \varphi(x)\,dx\,dx \qquad \textbf{EQ 8}$$

Where:

E_c = Modulus of Elasticity of Concrete (Composite)

I_c Composite Moment of Inertia

e) The resulting deflection due to the relaxation is the sum of the deflections obtained from the applied curvature (Equation 6) and the application of the point load determined in (d) upon the structure shown in Figure 11. Equations for calculating the deformation along the length of the beam can be found the Section A.5.

A.3.6 Carry Out Remainder of Design

Author Note: This would include the design of other bridge components.

A.3.7 Precast Deck Panels

All grout, and/or adhesives must be adequately cured prior to lowering the interior support. The creep and shrinkage properties of the materials must be compatible with the intended use.

A.4 Design Flowchart

```
                        ┌──────────────────┐
                        │  Design criteria │
                        └────────┬─────────┘
                                 │
         ┌──────────────────┐    │
         │ determine bridge │    │
         │  geometry and    │    │
         │   dimentions     │    │
         └──────────────────┘    │
                                 │
  ┌──────────────────┐       ┌───┴──────────────────┐
  │ Conventional     │◄──────┼──────►│ Self-stressing │
  │ design method    │       │       │ design method  │
  └────────┬─────────┘       │       └───────┬────────┘
           │                 │               │
  ┌────────▼─────────┐       │       ┌───────▼────────┐
  │    calculate     │       │       │ choose level of│
  │ loads/stress due │       │       │ compressive    │
  │ to girder weight │       │       │ stress         │
  └────────┬─────────┘       │       └───────┬────────┘
           │                 │               │
  ┌────────▼─────────┐       │       ┌───────▼────────┐
  │ calculate        │       │       │ determine amount│
  │ load/stress due  │       │       │ of displacement │
  │ to deck weight   │       │       └───────┬────────┘
  └────────┬─────────┘       │               │
           │                 │    ┌────────────┐  ┌──────────────┐
  ┌────────▼─────────┐       │    │ determine  │  │ determine    │
  │ check            │       │    │ force to   │  │ force need to│
  │ constructability │       │    │ anchor     │  │ raise bridge │
  │ (AASHTO LRFD)    │       │    │ girder ends│  └──────────────┘
  └────────┬─────────┘       │    └────────────┘
           │                 │               │
 ┌─────────▼──────────┐      │       ┌───────▼────────┐
 │ calculate load/    │◄─────┤       │ calculate load/│
 │ stress due to time-│      │       │ stress due to  │
 │ dependent effect   │      │       │ lifting        │
 └──────────┬─────────┘      │       └───────┬────────┘
            │                │               │
  ┌─────────▼────────┐       │       ┌───────▼────────┐
  │ calculate load/  │       └───────│ calculate load/│
  │ stress due to    │               │ stress due to  │
  │ live load        │               │ lowering       │
  └────┬────────┬────┘               └────────────────┘
       │        │
 ┌─────▼────┐ ┌─▼────────────┐
 │ service  │ │ strength     │
 │ limit    │ │ limit state  │
 │ state    │ │ (AASHTO LRFD)│
 │(AASHTO   │ └──────────────┘
 │ LRFD)    │
 └──────────┘
```
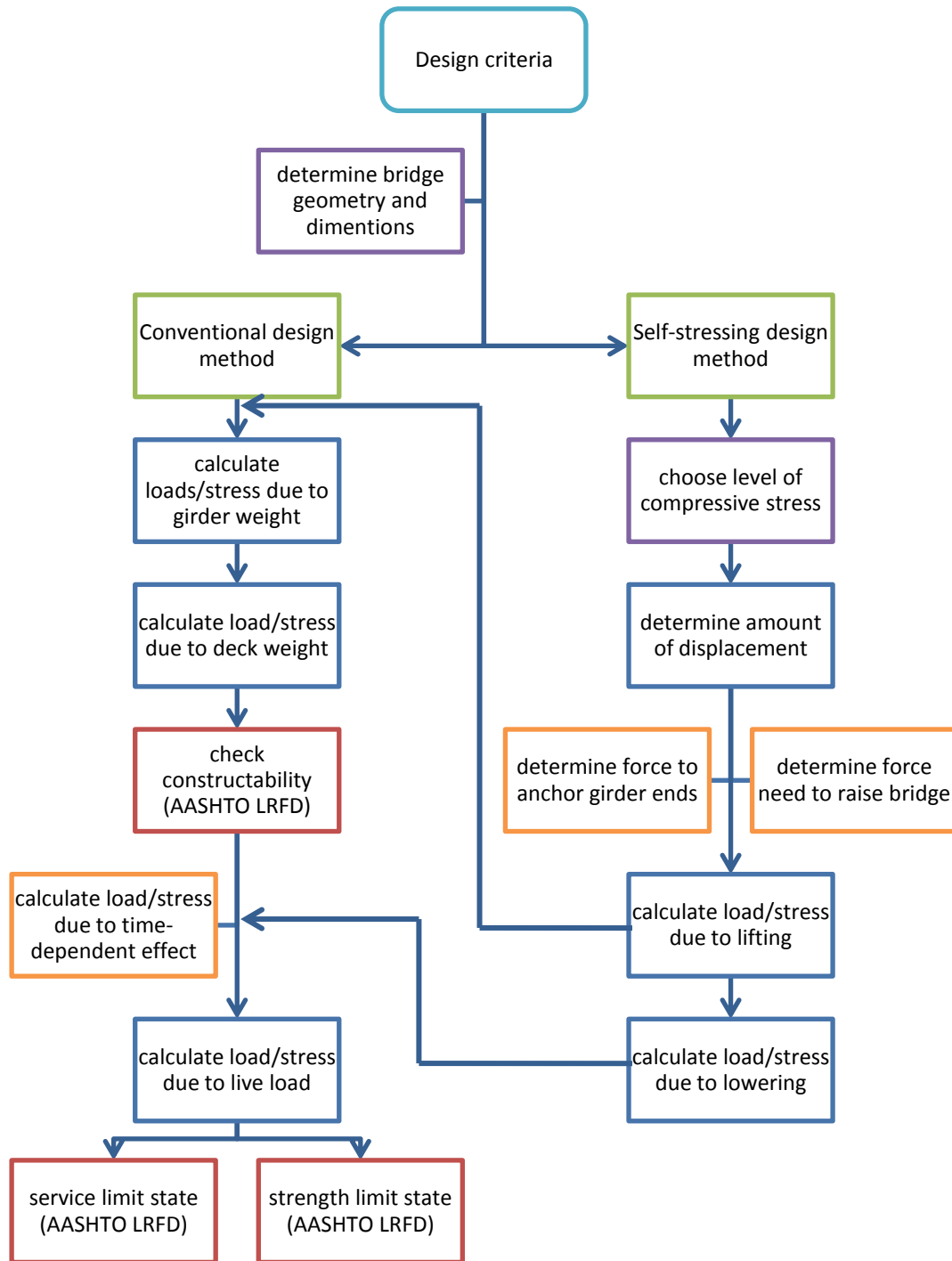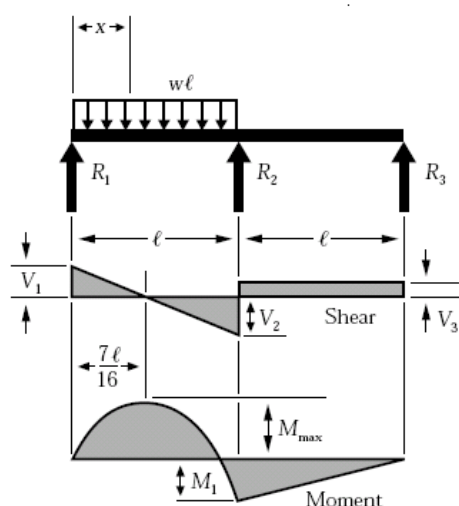
A.5 Design Aids for Two Spans Bridges

Content of this section keeps changing. Shears, Moments and Deflections of Needed Structure Types.

$$R_1 = V_1 \dots\dots\dots\dots\dots\dots\dots\dots = \frac{7}{16} wl$$

$$R_2 = V_2 + V_3 \dots\dots\dots\dots\dots\dots = \frac{5}{8} wl$$

$$R_3 = V_3 \dots\dots\dots\dots\dots\dots\dots\dots = -\frac{1}{16} wl$$

$$V_2 \dots\dots\dots\dots\dots\dots\dots\dots\dots\dots = \frac{9}{16} wl$$

$$M_{max} \left(at\ x = \frac{7}{16} l \right) \dots\dots\dots\dots = \frac{49}{512} wl^2$$

$$M_1 (at\ support\ R_2) \dots\dots\dots\dots = \frac{1}{16} wl^2$$

$$M_x (when\ x < l) \dots\dots\dots\dots\dots = \frac{wl^2}{16} (7l - 8x)$$

Figure 12.   **Continuous Beam – Two Equal Spans – Uniform Load on One Span**
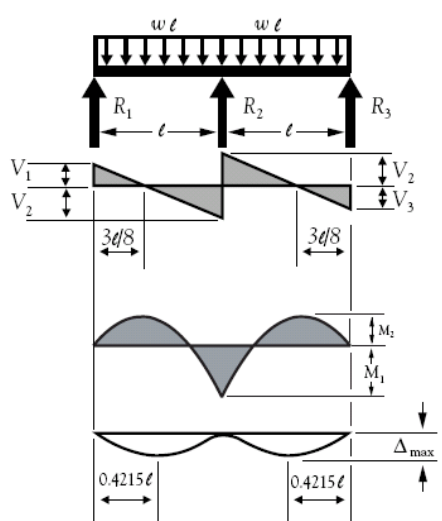
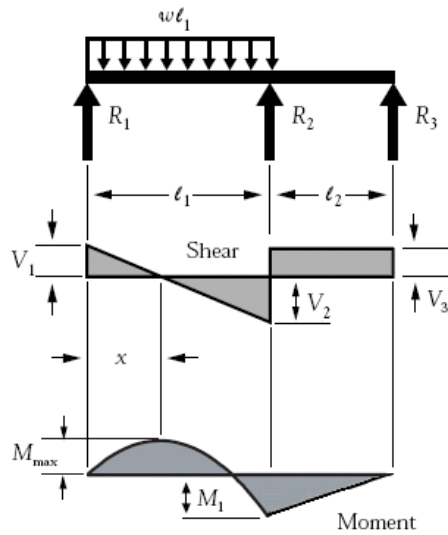$$R_1 = V_1 = R_3 = V_3 \dots\dots\dots\dots\dots\dots = \frac{3wl}{8}$$

$$R_2 \dots\dots\dots\dots\dots\dots\dots\dots\dots\dots\dots = \frac{10wl}{8}$$

$$V_2 = V_{max} \dots\dots\dots\dots\dots\dots\dots\dots = \frac{5wl}{8}$$

$$M_1 \dots\dots\dots\dots\dots\dots\dots\dots\dots\dots\dots = \frac{wl^2}{8}$$

$$M_2 \left(at\ \frac{3l}{8} \right) \dots\dots\dots\dots\dots\dots = \frac{9wl^2}{128}$$

$$\Delta_{max} (at\ 0.4215l, approx.from\ R_1\ and\ R_3) .. = \frac{wl^4}{185EI}$$

Figure 13.   **Continuous Beam – Two Equal Spans – Uniformly Distributed Load**

$$R_1 = V_1 \dots\dots\dots\dots\dots\dots = \frac{wl_1}{2} - \frac{M_1}{l_1}$$

$$R_2 \dots\dots\dots\dots\dots\dots\dots\dots = wl_1 - R_1 - R_3$$

$$R_3 \dots\dots\dots\dots\dots\dots\dots\dots = -\frac{M_1}{l_2}$$

$$V_2 \dots\dots\dots\dots\dots\dots\dots\dots = wl_1 - R_1$$

$$V_3 \dots\dots\dots\dots\dots\dots\dots\dots = R_3$$

$$M_1 \dots\dots\dots\dots\dots\dots\dots\dots = \frac{wl_2^3}{8(l_1 + l_2)}$$

$$M_{max}\left(\text{when } x = \frac{R_1}{w}\right)\dots\dots = R_1 x - \frac{w x^2}{2}$$

Figure 14. **Continuous Beam – Two Unequal Spans – Uniformly Distributed Load on One Span**
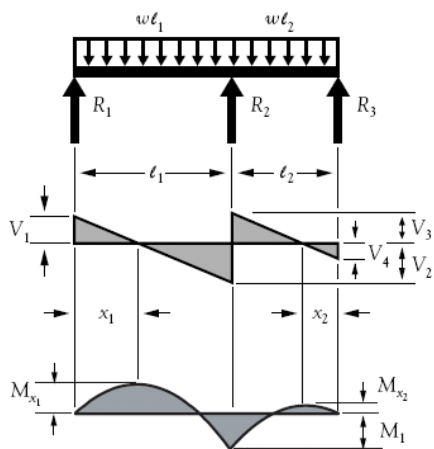
$$R_1 = V_1 \dots\dots\dots\dots\dots\dots = \frac{M_1}{l_1} + \frac{wl_1}{2}$$

$$R_2 \dots\dots\dots\dots\dots\dots\dots\dots = wl_1 + wl_2 - R_1 - R_3$$

$$R_3 = V_4 \dots\dots\dots\dots\dots\dots = \frac{M_1}{l_2} + \frac{wl_2}{2}$$

$$V_2 \dots\dots\dots\dots\dots\dots\dots\dots = wl_1 - R_1$$

$$V_3 \dots\dots\dots\dots\dots\dots\dots\dots = wl_2 - R_3$$

$$M_1 \dots\dots\dots\dots\dots\dots\dots\dots = \frac{wl_2^3 + wl_1^3}{8(l_1 + l_2)}$$
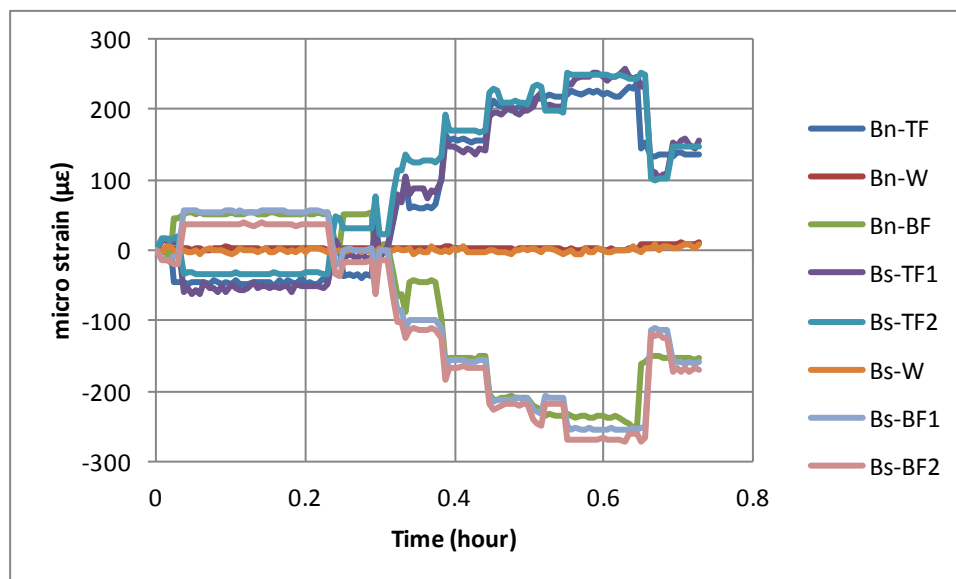
$$M_{x_1}\left(\text{when } x_1 = \frac{R_1}{w}\right)\dots\dots = R_1 x_1 - \frac{w x_1^2}{2}$$

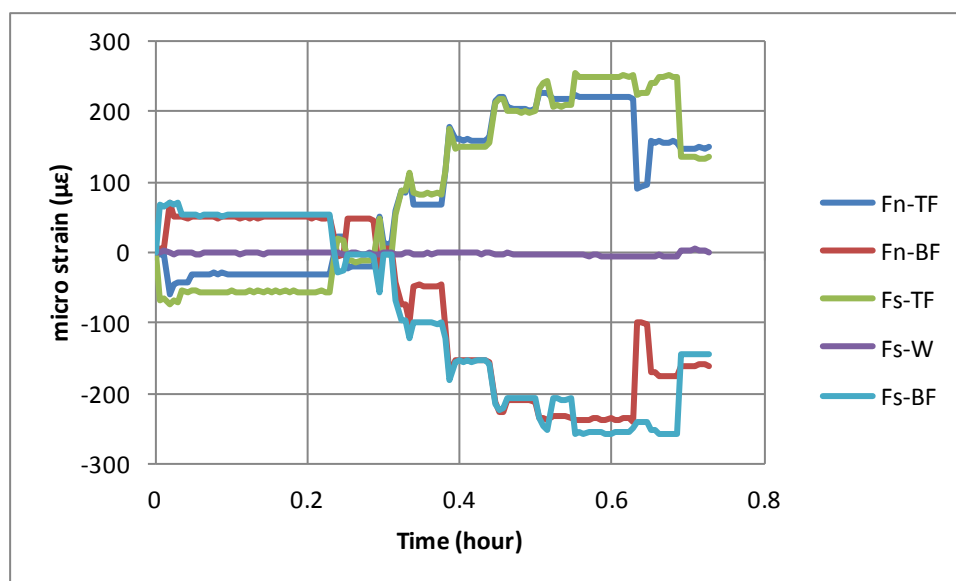$$M_{x_2}\left(\text{when } x_2 = \frac{R_3}{w}\right)\dots\dots = R_3 x_2 - \frac{w x_2^2}{2}$$

Figure 15. **Continuous Beam – Two Unequal Spans – Uniformly Distributed Load**
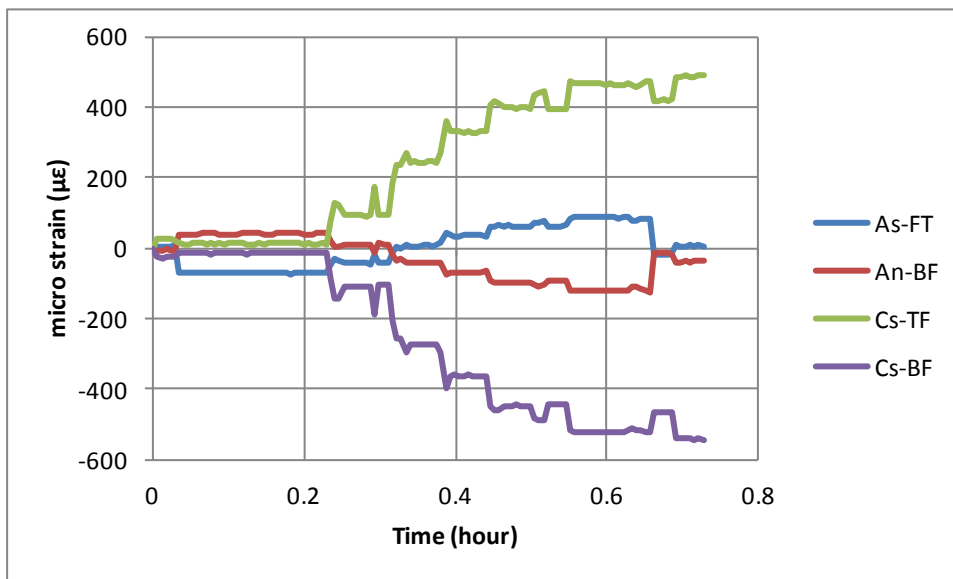
Appendix B   Experimental Data
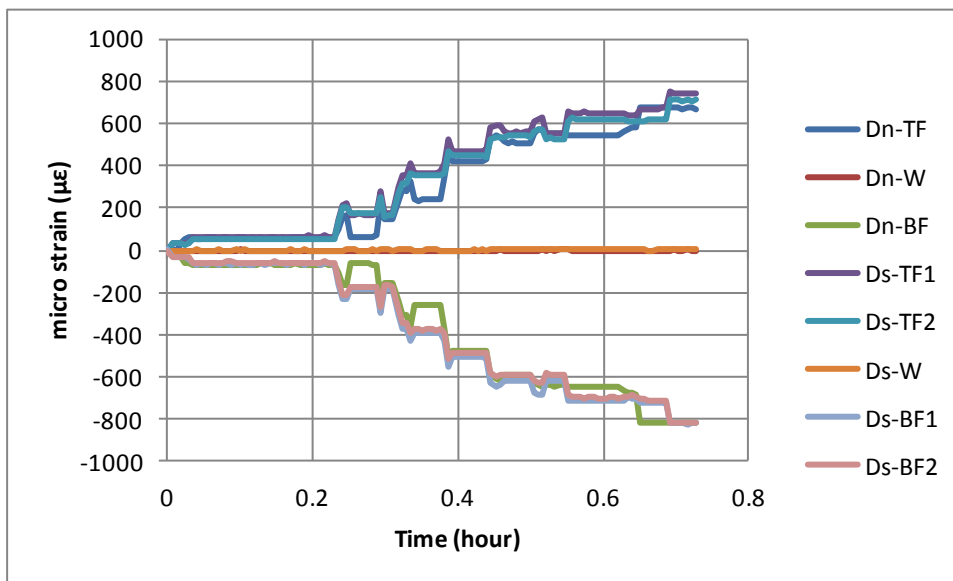
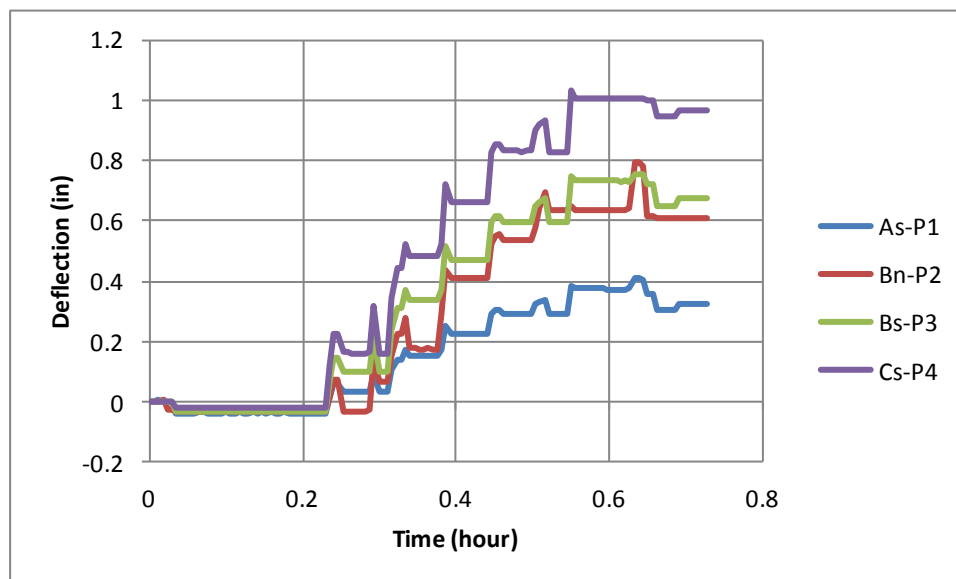# B.1 Drop of Initial Ballast and Shim Up Support

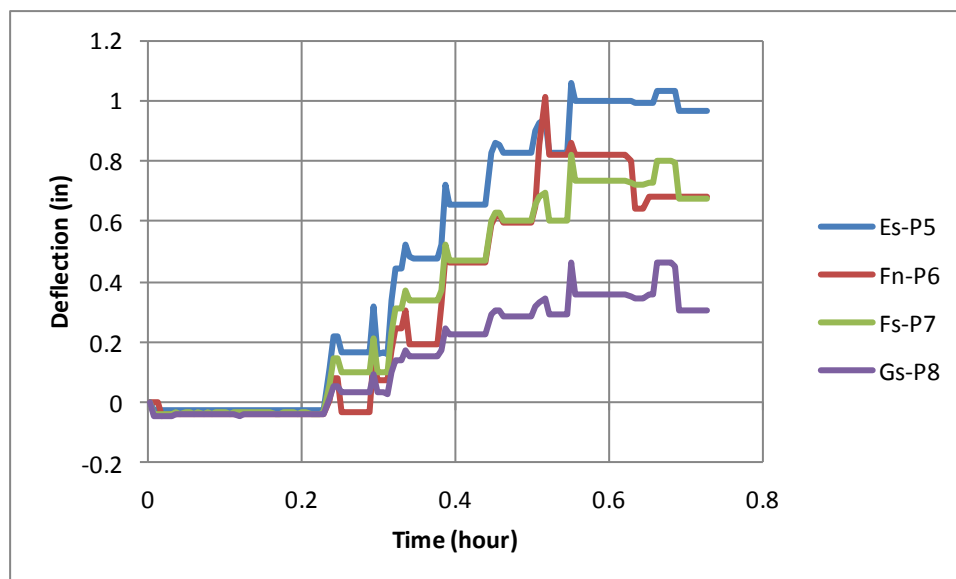
Mid-span (section B)

Mid-span (section F)

1/4 span (section A) and 3/4 span (section C)
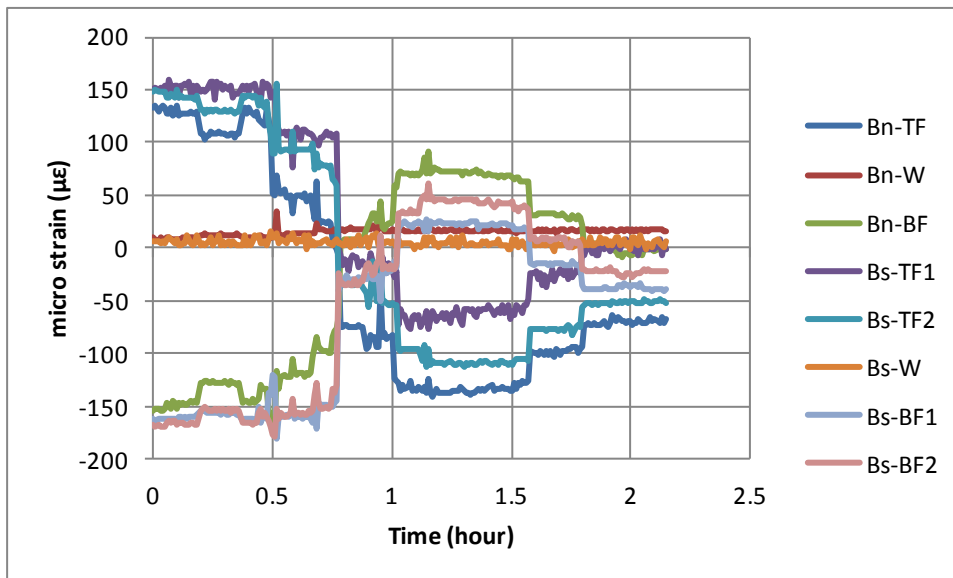

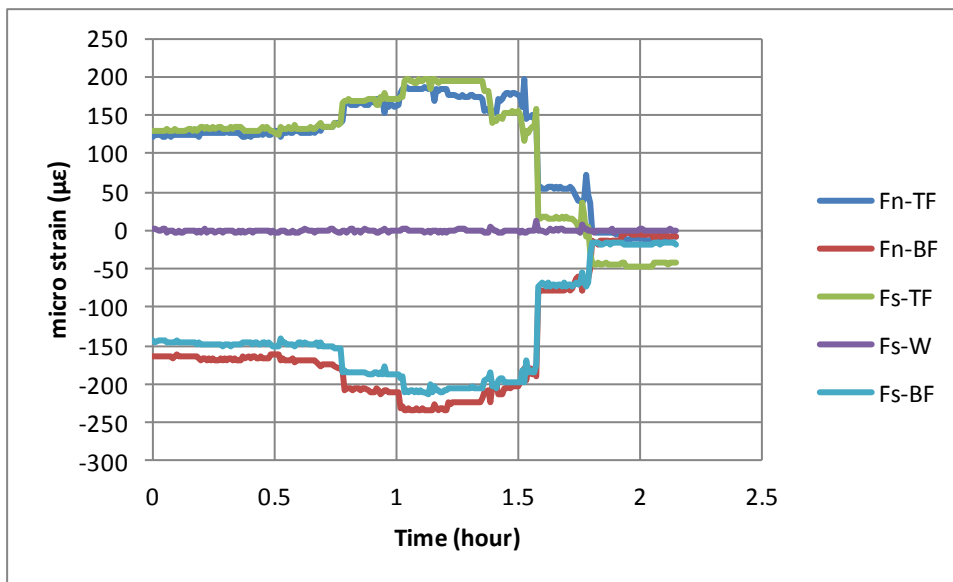**Interior support (section D)**

West span

East span

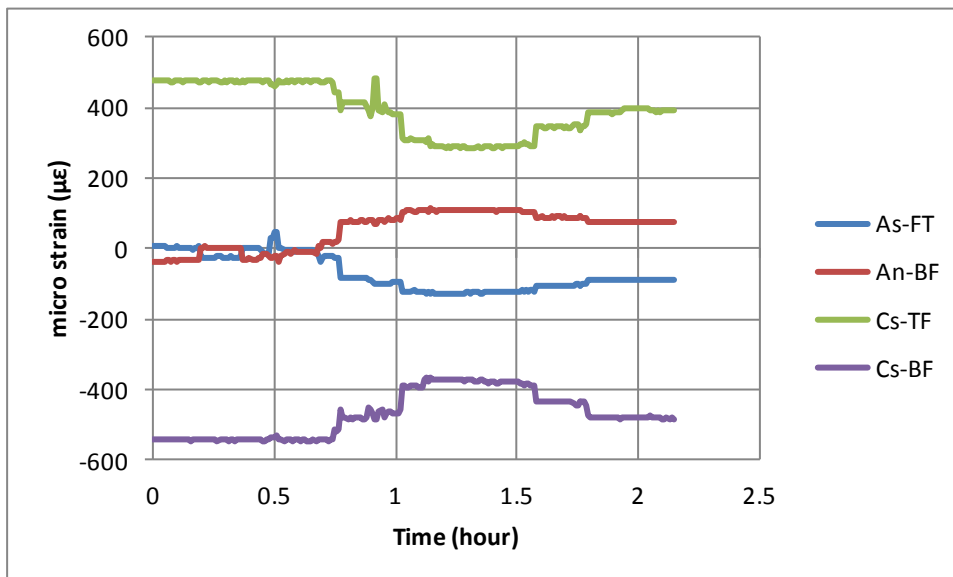# B.2 Drop of Remaining Ballast and Precast Placement

Mid-span (section B)

Mid-span (section F)

1/4 span (section A) and 3/4 span (section C)
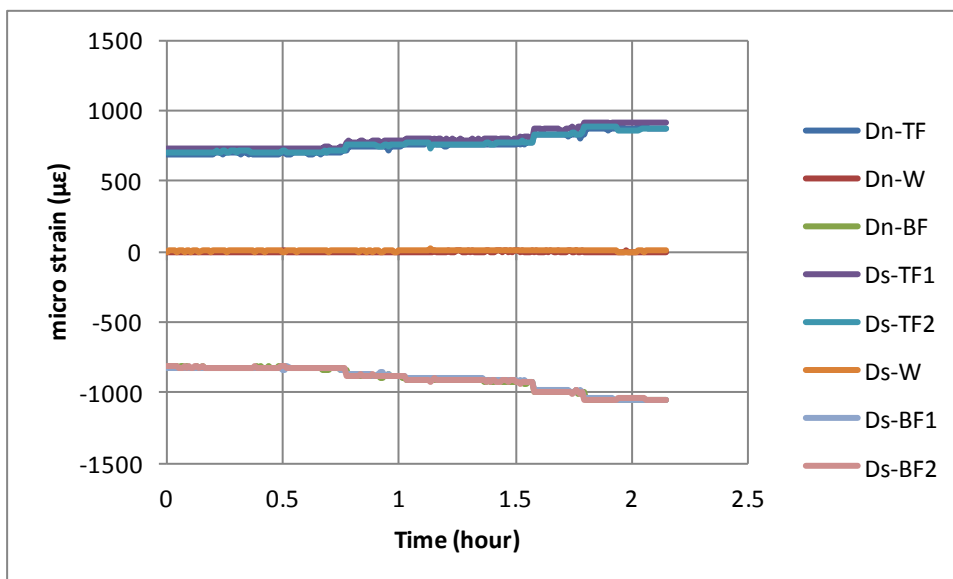
Interior support (section D)
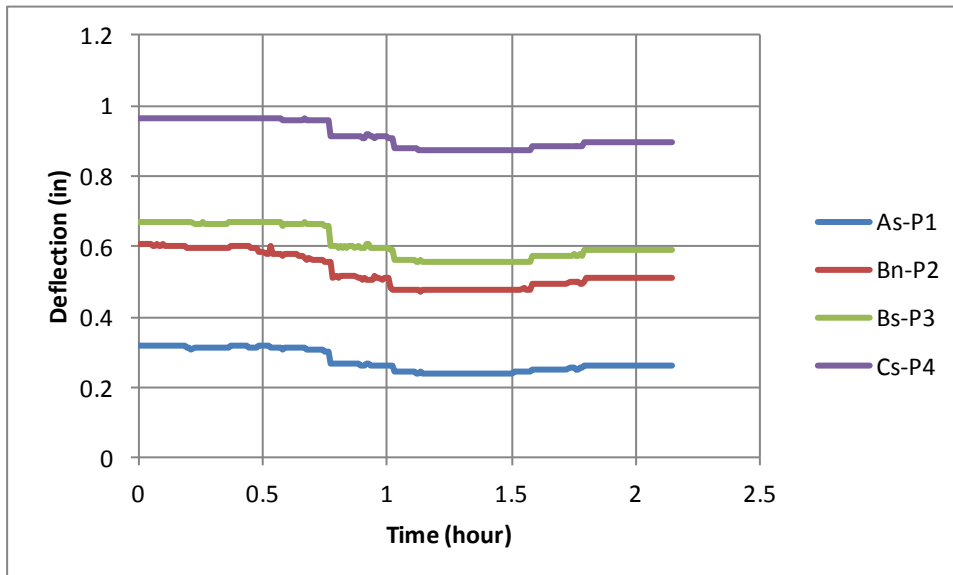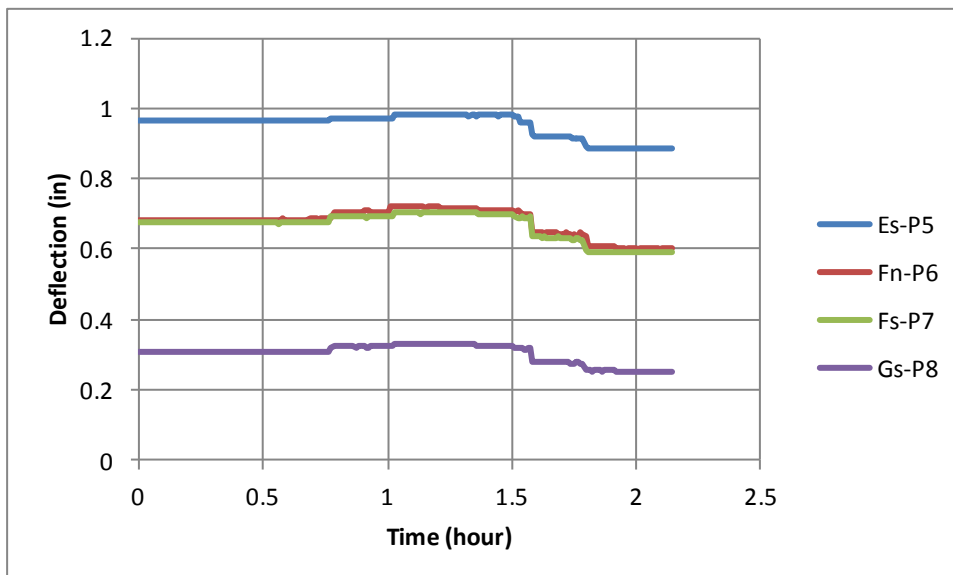
West span

East span

B.3 Shim Removal (self-stressing)
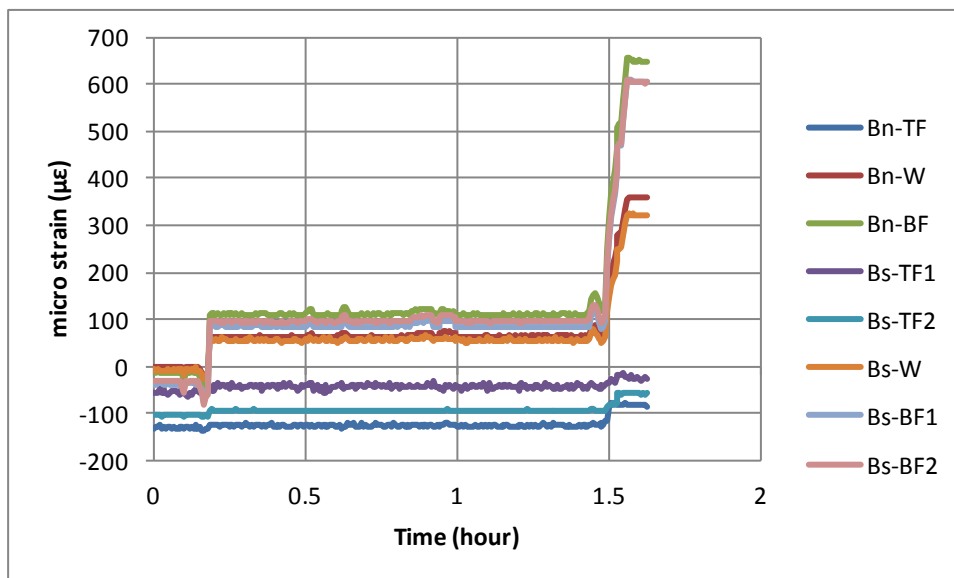
Mid-span (section B)
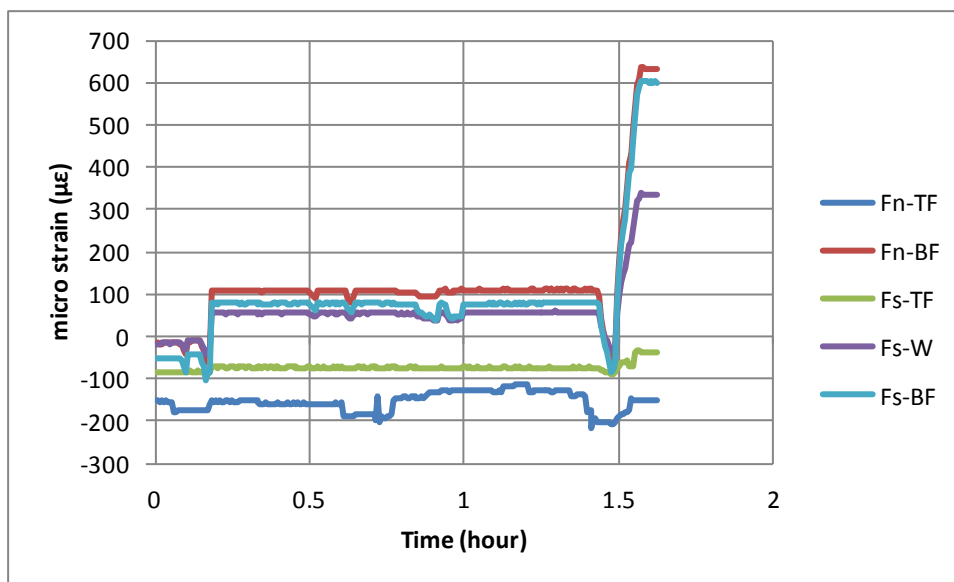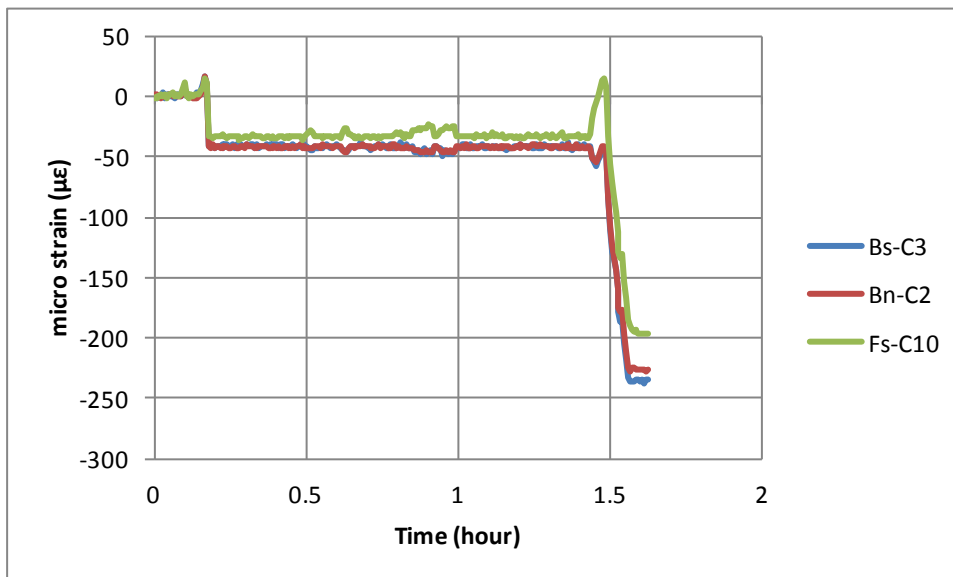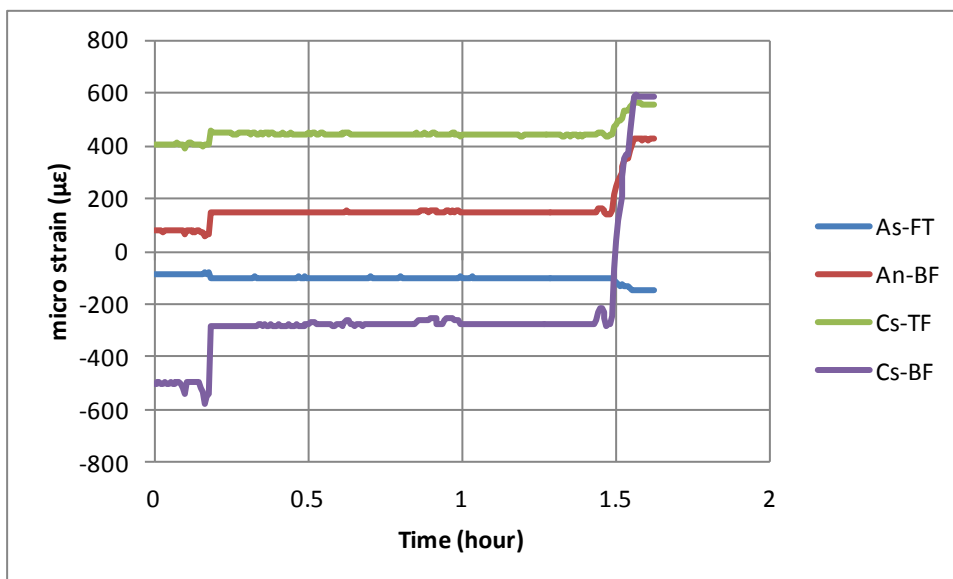
Mid-span (section F)

Mid-span (sections B & F) (concrete)

1/4 span (section A) and 3/4 span (section C)
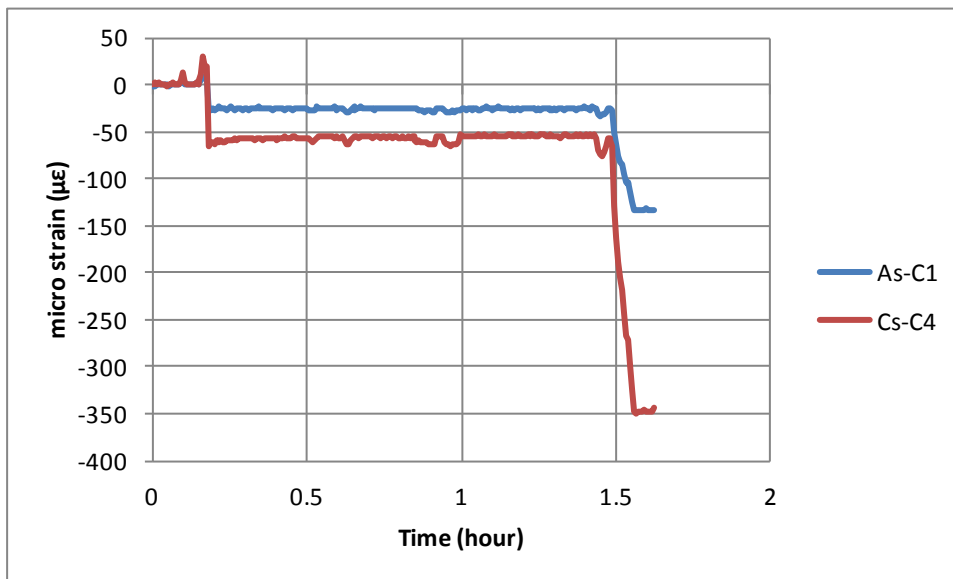
1/4 span (section A) and 3/4 span (section C) (concrete)
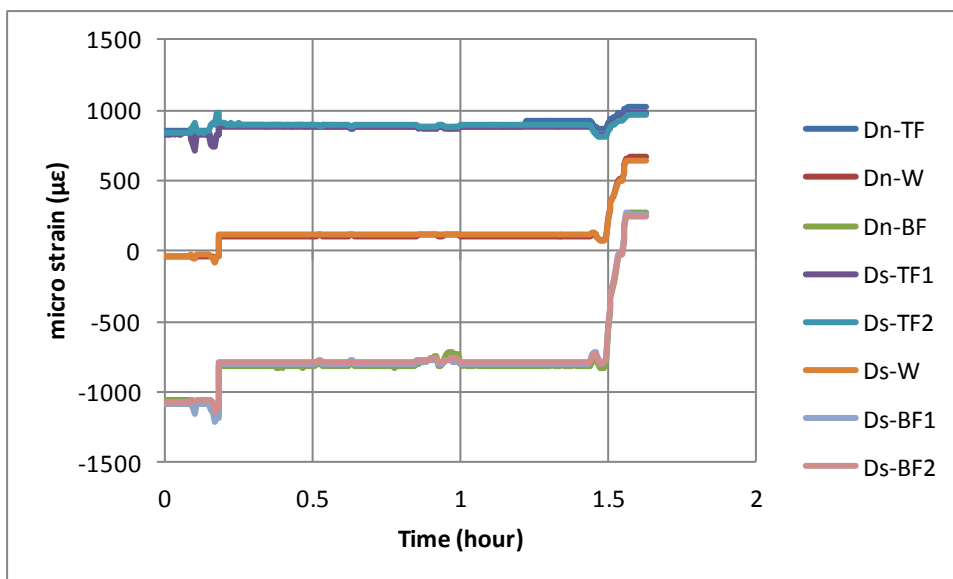
Interior support (section D)
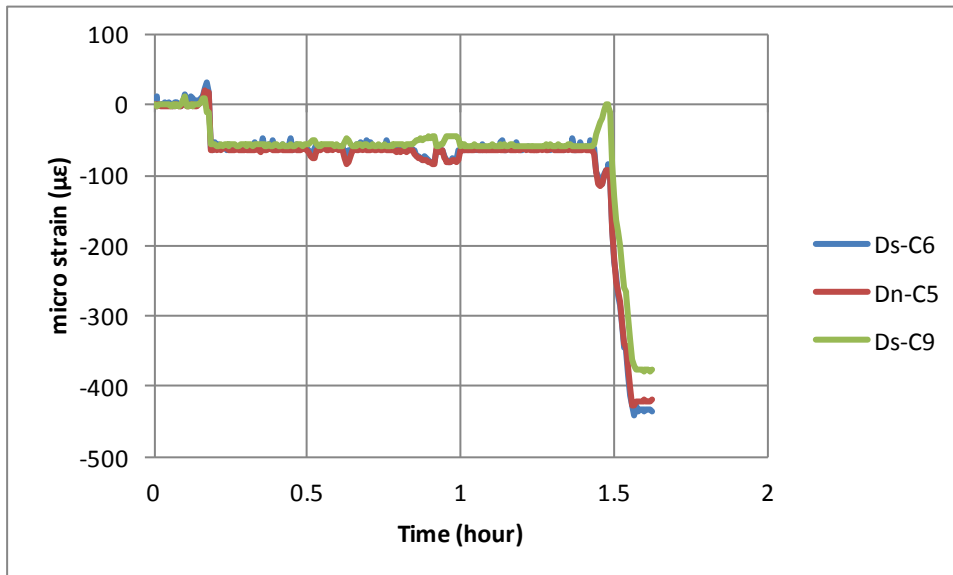
Interior support (section D) (concrete)
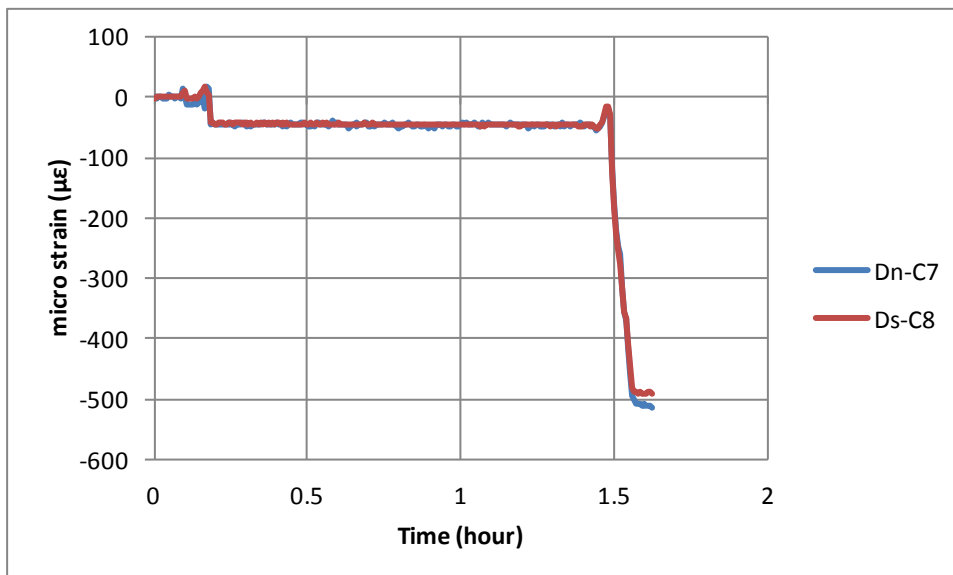
Interior support (section D) (grout)
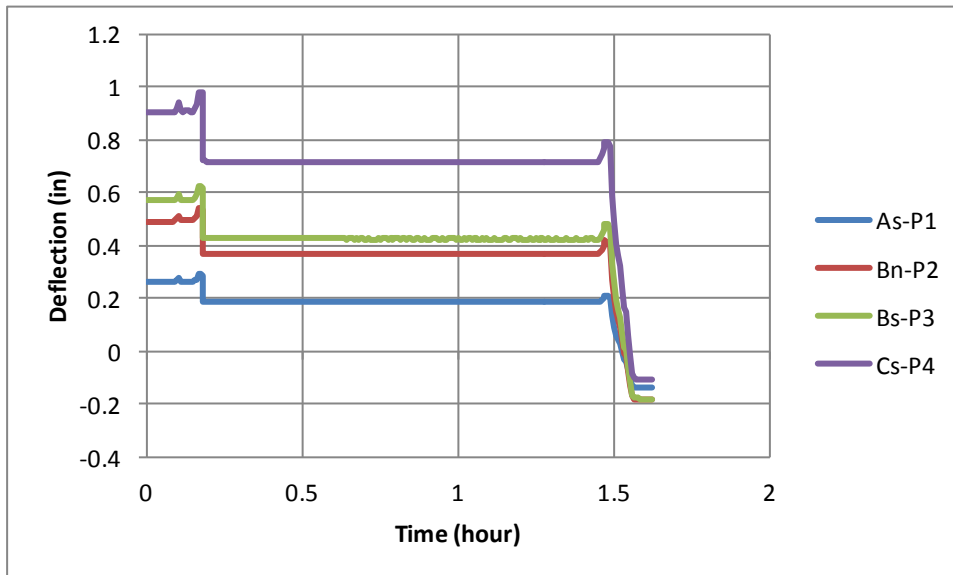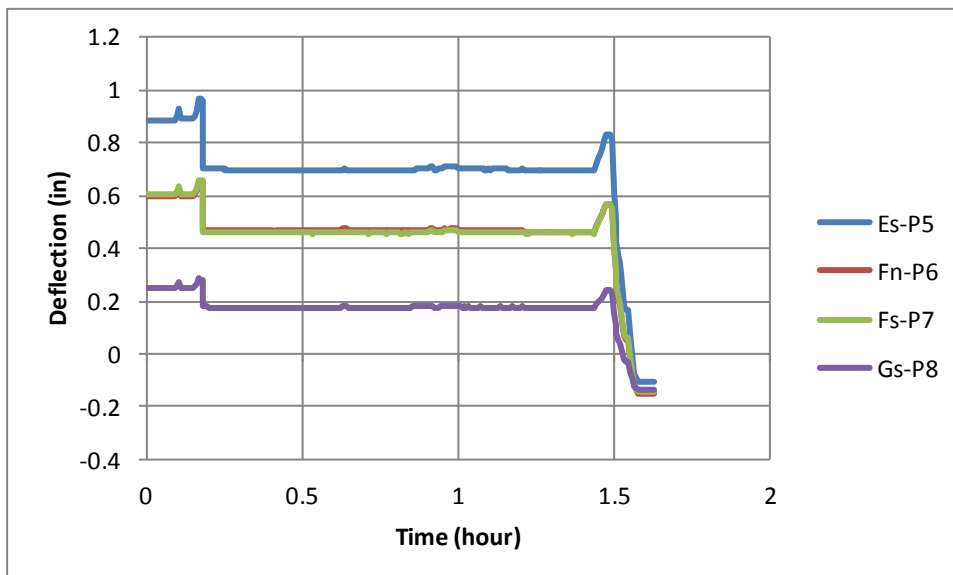
West span

East span

B.4 Long-term Monitoring
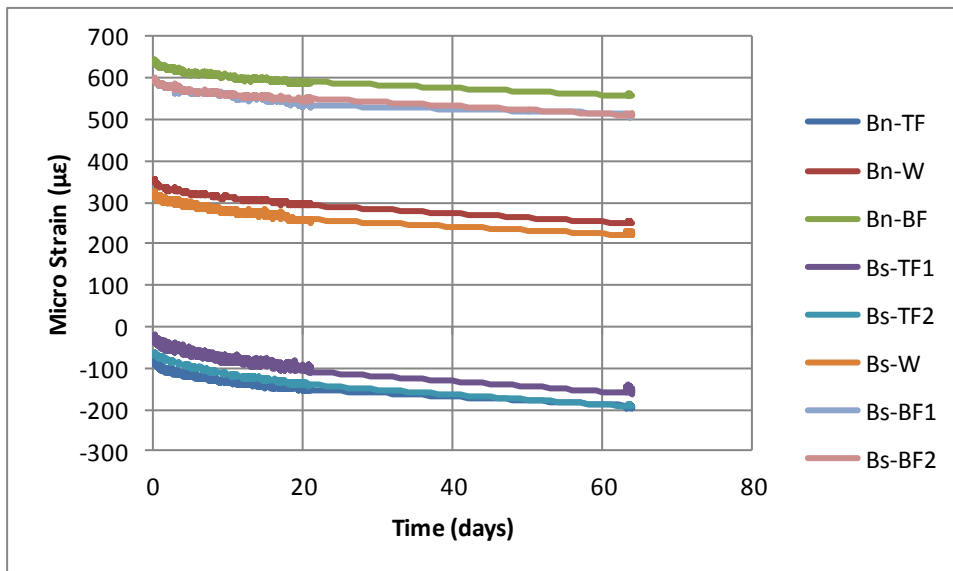
Mid-span (section B)
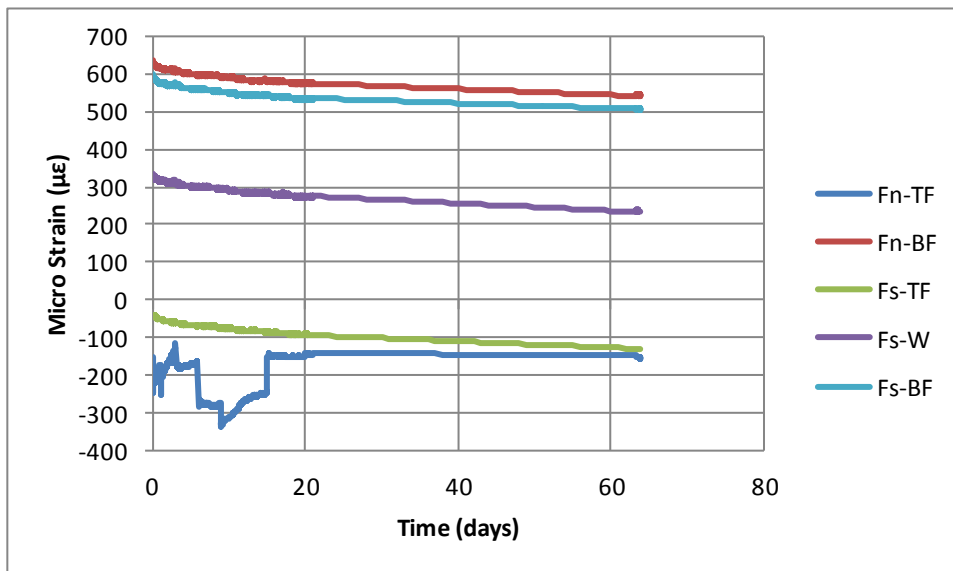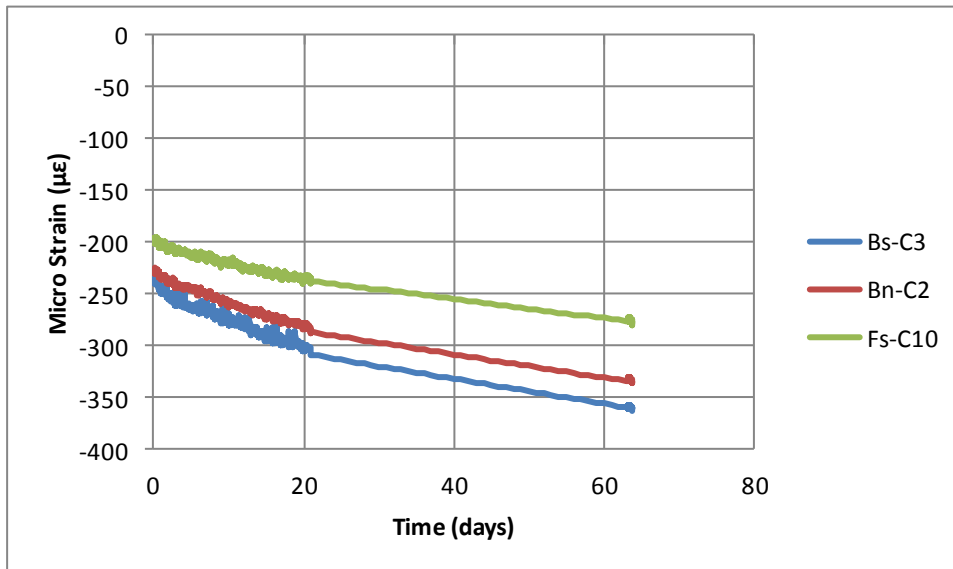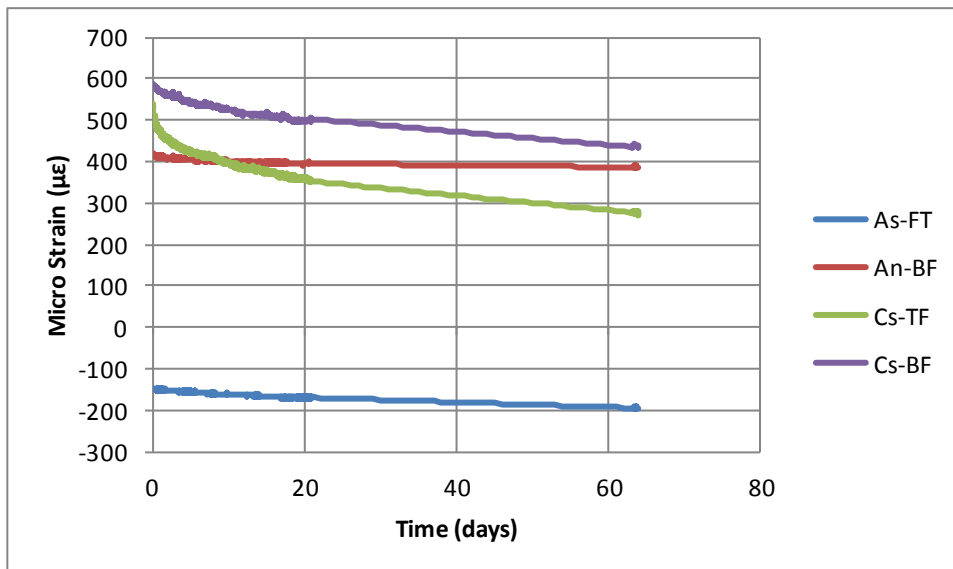
Mid-span (section F)

Mid-span (sections B & F) (concrete)

1/4 span (section A) and 3/4 span (section C)
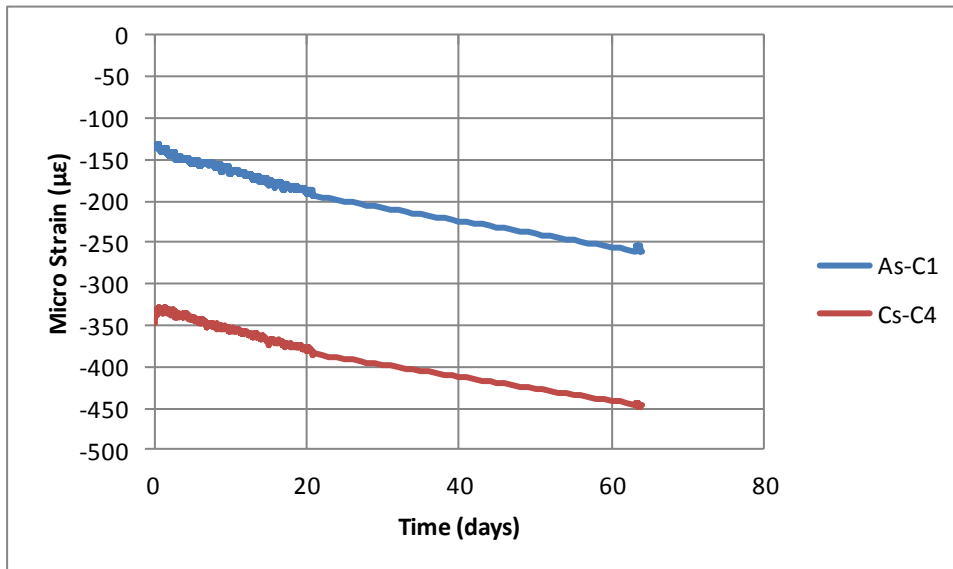
1/4 span (section A) and 3/4 span (section C) (concrete)
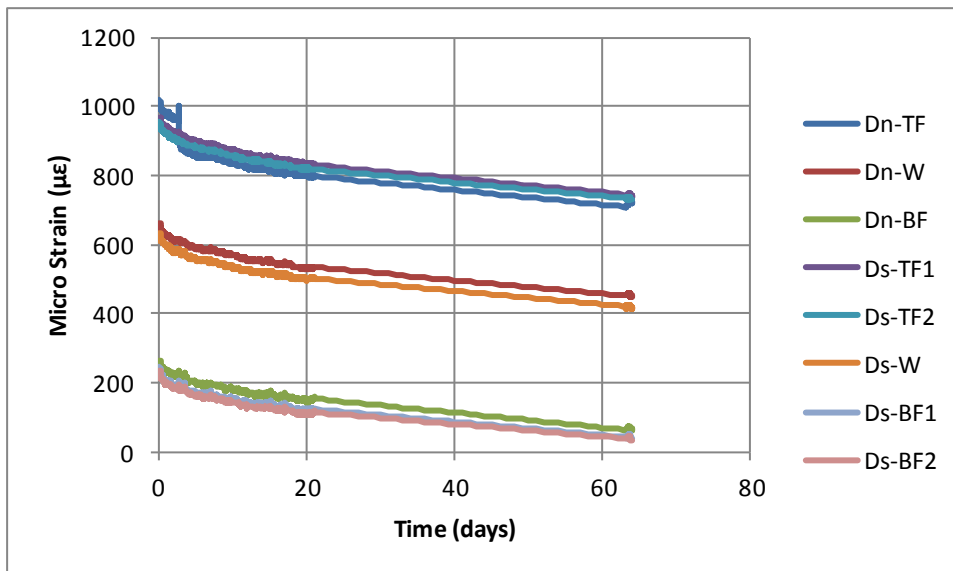
Interior support (section D)
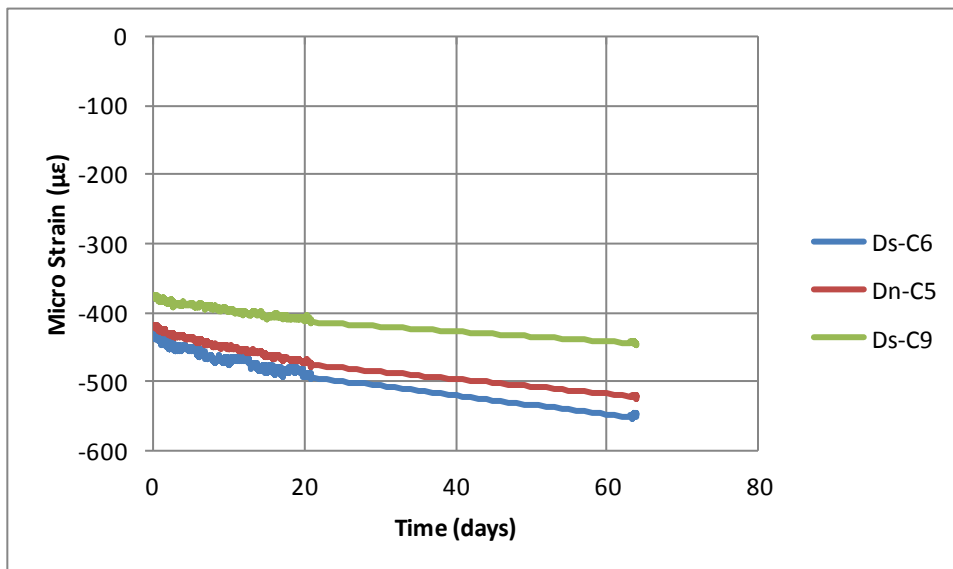
Interior support (section D) (concrete)
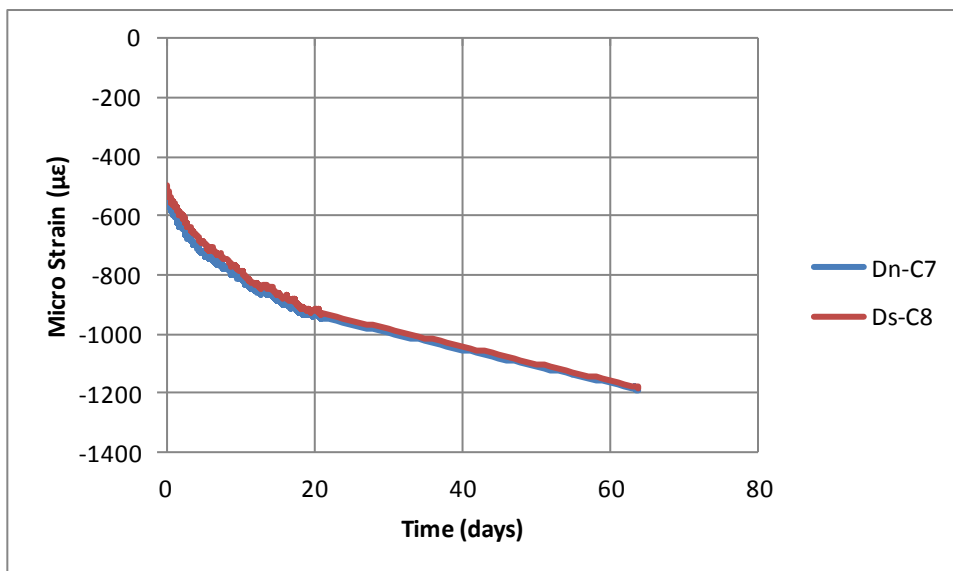
Interior support (section D) (grout)
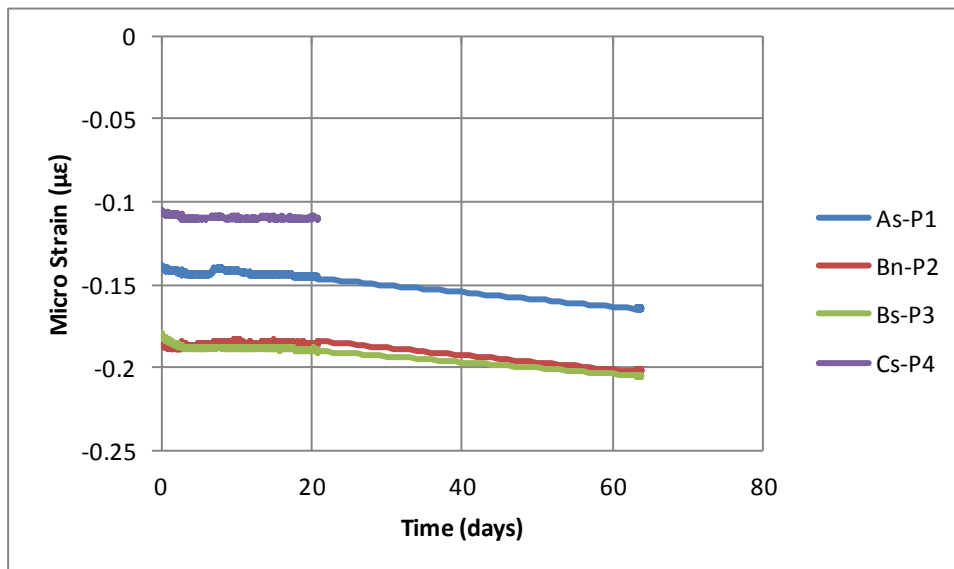
West span

* Cs-P4 was removed to be used in another testing
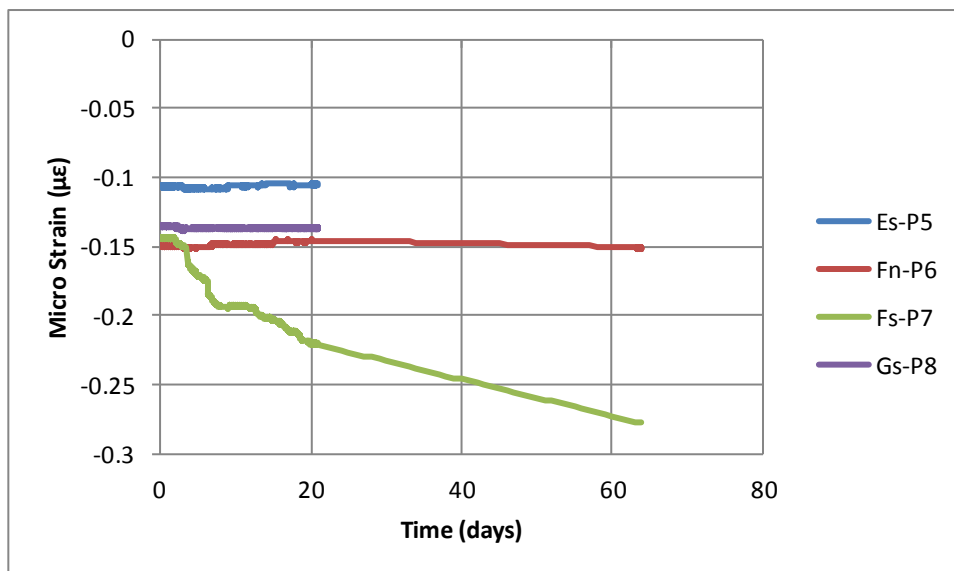
East span

* Es-P5 and Gs-P8 were removed to be used in another testing

B.5 Ultimate load testing
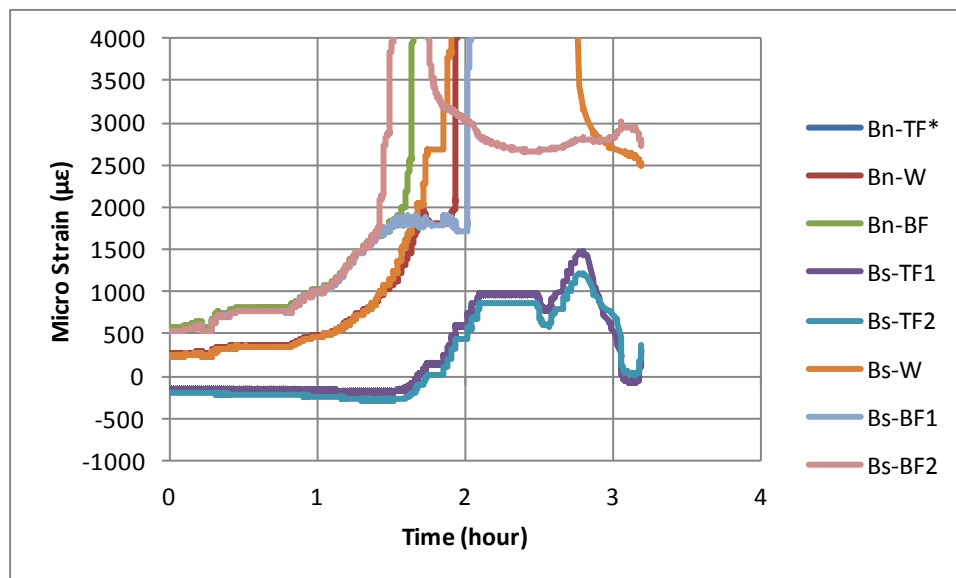
Mid-span (section B)

* Bn-TF gauge did not record data.
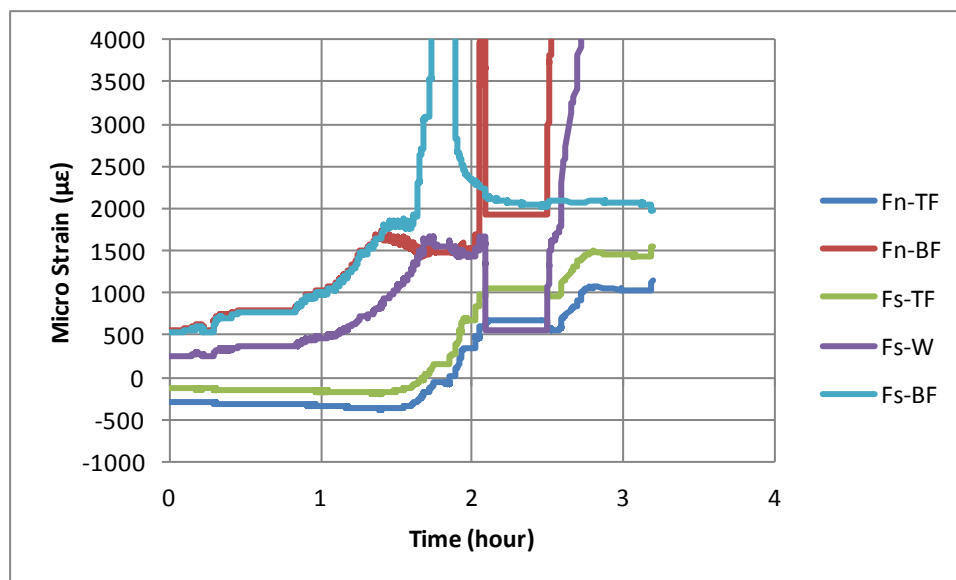
Mid-span (section F)
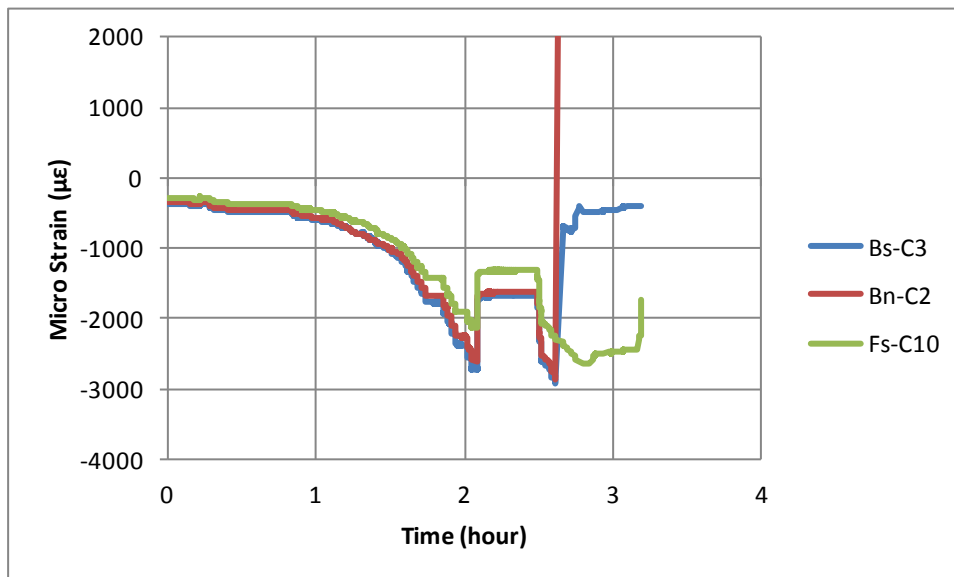
Mid-span (sections B & F) (concrete)
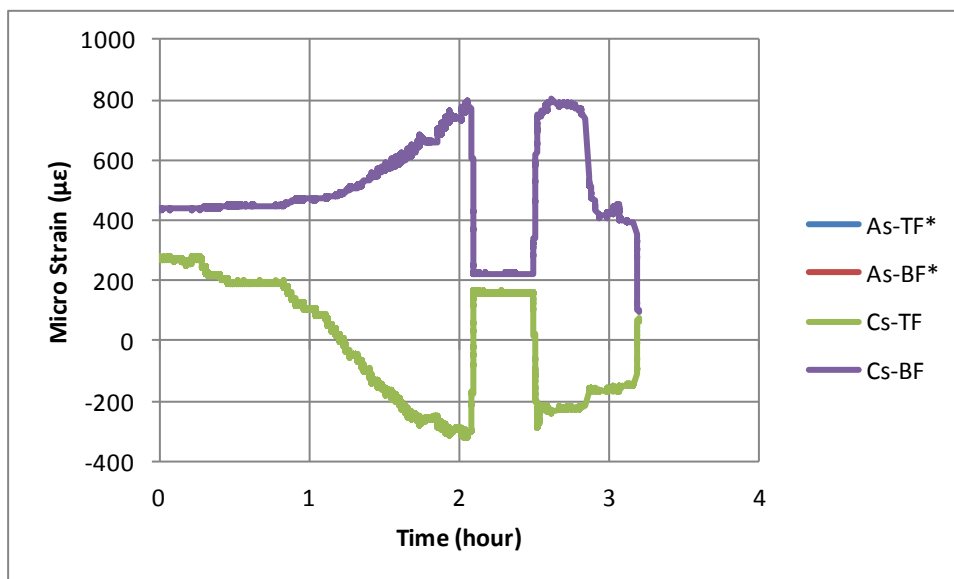
1/4 span (section A) and 3/4 span (section C)

* As-TF & As-BF gauge did not record data.
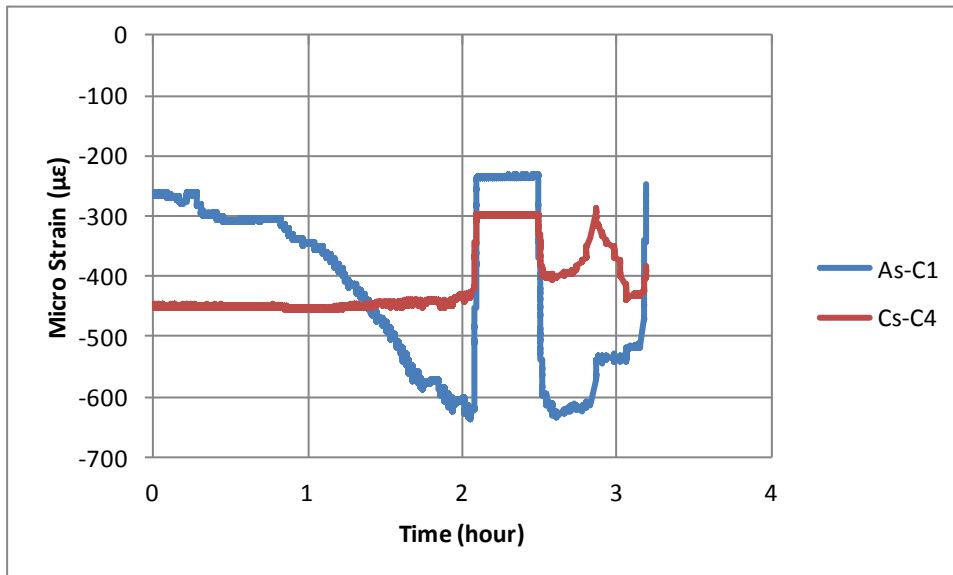
1/4 span (section A) and 3/4 span (section C) (concrete)
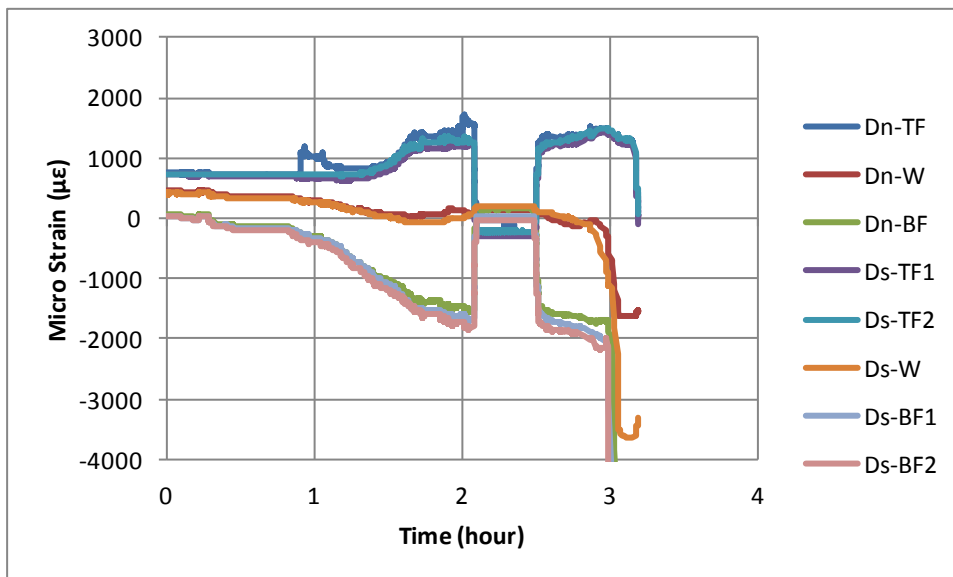
Interior support (section D)
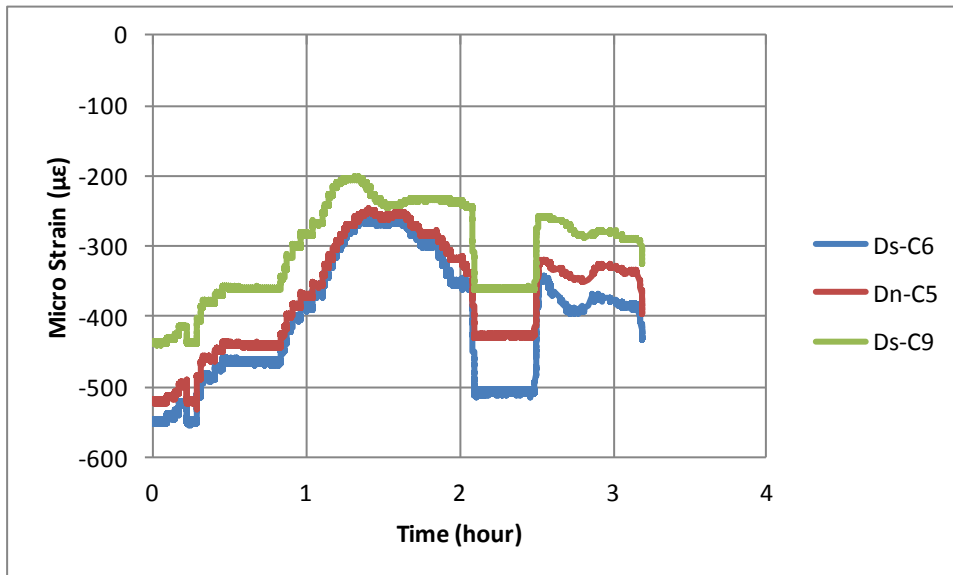
Interior support (section D) (concrete)
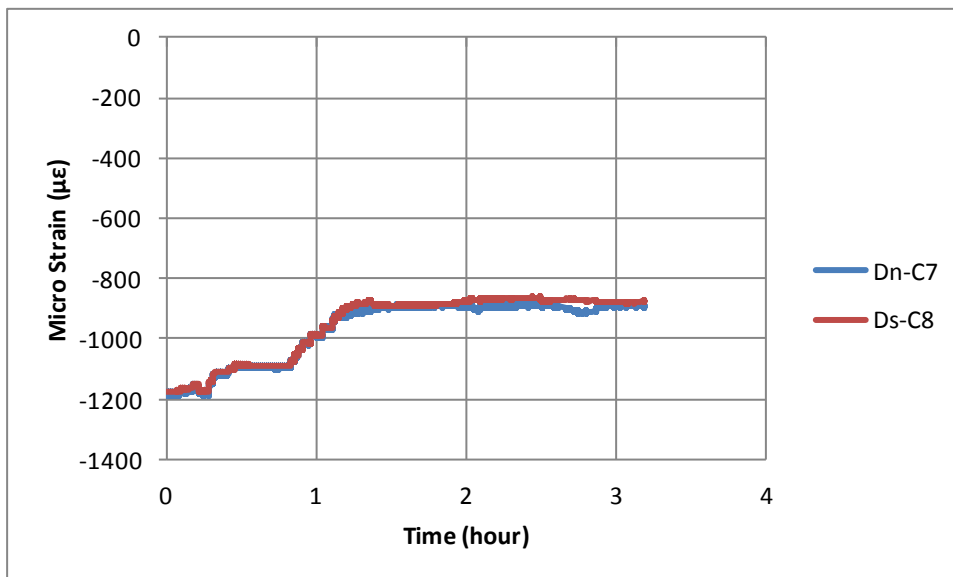
Interior support (section D) (grout)
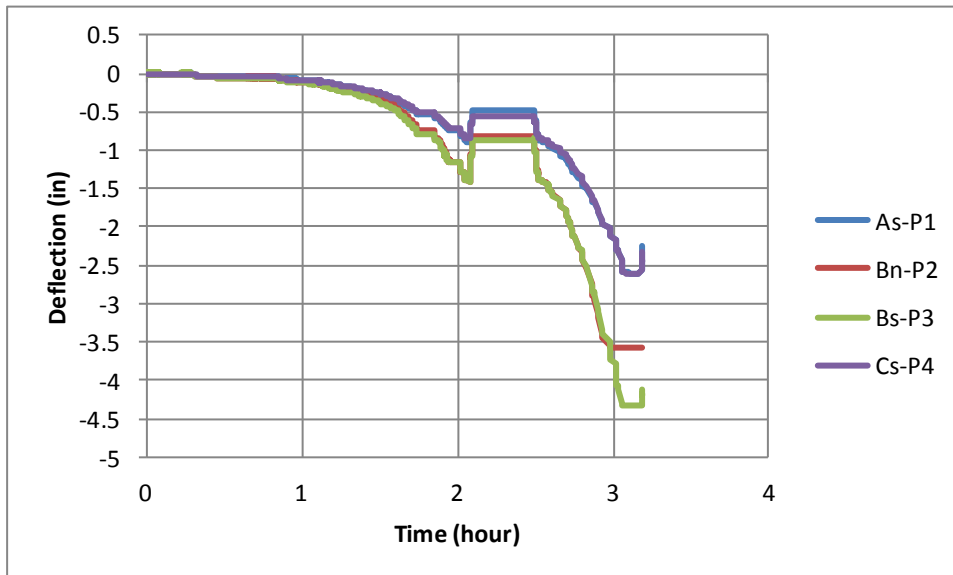
West span

* Potentiometers were zeroed.
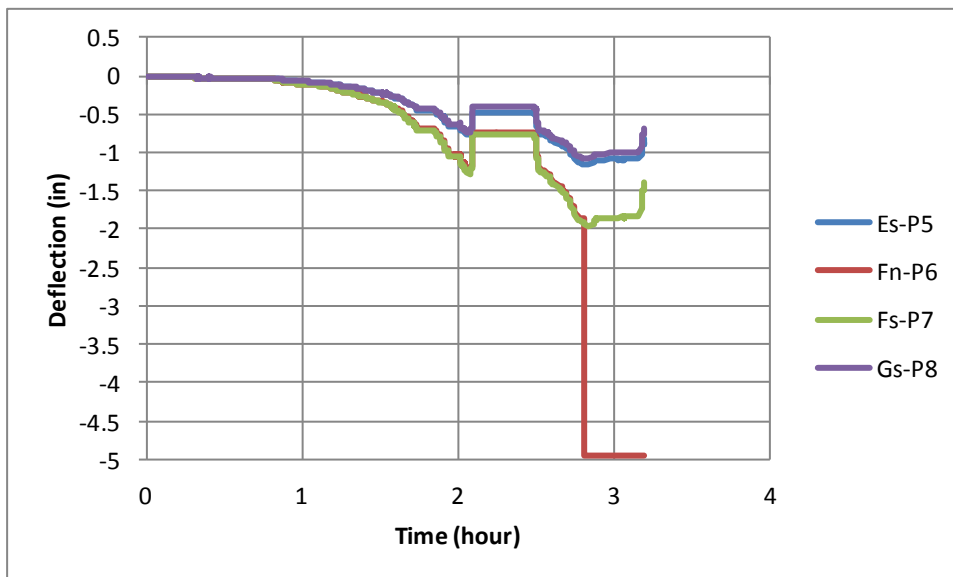
East span

* Potentiometers were zeroed.
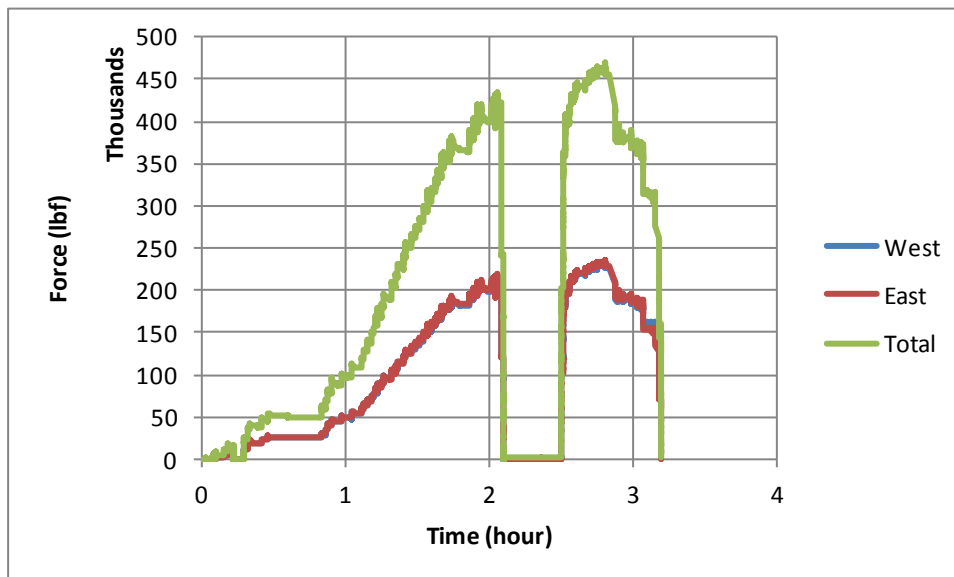
Loading
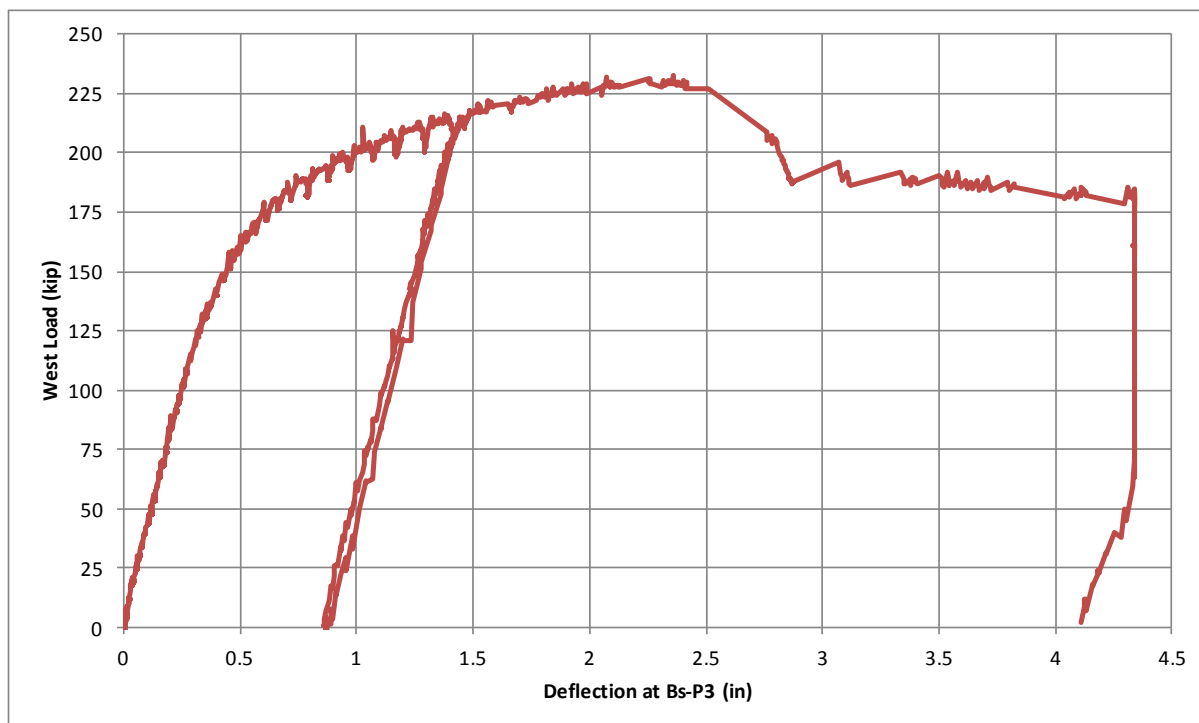
Load-deflection

Appendix C   Pictures

C.1 Ballast load

Weighting stack of train wheels
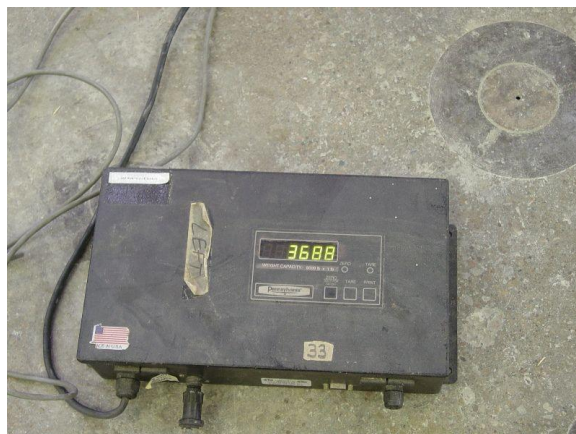
Digital scale

Stacks of train wheels

Stacks in the basement

Stacks in the basement

Washer and knot

C.2 Girder

Delivery of girders

Girders assembling

Shear studs

Steel hanger

Girder ready to placement

Supporting beam

C.3 Precast panels

Precast panels

Shear key detail

Delivery of panels

Precast set in sequence

Non-shrinkage grout

High-strength epoxy

C.4 Construction stages

Shim measurement

Pancake jacks

Overview of displaced girder

Girder curvature

Placing 2nd panel

Placing 3rd panel
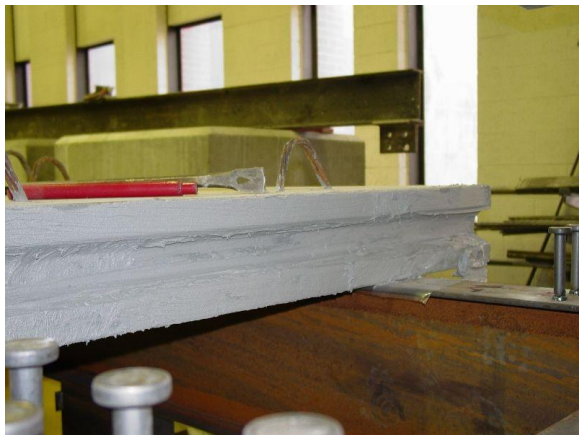
Spread epoxy

Placing 8th panel
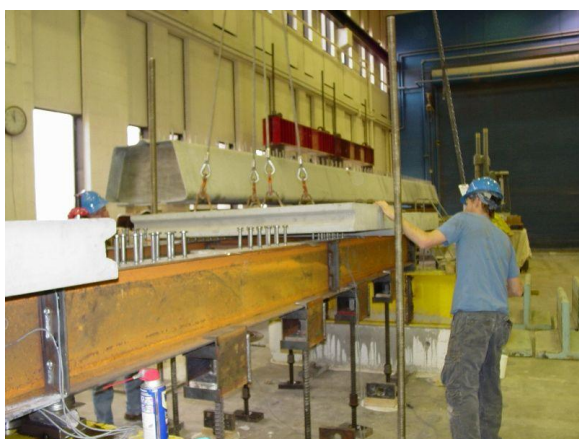
Placing 8th panel
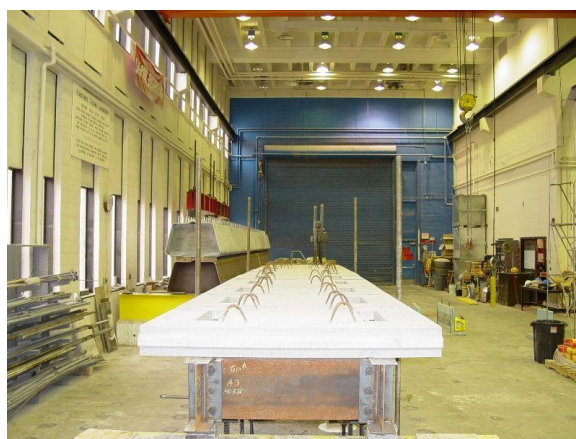
After placing all panels

Top of the panel
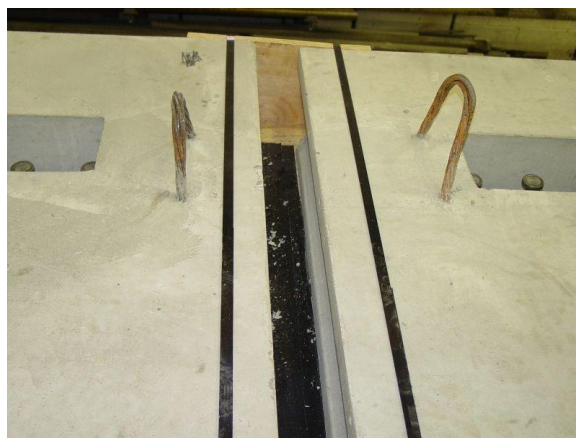
Clouse region formwork

Grout mixing

Grout pouring (begin)
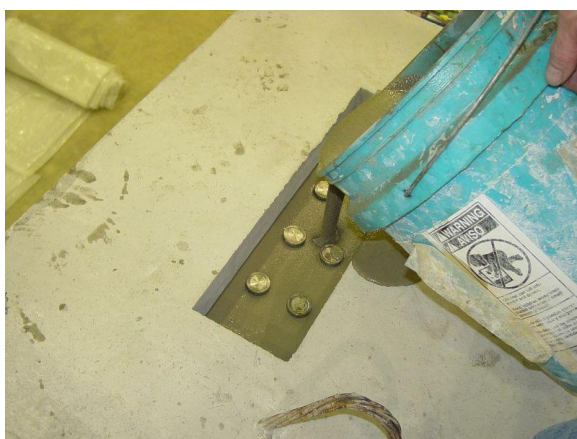
Grout pouring (end)

Grout cylinder samples

Shim removal (begin)

Shim removal (end)

C.5 Instrumentation
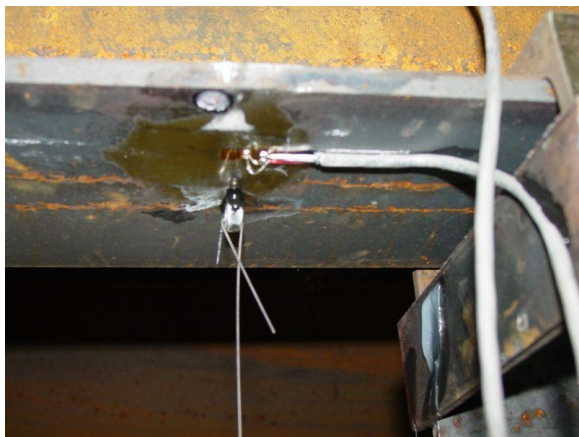
Strain gauge

Potentiometer

Concrete gauges (section D)
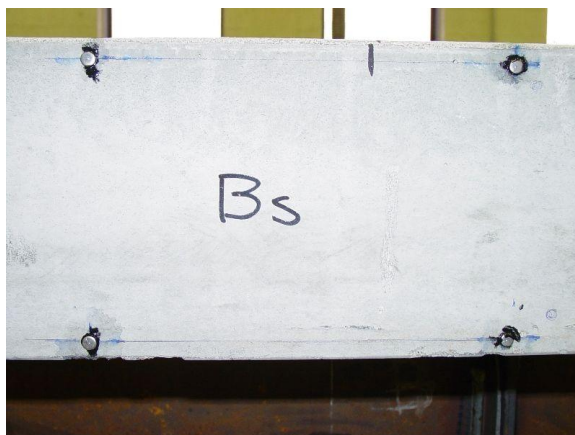
DEMEC points

C.6 Ultimate test

Ultimate load setup

Preload testing

Taking notes

Overall view

Close-up at closure region

Closure region (side view)

Cracking at closure region

Cracking at closure region

Cracking at closure region
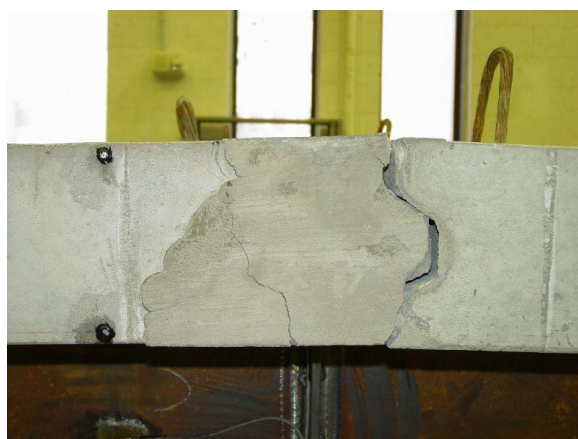
Cracking at closure region (ultimate)

West spreader beam

West mid-span (top view)

Overall view (longitudinal)

Concrete crush at west mid-span (north)

Concrete crush at west mid-span (south)
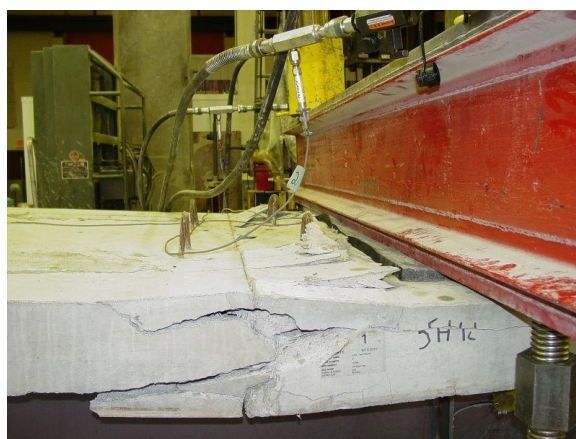
Concrete crush (top view)

Clouse-up flange buckling (north girder)

Clouse-up flange buckling (south girder)

C.7 After testing

Location of load (mid-span)

Precast panel (underneath)

Precast panel (west mid-span)

Precast panel (top view)

Precast panel reinforcement

Interior support (underneath)

Steel sample removal

West span (Interior support)

East span (over the dump truck)

Core removal

Concrete core

Core after tested

Appendix D   Additional calculations

D.1 Prediction of ultimate strength

Dimensions, material and section properties   ORIGIN := 1

Steel:

flange width	$bf := 5 \cdot in$
flange thickness	$tf := 0.335 in$
girder height	$h := 13.7 in$
web thickness	$tw := 0.23 in$
web depth	$d := h - 2 \cdot tf = 13.03 in$
area of steel	$As := 6.3469 in^2$
span	$L := 15 \cdot ft$
steel yield stress	$Fy := 50 \cdot ksi$
steel modulus	$Es := 29000 ksi$

Concrete:

slab thickness	$ts := 6 \cdot in$
slab width	$ws := 2.5 \cdot ft$
area of concrete	$Ac := ws \cdot ts = 180 in^2$
concrete strength	$fc := 8 \cdot ksi$
concrete ultimate strain	$\varepsilon u := 0.003$
concrete modulus	$Ec := 57 \cdot \sqrt{fc \cdot psi} = 5.098 ksi$
depth of NA	$c := 4.552245869 in$
total height	$ht := h + ts = 19.7 in$

Strain compatibility method

$$i := 1 .. 3$$

$$\varepsilon(t) := \varepsilon u \cdot \frac{(t - c)}{c}$$

Depth measured from top of slab

top concrete slab $yts := c - c = 0\,in$

girder top flange $yt := ts = 6\,in$

girder botton flange $yb := ht = 19.7in$

$$y := \begin{pmatrix} yts \\ yt \\ yb \end{pmatrix} \qquad y^T = (0 \quad 6 \quad 19.7)\,in$$

Strain calculation

at top concrete slab

at girder top flange $\varepsilon(y) = \begin{pmatrix} -0.003 \\ 0.001 \\ 0.01 \end{pmatrix}$

at girder botton flange

Force calculation

$$F_i := if\left(\varepsilon(y)_i < \frac{Fy}{Es}, \varepsilon(y)_i \cdot Es, Fy \right) \qquad F = \begin{pmatrix} -87 \\ 27.669 \\ 50 \end{pmatrix} ksi$$

Ultimate load estimation

<u>Location of PNA</u>

Guess $x := 1 \cdot in$

Given

$$F_3 \cdot bf \cdot tf + \left(\frac{F_3 + F_2}{2} \right) \cdot d \cdot tw + F_2 \cdot bf \cdot tf = 0.85 \, fc \cdot ws \cdot x$$

$ac := Find(x)$ $ac = 1.208 \, in$

<u>Depth measured from top of slab</u>

PNA bottom flange $db := ht - \dfrac{tf}{2} = 19.532 \, in$

PNA web $dw := ht - tf - \dfrac{d}{2} = 12.85 \, in$

PNA top flange $dt := ts + \dfrac{tf}{2} = 6.167 \, in$

NA concrete $dts := \dfrac{ac}{2} = 0.604 \, in$

Nominal capacity

$$Mn := F_3 \cdot bf \cdot tf \cdot db + \left(\frac{F_3 + F_2}{2} \right) \cdot d \cdot tw \cdot dw + F_2 \cdot bf \cdot tf \cdot dt - 0.85 \, fc \cdot ws \cdot ac \cdot dts = 272.358 \, ft \cdot kip$$

Plastic hinge theory

$W_{ext} = W_{int}$ $\theta := 1$

Given $P := 0 \cdot kip$

$$P \cdot \frac{L}{2} \cdot \theta = Mn \cdot (\theta + 2 \cdot \theta)$$

$Pn := Find(P)$ $Pn = 108.943 \, kip$

Predicted ultimate load

$Pu := 2 \cdot Pn = 217.886 \, kip$

The maximum load measured at the ultimate load test was 230 kip.

D.2 Lifting analysis

A beam analysis was conducted to determine whether or not the girder ends would be lifted while the shim in the interior support is applied.

Girder (W14x22)

Girder height	13.7 in
Area of girder	6.34 in2
Moment of inertia	192.0 in4
Steel modulus of elasticity	29000 ksi
Girder weight plus miscellaneous steel	0.035 kip/ft
Load	
Average ballast load weight	3.71 kip
Concrete panels weight	0.19 kip/ft

First analysis: dropping only the ballast near the ends.
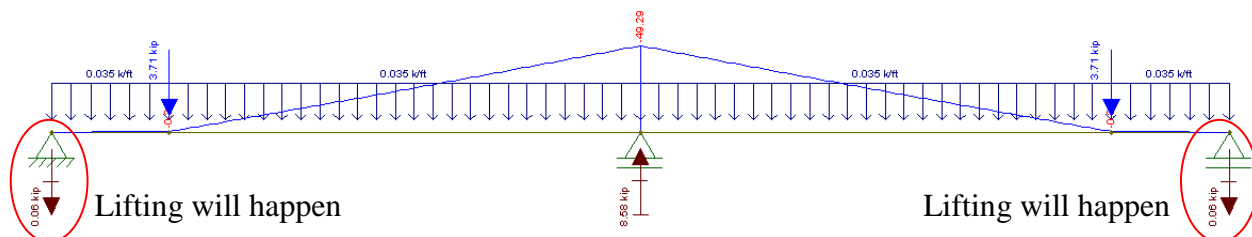
Second analysis: dropping next set ballast near to mid-span and also placing the precast panel weight only over the left span.
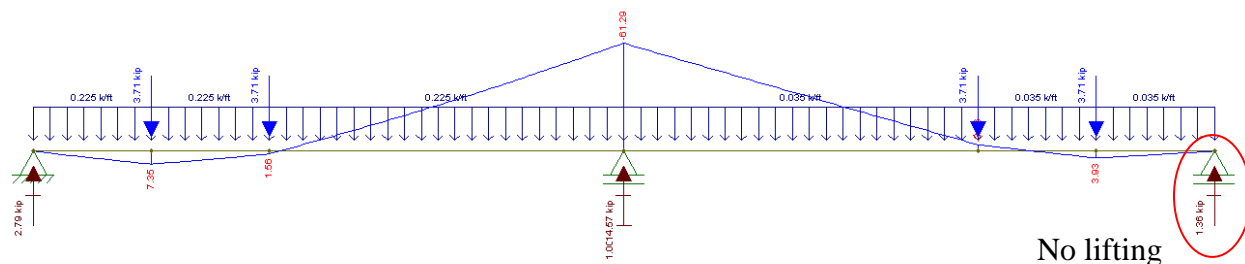
D.3 Time-dependent analysis

Dimensions and material properties

span length	$L := 15 \cdot ft$	beam depth	$D_s := 13.7 \cdot in$
deck thickness	$D_c := 6 \cdot in$	girder area	$A_{ss} := 6.35 in^2$
deck widht	$b := 2.5 \cdot ft$	girder inertia	$I_{ss} := 192.03 in^4$
		girder NA to top fiber	$d_{ss} := D_c + \dfrac{D_s}{2} = 12.85 in$
depth of top rebar	$d_{srt} := 1 \cdot in$	depth of bottom rebar	$d_{srb} := D_c - d_{srt} = 5 in$
area of top rebar	$A_{srt} := 4 \cdot \left(\dfrac{3 \cdot in}{8}\right)^2 \cdot \dfrac{\pi}{4} = 0.442 in^2$	area of bottom rebar	$A_{srb} := 4 \cdot \left(\dfrac{4 \cdot in}{8}\right)^2 \cdot \dfrac{\pi}{4} = 0.785 in^2$
steel modulus	$E_s := 29000 ksi$	shrinkage strain	$\varepsilon_{sh} := 0 \cdot 10^{-6}$
concrete strength	$f'_c := 8 \cdot ksi$	age adjusted factor	$\chi := 0.8$
concrete modulus	$E_c := 5422 ksi$	creep coeficient	$\phi := 0.6$
number of division	$NDiv := 10$	$i := 0 .. NDiv$	

Loading and moment during construction

girder linear weight	$w_g := 0.035 klf$	deck linear weight	$w_d := 0.187 klf$
ballast linear weight	$w_b := 1.278 klf$	total linear weight	$w := w_g + w_b + w_d = 1.5 klf$
bending moment (dead load)	$Mx(x) := w \cdot L \cdot x - \dfrac{w \cdot x^2}{2} - \dfrac{5}{4} \cdot w \cdot L \cdot \dfrac{x}{2}$		$M_{DL_i} := Mx\left(\dfrac{i}{NDiv} \cdot L\right)$

$M_{DL}^T =$

	0	1	2	3	4	5	6	7	8	
0	0	10.97	18.56	22.78	23.63	21.09	15.19	5.91	...	ft·kip
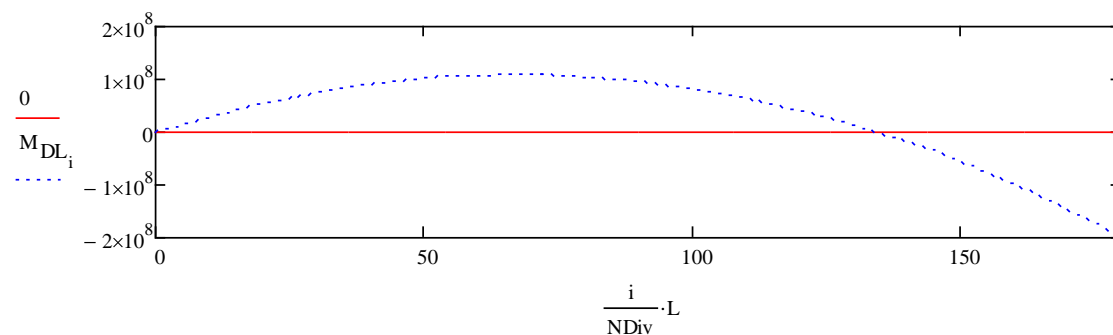
Noncomposite section properties (before self-stressing)

modular ratio $\quad n := \dfrac{E_s}{E_c} = 5.35$

transformed section area $\quad A_g := n \cdot A_{ss} = 33.963 \text{in}^2$

transformed section modulus $\quad B_g := n \cdot A_{ss} \cdot d_{ss} = 436.431 \text{in}^3$

transformed moment of inertia $\quad I_g := n \cdot \left(A_{ss} \cdot d_{ss}^2 + I_{ss} \right) = 6635.223 \text{in}^4$

moment of inertia at NA $\quad I_{NAg} := \dfrac{A_g \cdot I_g - B_g^2}{A_g} = 1027.088 \text{in}^4$

depth of NA (top of slab) $\quad d_{NAg} := \dfrac{B_g}{A_g} = 12.85 \text{in}$

upward displacement $\quad \delta_u := -1 \cdot \text{in}$

bending moment (lifting) $\quad M_{LI_i} := 3 \cdot \dfrac{E_c \cdot I_{NAg}}{L^2} \cdot \delta_u \cdot \dfrac{i}{NDiv}$

$M_{LI}^T =$

	0	1	2	3	4	5	6	7	8	ft·kip
0	0	-4.3	-8.59	-12.89	-17.19	-21.48	-25.78	-30.08	...	

total bending moment $\quad M_{NC} := M_{DL} + M_{LI}$

$M_{NC}^T =$

	0	1	2	3	4	5	6	7	ft·kip
0	0	6.672	9.969	9.89	6.437	-0.391	-10.594	...	
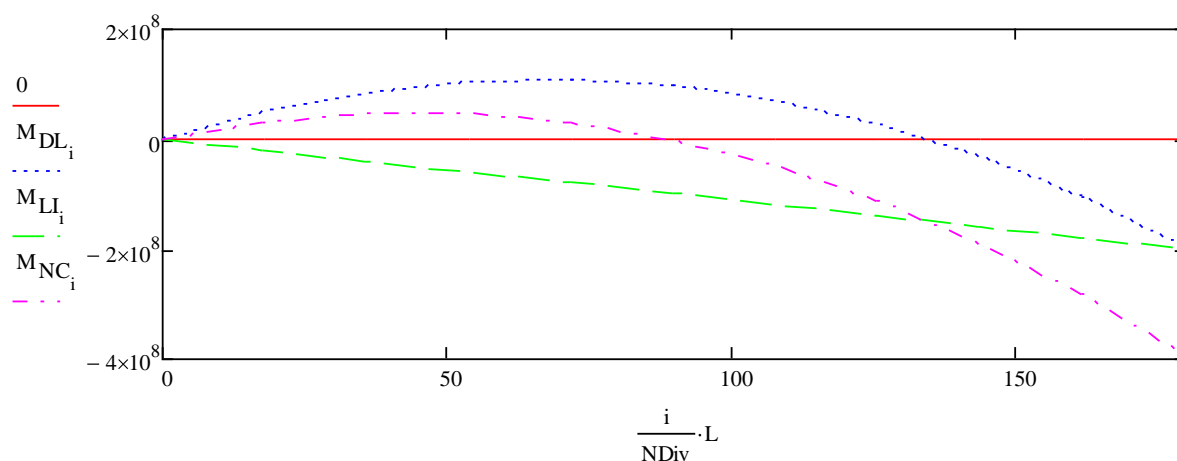
strain and curvature at top fiber (before self-stressing)

strain

$$\varepsilon_{g_i} := \frac{B_g \cdot M_{NC_i}}{E_c \cdot \left(A_g \cdot I_g - B_g^2\right)}$$

$\varepsilon_g{}^T =$		0	1	2	3	4	5	6
	0	0	$1.847 \cdot 10^{-4}$	$2.76 \cdot 10^{-4}$	$2.739 \cdot 10^{-4}$	$1.782 \cdot 10^{-4}$	$-1.083 \cdot 10^{-5}$	...

curvature

$$\rho_{g_i} := \frac{A_g \cdot M_{NC_i}}{E_c \cdot \left(A_g \cdot I_g - B_g^2\right)}$$

$\rho_g{}^T =$		0	1	2	3	4	5	6	$\frac{1}{in}$
	0	0	$1.438 \cdot 10^{-5}$	$2.148 \cdot 10^{-5}$	$2.131 \cdot 10^{-5}$	$1.387 \cdot 10^{-5}$	$-8.427 \cdot 10^{-7}$	...	

stress caused by the dead load moment (before self-stressing)

top girder

$$\sigma_{gsai_i} := E_s \cdot \left(\varepsilon_{g_i} - D_c \cdot \rho_{g_i}\right)$$

$\sigma_{gsai}{}^T =$		0	1	2	3	4	5	6	7	8	9	ksi
	0	0	2.86	4.27	4.23	2.76	-0.17	-4.53	-10.35	-17.6	...	

bottom girder

$$\sigma_{gsbi_i} := E_s \cdot \left[\varepsilon_{g_i} - \left| D_c + D_s \right| \cdot \rho_{g_i}\right]$$

$\sigma_{gsbi}{}^T =$		0	1	2	3	4	5	6	7	8	9	10	ksi
	0	0	-2.86	-4.27	-4.23	-2.76	0.17	4.53	10.35	17.6	26.31	36.45	

short-term section properties (at self-stressing)

transformed section area

$$A := b \cdot D_c + (n-1) \cdot \left| A_{srt} + A_{srb} \right| + n \cdot A_{ss} = 219.3 in^2$$

transformed section modulus

$$B := b \cdot D_c \cdot \frac{D_c}{2} + (n-1) \cdot \left| A_{srt} \cdot d_{srt} + A_{srb} \cdot d_{srb} \right| + n \cdot A_{ss} \cdot d_{ss} = 995.429 in^3$$

transformed moment of inertia

$$I := \frac{1}{3} \cdot b \cdot D_c^3 + (n-1) \cdot \left(A_{srt} \cdot d_{srt}^2 + A_{srb} \cdot d_{srb}^2 \right) + n \cdot \left(A_{ss} \cdot d_{ss}^2 + I_{ss} \right) = 8882.528 in^4$$

moment of inertia at NA

$$I_{NA} := \frac{A \cdot I - B^2}{A} = 4364.159 in^4$$

transformed stiffness

$$EI := E_c \cdot I_{NA} = 9.136 \times 10^{12} \frac{in^3 \cdot lb}{s^2}$$

depth of NA (top of slab)

$$d_{NA} := \frac{B}{A} = 4.539 in$$

cracked transf. section area

$$A_n := n \cdot \left| A_{srt} + A_{srb} \right| + n \cdot A_{ss} = 40.527 in^2$$

cracked transf. section modulus

$$B_n := n \cdot \left| A_{srt} \cdot d_{srt} + A_{srb} \cdot d_{srb} \right| + n \cdot A_{ss} \cdot d_{ss} = 459.797 in^3$$

cracked transf. moment of inertia

$$I_n := n \cdot \left(A_{srt} \cdot d_{srt}^2 + A_{srb} \cdot d_{srb}^2 \right) + n \cdot \left(A_{ss} \cdot d_{ss}^2 + I_{ss} \right) = 6742.605 in^4$$

down displacement

$$\delta_d := -\delta_u = 1 \, in$$

bending moment (release)

$$M_{RE_i} := 3 \cdot \frac{E_c \cdot I_{NA}}{L^2} \cdot \delta_d \cdot \frac{i}{NDiv} \qquad R_1 := 3 \cdot \frac{E_c \cdot I_{NA}}{L^3} \cdot \delta_d = 12.172 kip$$

strain and curvature at top fiber (at self-stressing)

strain

$$\varepsilon_{0_i} := \frac{B \cdot M_{RE_i}}{E_c \cdot \left| A \cdot I - B^2 \right|}$$

$\varepsilon_0^T =$	0	1	2	3	4	5	6
0	0	$4.203 \cdot 10^{-5}$	$8.406 \cdot 10^{-5}$	$1.261 \cdot 10^{-4}$	$1.681 \cdot 10^{-4}$	$2.101 \cdot 10^{-4}$	...

curvature

$$\rho_{0_i} := \frac{A \cdot M_{RE_i}}{E_c \cdot \left| A \cdot I - B^2 \right|}$$

$\rho_0^T =$	0	1	2	3	4	5	6	$\frac{1}{in}$
0	0	$9.259 \cdot 10^{-6}$	$1.852 \cdot 10^{-5}$	$2.778 \cdot 10^{-5}$	$3.704 \cdot 10^{-5}$	$4.63 \cdot 10^{-5}$	...	

stress caused by the release moment   (at self-stressing)

top slab

$$\sigma_{0_i} := E_c \cdot \varepsilon_{0_i}$$

$\sigma_{0i}{}^T =$		0	1	2	3	4	5	6	7	8	9	10	ksi
	0	0	0.23	0.46	0.68	0.91	1.14	1.37	1.6	1.82	2.05	2.28	

bottom slab

$$\sigma_{ai_i} := E_c \cdot \left(\varepsilon_{0_i} - D_c \cdot \rho_{0_i} \right)$$

$\sigma_{ai}{}^T =$		0	1	2	3	4	5	6	7	8	9	10	ksi
	0	0	-0.07	-0.15	-0.22	-0.29	-0.37	-0.44	-0.51	-0.59	-0.66	-0.73	

top reinforcement

$$\sigma_{srti_i} := E_s \cdot \left(\varepsilon_{0_i} - d_{srt} \cdot \rho_{0_i} \right)$$

$\sigma_{srti}{}^T =$		0	1	2	3	4	5	6	7	8	9	10	ksi
	0	0	0.95	1.9	2.85	3.8	4.75	5.7	6.65	7.6	8.55	9.5	

bottom reinforcement

$$\sigma_{srbi_i} := E_s \cdot \left(\varepsilon_{0_i} - d_{srb} \cdot \rho_{0_i} \right)$$

$\sigma_{srbi}{}^T =$		0	1	2	3	4	5	6	7	8	9	10	ksi
	0	0	-0.12	-0.25	-0.37	-0.5	-0.62	-0.74	-0.87	-0.99	-1.11	-1.24	

top girder

$$\sigma_{sai_i} := E_s \cdot \left(\varepsilon_{0_i} - D_c \cdot \rho_{0_i} \right) + \sigma_{gsai_i}$$

$\sigma_{sai}{}^T =$		0	1	2	3	4	5	6	7	8	9	ksi
	0	0	2.46	3.48	3.06	1.19	-2.13	-6.89	-13.09	-20.74	...	

bottom girder

$$\sigma_{sbi_i} := E_s \cdot \left[\varepsilon_{0_i} - \left| D_c + D_s \right| \cdot \rho_{0_i} \right] + \sigma_{gsbi_i}$$

$\sigma_{sbi}{}^T =$		0	1	2	3	4	5	6	7	8	9	ksi
	0	0	-6.93	-12.41	-16.45	-19.04	-20.19	-19.89	-18.15	-14.96	...	

long-term term section properties (after self-stressing)

Aged-adjusted elasticy modulus
$$E_e := \frac{E_c}{1 + \chi \cdot \phi} = 3663.514 \text{ksi}$$

long-term modular ratio
$$n_e := \frac{E_s}{E_e} = 7.916$$

transformed section area
$$A_e := b \cdot D_c + \left| n_e - 1 \right| \cdot \left| A_{srt} + A_{srb} \right| + n_e \cdot A_{ss} = 238.753 \text{in}^2$$

transformed section modulus
$$B_e := b \cdot D_c \cdot \frac{D_c}{2} + \left| n_e - 1 \right| \cdot \left| A_{srt} \cdot d_{srt} + A_{srb} \cdot d_{srb} \right| + n_e \cdot A_{ss} \cdot d_{ss} = 1216.132 \text{in}^3$$

transformed moment of inertia
$$I_e := \frac{1}{3} \cdot b \cdot D_c^3 + \left| n_e - 1 \right| \cdot \left(A_{srt} \cdot d_{srt}^2 + A_{srb} \cdot d_{srb}^2 \right) + n_e \cdot \left(A_{ss} \cdot d_{ss}^2 + I_{ss} \right) = 12118.979 \text{in}^4$$

moment of inertia at NA
$$I_{NAe} := \frac{A_e \cdot I_e - B_e^2}{A_e} = 5924.394 \text{in}^4$$

transformed stiffness
$$EI_e := E_e \cdot I_{NAe} = 8.38 \times 10^{12} \frac{\text{in}^3 \cdot \text{lb}}{\text{s}^2}$$

depth of NA (top of slab)
$$d_{NAe} := \frac{B_e}{A_e} = 5.094 \text{in}$$

cracked transf. section area
$$A_{en} := n_e \cdot \left| A_{srt} + A_{srb} \right| + n_e \cdot A_{ss} = 59.98 \text{in}^2$$

cracked transf. section modulus
$$B_{en} := n_e \cdot \left| A_{srt} \cdot d_{srt} + A_{srb} \cdot d_{srb} \right| + n_e \cdot A_{ss} \cdot d_{ss} = 680.5 \text{in}^3$$

cracked transf. moment of inertia
$$I_{en} := n_e \cdot \left(A_{srt} \cdot d_{srt}^2 + A_{srb} \cdot d_{srb}^2 \right) + n_e \cdot \left(A_{ss} \cdot d_{ss}^2 + I_{ss} \right) = 9979.055 \text{in}^4$$

concrete section area
$$A_c := b \cdot D_c + (-1) \cdot \left| A_{srt} + A_{srb} \right| = 178.773 \text{in}^2$$

concrete section modulus
$$B_c := b \cdot D_c \cdot \frac{D_c}{2} + (-1) \cdot \left| A_{srt} \cdot d_{srt} + A_{srb} \cdot d_{srb} \right| = 535.631 \text{in}^3$$

concrete moment of inertia
$$I_c := \frac{1}{3} \cdot b \cdot D_c^3 + (-1) \cdot \left(A_{srt} \cdot d_{srt}^2 + A_{srb} \cdot d_{srb}^2 \right) = 2139.923 \text{in}^4$$

restrained actions

$$\Delta N_{neg_i} := -E_e \cdot \left[\phi \cdot \left(A_c \cdot \varepsilon_{0_i} - B_c \cdot \rho_{0_i} \right) + \varepsilon_{sh} \cdot A_c \right]$$

$\Delta N_{neg}^T =$	0	1	2	3	4	5	6	7	8	9	kip
0	0	-5.61	-11.23	-16.84	-22.46	-28.07	-33.68	-39.3	-44.91	...	

$$\Delta M_{neg_i} := -E_e \cdot \left[\phi \cdot \left(-B_c \cdot \varepsilon_{0_i} + I_c \cdot \rho_{0_i} \right) - \varepsilon_{sh} \cdot B_c \right]$$

$\Delta M_{neg}^T =$	0	1	2	3	4	5	6	7	8	9	10	ft·kip
0	0	0.49	0.99	1.48	1.98	2.47	2.97	3.46	3.95	4.45	4.94	

change in strain and curvature at top fiber (after seft-stressing)

strain

$$\Delta\varepsilon_i := \frac{-\left(B_e \cdot \Delta M_{neg_i}\right) - I_e \cdot \Delta N_{neg_i}}{E_e \cdot \left(A_e \cdot I_e - B_e^2\right)}$$

$\Delta\varepsilon^T =$		0	1	2	3	4	5	6
	0	0	$1.174 \cdot 10^{-5}$	$2.348 \cdot 10^{-5}$	$3.521 \cdot 10^{-5}$	$4.695 \cdot 10^{-5}$	$5.869 \cdot 10^{-5}$	...

curvature

$$\Delta\rho_i := \frac{-\left(A_e \cdot \Delta M_{neg_i}\right) - B_e \cdot \Delta N_{neg_i}}{E_e \cdot \left(A_e \cdot I_e - B_e^2\right)}$$

$\Delta\rho^T =$		0	1	2	3	4	5	6	$\frac{1}{in}$
	0	0	$1.044 \cdot 10^{-6}$	$2.089 \cdot 10^{-6}$	$3.133 \cdot 10^{-6}$	$4.177 \cdot 10^{-6}$	$5.222 \cdot 10^{-6}$	...	

change in the stress caused by time-dependent effect (after self-stressing)

top slab

$$\Delta\sigma_{c0_i} := -E_e \cdot \left[\phi \cdot \left(\varepsilon_{0_i} - 0 \cdot \rho_{0_i}\right) + \varepsilon_{sh} - \left| \Delta\varepsilon_i - 0 \cdot \Delta\rho_i \right| \right]$$

$\Delta\sigma_{c0}^T =$		0	1	2	3	4	5	6	7	8	9	10	ksi
	0	0	-0.05	-0.1	-0.15	-0.2	-0.25	-0.3	-0.35	-0.4	-0.44	-0.49	

bottom slab

$$\Delta\sigma_{ca_i} := -E_e \cdot \left[\phi \cdot \left(\varepsilon_{0_i} - D_c \cdot \rho_{0_i}\right) + \varepsilon_{sh} - \left| \Delta\varepsilon_i - D_c \cdot \Delta\rho_i \right| \right]$$

$\Delta\sigma_{ca}^T =$		0	1	2	3	4	5	6	7	8	9	10	ksi
	0	0	0.05	0.1	0.15	0.2	0.25	0.3	0.35	0.4	0.45	0.5	

top reinforcement

$$\Delta\sigma_{srt_i} := E_s \cdot \left| \Delta\varepsilon_i - d_{srt} \cdot \Delta\rho_i \right|$$

$\Delta\sigma_{srt}^T =$		0	1	2	3	4	5	6	7	8	9	10	ksi
	0	0	0.31	0.62	0.93	1.24	1.55	1.86	2.17	2.48	2.79	3.1	

bottom reinforcement

$$\Delta\sigma_{srb_i} := E_s \cdot \left| \Delta\varepsilon_i - d_{srb} \cdot \Delta\rho_i \right|$$

$\Delta\sigma_{srb}^T =$		0	1	2	3	4	5	6	7	8	9	10	ksi
	0	0	0.19	0.38	0.57	0.76	0.94	1.13	1.32	1.51	1.7	1.89	

tob girder

$$\Delta\sigma_{sa_i} := -E_e \cdot \left[-\left| \Delta\varepsilon_i - D_c \cdot \Delta\rho_i \right| \right]$$

$\Delta\sigma_{sa}{}^T =$		0	1	2	3	4	5	6	7	8	9	10	ksi
	0	0	0.02	0.04	0.06	0.08	0.1	0.12	0.14	0.16	0.18	0.2	

bottom girder

$$\Delta\sigma_{sb_i} := -E_e \cdot \left[-\left[\Delta\varepsilon_i - \left| D_c + D_s \right| \cdot \Delta\rho_i \right] \right]$$

$\Delta\sigma_{sb}{}^T =$		0	1	2	3	4	5	6	7	8	9	10	ksi
	0	0	-0.03	-0.06	-0.1	-0.13	-0.16	-0.19	-0.23	-0.26	-0.29	-0.32	

final stress

top of concrete deck

$$\sigma_c := \sigma_{0i} + \Delta\sigma_{c0}$$

$\sigma_c{}^T =$		0	1	2	3	4	5	6	7	8	9	10	ksi
	0	0	0.18	0.36	0.54	0.71	0.89	1.07	1.25	1.43	1.61	1.78	

bottom of concrete deck

$$\sigma_{ca} := \sigma_{ai} + \Delta\sigma_{ca}$$

$\sigma_{ca}{}^T =$		0	1	2	3	4	5	6	7	8	9	10	ksi
	0	0	-0.02	-0.05	-0.07	-0.09	-0.12	-0.14	-0.16	-0.19	-0.21	-0.24	

top reinforcement

$$\sigma_{srt} := \sigma_{srti} + \Delta\sigma_{srt}$$

$\sigma_{srt}{}^T =$		0	1	2	3	4	5	6	7	8	9	10	ksi
	0	0	1.26	2.52	3.78	5.04	6.3	7.56	8.82	10.08	11.34	12.6	

bottom reinforcement

$$\sigma_{srb} := \sigma_{srbi} + \Delta\sigma_{srb}$$

$\sigma_{srb}{}^T =$		0	1	2	3	4	5	6	7	8	9	10	ksi
	0	0	0.07	0.13	0.2	0.26	0.33	0.39	0.46	0.52	0.59	0.65	

top girder

$$\sigma_{sa} := \sigma_{sai} + \Delta\sigma_{sa}$$

$\sigma_{sa}{}^T =$		0	1	2	3	4	5	6	7	8	9	ksi
	0	0	2.48	3.52	3.12	1.27	-2.03	-6.77	-12.95	-20.58	...	

bottom girder

$$\sigma_{sb} := \sigma_{sbi} + \Delta\sigma_{sb}$$

$\sigma_{sb}{}^T =$		0	1	2	3	4	5	6	7	8	9	ksi
	0	0	-6.96	-12.47	-16.54	-19.17	-20.35	-20.09	-18.38	-15.22	...	

constant

uncracked region

$$\alpha_1 := \frac{\varepsilon_{sh} \cdot \left| B_e \cdot A_c - A_e \cdot B_c \right|}{A_e \cdot I_e - B_e^2} \qquad \alpha_1 = 0$$

$$\beta_1 := \frac{1}{E_c \cdot \left| A \cdot I - B^2 \right|} \cdot \left[A + \frac{\phi \cdot \left| A_c \cdot B \cdot B_e - B_c \cdot A \cdot B_e - B_c \cdot B \cdot A_e + I_c \cdot A \cdot A_e \right|}{A_e \cdot I_e - B_e^2} \right] \qquad \beta_1 = 1.218 \times 10^{-13} \frac{s^2}{in^3 \cdot lb}$$

$$\gamma_1 := \frac{A_e}{E_e \cdot \left(A_e \cdot I_e - B_e^2 \right)} \qquad \gamma_1 = 1.193 \times 10^{-13} \frac{s^2}{in^3 \cdot lb}$$

Restoring moment analysis

Define the Primary Moment (Broken into components and Summed)

$$M_w(x) := \frac{w \cdot (2 \cdot L)}{2} x - \frac{w \cdot x^2}{2} \qquad M0x(x) := M_w(x) \qquad M0x(L) = 168.75 ft \cdot kip$$

Define Virtual Moment Due to Force at Reaction Location

$$M1x(x) := 1kip \cdot \frac{(2 \cdot L - L)}{2 \cdot L} \cdot x - 1kip \cdot \Phi(x - L)(x - L)$$

$$M1x(L) = 7.5 ft \cdot kip$$

Break Crap up in Preparation for Numerical

$$j := 0.. 2 \cdot NDiv \qquad x_j := j \cdot \frac{2 \cdot L}{2 \cdot NDiv} \qquad M0_j := M0x\left(x_j \right) \qquad M1_j := M1x\left(x_j \right)$$
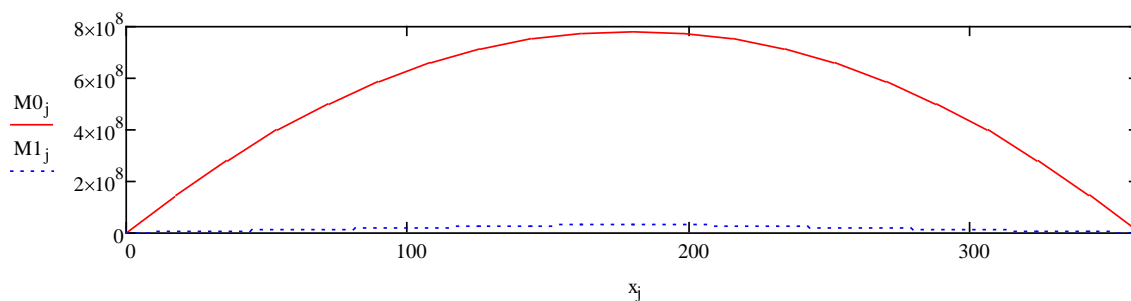
short-term moment

effective stifness $\qquad EI_{eff_j} := EI$

first integrant $\qquad Int1_j := M1_j \cdot \dfrac{M0_j}{EI_{eff_j}}$

second integrant $\qquad Int2_j := M1_j \cdot \dfrac{M1_j}{EI_{eff_j}}$

$$m1 := \sum_{k=1}^{2 \cdot NDiv} \left[\left(\frac{Int1_{k-1} + Int1_k}{2} \right) \cdot \frac{2 \cdot L}{2 \cdot NDiv} \right] = 0.096 \, ft \cdot kip \qquad m2 := \sum_{k=1}^{2 \cdot NDiv} \left[\left(\frac{Int2_{k-1} + Int2_k}{2} \right) \cdot \frac{2 \cdot L}{2 \cdot NDiv} \right] = 3.44 \times 10^{-3} \, ft \cdot kip$$

short-term restoring force $\qquad X := -\dfrac{m1}{m2} = -28.041$

short-term bending moment $\qquad M_i := M0_i + X \cdot M1_i$

long-term moment

effective stifness $\qquad EI_{eeff_j} := EI_e$

first integrant $\qquad Int1_j := M1_j \cdot \dfrac{M0_j}{EI_{eeff_j}}$

second integrant $\qquad Int2_j := M1_j \cdot \dfrac{M1_j}{EI_{eeff_j}}$

third integrant $\qquad \Delta\rho_{s_j} := \begin{vmatrix} \Delta\rho_j & \text{if } j \le NDiv \\ \Delta\rho_{2 \cdot NDiv - j} & \text{otherwise} \end{vmatrix} \qquad\qquad Int3_j := M1_j \cdot \Delta\rho_{s_j}$

$$m1 := \sum_{k=1}^{2 \cdot NDiv} \left[\left(\frac{Int1_{k-1} + Int1_k}{2} \right) \cdot \frac{2 \cdot L}{2 \cdot NDiv} \right] = 0.105 \, ft \cdot kip \qquad m2 := \sum_{k=1}^{2 \cdot NDiv} \left[\left(\frac{Int2_{k-1} + Int2_k}{2} \right) \cdot \frac{2 \cdot L}{2 \cdot NDiv} \right] = 3.751 \times 10^{-3} \, ft \cdot kip$$

$$m3 := \sum_{k=1}^{2 \cdot NDiv} \left[\left(\frac{Int3_{k-1} + Int3_k}{2} \right) \cdot \frac{2 \cdot L}{2 \cdot NDiv} \right] = 9.446 \times 10^{-3} \, ft \cdot kip$$

long-term restoring force $\qquad X_e := -\dfrac{m1 + m3}{m2} = -30.56$

long-term bending moment $\qquad M_{e_i} := M0_i + X_e \cdot M1_i$

final restoring force and moment

restoring force $\quad R_i := X \cdot kip = -28.041 kip \qquad \delta R := \left| X_e - X \right| \cdot kip = -2.518 kip \qquad R := R_i + \delta R = -30.56 kip$

restoring moment $\quad \delta M_i := M_{e_i} - M_i$

$M^T =$		0	1	2	3	4	5	6	7	8	
	0	0	11.032	18.688	22.97	23.877	21.409	15.565	6.347	...	ft·kip

$\delta M^T =$		0	1	2	3	4	5	6	7	8	9	
	0	0	-1.89	-3.78	-5.67	-7.56	-9.44	-11.33	-13.22	-15.11	...	ft·kip
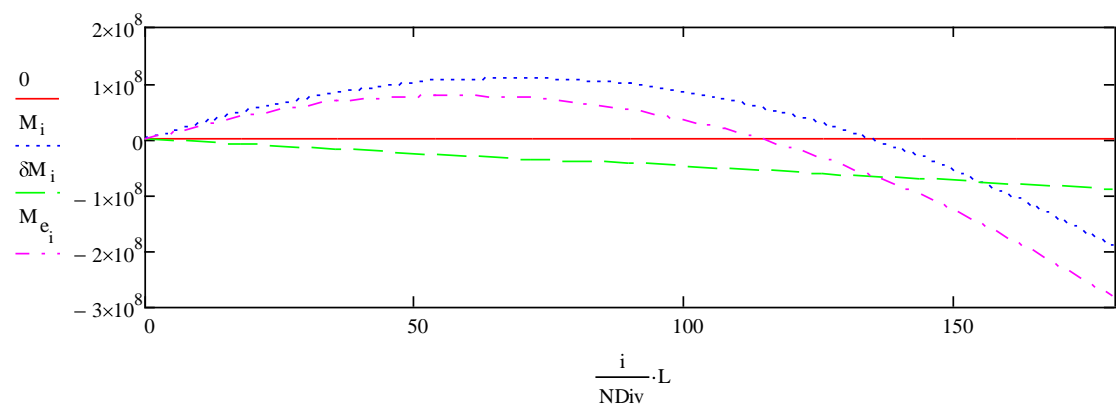
additional strain and curvature at top fiber (after self-stressing)

strain

$$\delta \varepsilon_i := \frac{B_e \cdot \gamma_1 \cdot \delta M_i}{A_e}$$

$\delta \varepsilon^T =$		0	1	2	3	4	5	6
	0	0	$-5.32 \cdot 10^{-6}$	$-1.064 \cdot 10^{-5}$	$-1.596 \cdot 10^{-5}$	$-2.128 \cdot 10^{-5}$	$-2.66 \cdot 10^{-5}$	...

curvature

$$\delta \rho_i := \gamma_1 \cdot \delta M_i$$

$\delta \rho^T =$		0	1	2	3	4	5	6	
	0	0	$-1.044 \cdot 10^{-6}$	$-2.089 \cdot 10^{-6}$	$-3.133 \cdot 10^{-6}$	$-4.177 \cdot 10^{-6}$	$-5.222 \cdot 10^{-6}$	...	$\frac{1}{in}$

additional stress at top fiber caused by restoring moment (after self-stressing)

top slab

$$\delta\sigma_{c0} := E_e \cdot (\delta\varepsilon - 0 \cdot \delta\rho)$$

$\delta\sigma_{c0}{}^T =$		0	1	2	3	4	5	6	7	8	9	ksi
	0	0	-0.02	-0.04	-0.06	-0.08	-0.1	-0.12	-0.14	-0.16	...	

bottom slab

$$\delta\sigma_{ca} := E_e \cdot \left| \delta\varepsilon - D_c \cdot \delta\rho \right|$$

$\delta\sigma_{ca}{}^T =$		0	1	2	3	4	5	6	7	8	9	10	ksi
	0	0	0	0.01	0.01	0.01	0.02	0.02	0.02	0.03	0.03	0.03	

top reinforcement

$$\delta\sigma_{srt} := E_s \cdot \left| \delta\varepsilon - d_{srt} \cdot \delta\rho \right|$$

$\delta\sigma_{srt}{}^T =$		0	1	2	3	4	5	6	7	8	9	10	ksi
	0	0	-0.12	-0.25	-0.37	-0.5	-0.62	-0.74	-0.87	-0.99	-1.12	-1.24	

bottom reinforcement

$$\delta\sigma_{srb} := E_s \cdot \left| \delta\varepsilon - d_{srb} \cdot \delta\rho \right|$$

$\delta\sigma_{srb}{}^T =$		0	1	2	3	4	5	6	7	8	9	10	ksi
	0	0	-0	-0.01	-0.01	-0.01	-0.01	-0.02	-0.02	-0.02	-0.03	-0.03	

tob girder

$$\delta\sigma_{sa} := E_s \cdot \left| \delta\varepsilon - D_c \cdot \delta\rho \right|$$

$\delta\sigma_{sa}{}^T =$		0	1	2	3	4	5	6	7	8	9	10	ksi
	0	0	0.03	0.05	0.08	0.11	0.14	0.16	0.19	0.22	0.25	0.27	

bottom girder

$$\delta\sigma_{sb} := E_s \cdot \left\lceil \delta\varepsilon - \left| D_c + D_s \right| \cdot \delta\rho \right\rceil$$

$\delta\sigma_{sb}{}^T =$		0	1	2	3	4	5	6	7	8	9	10	ksi
	0	0	0.442	0.885	1.327	1.769	2.212	2.654	3.097	3.539	3.981	4.424	

final stress

top of concrete deck

$$\sigma_{cf} := \sigma_{0i} + \Delta\sigma_{c0} + \delta\sigma_{c0}$$

$\sigma_{cf}{}^{T} =$

	0	1	2	3	4	5	6	7	8	9	10
0	0	0.16	0.32	0.48	0.64	0.8	0.95	1.11	1.27	1.43	1.59

ksi

bottom of concrete deck

$$\sigma_{caf} := \sigma_{ai} + \Delta\sigma_{ca} + \delta\sigma_{ca}$$

$\sigma_{caf}{}^{T} =$

	0	1	2	3	4	5	6	7	8	9	10
0	0	-0.02	-0.04	-0.06	-0.08	-0.1	-0.12	-0.14	-0.16	-0.18	-0.2

ksi

top reinforcement

$$\sigma_{srtf} := \sigma_{srti} + \Delta\sigma_{srt} + \delta\sigma_{srt}$$

$\sigma_{srtf}{}^{T} =$

	0	1	2	3	4	5	6	7	8	9	10
0	0	1.14	2.27	3.41	4.55	5.68	6.82	7.96	9.09	10.23	11.36

ksi

bottom reinforcement

$$\sigma_{srbf} := \sigma_{srbi} + \Delta\sigma_{srb} + \delta\sigma_{srb}$$

$\sigma_{srbf}{}^{T} =$

	0	1	2	3	4	5	6	7	8	9	10
0	0	0.06	0.12	0.19	0.25	0.31	0.37	0.44	0.5	0.56	0.62

ksi

top girder

$$\sigma_{saf} := \sigma_{sai} + \Delta\sigma_{sa} + \delta\sigma_{sa}$$

$\sigma_{saf}{}^{T} =$

	0	1	2	3	4	5	6	7	8	9
0	0	2.51	3.58	3.2	1.38	-1.89	-6.6	-12.76	-20.36	...

ksi

bottom girder

$$\sigma_{sbf} := \sigma_{sbi} + \Delta\sigma_{sb} + \delta\sigma_{sb}$$

$\sigma_{sbf}{}^{T} =$

	0	1	2	3	4	5	6	7	8	9
0	0	-6.52	-11.59	-15.22	-17.4	-18.14	-17.43	-15.28	-11.68	...

ksi

Prediction of prestressing loss

initial self-stressing $\qquad \sigma_{0i_{NDiv}} = 2.279 \text{ksi}$

fianl self-stressing $\qquad \sigma_{cf_{NDiv}} = 1.59 \text{ksi}$

percentage of loss $\qquad \text{loss} := \dfrac{\left|\sigma_{cf_{NDiv}} - \sigma_{0i_{NDiv}}\right|}{\sigma_{0i_{NDiv}}} \cdot 100 = 30.222$